^{14}C and ^{14}C–^{10}Be Terrestrial Age Dating System for Stony Meteorites

Inaugural dissertation
of the Faculty of Science,
University of Bern

Presented by
Mohammad Tauseef

Supervisor of the doctoral thesis:
Prof. Dr. Ingo Leya
Physics Institute, University of Bern

Referee: Dr. Jérôme Gattacceca
CEREGE Institute, France

^{14}C and ^{14}C–^{10}Be Terrestrial Age Dating System for Stony Meteorites

Inaugural dissertation
of the Faculty of Science,
University of Bern

Presented by
Mohammad Tauseef

Supervisor of the doctoral thesis:
Prof. Dr. Ingo Leya
Physics Institute, University of Bern

Referee: Dr. Jérôme Gattacceca
CEREGE Institute, France

Accepted by the Faculty of Science

Bern, 31. March 2025

The Dean
Prof. Dr. Jean-Louis Reymond

Table of Contents

List of Tables

List of Figures

Acknowledgements

All praise belongs to Allah, the planner of all souls. It is by His boundless compassion and generosity that I have been able to complete this PhD journey. This experience has been one of the most transformative periods of my life, filled with learning, growth, and moments of joy. These past four years have been nothing short of incredible, and I will forever cherish the knowledge gained and the friendships formed along the way.

First and foremost, I extend my deepest gratitude to my PhD supervisor, **Prof. Dr. Ingo Leya**. His patience, motivation, and immense knowledge have been a guiding light throughout this journey. His unwavering encouragement, pioneering ideas, and insightful suggestions from the very beginning have shaped this thesis and made this research possible. I will always be grateful for his support, which has not only strengthened my scientific understanding but has also helped me grow as a researcher.

I am also sincerely thankful to **Dr. Jérôme Gattacceca, Dr. Régis Braucher, and the ASTER-Team at CEREGE, France**, for their invaluable assistance with the **^{10}Be** analysis. Their generosity and expertise were instrumental in this work. My visit and stay at CEREGE for two weeks were an enriching experience, and I am grateful for their warm hospitality, insightful discussions, and the opportunity to learn from their expertise firsthand. I would also like to express my sincere gratitude to **Prof. Dr. Sönke Szidat, Dr. Thomas Laemmel, Dr. Gary Salazar, Dr. Tiberiu Sava and Dr. Franziska Lechleitner** for their invaluable help and guidance in teaching me **^{14}C measurement using MICADAS AMS**. Their expertise, patience, and willingness to share their knowledge have greatly contributed to my understanding and the success of this work.

No words can truly express my gratitude to my **family** and my **to-be wife, Zainab**. From the depths of my heart, I thank them for their unconditional love, endless support, and unwavering prayers. Being far from home was never easy, but their belief in me kept me strong and gave me the courage to keep pushing forward.

A special thanks to my incredible **lab mates**—**Jason Hirtz, Hammad Khan, Parastoo Ghaznavi, and Farshid Nozarian**—for their support, insightful discussions, and the many moments of laughter that made the long hours in the lab enjoyable. My gratitude also goes to **Anna Zappatini and Carine Sadaka**, whose collaboration and friendship have enriched my research and made the journey even more fulfilling. I am thankful to **Jan Wenger, Andreas Schmitt, and Samuel Meier** for their technical expertise and constant support in the lab—without their help, my measurements would not have been as smooth and successful.

I am also thankful to **Dora Zimmerer, Tina Rothenbühler** and **Gisela Herren** for their help with the administrative aspects during my PhD studies.

Beyond the lab, I have been blessed with the companionship of wonderful **friends** who made my time at the university unforgettable. My heartfelt thanks go to **Harsh Vasoya, Vrushali Godse, Kaushavi Cholke, Tipu Khan, Mohammed Yagoubi, Bahare Masoumi, and Aryavart Anand**, for their encouragement, warmth, and the many cherished memories we shared. I am also grateful to my friend **Mazhar Sadiq** for visiting Bern and for the memories we created while exploring Switzerland together. A special mention to my **flatmates, Flavian, Leïla, and Isabella**, whose presence turned my stay into a home away from home.

To each and every one of you—thank you for being part of this journey. This PhD is not just my achievement, but a reflection of all the kindness, support, and love I have received along the way.

*This PhD is dedicated to my **father** and **mother**,*

I am a mere reflection of both.

Chapter 1

Introduction: Meteorites and The Scope of This Project

1.1. Project Focus and Goals

Meteorites provide important clues about the history of the Solar System and the processes that shape planetary bodies. One of the key aspects in meteorite research is determining how long a meteorite has been on Earth—its terrestrial age. These ages are determined by comparing the initial (at time of fall) and present-day concentrations of cosmogenic radionuclides (e.g., ^{14}C, ^{10}Be, ^{36}Cl, ^{41}Ca). This information helps scientists understand the rate at which meteorites arrive (meteorite flux), how they weather over time, i.e., their interaction with different hot and cold desert environments, and their potential role in delivering important elements to our planet. Among different types of meteorites, terrestrial ages of stony meteorites are very often determined using the ^{14}C and ^{14}C-^{10}Be dating system. This system is well-suited for dating stony meteorites from desert environment, which are typically younger than 50 ka. However, a major challenge in ^{14}C and ^{14}C-^{10}Be dating system is the uncertainty in initial activity concentrations (saturation activities) of ^{14}C and $^{14}C/^{10}Be$ ratios at the time meteorite fell on Earth. These saturation activities correspond to the production rates in space, which essentially depends on the meteorite's chemical composition, size, and shielding depth. While they can be estimated by analyzing recently fallen meteorites, previous studies have relied on very few measurements, assuming an average, constant saturation value. This approach ignores shielding-dependent variations in ^{14}C saturation activities and $^{14}C/^{10}Be$ ratios, leading to inaccurate terrestrial age estimates and size-dependent biases in terrestrial age histograms.

This project aims to improve the accuracy of meteorite terrestrial age dating by refining the ^{14}C and ^{14}C-^{10}Be dating system. By studying how ^{14}C production rates and $^{14}C/^{10}Be$ ratios vary with shielding depth, this research will develop a more reliable method for determining terrestrial ages. A combination of model calculations and experimental data will be used to estimate ^{14}C saturation activities and $^{14}C/^{10}Be$ saturation ratios in meteorites and understand how it varies with shielding depth. The isotopic concentrations of light noble gases He, Ne, and Ar will be measured, and cosmogenic $(^{22}Ne/^{21}Ne)_{cos}$ will be determined to estimate shielding depth of studied samples. Additionally, cosmic ray exposure age of meteorites will be estimated to evaluate ^{10}Be saturation equilibrium, which help constrain the $^{14}C/^{10}Be$ dating system. The results of the improved ^{14}C and $^{14}C/^{10}Be$ dating system will be applied to refine terrestrial age of strewnfield meteorites from Oman, and refining ages of other hot desert meteorites, such as meteorites from Saharan Desert and Australia. Ultimately, this research will contribute to a better understanding of cosmogenic (^{14}C and ^{10}Be) nuclide production in meteorite in space,

and improve the methods used for dating meteorites that have fallen to Earth, which in turn helps in other scientific topics such as the meteorite flux estimates and its life on Earth.

1.2. Meteorites

Meteorites are extraterrestrial rock fragments from space that reaches on the Earth surface. They originate from celestial bodies, typically asteroids, that experience collision and fragmentation due to impacts. These fragments travel through space, sometimes for millions of years, before their trajectories bring them into Earth's gravitational influence. After landing, meteorites can be affected by terrestrial weathering, which alters their chemical and physical characteristics. Studying fresh falls and well-preserved meteorites provides the most accurate insights into their extraterrestrial origins. While majority of meteorites originate from the asteroids, which are located in between Mars and Jupiter, some rock fragments ejected off from the surface of the Moon and the Mars, due to cratering impacts, also make their way to Earth, termed as Lunar and Martian meteorites. Meteorites are falling on Earth throughout the geological time. From the earlier Late Heavy Bombardment delivering volatiles, to Permian-Triassic causing extinction of life, to present day catastrophic events such as Chelyabinsk (2013). Humans have been observing and interpreting meteorite falls for thousands of years, often as divine signs or sacred objects. Archaeological excavation also found tools and artifacts made of meteoritic materials. Roman historians recorded meteorite falls as omens linking to war and political changes.

1.3. Meteoroids, Meteorites and Meteors

A meteorite journey through the solar system is distinctly divided into three stages. First stage is when rock fragments travelling through the space after ejecting off from its parent body until it gets attracted by planetary gravitational force or it falls into the sun, are called meteoroid (e.g., Norton 2002). This can vary in size from a grain to a few meter-sized objects. Second stage is when meteoroids entering the Earth’s atmosphere creating a bright streak of light due to frictional heating and burns up completely in the atmosphere, these are termed meteors or shooting stars. Not all objects survive their passage through Earth’s atmosphere. Their survival rate depends on many factors, such as size and shape of the object, entry angle and entry velocity. Only those meteoroids which survive Earth’s atmosphere and finally land of surface are called meteorites. These objects can be as small as grain-sized to big few centimetres

weighing tons of kilogram. The different small bodies terminologies associated with meteorites are shown in Fig. 1.1.

Meteorites are windows to early solar system helping in understanding the conditions exist during the early solar system. These space rocks provide valuable insights into (i) the formation and evolution of the solar system, (ii) the composition of celestial bodies that no longer exist (iii) the planetary formation processes that led to the development of Earth and other planets, (iv) the delivery of water and organic molecules to Earth, which may have contributed to the emergence of life and, (v) the cosmic ray exposure history of space objects, offering insights into galactic cosmic rays (GCR) and solar activity (solar cosmic rays – SCR) over time.

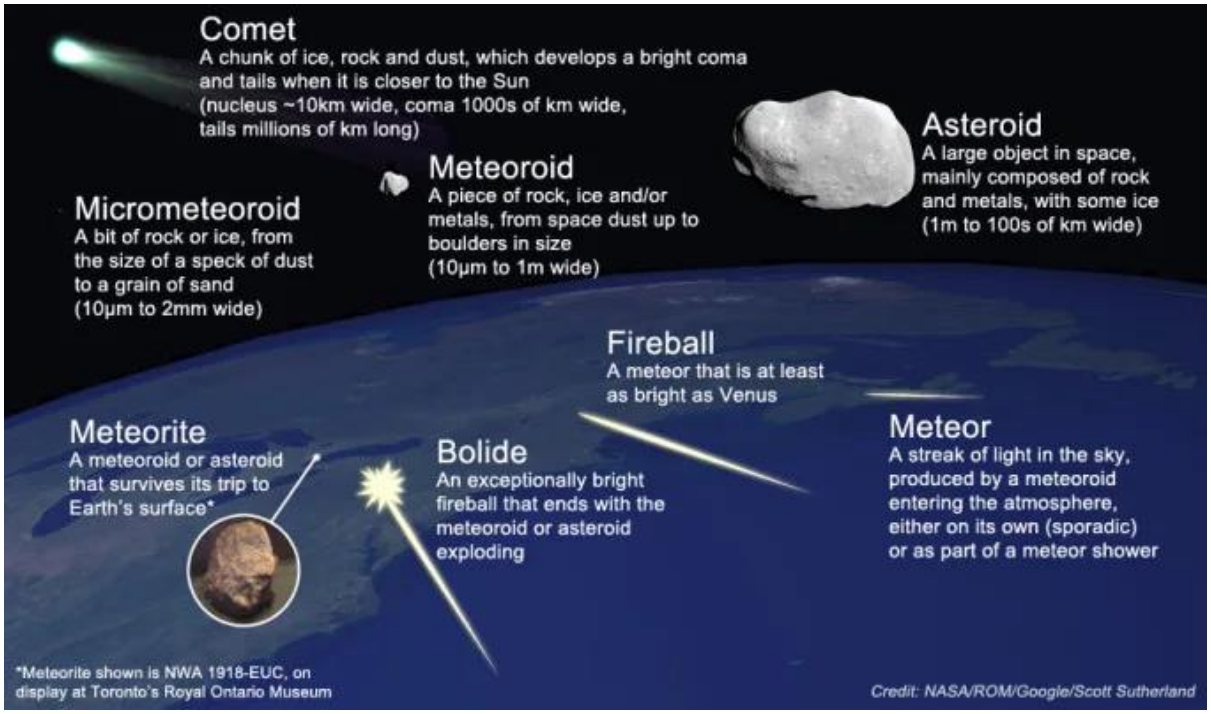

Fig. 1.1. Different terminologies and small bodies associated with meteorites

1.4. Classification of Meteorites

A simplified classification of meteorites consists of three groups: (i) stony meteorites, (ii) iron meteorites, and (iii) stony-iron meteorites. This division is based on the stone to iron ratio. The widely accepted classification is the two groups: (i) undifferentiated meteorites (chondrites), and (ii) differentiated meteorites (achondrites). These are further divided into various groups, sub-groups and clans (Weisberg et al., 2006). This classification systematically organizes meteorites based on chemical, petrological and isotopic properties, providing a framework for

understanding their origin and evolution. The undifferentiated meteorites are called chondrites (Table 1.1) that have solar-like compositions and are derived from asteroids that did not experience planetary differentiation (Weisberg et al., 2006). The name derived from the spherical grains called chondrules, present in these meteorites, which are believed to be the oldest material in the solar system. Chondrites make up ~92% of total documented meteorites. Chondrites are further classified based on petrographic types, labelled from 1 to 6 (Van Schmus and Wood, 1967), weathering grades from W0 for fresh un-weathered to W6 for highly weathered, altered silicates (Wlotzka, 1993).

Achondrites are igneous rocks derived from the differentiated parent bodies, which have separated into different density and compositional layers as a result of melting and gravitational separation. Differentiated meteorites contribute ~10% of the total meteorite, which includes stony (Table 1.2), stony-iron (Table 1.3) and iron meteorites (Table 1.4). Some meteorites show igneous texture (recrystallised) but retain chemical signatures similar to chondritic meteorites are termed as primitive achondrites e.g., Ureilites. Stony-iron meteorites are believed to be originated from core-mantle boundary of differentiated parent bodies. Iron meteorites have crystallized from metallic melts and derived mostly from the cores of differentiated parent bodies due to impacts.

Table 1.1. Chondrite group meteorites and their characteristics.

Group	Characteristics
Ordinary Chondrites	Most common; moderate Fe content
- H (High Fe)	~25–31% total Fe, low Fe/Ni metal
- L (Low Fe)	~20–25% total Fe, higher Fe/Ni metal
- LL (Very Low Fe)	~19–22% total Fe, highest Fe/Ni metal
Carbonaceous Chondrites	High volatile and organic content; primitive
- CI	No chondrules; rich in water, organics
- CM	Chondrules present; hydrated silicates
- CO	Small chondrules; low metal content
- CV	Large chondrules; some Fe-Ni metal
- CK	High Fe oxidation; abundant Fe-rich silicates
- CR	High Fe/Ni metal; aqueous alteration
- CH	High Fe/Ni metal (~20–30%)
- CB	Metallic components; early solar nebula processes
Enstatite Chondrites	Reduced, formed in an oxygen-poor environment
- EH (High Fe)	High Fe-Ni metal (~20–30%)
- EL (Low Fe)	Lower Fe-Ni metal (~10–15%)
Rumuruti (R) Chondrites	Oxidized; high FeO in silicates

Table 1.2. Achondrite group meteorites and their characteristics.

Group	Characteristics
Primitive Achondrites	Partial differentiation; some chondritic features
- Ureilites	Contains graphite & diamond, partially melted
- Acapulcoites & Lodranites	Transition between chondrites & achondrites
- Winonaites	Similar to silicate inclusions in IAB irons
Asteroidal Achondrites	Differentiated planetesimals
- (HED)	Origin from asteroid 4 Vesta
- Angrites	Basaltic; enriched in Ca, Al
- Aubrites	Enstatite-rich; formed in highly reduced conditions
Martian Meteorites (SNC)	From Mars, enriched in volatiles
Lunar Meteorites	Similar to Moon rocks; feldspathic and basaltic

HED= Howardites, Eucrites, and Diogenites; SNC= Shergottites, Nakhlites, and Chassignites

Table 1.3. Stony-iron group meteorites and their characteristics.

Group	Characteristics
Pallasites	Olivine + Fe-Ni metal (core-mantle boundary)
Mesosiderites	Brecciated silicates + Fe-Ni metal

Table 1.4. Iron meteorites and their characteristics.

Group (Chemical Class)	Characteristics
IAB	Mixed metal-silica, possibly from disrupted parent body
IIAB	Low Ni content; large Widmanstätten patterns
IIC, IID, IIE, IIF	Various Ni and trace element differences
IIIAB	Most common; moderate Ni content
IIICD	Rare; chemically distinct
IVA	High Ni, fine Widmanstätten patterns
IVB	Very high Ni, fine-grained

1.5. Meteorite Statistics

The number of approved meteorites is significantly increasing because of the systematic search campaigns in hot and cold deserts around the world. The Meteoritical Bulletin lists a total of 84206 meteorites in the database however, few of them are either pseudometeorites, uncategorised or doubtful stones. The total number of major types of meteorites documented is 77064 as of 8 Feb 2025 (Table 1.5). About 85% of the total account are ordinary chondrites. Among ordinary chondrites H chondrite comprises 45%, L chondrites make up 42%, and LL chondrites comprises 13%. Ordinary chondrites are followed by the carbonaceous chondrites and HED group in terms of number.

The Meteoritical Bulletin Database has documented 1401 confirmed meteorite falls (Table 1.6) as of 8 February 2025. These are the instances where meteorites were observed during their descent and subsequently recovered. Estimates suggest that thousands of meteorites larger than 0.1 kg fall on Earth, however, many of them go unobserved because they fall into oceans, remote areas, or during daylight when visibility is reduced. Among the documented falls, ordinary chondrite comprises ~70%. The number of reporting of meteorite falls are increasing, thanks to the developments in camera-networks focused on fireball observations, which have significantly improved the observation and documentation of meteorite falls (Colas et al., 2020; Bland et al., 2012).

Table 1.5. Distribution of meteorite types as of 8 February 2025.

	Type of meteorite	**No. of approved meteorites**	**% of total**
Chondrites	Ordinary	65114	84.49
	Carbonaceous	3261	4.24
	Enstatite	703	0.92
	Rumuruti	332	0.43
	Kakangari	4	0.01
Achondrites	Ureilites	726	0.94
	Angrites	54	0.07
	Aubrites	91	0.12
	HED	3095	4.03
	Winonaites	98	0.13
	Acapulcoites - Lodranites	201	0.26
	Branchinites	65	0.08
	Martian	395	0.51
	Lunar	717	0.93
Stony-Iron	Pallasites	189	0.25
	Mesosiderites	379	0.49
Iron	all class	1414	1.84
Others		226	
Total		**77064**	

There are other uncategorised, pseudometeorites and doubtful stones with a staggering total number of 7369.

Table 1.6. Fall vs. finds meteorite. Percentage of ordinary chondrite fall as of 08 Feb 2025.

Event	**Total**	**Finds**	**Falls**	**OC Fall**
Record	76737	75336	1401	984
(%)			1.8	70.2

OC=ordinary chondrite falls

1.6. Cosmogenic Nuclide Production in Meteorites

Meteoroids travelling through space are exposed to galactic cosmic rays (GCR) and solar cosmic rays (SCR). These interaction of GCR and SCR with meteoroids results in the production of different cosmogenic stable- and radionuclides. The stable nuclides (e.g., ^{3}He, ^{21}Ne) continue to accumulate with time, whereas the radioactive nuclides (e.g., ^{14}C, ^{10}Be, ^{26}Al), promptly undergo decay. However, after few half-lives, the production rate equals the decay rate and the radionuclide activity get into equilibrium state, called as saturation activity. In Fig. 1.2, the blue steadily increasing curve represents the continuous production (accumulation) of a stable cosmogenic nuclide (e.g., ^{21}Ne, ^{3}He) in a meteoroid over time. The red curve represents the production and decay of a radioactive cosmogenic nuclide (e.g., ^{14}C, ^{10}Be), which initially rises and then plateaus at saturation equilibrium when production and decay rates balance out. Cosmogenic nuclides which are discussed in this study are listed in Table 1.7.

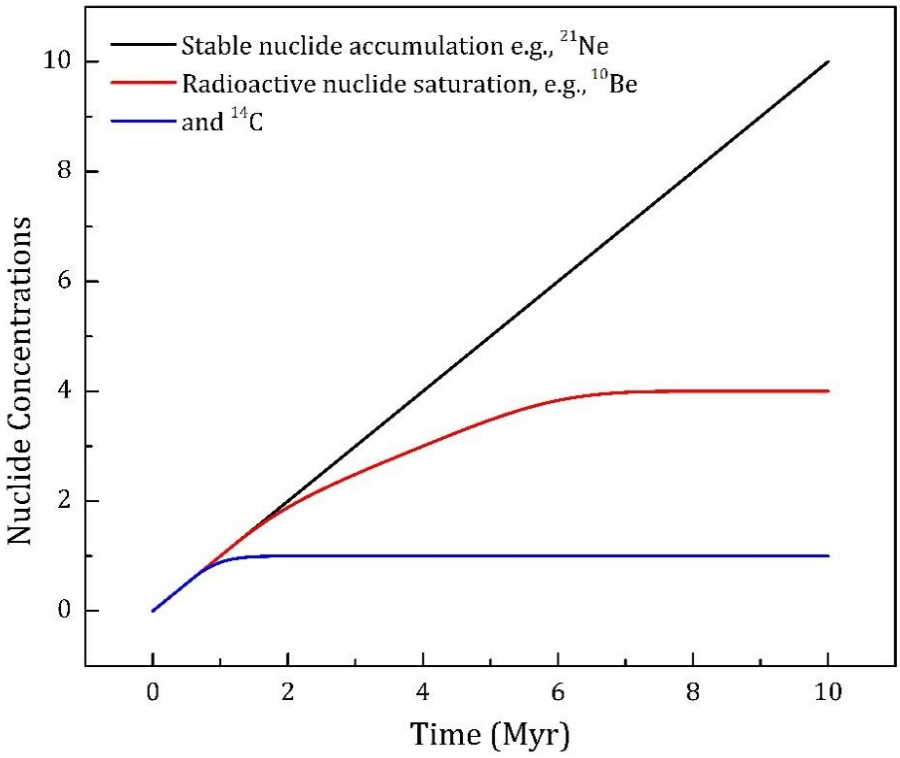

Fig. 1.2. Accumulation of stable and saturation of radionuclide concentrations in meteoroids with time.

Table 1.7. Cosmogenic nuclides discussed in this study.

Cosmogenic nuclides	Half-life (years)	Target Elements
^{14}C	5730	O, Mg, Al, Si, Ca, Fe, Ni
^{10}Be	1.39×10^6	O, Mg, Al, Si, Ca, Fe, Ni
^{26}Al	7.17×10^5	Al, Si, Ca, Fe, Ni
^{36}Cl	3.01×10^5	Cl, Ti, Ca, Fe, Ni
^{41}Ca	9.94×10^4	Ca, Fe, Ni
^{3}He, ^{4}He	stable	O, Mg, Al, Si, Ca, Fe, Ni
^{21}Ne, ^{22}Ne, ^{20}Ne	stable	Mg, Al, Si, Ca, Fe, Ni
^{36}Ar, ^{38}Ar, ^{40}Ar	stable	Cl, Ca, Ti, Fe, Ni

Details are taken from David and Leya, (2019).

1.7. Cosmic Ray Exposure History of Meteorites

Cosmic ray exposure (CRE) age estimates how long a meteoroid has been exposed to cosmic rays in space. Initially, the meteoroid's material is buried deep in its parent asteroid, shielded from cosmic rays. A collision ejects it into space, where it orbits the Sun and becomes fully exposed. This exposure continues until the meteoroid falls to Earth. During atmospheric entry, an estimated about 80% of its mass burns away, leaving only the innermost 20% (by mass) to reach the surface. After reaching on Earth, cosmic ray exposure effectively stops due to shielding by air, water, or ice. The CRE age (T_{exp}) is the time between ejection from the parent body (T_i) and arrival on Earth (T_f), calculated as $T_{exp} = T_f - T_i$. To determine T_{exp}, we measure cosmogenic nuclides—either stable (e.g., ^{21}Ne) or radioactive nuclides (^{10}Be, ^{26}Al). Among the stable noble gas isotopes, e.g., ^{3}He, ^{21}Ne, and ^{38}Ar, CRE ages derived using ^{21}Ne are the most common and robust method. The exposure age is calculated using the isotopic concentration and production rate in meteorites. For example, CRE age derived using ^{21}Ne is expressed as: $T_{21} = N(^{21}Ne)/P(^{21}Ne)$, where N is the measured concentration of cosmogenic $^{21}Ne_{cos}$ (in units 10^{-8} cm^3 STP/g) and P is the $^{21}Ne_{cos}$ production rate (in units 10^{-8} cm^3 STP/g/Ma). The concentration of stable nuclides (e.g., $^{21}Ne_{cos}$) are measured using mass spectrometry, whereas the production rates are usually determined by model calculations (e.g., Leya and Masarik, 2009). The production rate of $^{21}Ne_{cos}$ depends on shielding depth of sample within the meteoroid, which is a priori unknown and has to be assumed or deduced by some means. Since, a meteoroid may lose well over 80% of its pre-atmospheric mass when passing through the Earth's atmosphere, and moreover may disintegrate into many fragments, which can render the shielding depth estimates. Nonetheless, the shielding depth are usually deduced by using shielding indicators such as cosmogenic $(^{22}Ne/^{21}Ne)_{cos}$. Most meteorites have CRE ages in the

range of millions of years, reflecting their long journey in space before reaching Earth. The CRE age calculations assume a constant GCR flux, and single-stage exposure, meaning the meteoroid was ejected from a well-shielded depth and travelled as a single piece without further collisions. In this case, measured radionuclide activity reliably indicates stable nuclide production rates. However, if the meteoroid underwent breakups (complex exposure history), production rates change, leading to incorrect CRE ages. The impact of breakups, i.e., multi-collisional history of meteorites is reflected by the activity concentrations of radionuclide of different half-lives. For example, ^{53}Mn (half-life: 3.7 Ma) retains its original exposure history, while ^{44}Ti (half-life: 60 years) reflects only recent changes (David and Leya, 2019).

Analysis of CRE age histograms (Fig. 1.3) reveals two key observations (Wieler, 2002; Graf and Marti, 1995). First, most stony meteorites have exposure ages between a few million years and ~70 million years (David and Leya, 2019). Second, the distribution of CRE ages shows clusters, suggesting that many meteorites of the same type (e.g., H chondrites) originated from a single, large collision on a parent asteroid. This implies that meteorite delivery to Earth is not continuous but occurs in bursts following major asteroid belt collisions. For example, about 45% of all studied H chondrites have CRE ages of ~7 Ma, indicating they likely originated from a single, significant impact event. Similar peak clusters can be observed for L (20–30 Myr and 40 Ma), LL (~17 Ma) and E chondrites (~20–30 Ma). These peaks are likely indicating collision events that resulted in meteorite delivery to Earth.

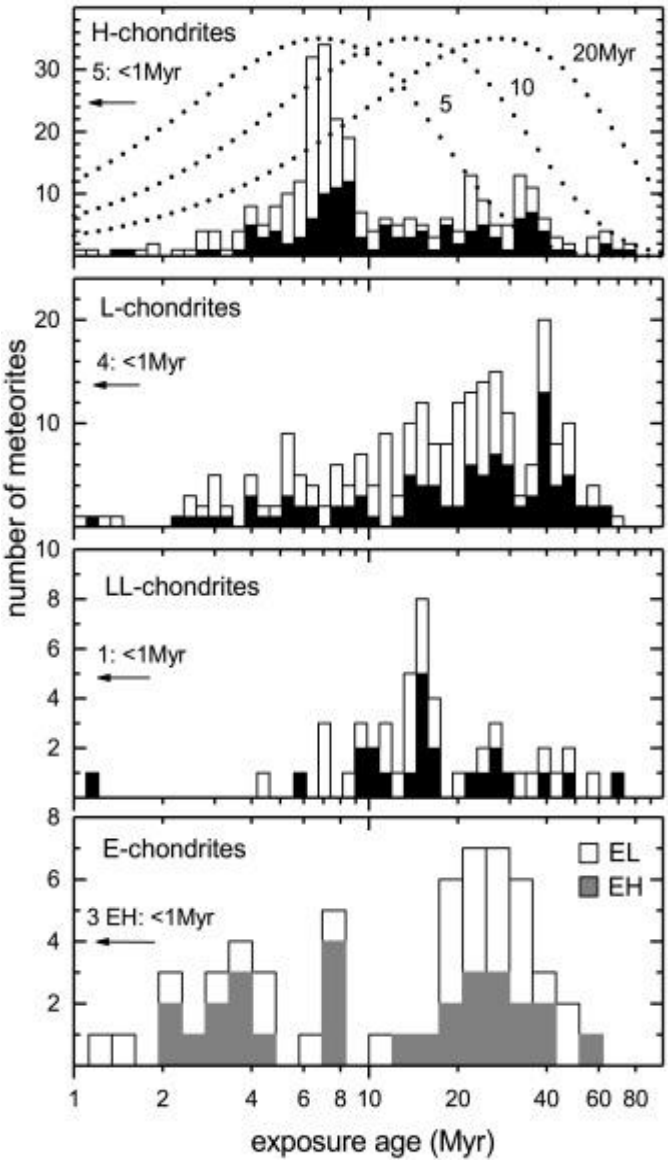

Fig 1.3. CRE age histogram for H, L, LL and enstatite chondrites. The graph is taken from Wieler, (2002).

1.8. Terrestrial Age of Meteorites

Terrestrial age of a meteorite is the time spent on Earth before being found. Knowing terrestrial ages of meteorites is crucial for multiple scientific questions. *First*, they help in understanding terrestrial weathering processes, as meteorite preservation varies significantly across different desert environments. While meteorites found in the Sultanate of Oman, North Africa, the United States, and Australia have average terrestrial ages of 30–50 ka (Al-Kathiri et al. 2005; Sliz et al. 2022; Jull 1993, 2006), those in the Atacama Desert and Antarctica can reach ages of up to millions of years (Cassidy 2003; Gattacceca et al. 2011; Drouard et al. 2019). *Second*, pairing corrections—determining if multiple meteorites originate from the same meteoroid that fragmented during atmospheric entry—rely partly on terrestrial ages. *Third*, these ages contribute to studying the dynamics of small solar system bodies, particularly in determining ejection ages (the sum of CRE age and terrestrial age). Although the terrestrial age is typically much shorter than the CRE age, in meteorite types with low CRE ages (e.g., lunar meteorites, carbonaceous chondrites), terrestrial age plays a significant role. *Lastly*, terrestrial ages provide insights into the meteorite influx to Earth, helping address whether the flux rate and composition have remained constant or changed over time. Terrestrial ages are commonly determined using the cosmogenic radionuclides produced in space. The radionuclides are continuously produced in meteoroid in space, after landing on Earth they get shielded from cosmic rays, and with no production these radionuclides subsequently undergo decay based on their half-lives. Measuring the present-day activity concentration of a radionuclide and comparing it with the initial activity concentration at the time of arrival, gives the time elapsed on Earth. However, to achieve this, first, we need to know the initial activity of that radionuclide at the time of fall, which is a priori unknown. These initial activities are also called saturation activities of a radionuclide, which can be determined by measuring their concentrations in freshly fallen meteorites. These saturation activities can be subsequently used to determine the terrestrial ages of meteorite finds. However, these saturation activities are not constant and depends on many factors such as the pre-atmospheric size of the meteorite, its shape, the position of the studied sample within the pre-atmospheric body (shielding depth), and the chemical composition of the meteorite. The chemical dependency, to some extent, can be overcome by coupling two radionuclides with different half-lives, which are produced from the same parent element (e.g., ^{14}C with ^{10}Be). The shielding dependency, however, needs to be estimated by some means, for instance, using the measured $(^{22}Ne/^{21}Ne)_{cos}$ in the same sample aliquot can put some constraint on shielding depth.

1.9. Terrestrial Age Dating Using ^{14}C and ^{14}C – ^{10}Be Technique

Terrestrial ages of stony meteorites are commonly determined using the ^{14}C and $^{14}C/^{10}Be$ dating systems, which have also been applied to mesosiderites (Jull et al., 2009) and iron meteorites (Schnitzer et al., 2012). Both ^{14}C and ^{10}Be, with a half-life of 5730 yrs, produced in meteoroids as a result of spallation on O-atom by the interaction of high-energy cosmic ray particles. ^{14}C dating technique can potentially date meteorites terrestrial age up to 30–40 ka old, which is suitable for most of the stony meteorites (Jull et al., 1989). For meteorites that are older and not suitable for ^{14}C dating, radionuclides, for example ^{10}Be ($t_{1/2}$ = 1.37 Ma) or ^{36}Cl ($t_{1/2}$ = 301 ka) with a relatively longer half-lives are used to determine terrestrial ages (Drouard et al., 2019; Hutzler et al., 2016).

^{14}C dating of meteorites is considered as a robust technique and has been applied to date meteorites from different terrestrial settings (Al-Kathiri et al., 2005; Jull et al., 2010). Despite the significance of these methods, only three laboratories worldwide conduct such studies: the University of Arizona, USA (Jull et al., 2013), Nagoya University, Japan (Minami et al., 2006), and the University of Bern, Switzerland (Mészáros et al., 2018; Sliz et al., 2019, 2022). Currently, new data on ^{14}C ages are being published only from University of Bern and University of Arizona. Due to analytical challenges, ^{14}C-based terrestrial ages are often less precise and reliable than desired, given the importance of the data. A key factor in these calculations is the ^{14}C saturation activity at the time of the meteorite's fall. Saturation activity refers to the equilibrium activity concentration of a radionuclide that has reached a steady-state during cosmic-ray irradiation in space and has not yet started to decay after the meteorite lands on Earth. This value is equivalent to the production rate, defined as the rate at which a nuclide is generated per unit mass and time during space exposure. For practical applications, average ^{14}C saturation activities of 46 dpm/kg for H chondrites, 51.1 dpm/kg for L chondrites, and 55.2 dpm/kg for LL chondrites are commonly used (e.g., Jull et al., 1998). Very often an uncertainty of 15% is assigned to the average ^{14}C saturation activity. The terrestrial ages determined using these average values thus have uncertainties of 1–2 ka (Jull et al., 1989; 1993; 1998).

However, ^{14}C production rates are strongly influenced by shielding conditions, which are often unknown for the studied samples. Measured ^{14}C activity concentrations in fresh falls range from 34 to 70 dpm/kg—a variation of more than a factor of 2 (Minami et al., 2006; Jull et al., 1989; Leya et al., 2001). Earlier model calculations (Wieler et al., 1996; Knauer et al., 1995) have confirmed these variations, revealing the limitations of using constant values in terrestrial age determinations. However, these findings were ignored due to the lack of experimental data

to prove model calculations, and average values were routinely used for age calculations. Consequently, relying on average values lead to size-dependent biases, and make significant over- or, in some cases, slight underestimations of terrestrial ages. The impact of shielding on ^{14}C production rates has been previously discussed (e.g., Jull et al., 1994; Knauer et al., 1995; Wieler et al., 1996). For instance, Knauer et al. (1995) highlighted the shielding dependency of ^{14}C production and proposed combining ^{14}C data with $(^{22}Ne/^{21}Ne)_{cos}$ ratios to improve dating accuracy. However, this approach was never widely implemented. Instead, the suggestion of Jull et al. (1993) assigning a 15% uncertainty to ^{14}C saturation activity for meteorites with unknown shielding conditions, has been adopted.

To address shielding effects, some studies have employed the $^{14}C/^{10}Be$ production rate ratio, which partially corrects for shielding effects and typically provides more reliable terrestrial ages than calculations based solely on ^{14}C (e.g., Kring et al., 2001; Jull et al., 2010). A commonly assumed $^{14}C/^{10}Be$ ratio of 2.5 ± 0.1 has been used for age calculations (Jull et al., 1990, 2010; Kring et al., 2001; Welten et al., 2001). However, experimental data and model calculations indicate that this ratio is not constant. For example, measured $^{14}C/^{10}Be$ ratios for meteorite falls vary significantly from the assumed value, with reported ratios of 2.1 for the L/LL6 chondrite Knyahinya (Jull et al., 1994), and 3.3 ± 0.1 for the H4–5 chondrite Carancas (Jull et al., 2009). Even within a single meteorite, such as St-Robert (H5), values range from 2.3 to 3.7 (Leya et al., 2001). Additionally, model predictions by Jull et al. (2010) suggest $^{14}C/^{10}Be$ ratios between 1.2 for small meteorites and 3.0 for large ones.

In summary, these findings clearly indicate that neither ^{14}C saturation activities nor the $^{14}C/^{10}Be$ production rate ratio are constant; both vary with shielding conditions. ^{14}C and ^{14}C -^{10}Be system are robust technique for dating terrestrial ages of meteorites but the assumption of constant saturation activities and saturation ratios can create size-dependent bias in terrestrial ages which results in overestimation, and in some case, underestimation of true ages of meteorites. To overcome this, it is needed to employ shielding indicator, e.g., $(^{22}Ne/^{21}Ne)_{cos}$ to estimate shielding-based saturation activities and ratios in terrestrial age calculation. This study, as mentioned earlier, investigates the shielding-dependent ^{14}C saturation activities and $^{14}C/^{10}Be$ saturation ratios using experimental data and model calculation.

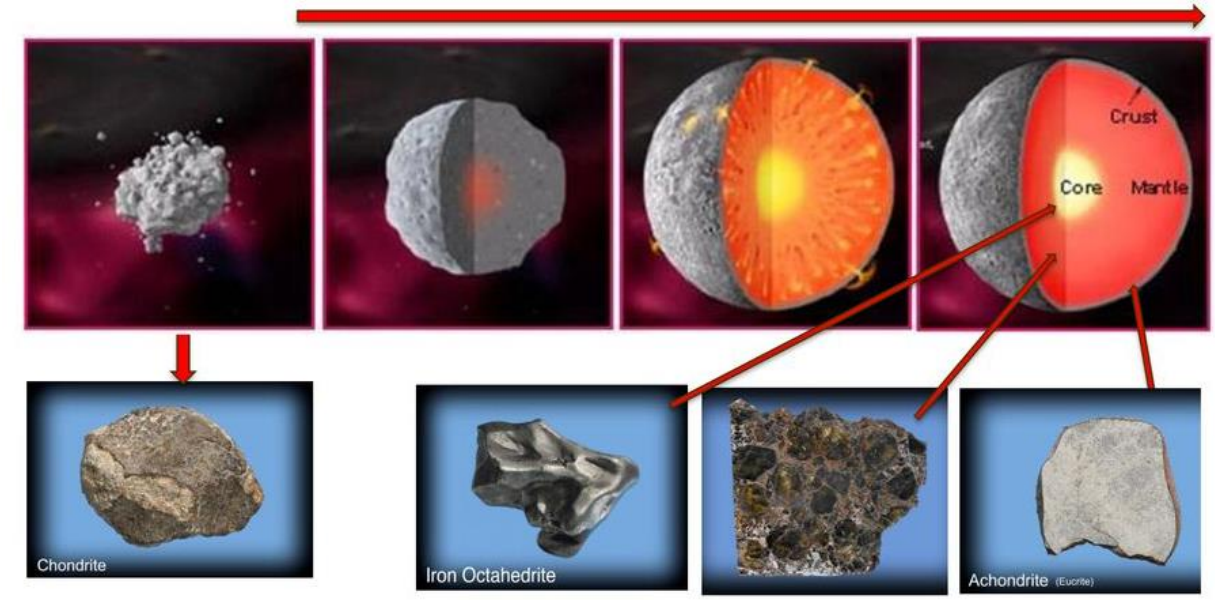

Fig. 1.4. Chondrites derived from undifferentiated parent bodies. Achondrites (Iron, stony-iron and achondrites) derived from differentiated parent bodies. Initial heating of these parent bodies causes melting and differentiation. Mainly by the short-lived isotopes, e.g., ^{26}Al ($t_{1/2} = 7.17 \times 10^5$ years) and ^{60}Fe ($t_{1/2} = 2.6 \times 10^6$ years). Picture credit: An Introduction to Meteorites & Impactites: Dr. Jana Horak.

Fig. 1.5. Allende chondrite (left) showing chondrules and CAI in the meteorite matrix (pic credit: mdpi.com/2075-163X/13/1/31). Esquel pallasite in middle and Widmanstätten pattern in the Staunton iron meteorite (right). Picture credit: The Smithsonian History Museum

Chapter 2

Studied Meteorites in This Project and Methods of Analysis

2.1. Meteorites Studied in This Project

This study focuses on ordinary chondrites. We started a systematic study for evaluating the ^{14}C saturation activities and $^{14}C/^{10}Be$ saturation activity ratios for different shielding depth. For this project, we selected recently fallen H, L and LL chondrites (Table 2.1) from our collection at the Physics Institute, University of Bern. The results of these meteorites are discussed in chapter 3 and 4. We emphasised to select meteorites with CRE ages > 7 Myr that to make sure ^{10}Be is in saturation and can be combined to study $^{14}C/^{10}Be$ production rate ratios. The selection of meteorites also depends on the amount of available material. In addition, we studied (chapter 5) CRE ages, pre-atmospheric size, and refined terrestrial ages of strewnfield meteorites from the Omani desert (Table 2.2). ^{14}C and ^{10}Be data for these meteorites are already published by Sliz et al. (2022). Five L chondrites from the Atacama Desert were investigated for terrestrial ^{14}C production (details in chapter 6).

Table 2.1. Recently fallen meteorites analyzed for ^{14}C, ^{10}Be and noble gas in this study.

Meteorite	Type	Fall	Country	TKW (kg)	Collection
SaU 606	H5	_1	Oman	0.136	NHM, Bern
Castalia	H5	1874	USA	7.3	WP, UniBern
Ehole	H5	1961	SW Africa	2.4	WP, UniBern
Farmville	H4	1934	USA	56	WP, UniBern
Ochansk	H4	1887	Russia	500	WP, UniBern
Al-Khadhaf	H4-5	2023	Oman	0.012	NHM, Bern
Mount Tazerzait	L5	1991	Niger	110	WP, UniBern
Boumdeid	L6	2011	Mauritania	3.6	WP, UniBern
Ausson	L5	1858	France	50	WP, UniBern
Kandahar	L6	1959	Afghanistan	0.299	WP, UniBern
Suizhou	L6	1986	China	260	WP, UniBern
Tennasilm	L4	1872	Estonia	28.5	WP, UniBern
Renchen	L5-6	2018	Germany	0.999	WP, UniBern
Antonin	L5	2021	Poland	0.35	WP, UniBern
Leedey	L6	1943	USA	51.5	WP, UniBern
Bensour	LL6	2002	Morocco	45	WP, UniBern
Stubenberg	LL6	2016	Germany	1.473	WP, UniBern
Sulagiri	LL6	2008	India	110	WP, UniBern
Kilabo	LL6	2002	Nigeria	19	WP, UniBern
Mangwendi	LL6	1934	Zimbabwe	22.3	WP, UniBern
Moshampa	LL5	2015	Iran	2.26	CEREGE

[1]SaU606 is not an observed fall. Collection indicates the locations from where the samples are obtained.
NHM Bern is the meteorite collection at National History Museum, Bern.
WP, UniBern is the meteorite collection at the Physics Institute, University of Bern.

Table 2.2. Strewnfield Meteorites studied for noble gas (chapter 5). Samples from NHM, Bern.

Meteorites	Field Nr.	Type	Location	TKW (kg)	References
JaH073	0201–640	L6	Al Wusta	650	Al-Kathiri et al. (2005)
JaH091	0210–11	L5	Al Wusta	4600	Al-Kathiri et al. (2005)
SaU001_243	0201–243	L4-5	Al Wusta	423	Sliz et al. (2022)
SaU001_04	0201–04	L4-5	Al Wusta	423	Sliz et al. (2022)
Shisr015_1942	0212–1942	L5	Zufar	3.41	Sliz et al. (2022)
Shisr015_165	0102–165	L5	Zufar	3.41	Sliz et al. (2022)
Shisr015_78	0301–78	L5	Zufar	3.41	Sliz et al. (2022)
Dhofar 005	0102–200	L6	Dhofar	125.5	Sliz et al. (2022)
SaU 163	0101–002	H5	Al Wusta	1.88	Al-Kathiri et al. (2005)
RaS 267	0801–005	LL6	Al Wusta	0.117	Zurfluh et al. (2016)

2.2. Sample Preparation for ^{14}C, ^{10}Be and Noble Gas Measurements

Sample preparation is highly important step in laboratory work. It ensures, *first*, that only the material of interest is separated and purified in a suitable form, and *second*, some of the material might be chemically processed before being analysed. The ordinary chondrites selected in this study are a mixture of common minerals, mostly silicates, and some metal in the form of iron-nickel alloys (FeNi). Terrestrial contamination such as carbonates and organic matter can significantly affect the final results. Consequently, a well performed sample preparation technique is the essential groundwork for further processing of samples. Sample preparation comprises of (i) fragmentation and milling, and (ii) chemical treatments.

2.2.1. *Physical treatment: Milling and grinding*

About 500–1000 mg of each meteorites sample was subjected to milling and grinding in Agate Mortar-Pester. Hammer was used to fragment larger material by placing sample in a seal bag to prevent any contact between hammer and sample. Small fragments were grinded, and the produced powdered samples were then sieved into different size fractions. Three sieves of <125 µm, 125–200 µm, and >200 µm sizes were used for grain size separation. The large grain sizes were mostly metal that were difficult to be grinded, were transferred to vial. The major portion was made of fine grained powdered (<125um) sample material, which were selected for further treatment and analysis. All the fractions were weighed and noted down. In addition to the fine-grained samples, I also leached some coarse-grained samples to check if there is any effect of grain size on the concentrations of radionuclides.

2.2.2. *Chemical Leaching*

The weights of the powdered samples selected for analysis were, first, noted down to track the changes or mass loss occurred during leaching. Chemical treatments were performed in following steps:

- Samples were then put into a glass crucible and 6.0M HCl was added to them until submerged. Stirred a little bit and left for about 45 minutes to make sure a good dissolution of carbonates.
- Second, sample solutions were then poured into a centrifuge tube and placed in the centrifugation system @ 4000 rpm for 4–5 min.
- The solvents from the samples were then poured out into waste container and MilliQ (18.2 MΩ cm @ 25 °C) was added to samples and centrifuged again for 2–3 times to make sure that there are no solvent/acid left in the samples.
- The cleaned samples were then kept for drying under UV lamp overnight.
- The dried samples were transferred to Teflon beakers and treated with Ethanol-amine-thioglycolate (EGTA) and kept for 48 hours to dissolve weathering products such as Fe-oxides and hydroxides.
- The samples were then centrifuged to remove the solution, cleaned with MilliQ water for 2–3 times, and dried under UV lamp until they were completely dry.
- Mass of leached samples were recorded, and the mass loss (%) due to leaching were calculated.

The leaching procedure essentially removes any carbonates and weathering products that are the likely sources of secondary terrestrial ^{14}C contamination, without affecting the original ^{14}C budget of meteorites. The changes in chemical composition of meteorites due to the chemical leaching are discussed in detail in chapter 4.

2.3. Preparation of ^{14}C Extraction Line at the Physics Institute, University of Bern

About 50 mg of leached samples powder were wrapped in pre-cleaned Al-foil of 3×3 cm^2 and loaded into the sample holder of the extraction line. Heating wires were placed around the sample holder and heated at 80 °C for 24 h, and subsequently pumped, in order to remove any condensed atmospheric gases, which might have introduced during opening and sample loading in the extraction line. The sample melting takes place in a platinum crucible, resting on glass shards, inside a glass crucible (Fig. 2.1). This crucible set-up was also heated in a

cyclic manner for few times to make sure it's clean, and there is no water molecules or atmospheric gases attached inside it. These heating cycles allow us to significantly lower the background blank level. Heating wires were also wrapped on some part of the extraction line and heated to 80 °C for 24 h to make sure no residual gas is attached in the inside wall of the stainless-steel tubes.

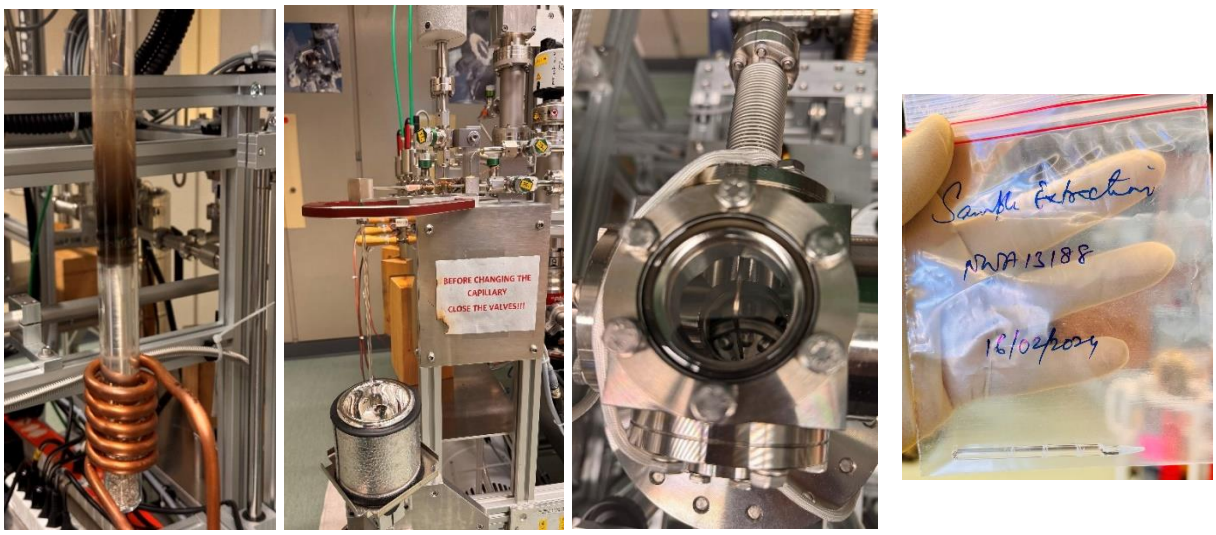

Fig. 2.1. Pictures of different constituent of ^{14}C extraction line at the Physics Institute, University of Bern. From left to right: crucible set-up, capillary for $^{14}CO_2$ collection, sample holder unit and prepared capillary to be introduced in gas-interface system of MICADAS-AMS..

2.3.1. *Sample Extraction in the ^{14}C Line*

The extraction process consists of four distinct stages:

- Pre-heating – The sample is pre-heated at 60.0 A (~500 °C) in an ultra-high purity (UHP) O_2 flow for 1 hour. This step removes residual adsorbed water and terrestrial contaminants. No gas is collected, all released gases are pumped away unless specifically required for contamination studies.
- Gas Extraction – The sample is heated at 121.0 A (~1600 °C) under an O_2 partial pressure of 30±5 mbar for 10 minutes. Released gas passes through a gas purification furnace (Carbolite-Gero®) before being collected in a liquid nitrogen-cooled helix.
- Gas Purification – The extracted gas undergoes further cleaning in a dedicated gas purification unit. Water is removed using a trap at -78 °C, while remaining contaminants are eliminated in a cold trap at -100 °C.
- Sample Collection – The purified CO_2 gas is collected in a glass capillary tube.

Schematic diagram of different components of the extraction line has been shown in Fig. 2.2. Depending on the required analysis, the sample may be: (i) directly collected, (ii) spiked with ^{14}C-free CO_2 gas, or (iii) diluted, with only a portion of the gas retained. For a reliable AMS measurement, the extracted CO_2 must contain at least 10 µg of carbon (µg C). A complete $^{14}CO_2$ extraction takes approximately 3 hours.

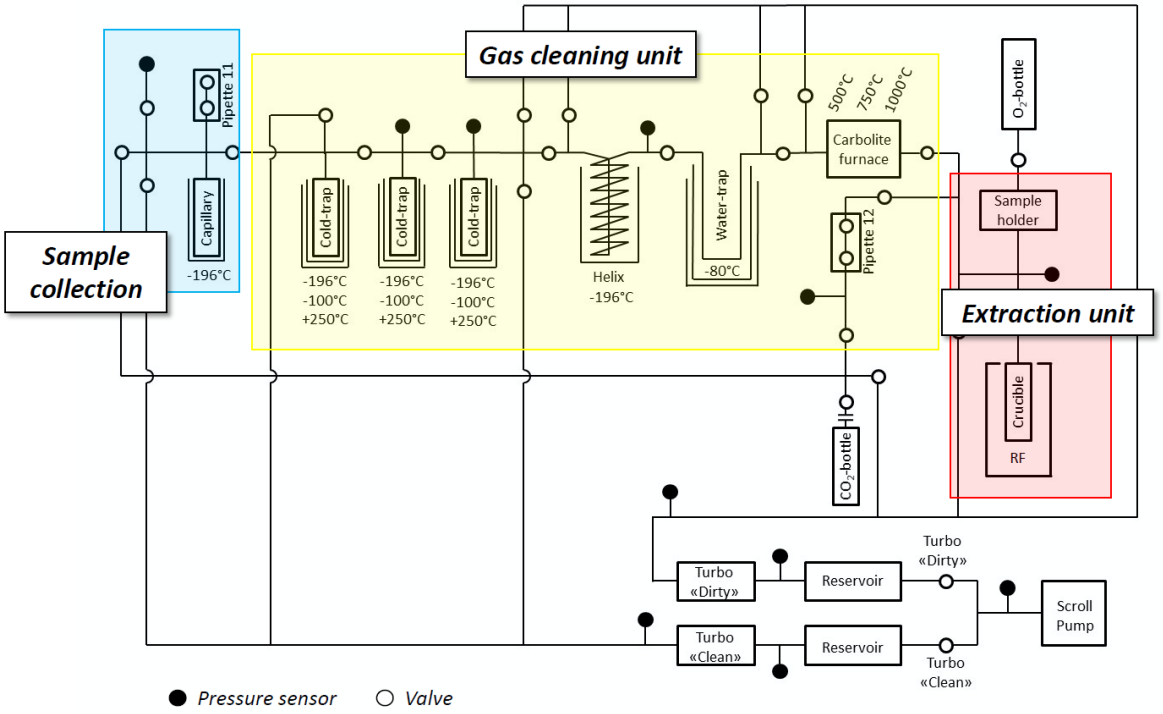

Fig. 2.2. Schematic diagram of the ^{14}C extraction line at the Physics Institute, University of Bern.

2.3.2. *Sequence of Measurements for one Meteorite*

To complete analysis of a single meteorite, a sequence of four measurements is required:

- Cylinder CO_2 Blank – A known amount of ^{14}C-free CO_2 gas (~1 cm³, measured using a pipette) is analysed. This system blank is used to assess the background level of ^{14}C in the system, which is particularly crucial after multiple meteorite aliquot measurements.
- Al-Foil Blank – Measurement of the Al foil used for wrapping samples. This helps determine the amount of ^{14}C extracted from the foil and serves as a blank correction for sample ^{14}C concentration.

- Sample Extraction – The primary measurement of the powdered, purified silicate separates from the meteorite, wrapped in Al foil, to determine its ^{14}C content.
- Sample Re-extraction – A second measurement of the same meteorite aliquot at a slightly higher temperature to extract any remaining ^{14}C. The data from both the sample extraction and re-extraction are combined to obtain the final ^{14}C activity concentrations.

2.4. Maintenance, Leak Testing and Calibration of the ^{14}C Extraction Line

Regular maintenance of the ^{14}C extraction line involves several essential tasks to ensure optimal performance. Routine activities include replacing the glass capillary used for sample collection, loading new samples in the sample holder, and applying heating wires to the sample holder after loading. Additionally, the Pt-crucible must be periodically cleaned and replaced as needed. I used to check the crucible after every 12–15 samples. In case of any damage or cracks, change the crucible otherwise cleaning and heating would be adequate for reuse of the crucible. Detailed protocols for these procedures are outlined in Sliz et al. (2020). External heating is a crucial aspect of maintaining the extraction line. Heat is applied to specific sections, such as the sample holder, the connection line between the oven and helix and the water trap, to remove any adsorbed gases. The cold fingers require degassing at 250 °C, although they are typically heated to 180 °C as standard condition. However, for samples with high carbon content, additional heating is recommended. The standard protocol for heating the sample holder can be adapted for other components as required.

Valves are susceptible to leaks after prolonged use or improper handling. To prevent damage to the washers at the connection, tightening the valve beyond 1.5 Torque is discouraged. If the pressure readings for the crucible, helix, or cold traps exceed 10^{-5} mbar, it may indicate a leak in the system. In such cases, leak testing should be performed with the assistance of technical staff. Sample measurements must always be conducted under standard vacuum pressure to ensure accurate results.

Calibration between the pipette and capillary is performed by taking a CO_2 shot into the pipette, which is then released and trapped in the capillary. This calibration can be conducted using either the short route (cold test) or the long route (hot test). The cold test involves direct transfer between the pipette and capillary, while the hot test requires transferring CO_2 to a hot crucible at extraction temperature, following the same procedure as a CO_2 blank measurement, except that the gas is not collected. Typically, a calibration factor of ~17 is observed between the

pipette and capillary volumes, regardless of the chosen route. Throughout this process, vacuum pressures and sensor readings must be continuously monitored before, during, and after gas collection to ensure accuracy and system integrity. The operator of the extraction line is responsible for performing these routine maintenance tasks. However, more complex procedures, such as servicing the vacuum system, are handled in coordination with the technical staff. A summary of material suppliers for equipment and required consumables is available in Appendix A.

2.5. ^{14}C Measurements at the MICADAS-AMS

The $^{14}C/^{12}C$ ratio analyses were conducted using the Mini Radiocarbon Dating System (MICADAS) at the Laboratory for the Analysis of Radiocarbon with AMS (LARA), part of the Oeschger Centre for Climate Change Research and the Department of Chemistry, Biochemistry, and Pharmaceutical Sciences at the University of Bern (Szidat et al., 2014). The extracted CO_2 gas, sealed in glass ampules, was introduced into the automated gas interface system (GIS) of the MICADAS, where the ampules were cracked open. In some cases, capillaries needed to be manually cracked using a hammer due to insufficient scratching of the glass capillaries. The released CO_2 was then mixed with helium gas and transported to the gas ion source for measurement.

A single cracker magazine holds eight capillaries, and typically two to three magazines are present in the lab to fill all the ampoules. Once the measurements are complete, these magazines are replaced. A typical batch of ampules submitted from our laboratory contained 16 to 24 samples. The maximum number of ampules I measured in a single day was 26, excluding four Oxa II standards and blanks. However, a best practice is to limit the measurements to a maximum of 24 ampules per day, allowing for the analysis of approximately six meteorite samples in a single batch. The ^{14}C results are reported as $F^{14}C$ (fraction modern carbon) values.

The MICADAS AMS system accounts for multiple sources of uncertainty, including counting statistics, blank subtraction, standard normalization, correction for isotope fractionation, and an additional 1.5‰ uncertainty to account for day-to-day variability in ^{14}C measurements (Szidat et al., 2014). As a result, the raw AMS data already incorporates a significant number of individual uncertainties, simplifying the calculation of ^{14}C activity concentrations and making the process more straightforward.

2.6. ^{10}Be Extraction and Sample Preparation at CEREGE, France

About ~200 mg aliquots of leached meteorite samples were brought over to the CEREGE Institute in Aix-en-Provence, France, for further chemical processing under the supervision of Dr. Jérôme Gattacceca and Dr. Régis Braucher. The established protocol for ^{10}Be extraction from meteorites was a modified version of the procedure typically used for terrestrial samples. This modification significantly streamlines the extraction process, allowing for complete sample preparation—including AMS target preparation—within 6 to 8 days, depending on the dissolution time in hydrofluoric acid (HF).

The final BeO targets were prepared with assistance from the *Laboratoire National des Nucléides Cosmogéniques* (LN2C; National Laboratory for Cosmogenic Nuclides) and subsequently submitted to the ASTER AMS facility (*Accélérateur pour les Sciences de la Terre*) in CEREGE, for ^{10}Be measurements.

The key steps in BeO preparation include:

- Sample Transfer & Spiking – Meteorite samples were transferred to Nalgene containers, and 300 μg of ^{10}Be spike was added.
- Silicate Dissolution – 10 mL of HF was introduced to dissolve the silicates over 48 hours on a shaker.
- Be Recovery – Following HF evaporation, acetylacetone ($C_5H_8O_2$) was used to recover Be, which was later combined with carbon tetrachloride (CCl_4) to extract the Be-bearing organic phase from the solution.
- BeO Formation – The extracted Be was converted to BeO powder by oxidation in a furnace at 800°C for one hour.

This refined protocol ensures efficient ^{10}Be extraction while maintaining high analytical precision for subsequent AMS measurements.

Targets of BeO powder for AMS measurements were prepared at the ASTER sample preparation laboratory in the following steps:

- Mixing of prepared BeO powder with niobium (Nb) powder – 1:1.5 volume ratio,
- Assembly of AMS cathodes,
- Pressing of powder mix into cathodes using a pressing machine – 2 GT for 30 sec.

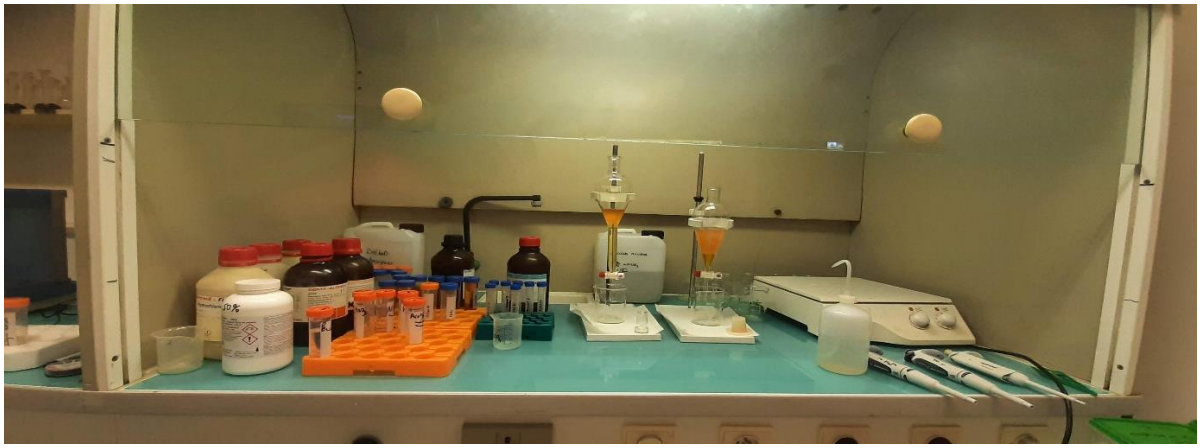

Fig. 2.3. Image displaying the setup for ^{10}Be extraction at CEREGE, France.

As part of this project a two week visit at the CEREGE Institute in February 2023 took place, where all samples were chemically processed (Fig. 2.3) and their BeO targets prepared. The batch comprised of 16 samples and a blank were submitted to ASTER AMS for Be measurements. The AMS data for the samples were received shortly afterwards. ^{10}Be activities were determined and combined with ^{14}C data to calculate ^{14}C/^{10}Be production rate ratios in the studied meteorites. During the single visit at the CEREGE Institute, following project objectives were achieved: (i) chemical extraction of Be from samples, (ii) completion of chemical processing and preparation of BeO powder, (iii) preparation of the AMS targets for ^{10}Be measurements. After the Be extraction, residual materials were subjected to X-ray diffraction (XRD) analysis. The results indicated the presence of fluoride salts but no remaining silicates, confirming that all Be was successfully extracted from the samples. This streamlined approach ensured efficient sample processing and high-precision AMS measurements for accurate production rate calculations.

2.7. ^{10}Be Measurements at ASTER-AMS Facility, CEREGE, France

The ^{10}Be/^{9}Be ratios were measured at the ASTER AMS facility in Aix-en-Provence, France. ASTER is a 5 MV Accelerator Mass Spectrometry (AMS) system, where ^{10}Be measurements are routinely conducted in a fully automated mode. The spectrometer is equipped with a sample wheel that holds up to 200 samples. To ensure stable operation, graphite targets are strategically placed within the wheel, acting as a buffer when the ion source is switched on or off and aiding in cleaning procedures (Arnold et al., 2010; Arnold et al., 2013). Additionally, three reference

targets of the NISTSRM4325 standard and one machine blank were included in each measurement sequence (Arnold et al., 2010). The remaining slots in the sample wheel are occupied by the unknown samples for analysis.

Similar to the ^{14}C AMS measurements, the raw ^{10}Be data incorporate multiple sources of uncertainty, including statistical error, standard uncertainty, instrumental variability (from the mean of standard measurements), and an additional systematic error of ~0.5% (Arnold et al., 2010). Consequently, the final calculated ^{10}Be activities account for all systematic and statistical uncertainties, ensuring accurate and precise results.

2.8. Noble Gas Line and Measurement of He, Ne and Ar Isotopes at the Physics Institute, University of Bern

The isotopic analysis of Helium (He), Neon (Ne), and Argon (Ar) followed well-established protocols for stony meteorites, as described in prior studies (e.g., Leya et al., 2013). ~20 mg of leached samples were carefully wrapped in Al-foil and loaded into the sample holder of the extraction line. To remove adsorbed atmospheric gases, the samples underwent vacuum heating at ~80 °C for up to 48 hours. This was followed by degassing in a molybdenum crucible, where the samples were held at 1750°C for 20 minutes. The released gases were purified using SAES® getters operated at temperatures between 180 °C and 450 °C, ensuring the removal of unwanted species. The He-Ne fraction was separated from the Ar fraction using activated charcoal maintained at liquid nitrogen temperature. The He-Ne fraction was then analysed using a small-volume static sector field mass spectrometer, custom-built in-house, at the Physics Institute, University of Bern. During the measurement process, additional purification was carried out using Ti getters to reduce H_2 contamination and activated charcoal at liquid nitrogen temperature to eliminate hydrocarbons and residual Ar, ensuring high-precision noble gas measurements.

The Ar fraction underwent additional purification using supplementary getters and was subsequently measured in a static noble gas tandem spectrometer, also designed and constructed at the University of Bern. This design aimed to minimize baseline variations resulting from scattered ions. Gas concentrations were calculated by comparing the peak height of the sample signal to signals from the established standards. Calibrations gas was routinely measured, which composed of known amounts of standard gases reflecting atmospheric isotopic compositions. Notably, Helium (He) exhibited an enrichment in ^{3}He relative to ^{4}He

compared to the terrestrial atmosphere. We systematically measured blanks both before and after samples extractions, with typical values in units of 10^{-12} cm^3STP. Our noble gas dataset was carefully corrected for potential interferences and instrument nonlinearities. The dataset includes comprehensive adjustments for uncertainties, such as blank corrections and standard measurements. These corrections account for a systematic uncertainty of 4% for gas amounts and 2% for isotope ratios, ensuring high accuracy in the results. Fig. 2.4 displays the noble gas line located at the Physics Institute, of University of Bern, where all the noble gas measurements took place.

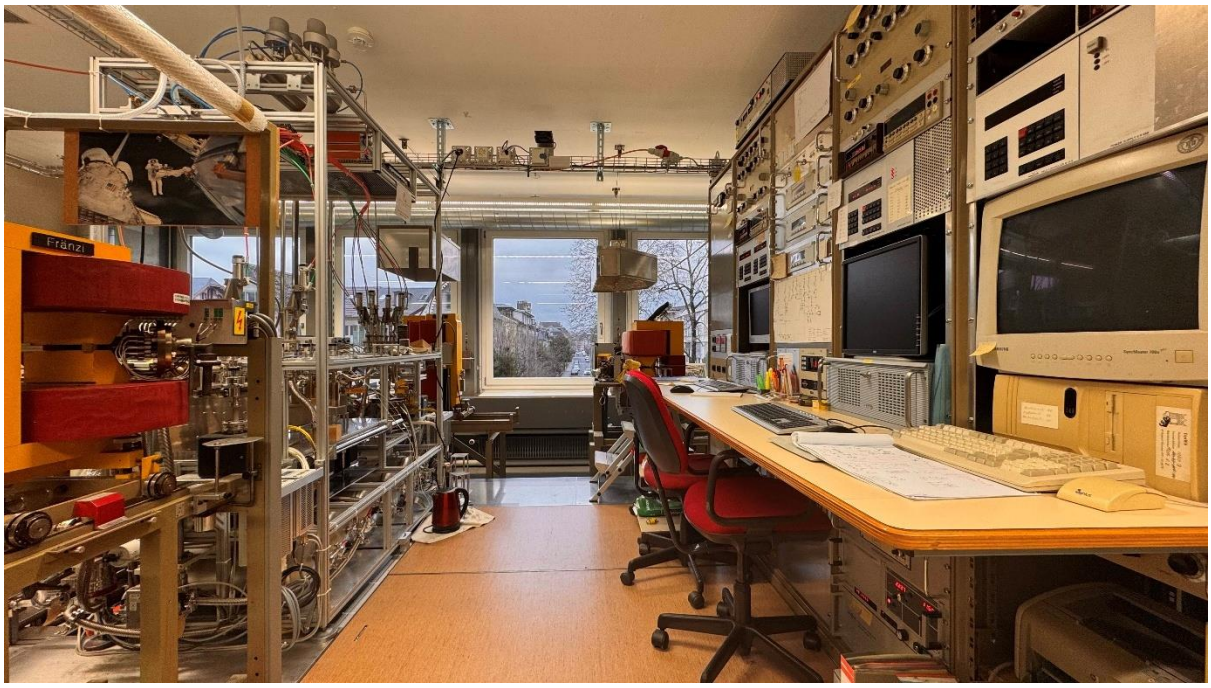

Fig. 2.4. Noble gas line at the Physics Institute, University of Bern.

Chapter 3

Preliminary study on Improving the ^{14}C and ^{14}C-^{10}Be Terrestrial Age Dating System for Meteorites: Model Calculations and experimental data

Based on article published in the ***Meteoritics & Planetary Science*** Journal. **https://doi.org/10.1111/maps.14144** published under **CC-BY-NC-ND** license.

Numbering of Title, tables and figures presented in this chapter are formatted to fit the layout of this thesis.

^{14}C and ^{14}C-^{10}Be terrestrial age dating system for meteorites – New data for four recently fallen meteorites

Mohammad Tauseef[1]*, Ingo Leya[1], Jérôme Gattacceca[2], Beda Hofmann[3], Sönke Szidat[4], Régis Braucher[2], Thomas Laemmel[4], ASTER Team[2]

[1]Space Research and Planetary Science, Physics Institute, University of Bern, Sidlerstrasse 5, 3012 Bern, Switzerland

[2]CNRS, Aix Marseille Univ, IRD, INRAE, CEREGE, Aix-en-Provence, France

[3]Natural History Museum Bern, Bernastrasse 15, 3005 Bern, Switzerland

[4]Department of Chemistry, Biochemistry and Pharmaceutical Sciences & Oeschger Center for Climate Change Research, University of Bern, Freiestrasse 3, 3012 Bern, Switzerland

***Corresponding author**. Email: mohammad.tauseef@unibe.ch

ABSTRACT

We perform a systematic and detailed study of the ^{14}C and ^{14}C-^{10}Be dating systems for meteorite terrestrial ages. Physical model calculations indicate that neither the ^{14}C production rates nor the $^{14}C/^{10}Be$ production rate ratios are constant enough to be reasonably approximated by average values. By using simple averages, one introduces a significant size dependent bias into the database for meteorite terrestrial ages. By combining modeled ^{14}C production rates and $^{14}C/^{10}Be$ production rate ratios with $(^{22}Ne/^{21}Ne)_{cos}$ ratios and assuming ~80% ablation losses, relatively easy to use correlations of ^{14}C production rates and $^{14}C/^{10}Be$ production rate ratios as a function of $(^{22}Ne/^{21}Ne)_{cos}$ are established. The new correlations enable to determined terrestrial ages much more accurate than ages based solely on average values for ^{14}C and/or $^{14}C/^{10}Be$. We validate the model predictions by measuring ^{14}C activity concentrations, $^{14}C/^{10}Be$ production rate ratios, $^{21}Ne_{cos}$ concentrations, and $(^{22}Ne/^{21}Ne)_{cos}$ ratios in four recently fallen meteorites: Mt. Tazerzait, Boumdeid (2011), Bensour, and SaU 606. The experimental data confirmed the model predictions, though the database is too scarce to be conclusive. More data from freshly fallen meteorites are needed for validating the model predictions, especially for validating them for different chondrite types.

3.1. Introduction

Terrestrial ages of meteorites, i.e., the time the meteorite spent on Earth before being found and collected, provide essential information for several highly relevant scientific questions. First, terrestrial ages are needed to better understand terrestrial weathering. For example, the conditions supporting or limiting meteorite preservations differ significantly among the different deserts. While meteorites found in the deserts of the Sultanate of Oman, North Africa, the United States, and Australia have average terrestrial ages in the range 30–50 ka (e.g., Al-Kathiri et al., 2005; Sliz et al., 2022; Jull, 1993; 2006), meteorites found in the Atacama Desert or in Antarctica can have terrestrial ages up to millions of years (e.g., Cassidy, 2003; Gattacceca et al., 2011, Drouard et al., 2019). Terrestrial ages are crucial data for comprehending and quantifying the processes involved in weathering. Second, correcting meteorite finds for pairing, i.e., for determining if two meteorites belong to the same object in space that broke up during atmospheric entry, is based, among other information, on terrestrial ages. Third, terrestrial ages are essential information to study the dynamics of small solar system bodies. In such studies, the ejection age, which is the sum of the cosmic ray exposure (CRE) age and the terrestrial age, is analysed for a large variety of meteorites. Though, in most cases the ejection age is very similar to the CRE age, i.e., the terrestrial age is short compared to the CRE age, there are meteorite classes with typically low CRE ages (lunar meteorites, carbonaceous chondrites) for which knowledge of the terrestrial age is crucial. A thorough study of ejection ages enables evaluating several parameters relevant for understanding the evolution and habitability of Earth. For example, asteroid/meteoroid impacts delivered most likely a large fraction of the Earth's volatile components (e.g., Marty, 2012; Marboeuf et al., 2014) and influenced the evolution of the Earth atmosphere (Schlichting et al., 2015). In addition, large asteroid impacts led to mass extinctions at the Cretaceous-Paleogene boundary (e.g., Alvarez et al., 1980; Hildebrand et al., 1991; Schulte et al., 2010) and possibly also at other times throughout geological history (e.g., Koeberl and Montanari, 2009; Schmieder et al., 2014). Finally, the accretion of asteroidal dust might even affect the Earth`s climate (e.g., Farley et al., 2006; Muller and MacDonald, 1997). Currently, however, the mechanisms responsible for the delivery of meteorites in the aftermath of an asteroid collision or break-up event are not understood well and CRE age histograms provide the ground truth against which the dynamical models must be tested. Closely connected, fourth, studies of the meteorite influx to Earth are all based on terrestrial ages. Relevant questions thereby are: Was the meteorite influx in a given area constant and/or was the composition of the meteorite flux variable over time? For example,

studies based on sediment dispersed meteorites demonstrate that before the Palaeozoic (550–250 Ma ago), the flux of LL chondrites relative to other chondrite groups was larger than today. Data also indicate that in the Ordovician, i.e., before 466 Ma, primitive achondrites had a similar or higher abundance than ordinary chondrites (e.g., Heck et al., 2017; Schmitz et al., 2017; Schmitz et al., 2019a, b). In addition, a recent study indicates that there might have been a change in the composition of the meteorite flux with a higher (compared to recent falls) abundance of H chondrites between 1–0.5 million years ago (Drouard et al., 2019).

For stony meteorites, terrestrial ages are often determined using the ^{14}C and/or ^{14}C-^{10}Be dating systems (see below). Carbon-14 and ^{14}C-^{10}Be terrestrial age dating has also been applied to mesosiderites (Jull et al., 2009) and iron meteorites (Schnitzer et al., 2012). However, despite the immense potential of this dating system and the importance of the data, there are currently only three laboratories world-wide performing such studies; the University of Arizona, USA (e.g., Jull et al., 2013), the Nagoya University, Japan (Minami et al., 2006), and our group at the University of Bern (Mészáros et al., 2018; Sliz et al., 2019,2022).

Due to analytical challenges, the ^{14}C terrestrial ages are very often not as precise and reliable as one would like them to be considering the importance of the data. For example, for calculating ^{14}C terrestrial ages, the ^{14}C saturation activity concentration at the time of fall must be known. Note that saturation activities at the time of fall, i.e., the activity concentration for a radionuclide that reached saturation during irradiation and that has not yet started to decay after the irradiation ended, i.e., after the meteorite fell on Earth, are equal to production rates, i.e., the rate of a nuclide produced per unit of mass and time during irradiation in space. In the following, we use the term saturation activity and production rate synonymic. For practical applications, constant (average) ^{14}C saturation activities of 46 ± 1.0 dpm/kg, 51.1 ± 1.0 dpm/kg, and 55.2 ± 1.0 dpm/kg are used for H, L, and LL chondrites, respectively (e.g., Jull et al., 1998). The ^{14}C production rates significantly depend on shielding, which is usually not known for the studied samples. Consequently, using average values can result in a significant over- and sometimes also in a slight underestimation of the true terrestrial age.

Starting the discussion with H chondrites, Jull et al. (1989) measured for the two H chondrite falls Richardton and Nuevo Mercurino ^{14}C activity concentrations of 34.6 ± 0.8 and 35.3 ± 0.4 dpm/kg, i.e., up to 20% lower than the recommended value of 46 ± 1.0 dpm/kg. For the H6 chondrite Torino, Wieler et al. (1996) measured a ^{14}C activity concentration of 42.2 ± 2.1 dpm/kg. According to their study, Torino had a complex exposure history; the pre-atmospheric radius of the final meteorite was likely in the range of 20 cm and the second stage exposure

time was long enough that ^{14}C reached saturation (see also Herzog et al., 1991). Recently, Jull et al. (2009) measured a ^{14}C activity concentration for the H4–5 chondrite fall Carancas of 56.9 ± 1.5 dpm/kg, i.e., much higher than other published values and much higher than the recommended average. Vogt et al. (1993) measured for the Bur Gheluai H5 chondrite fall ^{14}C activity concentrations between 37.7 dpm/kg and 53.1 dpm/kg, i.e., the data vary by ~30%. Even larger variations were detected by Leya et al. (2001) for the H5 chondrite fall St-Robert, for which the authors determined ^{14}C activity concentrations ranging from 49 ± 12 to 75 ± 4 dpm/kg, i.e., the values vary by ~50%. To summarize, the published ^{14}C saturation activities for H chondrite falls range from 34.6 dpm/kg to 75 ± 4 dpm/kg, i.e., they vary by more than a factor of 2. The average ^{14}Csaturation activity considering all data is 51 ± 12, which agree with the typically used value of 46 ± 1.0 dpm/kg (e.g., Jull et al., 1998) only due to the large (1σ) standard deviation. However, the large standard deviation renders the average value essentially useless for calculating terrestrial ages.

The ^{14}C saturation activities found in literature for L chondrites range between 44 ± 1 dpm/kg and 60.1 ± 0.9 dpm/kg, i.e., they vary by more than 35% (see Minami et al., 2006 for references). The average ^{14}C saturation activity is 53.5 ± 4.4 dpm/kg, i.e., reasonably close to the typically used value of 51.1 ± 1.0 dpm/kg (e.g., Jull et al., 1998), but with a much higher uncertainty. To our knowledge, there is so far no measurement of ^{14}C saturation activities for LL chondrites.

To summarize, the data so far indicate that there is a large spread in published ^{14}C saturation activities. This finding is supported by earlier model calculations that also indicate a significant depth and size dependency of the ^{14}C production rates. For example, Wieler et al. (1996) predicted ^{14}C production rates ranging from ~12 dpm/kg for surface samples of small meteorites to ~52 dpm/kg for shielded samples in objects with pre-atmospheric radii in the range of 45 cm.

To overcome the problem of variable ^{14}C production rates, $^{14}C/^{10}Be$ ratios can be used instead; the ^{10}Be data serve as a proxy for the shielding dependence of the ^{14}C production rates. The $^{14}C/^{10}Be$ production rate ratios are supposed to be less shielding dependent than ^{14}C production rates, making $^{14}C/^{10}Be$ ages more reliable than ^{14}C ages. However, the $^{14}C/^{10}Be$ production rate ratio and its dependence on shielding is not well constrained. In literature, one often finds an average $^{14}C/^{10}Be$ production rate ratio of 2.5 ± 0.1, whereas it is difficult to find the proper references and/or the underlying data. For example, for calculating the terrestrial age of the Gold Basin strewn field, Kring et al. (1991) used the ratio of 2.5 ± 0.1, giving Jull et al. (1990)

as a reference. However, in their study of meteorites from western Libya, there is no mentioning of a $^{14}C/^{10}Be$ production rate ratio. The other reference often given, Welten et al. (2001), used a $^{14}C/^{10}Be$ production rate ratio of 2.65 ± 0.20 with a reference to Jull et al. (2000). In the latter study, the author has used data from few irradiation experiments and from recently fallen meteorites (e.g., Jull et al., 1994). The actual data, however, indicate that the $^{14}C/^{10}Be$ production rate ratio scatter around 2.5 but with a spread of larger than 0.1. As an example, the data for Knyahinya gives a $^{14}C/^{10}Be$ production rate ratio of 2.1 (Jull et al., 1994), i.e., lower than the recommended average. In contrast, the $^{14}C/^{10}Be$ production rate ratio for the H chondrite Carancas is 3.3 ± 0.1 (Jull et al., 2009), i.e., significantly higher than the average value. Even worse, the $^{14}C/^{10}Be$ production rate ratios for St-Robert (H5) vary from 2.3 to 3.7, i.e., they vary by more than 60% (Leya et al., 2001). This variation is for samples from the very same meteorite, clearly contradicting the basic assumption that $^{14}C/^{10}Be$ production rate ratios are constant or at least relatively constant. The large spread is confirmed in a more systematic study, in which Jull et al. (2001) studied the dependence of $^{14}C/^{10}Be$ production rate ratios on meteoroid size and shielding. Based on model calculations, the authors found ratios between 1.2 at the surface of small meteoroids and 3.0 for deeper samples in larger meteoroids. However, the $^{14}C/^{10}Be$ ratio in meteoroids with pre-atmospheric sizes in the range 25–100 cm, which is a very common size for chondrites, indeed scatter around 2.5, but with a spread much larger than the very often used 0.1.

To summarize, neither the ^{14}C production rates nor the $^{14}C/^{10}Be$ production rate ratios are constant enough to enable accurate and reliable terrestrial age dating using only average values. In addition, the average values are not well constrained. We therefore started a systematic study to better understand and quantify ^{14}C production rates and $^{14}C/^{10}Be$ production rate ratios and especially their dependence on meteorite size and shielding. Doing so, we use new model calculations, and we will validate the model predictions with new experimental data for recently fallen meteorites. In addition to ^{14}C and ^{10}Be activity concentrations we also add the cosmogenic noble gases $^{21}Ne_{cos}$ and the well-known shielding indicator $(^{22}Ne/^{21}Ne)_{cos}$ to the dating system. In doing so, $(^{22}Ne/^{21}Ne)_{cos}$ is used for additional shielding corrections and $^{21}Ne_{cos}$ is used to check if ^{10}Be is in saturation. Here we will present in some detail the model predictions and first experimental data. A more extensive database for H, L, and LL chondrites will be published in a follow-up study.

3.2. New Model Calculations

The model is similar as described earlier (Leya et al., 2021). Briefly, the model is based on the particle spectra for primary and secondary particles and the cross sections for the relevant nuclear reactions. The new version of the model calculations (labelled version V03) benefits from some major improvements compared to earlier approaches. *First*, the particle spectra are calculated using the Geant4 toolkit (e.g., Agostinelli et al., 2003), which provides a comprehensive set of models covering all physical processes important for nuclear interactions and transport over a wide energy range, i.e., from a few MeV for neutrons up to TeV for all particles. We use Geant4 to routinely and reliably calculate particle spectra for meteoroids (spherical and elliptical), planetary surfaces, and planetary atmospheres (including magnetic fields). For the calculation, we use the physics list "FTFP_INCLXX_HP". In this set-up, INCL is used to treat nucleons, i.e., protons and neutrons, between 1 MeV and 20 GeV and heavy ions, e.g., ^{4}He-particles, between 0 and 3 GeV/nucleon. Importantly, the current version of INCL can reliably handle α-induced reactions and is also able to properly treat the emission of light charged ejectiles up to mass number A = 8 (Mancusi et al. 2014). Connected to this comes the *second* improvement; the new model generation is the first ever able to fully include primary and secondary galactic α-particles. *Third*, all relevant cross sections have been adjusted according to recent changes in AMS standards and/or half-lives. *Fourth*, the new model gives, for the first time, uncertainties. For more information, see Leya et al. (2021).

Using the new model calculations, we calculated ^{10}Be and ^{14}C production rates for various types of meteorites and for the Apollo 15 and Apollo 17 drill cores. For the meteorites we consider pre-atmospheric radii between 4 cm and 500 cm and for the Apollo 15 and 17 drill cores we calculated production rates down to a depth of ~450 g/cm^2, using a density of 1.76 g/cm^3 and 1.83 g/cm^3 for Apollo 15 and Apollo 17, respectively. In addition, we calculated ^{21}Ne production rates and $(^{22}Ne/^{21}Ne)_{cos}$ ratios. The modeling results are combined to test and improve the basics of the ^{14}C and $^{14}C/^{10}$Be dating system for meteorite terrestrial ages.

Before doing so, we first need to prove that the model can accurately calculate ^{14}C and ^{10}Be production rates. Fig. 3.1 depicts modeled and experimental ^{10}Be and ^{14}C data from the L/LL5 chondrite Knyahinya (upper row) and the Apollo 15 and Apollo 17 drill cores (lower row). We start discussing the data for Knyahinya first. The ^{10}Be data are from Graf et al. (1990) and the ^{14}C data are from Jull et al. (1994). The results of the model calculations are shown by the solid black line together with the 1σ uncertainties indicated by the gray area. There are some important findings. First, the model predictions accurately describe the experimental data. The

agreement is within the uncertainties. Second, the uncertainties of the model calculations increase from the surface towards the centre. This is understandable considering that for both nuclides, contributions from secondary neutrons increase from the surface towards the centre and such contributions are more uncertain due to less well-known neutron cross sections. To summarize, the model is well capable of calculating ^{10}Be and ^{14}C production rates, at least in the L/LL chondrite Knyahinya. Next, we can demonstrate that the model is able to accurately describe ^{10}Be and ^{14}C in larger objects by comparing model predictions and experimental data for Apollo drill cores (Fig. 3.1, lower row).

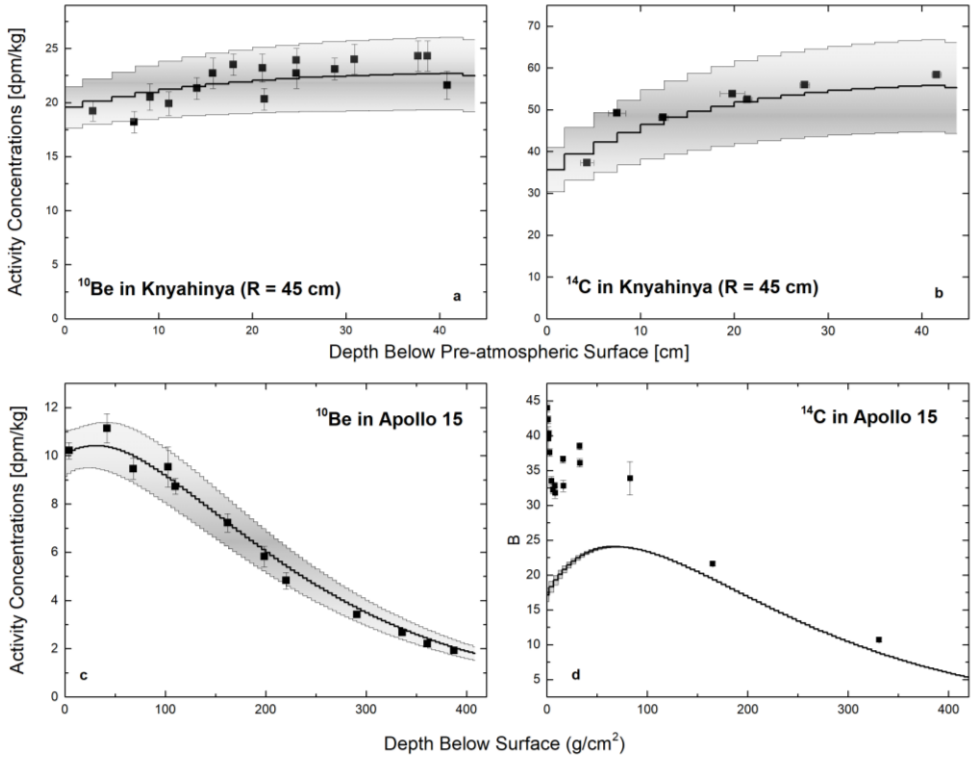

Fig. 3.1. ^{10}Be and ^{14}C depth profiles for the L/LL chondrite Knyahinya (upper row) and the Apollo 15 drill core (lower row). The experimental data are from Graf et al. (1990) (^{10}Be in Knyahinya), Jull et al. (1994) (^{14}C in Knyahinya), Nishiizumi et al. (1984) (^{10}Be in Apollo 15), and Jull et al. (1998) (^{14}C in Apollo 15). The solid black lines are the results from physical model calculations and the grey area gives 1σ uncertainties for the model predictions. The first few cm of the Apollo 15 drill core samples are affected by contributions from solar cosmic rays.

The ^{10}Be data for the Apollo 15 drill core are from Nishiizumi et al. (1984). The agreement for ^{10}Be is very good, all experimental data plot within the 1σ-uncertainty envelope. The comparison is more difficult for ^{14}C because the experimental database is scarce. In addition, in the only existing database (e.g., Jull et al., 1998) most of the samples are from close to the

surface, hence, they are affected by solar cosmic ray (SCR) produced ^{14}C and are therefore not suitable for such a validation. This leaves only the two data at 165 g/cm^2 and 331 g/cm^2 for a comparison. The model predictions are slightly too low by about 10–15%, a discrepancy that has also been observed with earlier models (e.g., Jull et al., 1998). A possible explanation for too low model predictions could be a lower solar activity, i.e., a lower solar magnetic field, during the last few tens of ka compared to the solar activity during the last few Ma. For example, assuming a solar modulation of M = 550 MV instead of M = 650 MV, i.e., a lower solar magnetic field and consequently a higher GCR flux reaching the Moon, would bring model and experimental data into agreement. However, this is somewhat speculative, and more data are needed to proof or reject this hypothesis. Anyway, these minor discrepancies are of little consequence for our study.

3.3. Production Rates for ^{14}C

Fig. 3.2 depicts the modeled ^{14}C production rates for L chondrites with pre-atmospheric radii between 4 cm and 100 cm. For all objects with radii less or equal 80 cm, there is an increase in ^{14}C production rates with increasing shielding depth. This increase becomes larger with increasing radius; it is a factor of 1.28 for 10 cm objects and a factor of 1.55 for 80 cm objects. In addition, there is a strong dependence of the ^{14}C production rates on the pre-atmospheric radius. For example, the production rate at the centre of a 10 cm object is 31.2 dpm/kg and for a 45 cm object it is 54.8 dpm/kg, i.e., there is an increase of more than a factor of 1.75. Consequently, the model predictions clearly demonstrate that the ^{14}C production rates not only depend on the shielding depth but also on the pre-atmospheric size of the meteorite. From the data in Fig. 3.2, it is obvious that giving one average ^{14}C production rate that it applicable to all L chondrites is impossible. Depending on size and shielding, there would be either a significant over- or underestimation of the (real) ^{14}C production rate. This is made clear by the horizontal line at a ^{14}C production rate of 51.1 ± 1.0 dpm/kg, which is the average ratio very often used for calculating ^{14}C terrestrial ages for L chondrites (e.g., Jull et al., 1998). Considering the entire range of modeled data, which is from 21.7 dpm/kg to 55.2 dpm/kg, the deviation from the assumed average can reach a factor of 2.3. The consequences for the terrestrial ages are discussed below.

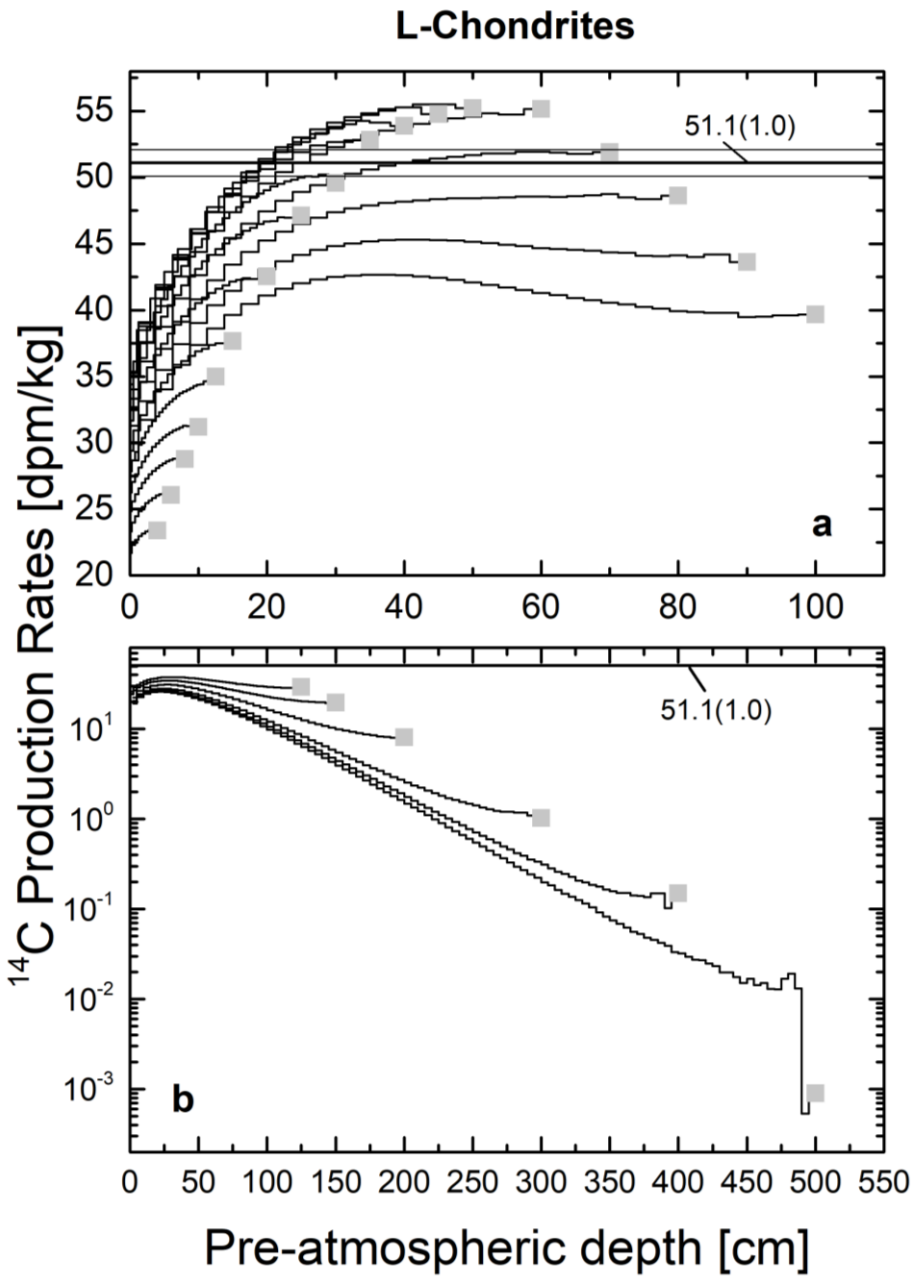

Fig. 3.2. Modeled ^{14}C production rates as a function of depth below the surface for L chondrites with pre-atmospheric radii between 4 cm and 100 cm (panel a) and with pre-atmospheric radii between 125 cm and 500 cm (panel b). Also shown is the average ^{14}C production rate of 51.1 ± 1.0 dpm/kg often used for ^{14}C terrestrial age dating of L chondrites.

Using the average ^{14}C production rate of 51.1 dpm/kg is a better match for objects in the radius range 20–90 cm than it is for smaller or larger objects. Therefore, using an average production rate produces a size-dependent bias into the terrestrial age database. Due to this bias, the terrestrial ages for smaller meteorites are systematically too old, which seriously compromises the interpretation of terrestrial age distribution because some samples might not necessarily be old but simply originate from smaller objects. To elaborate on this size-dependent bias, we

calculated the deviation of the modeled production rate from the normally used average value as a function of meteorite size. For the calculation, we consider only the innermost 58% of each radius. Ignoring the outermost layer accounts for the typically ~80% ablation losses during atmospheric entry (in mass). Doing so, we simply assume that atmospheric entry homogeneously reduces the radius. The thus produced data is shown in Fig. 3.3 as the ratio of average production rate (51.1 dpm/kg) divided by the modeled production rates as a function of pre-atmospheric radius.

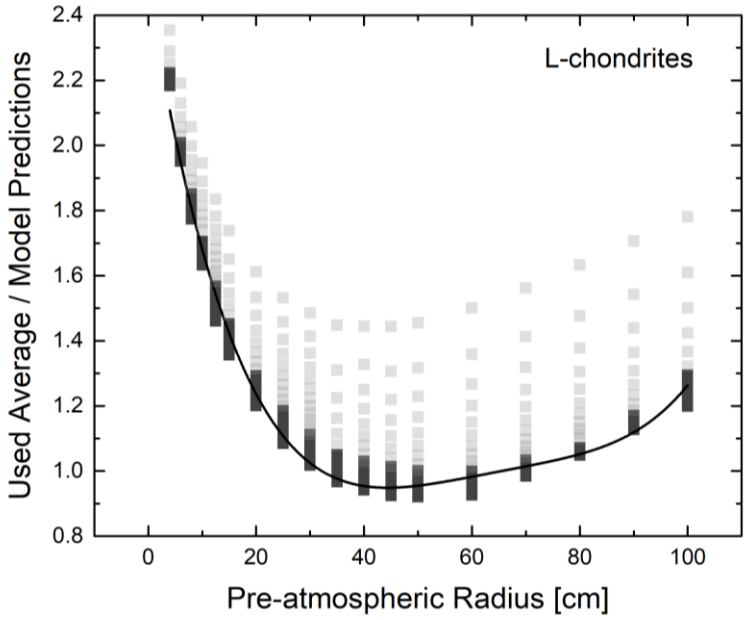

Fig. 3.3. Ratio of used average ^{14}C production rate relative to the model predictions as a function of pre-atmospheric radius of the meteoroid. For modeling 80% ablation losses are assumed, i.e., only the innermost 58% of the meteoroid is considered. The dark gray bars shown for each radius indicate the shielding dependence of the ratios for a given meteoroid radius. The light gray symbols show the data for the outermost 42% of radius, i.e., for the outermost 40% of mass. The solid black line is a best fit through the data (considering ablation).

Since the ratios are shielding dependent, there are more data for each radius. The best fit line through the data is given by (solid black line):

$$Ratio = 2.474 - 0.1011 \times R + 0.00242 \times R^2 - 2.503 \times 10^{-5} \times R^3 + 9.696 \times 10^{-8} \times R^4 \qquad \textbf{(eq. 3.1)}$$

with R the pre-atmospheric radius of the meteorite (cm). The ratio between the normally assumed average production rate ratio and the modeled values can be translated into age differences. Using the equations for the radioactive decay enables calculating the ratio of terrestrial ages T_{true}, i.e., the age calculated using the true production rate $P_{14}(true)$, relative to

the terrestrial age T_{av} calculated using the average production rate $P_{14}(av)$. The obtained equation is:

$$\frac{T_{true}}{T_{av}} = 1 - \frac{ln\left(\frac{P_{14}(true)}{P_{14}(av)}\right)}{ln\left(\frac{A\left(^{14}C\right)}{P_{14}(av)}\right)} \qquad \textbf{(eq. 3.2)}$$

with $P_{14}(av)$ the average production rate (e.g., 51.1 dpm/kg for L chondrites), $P_{14}(true)$ the true production rate for ^{14}C fully considering radius and shielding dependence, and $A(^{14}C)$ the measured ^{14}C activity concentration. As an example, by assuming a measured ^{14}C activity of 25 dpm/kg and by using the average ^{14}C production rate of 51.1 dpm/kg, we calculate a terrestrial age of ~5910 years. This age is only close, i.e., to within 10%, to the "true" terrestrial age for meteoroids in the size range 25–100 cm. If the sample would originate from a small meteorite, i.e., a 10 cm object, the real terrestrial age would only be ~1620 years, i.e., significantly shorter. The relative differences become smaller for lower measured ^{14}C activities. For example, assuming a ^{14}C activity of 5 dpm/kg gives a nominal age (calculated using the average production rate) of ~19,200 years. If the sample originated from a small meteoroid (again assuming 10 cm), the age would be in the range ~14,920 years, i.e., significantly lower. These examples already demonstrate that using one average value for the ^{14}C production rates introduces a bias into the calculated terrestrial ages. Ages from small meteorites are overestimated and depending on the measured ^{14}C activity concentration, this overestimation can be significant.

3.4. ^{14}C/^{10}Be Production Rate Ratios

To circumvent the problem of the radius and shielding dependence of the ^{14}C production rates, the ^{14}C/^{10}Be production rate ratio is often used for calculating so-called ^{14}C-^{10}Be terrestrial ages. However, it has already been shown by Jull et al. (2001) that the ^{14}C/^{10}Be production rate ratio is not as constant as it should be for reliable terrestrial age determination. Using model calculations similar to ours and studying L chondrites with radii between 10 cm and 1000 cm, these authors calculated ^{14}C/^{10}Be production rates ratios in the range ~1.2 at the surface of small meteoroids, and up to ~3.0 for samples at larger shielding depths in larger meteoroids. They conclude, that for meteoroids in the size range 25–100 cm the ^{14}C/^{10}Be ratios scatter around 2.5 but with a spread much larger than 0.1. Their results are confirmed by our new model. Fig. 3.4 (upper panel) depicts the modeled ^{14}C/^{10}Be production rate ratios as a function of ^{10}Be production rates for H chondrites with pre-atmospheric radii between 4 cm and 100

cm. For modeling, we again assume 80% ablation losses, i.e., we only consider the innermost 58% of the radius. In contrast to the earlier model, we also give uncertainties (shown by the light gray error bars). For producing the diagram shown in Fig. 3.4 (lower panel), we calculated mass weighted averages for each meteoroid, i.e., we used the masses of the individual spherical shell as weights. Doing so, we produce one data point for each meteoroid (shown by the solid black symbols with error bars). Fig. 3.4 (lower panel) depicts the thus calculated averages for meteoroids with pre-atmospheric radii between 4 cm and 500 cm. The red line is a best fit through the data.

$$\frac{^{14}C}{^{10}Be} = \begin{cases} a - b \times P\left(^{10}Be\right)^{c} \text{ for } R \geq 35\ cm \\ f + g \times P\left(^{10}Be\right) \text{ for } R < 35\ cm \end{cases} \qquad \textbf{(eq. 3.3)}$$

Table 3.1. Parameters for the two fit functions describing the relationship of $^{14}C/^{10}Be$ production rate ratios as a function of ^{10}Be production rates (eqn. 3.3).

Meteorite Type	***a***	***b***	***c***	***f***	***g***
H Chondrite	2.80 ± 0.01	$7.73\times10^{-10} \pm 2.11\times10^{-9}$	6.72 ± 0.91	-2.54 ± 0.23	0.229 ± 0.013
L Chondrite	2.82 ± 0.01	$3.71\times10^{-10} \pm 1.08\times10^{-9}$	6.76 ± 0.95	-3.00 ± 1.44	0.237 ± 0.008
LL Chondrite	2.80 ± 0.01	$3.12\times10^{-10} \pm 9.98\times10^{-11}$	7.50 ± 1.03	-2.90 ± 0.09	0.228 ± 0.005

Valid for all radii from 4 cm to 500 cm.
For determining the fit function, 80% ablation losses are assumed

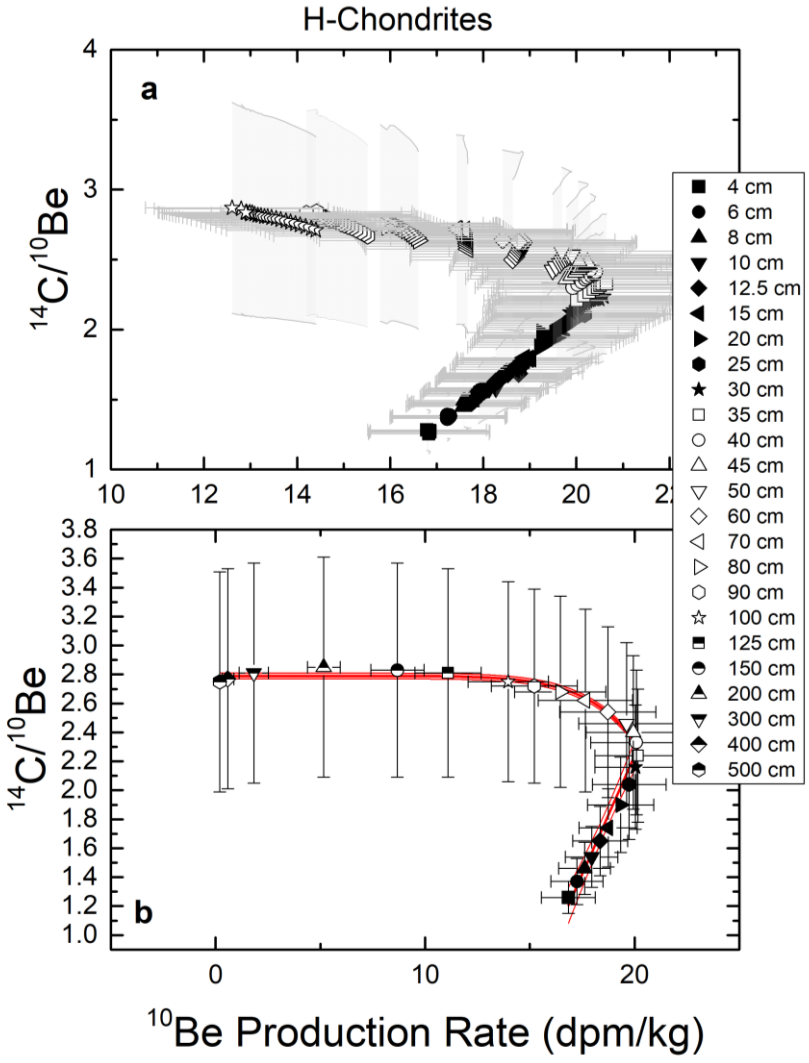

Fig. 3.4. $^{14}C/^{10}Be$ production rate ratios as a function of ^{10}Be production rates for H chondrites. (a) depicts the data for meteorites with pre-atmospheric radii less or equal 100 cm. The data are for various shielding depths assuming 80% ablation losses, i.e., only considering the innermost 58% of the radius. The different symbols shown for each radius indicate the data for different shielding depths. (b) depicts the data but using weighted averages and considering all meteorites with pre-atmospheric radii less or equal 500 cm. As weights, the mass for each spherical shell was used. The red line shows the best-fit line through the data.

The values for *a*, *b*, *c*, *f*, and *g* for H, L, and LL chondrites are given in Table 3.1. Note that the values for the fit depend only very little on the assumption of 80% ablation losses. Considering all data and not calculating weighted averages would give correlations less than 10% different from the ones shown in Fig. 3.4 (lower panel). The $^{14}C/^{10}Be$ ratio is relatively constant for a large range of ^{10}Be production rates. For example, for meteoroids with radii larger than ~40 cm, the average $^{14}C/^{10}Be$ production rate ratio is relatively constant at 2.53 ± 0.21, 2.56 ± 0.23, and 2.55 ± 0.23 for H, L, and LL chondrites respectively. However, the difficulty arises from the fact that the relationship between ^{10}Be production rates and $^{14}C/^{10}Be$ ratios is surjective,

i.e., there is not a one-to-one relationship, and for some ^{10}Be data there is more than one ^{14}C/^{10}Be ratio possible. As an example, for a ^{10}Be production rate of 17.5 dpm/kg, which is possible either in a 10 cm meteorite or in a 60 cm object, the ^{14}C/^{10}Be production rate ratios can be either 1.4 for small objects or 2.7 for larger objects (see Fig. 3.4). To be more quantitative, assuming a measured ^{14}C/^{10}Be ratio of 1, 0.5, or 0.1 and a ^{14}C/^{10}Be production rate ratio of 2.7 (large object) gives terrestrial ages of 8.2 ka, 13.9 ka, and 27.2 ka, respectively. In contrast, assuming a ^{14}C/^{10}Be production rate ratio of 1.4 (small object) gives terrestrial ages of 2.8 ka, 8.5 ka, and 21.8 ka, respectively. Therefore, for small measured ^{14}C/^{10}Be ratios, the terrestrial ages can differ substantially depending on whether the sample is from a small or a large meteoroid. For the case ^{14}C/^{10}Be = 0.1, the differences are more than a factor of 3. Consequently, using simply one average ^{14}C/^{10}Be production rate ratio for all meteorites produces a significant size dependent bias into the terrestrial age database. Though, the ^{14}C/^{10}Be dating system is more robust than ^{14}C dating because the ^{14}C/^{10}Be production rate ratio is constant over a larger range of meteorites sizes than the ^{14}C production rate, it can nevertheless produce some seriously wrong ages and should therefore not be applied without further knowledge of the meteorite size.

To summarize, even though terrestrial ages for meteorites are highly relevant data for many applications and scientific questions, neither the ^{14}C production rates nor the ^{14}C/^{10}Be production rate ratios are well enough constrained for precise and reliable terrestrial age determinations.

3.5. Quantifying the Shielding Dependence of ^{14}C Production Rates

Fig. 3.5 depicts ^{14}C production rates as a function of cosmogenic (^{22}Ne/^{21}Ne)$_{cos}$ for L chondrites with pre-atmospheric radii of less than 90 cm. For producing the diagram, we again assume 80% ablation loses.

The relationship between ^{14}C production rates and (^{22}Ne/^{21}Ne)$_{cos}$ is bijective, i.e., for each (^{22}Ne/^{21}Ne)$_{cos}$ ratio there is only one ^{14}C production rate. The relationship is given by:

$$P(^{14}C) = \left(b \times \left({}^{22}Ne/_{21}Ne\right)_{cos} - a\right)^{-1} \left[\frac{dpm}{kg}\right] \qquad \textbf{(eq. 3.4)}$$

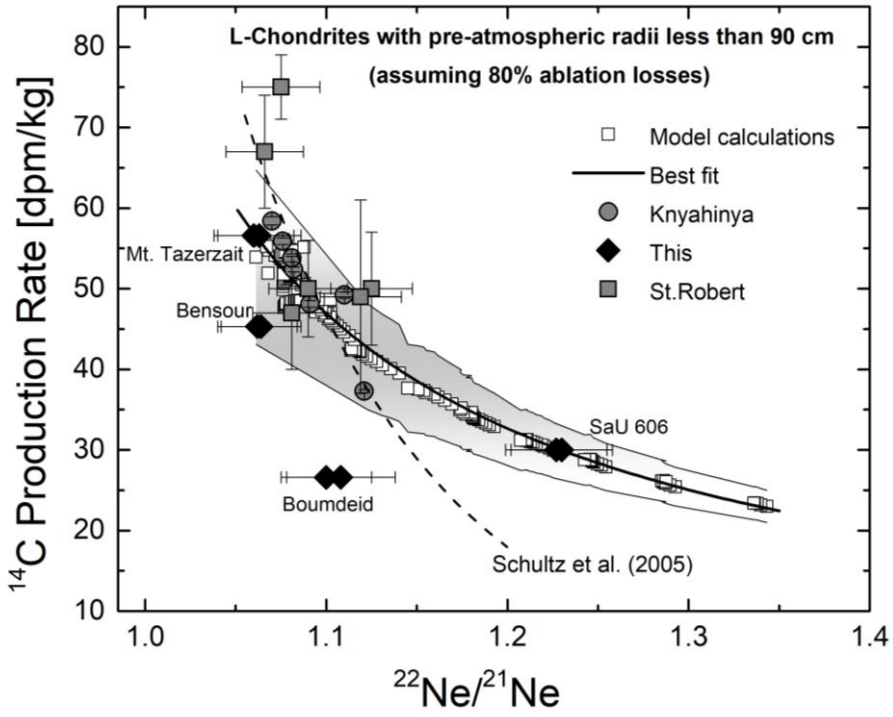

Fig. 3.5. ^{14}C production rates as a function of $(^{22}Ne/^{21}Ne)_{cos}$. The model calculations for L chondrites with radii between 4 cm and 90 cm are shown by the open squares. The gray area gives the 1σ standard deviation for the model calculations. The dashed line is the correlation given by Schultz et al. (2005). Also shown are experimental data for Knyahinya (Jull et al., 1994; Graf et al., 1990), St. Robert (Leya et al., 2001), and for the four meteorites studied here.

The parameters for H chondrites are $b = 0.099 \pm 0.001$ and $a = 0.084 \pm 0.001$. For L chondrites: $b = 0.093 \pm 0.001$ and $a = 0.081 \pm 0.001$, and for LL chondrites: $b = 0.091 \pm 0.001$ and $a = 0.079 \pm 0.001$. In addition to the model prediction (open symbols) and the best line (solid black line), Fig. 3.5 also shows experimental data for the L chondrite Knyahinya and for the four meteorites studied by us; Mt. Tazerzait, Bensour, Boumdeid (2011), and SaU 606. The experimental data are discussed in detail below.

In summary, the relationship of ^{14}C production rates as a function of $(^{22}Ne/^{21}Ne)_{cos}$ enables to determine ^{14}C production rates for all shielding depths in chondrites with pre-atmospheric radii of less than 90 cm, which covers the majority of the known chondrites. Considering that $(^{22}Ne/^{21}Ne)_{cos}$ can usually be measured to within better than ~2%, the ^{14}C production rates can be determined to within 10% for all chondrites with pre-atmospheric radii between 4 cm and less than 90 cm and for all shielding depths.

3.6. Quantifying the Shielding Dependence of $^{14}C/^{10}Be$ Production Rate Ratios

It is usually assumed that the $^{14}C/^{10}Be$ production rate ratios are less dependent on shielding than the ^{14}C production rates. We already demonstrated in Fig. 3.4 that this is not true, Fig. 3.6 depicts $^{14}C/^{10}Be$ production rate ratios as a function of the shielding indicator $(^{22}Ne/^{21}Ne)_{cos}$ ratios. The modeled data are for L chondrites with radii between 4 cm and 400 cm. Again, we only consider the innermost 58% of the radius, i.e., we assume 80% ablation losses. For the $^{14}C/^{10}Be$ ratio (open symbols), we also show the estimated uncertainties. Also shown are the experimental data for Knyahinya (Graf et al., 1990; Jull et al., 1994) and the results from our study for Mt. Tazerzait, Boumdeid (2011), Bensour, and SaU 606. The experimental data are discussed in detail below.

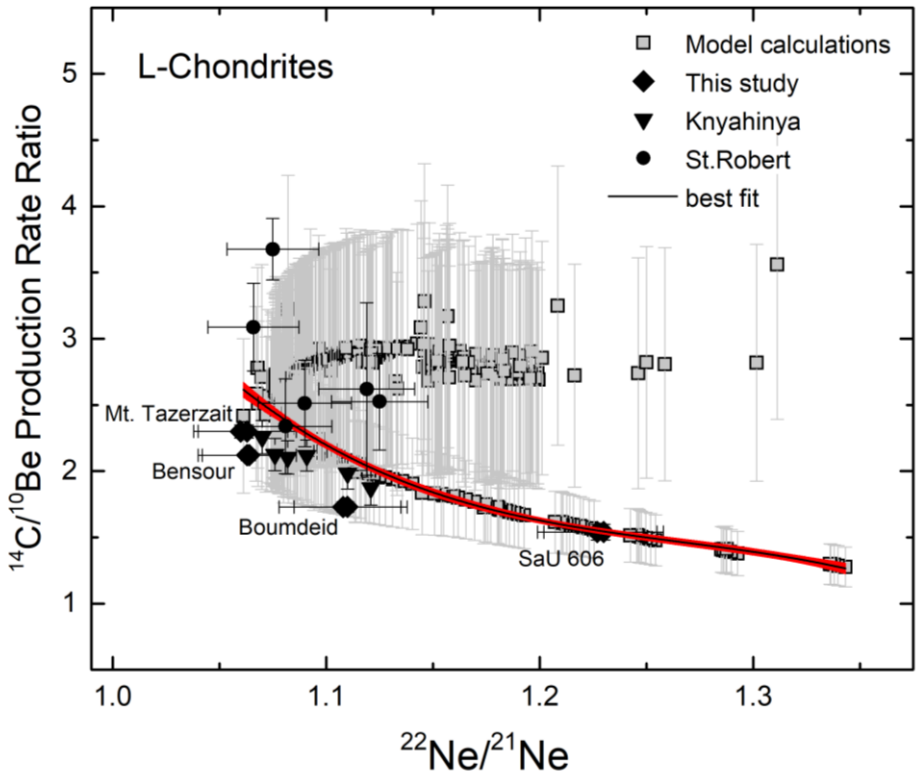

Fig. 3.6. $^{14}C/^{10}Be$ production rate ratios as a function of $(^{22}Ne/^{21}Ne)_{cos}$. The model calculations are for L chondrites with radii between 4 cm and 400 cm. The light gray error bars indicate the 1σ uncertainties of the model calculations. The red line is the best-fit line considering only meteorites with pre-atmospheric radii less or equal 60 cm. Also shown are experimental data for Knyahinya (Graf et al., 1990, Jull et al., 1994), St. Robert (Leya et al., 2001), and the data for the four chondrites studied here. The upper branch of modelled data is for larger meteorites (pre-atmospheric radius > 60 cm).

There is no one-to-one relationship between $^{14}C/^{10}Be$ production rates and $(^{22}Ne/^{21}Ne)_{cos}$ ratios, i.e., the relationship is surjective. For almost all $(^{22}Ne/^{21}Ne)_{cos}$ ratios there are two $^{14}C/^{10}Be$ ratios possible. For example, at a $(^{22}Ne/^{21}Ne)_{cos}$ ratio of 1.125 the $^{14}C/^{10}Be$ ratio can be ~1.9 for a small meteoroid (R ~ 20 cm) or ~2.9 for a larger object (R ~ 125 cm). The differences in $^{14}C/^{10}Be$ can be translated into terrestrial age differences. For a production rate ratio $^{14}C/^{10}Be$ = 1.9 or 2.9 and a measured $^{14}C/^{10}Be$ of 1.0 the terrestrial ages are ~5.3 ka and ~8.8 ka, respectively. For a measured ratio of 0.5 the terrestrial ages are ~11.0 ka and ~14.5. Finally, for a measured $^{14}C/^{10}Be$ ratio of 0.25 the terrestrial ages are ~16.7 ka and ~20.2 ka. Consequently, the differences in terrestrial ages can be substantial and using an average ratio introduces a significant size-dependent bias into the database.

Since the correlation $^{14}C/^{10}Be$ versus $(^{22}Ne/^{21}Ne)_{cos}$ is surjective, we cannot give a simple equation calculating $^{14}C/^{10}Be$ production rates from measured $(^{22}Ne/^{21}Ne)_{cos}$ ratios. We can, however, limit the database to produce such a one-to-one relationship. For example, if we consider only chondrites with pre-atmospheric radii less or equal 60 cm, the ambiguities disappear, and the $^{14}C/^{10}Be$ production rate ratios can be calculated from $(^{22}Ne/^{21}Ne)_{cos}$ ratios via:

$$\frac{P(^{14}C)}{P(^{10}Be)} = a - b \times \left(^{22}Ne/^{21}Ne\right)_{cos} + c \times \left(^{22}Ne/^{21}Ne\right)^2_{cos} - d \times \left(^{22}Ne/^{21}Ne\right)^3_{cos} \quad \textbf{(eq. 3.5)}$$

Table 3.2. Parameters for the fit function describing the relationship of $^{14}C/^{10}Be$ production rate ratios as a function of $(^{22}Ne/^{21}Ne)_{cos}$ (eqn. 5).

Meteorite Type	***a***	***B***	***c***	***d***
H Chondrite	148.1 ± 12.9	345.8±32.5	273.3 ± 27.2	72.4± 7.6
L Chondrite	173.4 ± 13.9	403.0±34.7	316.6 ± 28.7	83.3± 7.9
LL Chondrite	169.0 ± 12.9	391.5±32.1	306.6 ± 26.6	80.4± 7.3

Valid for all radii from 4 cm to 60 cm.
For determining the fit function, 80% ablation losses are assumed.

The result for L chondrites is shown by the solid black line and the 95% confidence interval is shown by the red area. The values for the parameters *a*, *b*, *c*, and *d* for H, L, and LL chondrites, respectively, are given in Table 3.2. Note that this correlation only holds for meteorites with pre-atmospheric radii less or equal 60 cm, which cannot easily be deduced from $(^{22}Ne/^{21}Ne)_{cos}$ ratios alone. For applying this equation, it is therefore mandatory to have an independent estimate of the pre-atmospheric size of the studied meteorite.

3.7. Experimental

3.7.1. *Meteorite Samples*

For this initiating study, four recently fallen meteorites were selected: Boumdeid (2011) (L6), Bensour (LL6), Mt. Tazerzait (L5), and Sayh al Uhaymir (SaU 606, H5). Bensour (LL6, shock stage S3) fell on February 11, 2002, at the border region between Morocco and Algeria. The total known mass of Bensour is 45 kg. Boumdeid (2011) is an L6 chondrite that fell on September 14, 2011, in the Assaba region of Mauritania. Two recent radionuclide studies (Buhl et al., 2014; Rosen et al., 2020) inferred a relatively small pre-atmospheric size for Boumdeid (2011) of (radius < 20 cm), which is consistent with the small total known mass of only 3.6 kg. The L5 chondrite Mt. Tazerzait fell on August 21, 1991, near Tohua in the Republic of Niger. In total, 110 kg of this meteorite has been recovered. Finally, SaU 606 is an H5 ordinary chondrite with shock stage S2 and a total known mass of 136.5 g. SaU 606 is not an observed fall, but an unweathered (W0) individual found in the Al-Wusta region of the Sultanate of Oman on February 12, 2017. The detectable activities of short-lived radionuclides indicate that SaU 606 fell very recently, likely in 2012 (Rosen et al., 2020). Such a short terrestrial age is negligible for ^{14}C studies, therefore SaU 606 can be included in this study.

3.7.2. *^{14}C Measurements and Data Reduction*

Sample preparation, CO_2 extraction, and ^{14}C measurements followed the procedures recently established in our laboratory by Mészáros et al. (2018) and Sliz et al. (2019, 2022). Briefly, samples were milled and the 125–200 μm grain size fraction was selected. The samples were leached first in 6 M HCl for 30 min to dissolve carbonates and to remove any terrestrial contamination. Next, after careful drying, the samples were leached for 48 hours in monoethanolamine thioglycolate (EATG) 65% to remove iron oxides and hydroxides. The leaching procedure results in losses of any oxidation products of metal and troilite and thus produces samples enriched in silicates. For correcting for such mass losses, we used the mean mass loss values determined by Mészáros et al. (2018). 50 mg of dried samples were wrapped in pre-cleaned Al-foil and were loaded into the Bernese ^{14}C extraction line. The extracted CO_2 gas had to be spiked with ^{14}C free CO_2 to provide enough carbon (> 10 μg) for the $^{14}C/^{12}C$ AMS measurements.

Measurements of the $^{14}C/^{12}C$ ratios were conducted at the MICADAS at the Laboratory for the Analysis of Radiocarbon with AMS (LARA) at the Department of Chemistry and

Biochemistry, University of Bern (Szidat et al., 2014; Szidat, 2020). Briefly, the glass ampoules containing the spiked sample gas were introduced into the gas interface system (GIS) of MICADAS, cracked open, and the CO_2 was mixed with He. This mixture was then transferred to the gas ion source. A normal measurement cycle also comprises a standard reference material (Oxalic acid II; NIST, Gaithersburg, USA), and blanks, which are essentially spiked background measurements following the same procedure as for the samples. The ^{14}C results are given in fraction modern carbon ($F^{14}C$) and they account for all possible uncertainties, i.e., correction for isotopic fractionation, uncertainties from blank subtraction and standard normalization, and a systematic uncertainty of 1.5‰ due to day to-day variabilities (Szidat et al., 2014).

To determine ^{14}C activity concentrations, we followed the procedure given by Hippe et al. (2013) and Hippe and Lifton (2014) and calculated the absolute $^{14}C/^{12}C$ ratio via:

$$\left(\frac{^{14}C}{^{12}C}\right)_{S,abs} = 1.1694 \times 10^{12} \times Ab12_S \times F^{14}C_S \times \left[1 + \delta^{13}C_S\right] \times e^{(1950-y)/8223} \qquad \textbf{(eq. 3.6)}$$

with $Ab12_S$ is the $^{14}C/^{12}C$ ratio of the sample determined by the observed $\delta^{13}C_S$ of the sample. $F^{14}C_S$ is the percentage of modern carbon in the sample normalized to $\delta^{13}C = -25‰_{VPDB}$ and y is the year of the measurement. Thereby, VPDB stands for Pee Dee Belemnite, a standard for the measurement of $\delta^{13}C$. The value of 1.1694×10^{-12} corresponds to the abundance of ^{14}C in modern carbon. The next step is the calculation of the number of ^{14}C atoms per gram of sample N_{14} using:

$$N_{14} = \left[\left(\frac{^{14}C}{^{12}C}\right)_{S,abs} \times N_A \times \frac{V_S}{V_A} - B\right] \Big/ M_S \quad \left(\frac{atoms}{g}\right) \qquad \textbf{(eq. 3.7)}$$

with N_A as Avogadro's number (6.022×10^{-23} atoms/mol), V_S the volume of CO_2 in the sample at 20°C and 1013 mbar, and V_A the volume of 1 mol CO_2 at 20°C and 1013 mbar. B is the number of ^{14}C atoms in the blank and M_S is the mass of the sample in gram. As usual when studying extraterrestrial samples, the final results are given as an activity concentration in disintegrations per minute per kilogram of sample (dpm/kg) calculated via: $A_m = \lambda_{14}$ (min^{-1}) × N_{14} × 1000.

3.7.3. *^{10}Be Measurements*

Sample preparation and AMS measurements of ^{10}Be were performed at the ASTER AMS facility, CEREGE, Aix-en-Provence, France. Details of the sample preparation procedure and the ^{10}Be measurements can be found in Arnold et al. (2010, 2013). In brief, ^{10}Be was extracted from 200 mg of sample material of 125–200 µm grain size. Silicate fractions were leached with HF, spiked with ^{9}Be carrier, and transformed into BeO powder. The BeO powder was then mixed with Niobium (Nb) powder (Aldrich, 325 mesh, 99.8%) in a 1:1.5 ratio and this mixture was pressed into the AMS cathodes. The standard reference material NIST SRM4325 with a ^{10}Be/^{9}Be ratio of $(2.79 \pm 0.03) \times 10^{-11}$ (Nishiizumi et al., 2007) and machine blanks were run before and after the samples. The measured ^{10}Be/^{9}Be ratios were corrected for procedural blanks. The AMS results include all sources of uncertainties, i.e., statistical uncertainties, uncertainty of the standard, uncertainty of the mean of the standard measurements (instrumental), and a systematic uncertainty of ~0.5% (Arnold et al., 2010). Finally, the ^{10}Be data are converted to activity concentrations in dpm/kg.

3.7.4. *Noble Gas Measurement*

The measurements of the isotopic He, Ne, and Ar concentrations were following our standard procedures for stony meteorites (e.g., Leya et al., 2013). Briefly, about 20 mg samples were wrapped in Al foil and were loaded into the extraction and cleaning line. After loading, samples were heated in vacuum at ~80°C for up to 48 hours to remove absorbed atmospheric gases. Samples were degassed in a Mo crucible held for 20 min at 1750°C. Blanks were regularly measured before and after sample extractions. Typical blanks (in units 10^{-12} cm^{3}STP) are ~13, ~17, ~7 for ^{3}He, ^{4}He, and ^{20}Ne, respectively. For ^{36}Ar and ^{40}Ar, typical blanks (in 10^{-10} cm^{3}STP) are ~0.5 and ~1.1, respectively. For all samples, blanks for He and Ne isotopes contribute less than 1% to the sample gas amounts; an exception is the ^{20}Ne blank for SaU 606, which contributes ~2% to the sample gas amount. The ^{36}Ar blank contributions range from ~7% for Bensour to ~40% for one SaU 606 aliquot. The ^{40}Ar blank contributes for most samples less than 1% to the measured gas amounts, an exception is one Boumdeid (2011) aliquot, for which the blank contributes ~8%. In addition to blank corrections, the noble gas data have also been corrected for interferences and instrument non-linearities. Calibrations were regularly performed; they consist of known amounts of standard gases having atmospheric isotopic composition. The only exception is He, which is enriched in ^{3}He relative

to ^{4}He relative to terrestrial atmosphere. Released gases were cleaned using SAES® getters operating at various temperatures between 180°C and 450°C. The He-Ne fraction was separated from the Ar fraction using activated charcoals held at the temperature of liquid nitrogen. The He-Ne fraction was measured in a (small volume) static sector field mass spectrometer built in-house. During the measurement, the gas was further cleaned, and the background was further reduced from remaining impurities using an additional Ti getter (for the reduction of H_2) and an activated charcoal held at the temperature of liquid nitrogen to reduce hydrocarbons and Ar. The Ar fraction was purified using additional getters and was measured in a static noble gas tandem spectrometer, also built at the University of Bern, designed to minimize baseline variations caused by scattered ions. Gas concentrations are calculated by comparing the peak height of the sample signal to signals from the standards. The given noble gas data reckons all possible sources of uncertainties, including uncertainties from blank correction and uncertainties from standard measurements. We added a systematic uncertainty of 4% for the gas amounts and 2% for the isotope ratios.

3.8. Results and Discussion

3.8.1. *^{14}C Activity Concentrations in Al-blank and Dead $^{14}CO_2$*

^{14}C concentrations measured in three Al-blanks ranged (in unts 10^4) from 10.7 ± 0.2 to 15.0 ± 0.5 ^{14}C atoms, with an average contribution of 12.8 ± 0.5 (10^4) ^{14}C atoms to the total ^{14}C concentration measured in samples. Similarly, the ^{14}C concentrations in ^{14}C-free cylinder CO_2 ranged (in unts 10^4) from 5.2 ± 0.4 to 31.6 ± 0.7 ^{14}C atoms, with an average contribution of 16.3 ± 0.3 (10^4) ^{14}C atoms to the measured sample concentrations. Combined, these blank contributions account for approximately 2% (Mount Tazerzait), 2.6% (Bensour), 4.4% (Boumdeid) and 3.7% (SaU 606) of the total ^{14}C concentrations in the samples. In contrast, the blank contribution to the standard JaH 073 was approximately 20%. Blank measurements were performed at the same extraction conditions as the samples. Both the Al-blanks and cylinder CO_2 blanks were also held at extraction temperature of 1600 °C in UHP O_2 for 10 min before trapping CO_2 in helix trap and later collecting it in glass capillaries. Consequently, the measured blanks (2–4%) represent the maximum possible background ^{14}C contribution from the extraction system. Details of the blank calculations and corrections are provided in Table 3.3.

Table 3.3. ^{14}C concentration in the procedural and system blanks.

Blanks	Diluted CO_2 (10^{-2} cm^3)	C equi. (µg)	$F^{14}C$	$\delta^{13}C$ (‰)	$^{14}C/^{12}C$ (10^{-12})	N14 (10^4 at)
CB_18102	3.1 ± 0.02	15.5	0.413 ± 0.008	-24.4	0.41 ± 0.008	31.6 ± 0.7
CB_20102	3.0 ± 0.02	15.3	0.233 ± 0.006	-23.8	0.23 ± 0.006	17.7 ± 0.5
CB_22102	3.0 ± 0.02	14.4	0.149 ± 0.005	-24.0	0.15 ± 0.005	10.7 ± 0.3
CB_27102	2.2 ± 0.02	14.8	0.071 ± 0.005	-24.3	0.07 ± 0.005	5.2 ± 0.4
AB_17102	3.9 ± 0.01	19.5	0.110 ± 0.005	-23.6	0.11 ± 0.002	10.7 ± 0.2
AB_21102	3.1 ± 0.01	15.6	0.165 ± 0.004	-24.2	0.16 ± 0.004	12.8 ± 0.3
AB_26102	3.0 ± 0.01	15.2	0.199 ± 0.008	-24.2	0.19 ± 0.006	15.0 ± 0.5

$F^{14}C$ is the Fraction modern carbon normalized to $\delta^{13}C$ of -25‰$_{VPDB}$ and AD 1950.
Average blank contribution (correction) of 29.1× 10^4 ^{14}C atoms was applied to the samples and re-extraction.

3.8.2. *^{14}C Activity Concentrations in Samples and Re-extractions*

The measured ^{14}C concentrations (blank-corrected) in the four recent falls show a small variation, ranging from 6.8 (±0.07) × 10^6 ^{14}C atoms for Boumdeid to 13.6 (±0.14) × 10^6 ^{14}C atoms for Mount Tazerzait. Blank corrections were applied to these measured values. The re-extractions contribution for each sample was less than 2%, except for SaU 606 for which the re-extraction accounts for 10%. The details of sample and re-extraction measurement are provided in Table 3.4.

Table 3.4. ^{14}C concentration in the studied meteorites and their re-extractions.

Meteorites	Diluted CO_2 (10^{-2} cm^3)	C equi. (µg)	$F^{14}C$	$\delta^{13}C$ (‰)	$^{14}C/^{12}C$ (10^{-12})	N14 (10^6 at)	N14[a] (10^6 at)
Mt. Taz.	3.6±0.03	17.75	13.5±0.08	-24.7	15.5±0.09	13.8±0.14	13.6±0.14
Reextract	3.2±0.03	15.76	0.676±0.01	-24.6	0.8±0.01	0.6±0.01	0.45±0.03
Bensour	3.7±0.03	18.50	10.7±0.07	-25.3	12.2±0.08	11.4±0.12	11.2±0.12
Reextract	3.1±0.03	15.60	0.323±0.01	-24.5	0.4±0.01	0.3±0.01	0.13±0.01
Boumdeid	3.7±0.03	18.58	6.4±0.04	-24.0	7.3±0.05	6.8±0.07	6.7±0.07
Reextract	3.1±0.03	15.51	0.127±0.02	-24.2	0.2±0.01	0.1±0.01	-0.5±0.01
SaU 606	3.7±0.03	18.58	6.9±0.05	-23.8	7.9±0.06	7.4±0.08	7.3±0.08
Reextract	3.1±0.03	15.51	0.986±0.02	-26.3	1.10±0.02	0.9±0.02	0.71±0.05
JaH 073	3.9±0.03	19.25	1.4±0.02	-25.7	1.6±0.02	1.5±0.02	1.4±0.02
Reextract	2.9±0.02	14.35	0.187±0.01	-24.6	0.2±0.01	0.2±0.01	-0.8±0.01

[a] N14 is the number of ^{14}C atoms after blank corrections.

3.8.3. *Noble Gases Cosmic Ray Exposure Ages and Meteorite Sizes*

The noble gas results for He and Ne isotopes are summarized in Table 3.5. The cosmogenic values $(^{22}Ne/^{21}Ne)_{cos}$ and $^{21}Ne_{cos}$ were calculated using a two-component deconvolution with

air and cosmogenic as endmembers. For the cosmogenic component we assume $(^{20}Ne/^{22}Ne)_{cos}$ = 0.844, which is the lowest ratio measured by us. For all samples two aliquots were measured, the $(^{22}Ne/^{21}Ne)_{cos}$ and $^{21}Ne_{cos}$ values for the two aliquots agree within the uncertainties, clearly demonstrating a good reproducibility. Using the $(^{22}Ne/^{21}Ne)_{cos}$ ratios we calculated ^{21}Ne production rates based on the correlation given by Dalcher et al. (2013). The CRE ages range from 9.84 ± 0.77 Ma for one SaU 606 aliquot to 51.5 ± 3.3 Ma for one Mt. Tazerzait aliquot. Again, for all samples the CRE ages determined from the two aliquots agree within the uncertainties.

The measured ^{36}Ar concentrations range from ~3.7×10^{-9} cm^3STP/g for one SaU 606 aliquot to ~3.0×10^{-8} cm^3STP/g for one Mt. Tazerzait sample. The $^{36}Ar/^{38}Ar$ ratios range between 0.72 and 4.36, indicating that measured argon is a mixture of cosmogenic and trapped argon; trapped is likely terrestrial contamination. Assuming $(^{36}Ar/^{38}Ar)_{cos}$ = 0.63 and $(^{36}Ar/^{38}Ar)_{air}$ = 5.32, the calculated cosmogenic $^{38}Ar_{cos}$ concentrations range between ~1.7×10^{-10} cm^3STP/g for one SaU 606 aliquot to ~1.9×10^{-8} cm^3STP/g for one Mt. Tazerzait sample. The reproducibility for $^{38}Ar_{cos}$ is fair. The $^{38}Ar_{cos}$ concentrations for the two aliquots from Bensour and Mt. Tazerzait agree within ~3% and ~13%, respectively. For SaU 606 both aliquots differ by a factor of ~5; the reason is not yet understood. Unfortunately, the argon phase for one Boumdeid (2011) aliquot was partly lost during extraction. All $^{40}Ar/^{36}Ar$ ratios are significantly higher than air, indicating a clear radiogenic ^{40}Ar signal. The CRE ages calculated using the correlation between $^{38}Ar_{cos}$ production rates and $(^{22}Ne/^{21}Ne)_{cos}$ given by Dalcher et al. (2013) range between 0.5 Ma for SaU 606 and 37.1 Ma for Mt. Tazerzait. All ^{38}Ar CRE ages (T_{38}) are lower than the ^{21}Ne CRE ages (T_{21}). The argon isotope concentrations are summarized in Table 3.6.

Bensour has been analysed for noble gases before (Cole et al., 2007) and there are some differences. While the CRE ages are in good agreement, 15.5 ± 1.0 Ma or 16.9 ± 1.1 Ma measured by us and 19.3 Ma (no uncertainty is given) measured by Cole et al. (2007), the latter authors give a $(^{22}Ne/^{21}Ne)_{cos}$ ratio for Bensour of 1.123, while we measure for both aliquots much lower ratios of 1.064 and 1.067. There is also a discrepancy for helium. The ^{3}He concentrations measured by us are (all in 10^{-8} cm^3STP/g) 30.6 and 26.8, whereas Cole et al. (2007) measured a lower ^{3}He concentration of ~21. Unlike ^{3}He, our measured ^{4}He concentration of 1570 and 1343 (10^{-8} cm3STP/g) are in good agreement with 1518 (10^{-8} cm3STP/g) measured by Cole et al. (2007), clearly indicating a significant radiogenic ^{4}He contribution. The measured ^{38}Ar concentrations of 0.39×10^{-8} cm^3STP/g and 0.41×10^{-8}

cm^3STP/g are surprisingly low and are not in agreement with the value of 0.73×10^{-8} cm^3STP/g given by Cole et al. (2007).

The relatively high $(^{22}Ne/^{21}Ne)_{cos}$ ratio for SaU 606 of 1.233 and 1.230 suggest a small pre-atmospheric size. This finding is consistent with the conclusion by Rosén et al. (2020). Based on short-lived radionuclide data, the authors suggest a mean shielding depth for the studied sample of just a few centimetres. The argon concentrations for both aliquots are low, rendering the data unreliable.

Mt. Tazerzait has been analyzed for noble gases before by Scherer and Schultz (2001). Our results are in good agreement with their data. Both studies determine a long exposure age, e.g., T_{21} = 57.6 Ma by Scherer and Schultz (2001) (no uncertainties are given in this study) and T_{21} of 46.0 ± 2.8 and 51.5 ± 3.3 Ma by us. The only difference is in the $(^{22}Ne/^{21}Ne)_{cos}$ ratio, which is 1.063 ± 0.026 and 1.066 ± 0.029 in our study, indicating large shielding, and 1.089 in the study by Scherer and Schultz (2001). The conclusion, however, is the same, Mt. Tazerzait comes from a shielded position and was thus part of a much larger object in space.

The measured $(^{22}Ne/^{21}Ne)_{cos}$ ratios for Boumdeid (2011) are 1.113 ± 0.025 and 1.111 ± 0.031, indicating an average sized meteorite with a pre-atmospheric radius of around 20−40 cm. This finding agrees with a size of 10−20 cm previously reported by Buhl et al. (2014). Their estimate is based on measured ^{60}Co, ^{54}Mn, and ^{22}Na activity concentrations. The T_{21} CRE ages for Boumdeid (2011) of 25.3 ± 1.7 Ma and 24.0 ± 1.7 Ma places this meteorite well in the CRE age peak for L chondrites.

To summarize, the CRE ages for all four studied samples are long enough that ^{10}Be has reached saturation. Therefore, all four samples can be used to validate the $^{14}C/^{10}Be$ terrestrial age dating system.

Table 3.5. He and Ne isotopic concentrations, cosmogenic ^{21}Ne and $(^{22}Ne/^{21}Ne)_{cos}$, and CRE ages for Bensour, SaU 606, Mt. Tazerzait, and Boumdeid.

Meteorite	Mass	Concentrations in 10^{-8} cm^{3}STP/g							
	(mg)	^{3}He	^{4}He	^{20}Ne	$^{20}Ne/^{22}Ne$	$^{21}Ne/^{22}Ne$	$(^{22}Ne/^{21}Ne)_{cos}$	$^{21}Ne_{cos}$	T_{21} (Ma)
Bensour (1)	50.33	30.6 ± 1.6	1570 ± 78	7.33 ± 0.39	0.862 ± 0.019	0.938 ± 0.020	1.063 ± 0.023	8.16 ± 0.44	17.8 ± 1.0
Bensour (2)	50.89	26.8 ± 1.4	1343 ± 67	6.55 ± 0.35	0.855 ± 0.020	0.936 ± 0.020	1.064 ± 0.022	7.32 ± 0.41	16.0 ± 0.9
SaU 606 (1)	20.30	11.6 ± 0.6	1548 ± 77	1.73 ± 0.11	0.844 ± 0.026	0.811 ± 0.018	1.230 ± 0.028	1.67 ± 0.12	9.75 ± 0.70
SaU 606 (2)	20.16	13.1 ± 0.7	1599 ± 81	1.95 ± 0.15	0.886 ± 0.058	0.809 ± 0.018	1.227 ± 0.028	1.79 ± 0.18	10.29 ± 1.03
Mt. Tazerzait (1)	20.74	98.3 ± 5.2	2953 ± 148	19.36 ± 1.04	0.860 ± 0.019	0.939 ± 0.020	1.060 ± 0.022	21.7 ± 1.2	46.5 ± 2.6
Mt. Tazerzait (2)	20.29	108.0 ± 5.7	3075 ± 157	21.40 ± 1.15	0.861 ± 0.021	0.937 ± 0.020	1.063 ± 0.023	23.9 ± 1.3	52.0 ± 2.9
Boumdeid (1)	21.33	47.0 ± 2.5	1635 ± 83	8.10 ± 0.49	0.854 ± 0.020	0.898 ± 0.020	1.110 ± 0.025	9.00 ± 0.52	25.2 ± 1.5
Boumdeid (2)	21.13	45.1 ± 2.9	1595 ± 96	8.10 ± 0.49	0.855 ± 0.020	0.899 ± 0.025	1.108 ± 0.030	8.62 ± 0.56	23.9 ± 1.6

$(^{22}Ne/^{21}Ne)_{cos}$ ratios, $^{21}Ne_{cos}$ concentrations and T_{21} ages are determined following Dalcher et al. (2013).

Table 3.6. Ar isotopic concentrations, cosmogenic ^{38}Ar, and CRE ages for Bensour, SaU 606, Mt. Tazerzait, and Boumdeid.

Meteorite	Mass	Concentrations in 10^{-8} cm^{3}STP/g				
	(mg)	^{36}Ar	$^{36}Ar/^{38}Ar$	$^{40}Ar/^{36}Ar$	$^{38}Ar_{cos}$	T_{38} (Ma)
Bensour (1)	50.33	1.65 ± 0.33	2.51 ± 0.13	2138 ± 194	0.397 ± 0.082	7.2 ± 1.5
Bensour (2)	50.89	1.77 ± 0.36	2.56 ± 0.13	2116 ± 193	0.411 ± 0.085	7.5 ± 1.5
SaU 606 (1)	20.30	0.374 ± 0.11	4.36 ± 0.35	12606 ± 1392	0.0177 ± 0.0015	0.5 ± 0.4
SaU 606 (2)	20.16	0.517 ± 0.13	2.91 ± 0.20	9820 ± 970	0.0923 ± 0.0041	2.8 ± 1.2
Mt. Tazerzait (1)	20.74	2.71 ± 0.55	1.32 ± 0.06	2030 ± 165	1.76 ± 0.36	32.4 ± 6.6
Mt. Tazerzait (2)	20.29	3.02 ± 0.61	1.31 ± 0.06	2031 ± 158	1.98 ± 0.40	37.1 ± 7.5
Boumdeid (1)	21.33	-	-	-	-	-
Boumdeid (2)	21.13	0.572 ± 0.14	0.72 ± 0.05	9248 ± 925	0.780 ± 0.17	17.7 ± 3.9

Boumdeid (1) was lost during measurement.

3.8.4. *^{14}C Activities and ^{14}C/^{10}Be Ratios*

The total ^{14}C atoms from each meteorite and thereby calculated activity concentrations in dpm/kg before and after mass loss correction are provided in Table 3.7. Measured ^{10}Be activity concentrations after mass loss corrections and the ^{14}C/^{10}Be production rate ratios are given in Table 3.7. The ^{14}C production rates range from 26.6 ± 0.1 dpm/kg for Boumdeid (2011) to 56.6 ± 0.1 dpm/kg for Mt. Tazerzait, i.e., they vary by more than a factor of 2. The high ^{14}C activity concentration for the L5 chondrite Mt. Tazerzait is consistent with previously reported values of 57.8 ± 0.8 and 60.1 ± 0.9 dpm/kg given by Minami et al. (2006) for the same meteorite. The average production rate for L chondrites used so far is 51.1 ± 1.0, which is only ~10% lower than the value for Mt. Tazerzait but significantly higher than the production rate of 26.6 ± 0.1 dpm/kg measured by us for the L chondrite Boumdeid (2011).

Table 3.7. Total ^{14}C atoms, ^{14}C and ^{10}Be activity concentration (dpm/kg), and ^{14}C/^{10}Be ratio in five chondrites.

Meteorites	Type	Mass (mg)	N14[a] (×10^6)	N14/g (×10^8)	^{14}C dpm/kg	^{14}C[b] dpm/kg	^{10}Be dpm/kg	^{14}C/^{10}Be
Mt. Taz.	L5	50.1	14.1±0.4	2.81±0.02	65.1±1.3	56.7±1.1	24.6±0.3	2.30±0.04
Bensour	LL6	50.2	11.4±0.4	2.26±0.02	52.3±1.0	45.6±0.9	21.4±0.3	2.13±0.04
Boumdeid	L6	50.4	6.6±0.3	1.32±0.02	30.5±0.6	26.6±0.5	15.3±0.2	1.73±0.04
SaU 606	H5	50.3	7.9±0.1	1.58±0.01	36.6±0.7	31.9±0.6	19.4±0.2	1.64±0.04
JaH 073	L6	50.9	1.4±0.4	0.28±0.01	6.4±0.1	5.6±0.1	n.d.	n.d.

All uncertainties are 1σ.
[a] N14 is the sum of blank corrected ^{14}C atoms in samples and re-extractions.
[b] ^{14}C[1] is the activity concentration after 12.8% mass loss correction.

Fig. 3.5 depicts ^{14}C production rates as a function of $(^{22}Ne/^{21}Ne)_{cos}$ for the measured data together with model calculations (see above). Though, the model calculations and therefore the best fit line are for L chondrites, we also plot the LL chondrite Bensour and the H chondrite SaU 606 in the same diagram. The differences between L and LL chondrites are small and are therefore of no relevance for the discussion. For H chondrites, the model predictions and the best fit line would be ~10% lower than for L chondrites, the basic trend, however, would remain the same. The data for Knyahinya (Jull et al., 1994; Graf et al., 1990) and the data for Mt. Tazerzait, Bensour, and SaU 606 plot within the uncertainties in the area given by the model calculations. The exception is Boumdeid (2011), for which either ^{14}C is ~50% too low or the $(^{22}Ne/^{21}Ne)_{cos}$ ratio is ~10% too low for both aliquots, which, however, show a good

reproducibility. Since experimental problems can be ruled out, other hypothesis like a complex exposure history, might be probable. Further studies, including more radionuclide data, are needed to finally solve this problem.

To summarize, experimental data confirm the trend given by model predictions of ^{14}C production rates as a function of $(^{22}Ne/^{21}Ne)_{cos}$. However, more experimental data are needed to properly validate the model calculations, especially independently validating them for the different chondrite types. The measured $^{14}C/^{10}Be$ ratios range from 1.54 ± 0.06 for SaU 606 to 2.30 ± 0.05 for Mt. Tazerzait, i.e., the ratios span almost the entire range of data predicted by the model calculations (see above). Fig. 3.6 shows $^{14}C/^{10}Be$ production rate ratios as a function of $(^{22}Ne/^{21}Ne)_{cos}$. The open symbols with the light gray error bars are the results of the model calculations for L chondrites discussed above. Also shown are the experimental data for the L chondrite Knyahinya (Graf et al., 1990; Jull et al., 1994), and the results obtained for Mt. Tazerzait, Bensour, Boumdeid (2011), and SaU 606. For the latter, each aliquot is plotted separately, i.e., for each meteorite there are two $(^{22}Ne/^{21}Ne)_{cos}$ values but only one $^{14}C/^{10}Be$ ratio. Again, we plot all data in the diagram for L chondrites; the diagrams for H and LL chondrites would only by slightly different. There is a good agreement between the model calculations and the experimental data (all chondrite types). The agreement is in all cases within the uncertainties. Therefore, the experimental data clearly confirm and validate the model calculations, indicating that the $^{14}C/^{10}Be$ ratio is not constant but varies significantly with shielding, i.e., with the $(^{22}Ne/^{21}Ne)_{cos}$ ratio. Again, more experimental data are needed to properly validate the model predictions.

3.9. Conclusions

We performed new and systematic model calculations for ^{10}Be and ^{14}C production rates in H, L, and LL chondrites. The focus of the model calculations was on the dependence of the ^{14}C production rates on shielding to better constrain terrestrial ages for meteorites. The modeled data clearly demonstrate that using average ^{14}C production rates, as it is usually done for calculating ^{14}C terrestrial ages, is not good enough for establishing a reliable and consistent terrestrial age database. For example, using average ^{14}C production rates introduces a size-dependent bias into the database, which can be significant, i.e., it overestimates terrestrial ages

for small objects and underestimates for larger objects. The introduced error can be significant. To be more quantitative, assuming a L chondrite with a pre-atmospheric radius of 10 cm, the ^{14}C production rates would rather be in the range 30 dpm/kg instead of the very often used 51.1 dpm/kg. This would have profound effects for the calculated terrestrial ages. For example, instead of the correct age of 1000 year we would calculate 5400 years, instead of 5000 years we would calculate 9400 years, and instead of a correct age of 10'000 year we would calculate 14'400 years, all ages are significantly too high. To circumvent or at least reduce the effects due to shielding, the $^{14}C/^{10}Be$ production rate ratio is often considered to give more reliable ages than the ^{14}C dating system. However, the model calculations clearly demonstrate that also the $^{14}C/^{10}Be$ ratios vary with shielding and that using an average value can produce unreliable terrestrial ages.

By combining ^{14}C production rates and $^{14}C/^{10}Be$ production rate ratios with the shielding indicator $(^{22}Ne/^{21}Ne)_{cos}$ and by assuming 80% ablation losses, i.e. by reasonably reducing the range of data, we were able to deduce easy-to-use correlations of ^{14}C production rates and $^{14}C/^{10}Be$ production rate ratios as a function of $(^{22}Ne/^{21}Ne)_{cos}$. The new correlations enable determining terrestrial ages based on ^{14}C or $^{14}C/^{10}Be$ ratios – if combined with $(^{22}Ne/^{21}Ne)_{cos}$ – more accurately than ages based solely on average values for ^{14}C and/or $^{14}C/^{10}Be$. However, the higher accuracy comes with a price, in addition to ^{14}C and ^{10}Be measurements, one also needs to measure the noble gases in aliquots of the samples. This, however, is not a serious limitation because, first, reliable He and Ne noble gas measurements can be performed on sample masses of ~10 mg and, second, cosmogenic ^{21}Ne concentrations are needed to demonstrate that measured ^{10}Be is in saturation and that the $^{14}C/^{10}Be$ dating system can be applied. Note that the thus determined correlations depend only very little on the assumption of 80% ablation losses. Considering all, data, i.e., also considering regions from the very surface of the pre-atmospheric meteorite, changes the correlations only within their given uncertainties.

To validate the model predictions, we measured ^{14}C activity concentrations, $^{14}C/^{14}Be$ production rate ratios, $^{21}Ne_{cos}$, and $(^{22}Ne/^{21}Ne)_{cos}$ in the four recently fallen meteorite: Mt. Tazerzait (L5), Boumdeid (2011) (L6), Bensour (LL6), and in SaU 606 (H5). Though, SaU 606 is not a witnessed fall, short-lived radionuclide activities indicate a very short terrestrial age of

only a few years, negligible for ^{14}C and $^{14}C/^{10}Be$ studies. The experimental data confirmed the model predictions, though the database is too scarce to be conclusive. More data from freshly fallen meteorites are needed to properly validate the model predications, especially validating them for the different chondrite types. We therefore started a follow-up study, extending the experimental database by analyzing ^{14}C, ^{10}Be, and the noble gases in a variety of H, L, and LL chondrite falls.

Chapter 4

Evaluating the ^{14}C Saturation Activities and $^{14}C/^{10}Be$ Saturation Activities Ratio in H, L, and LL chondrites

Based on article published in the ***Meteoritics & Planetary Science*** Journal. **https://doi.org/10.1111/maps.14355**

Numbering of the Title, tables and figures presented in this chapter are formatted to fit the layout of this thesis.

Evaluating ^{14}C and $^{14}C/^{10}Be$ terrestrial age dating systems for meteorites using experimental data and model calculations

Mohammad Tauseef[1]*, Ingo Leya[1], Jérôme Gattacceca[2], Sönke Szidat[3], Régis Braucher[2], Pascal M. Kruttasch[4], Anna Zappatini[4], ASTER Team[2]

[1]Physics Institute, Space Research and Planetology, University of Bern, Sidlerstrasse 5, 3012 Bern, Switzerland

[2]CNRS, Aix Marseille Université, IRD, INRAE, CEREGE, Aix-en-Provence, France

[3]Department of Chemistry, Biochemistry and Pharmaceutical Sciences & Oeschger Centre for Climate Change Research, University of Bern, Freiestrasse 3, 3012 Bern, Switzerland

[4]Institute of Geological Sciences, University of Bern, Baltzerstrasse 3, 3012, Ber, Switzerland

***Corresponding author**. Email: mohammad.tauseef@unibe.ch

ABSTRACT

This study presents a refined approach determining ^{14}C saturation activities and $^{14}C/^{10}Be$ saturation activity ratios in chondritic meteorites with the goal to improve terrestrial age dating. By combining new model calculations for ^{10}Be, ^{14}C and cosmogenic $(^{22}Ne/^{21}Ne)_{cos}$, along with experimental data from 17 freshly fallen chondrites, we established reliable correlations for ^{14}C production rates and $^{14}C/^{10}Be$ production rate ratios as a function of $(^{22}Ne/^{21}Ne)_{cos}$. The experimental data agree with the model calculations, and they fully confirm that ^{14}C production rates and $^{14}C/^{10}Be$ production rate ratios depend on shielding. Constrained correlations describe the experimental data for all shielding conditions and all ordinary chondrites mostly within the uncertainties given by the model. The new correlations therefore provide a significant improvement compared to the earlier approaches, in which average, meteorite-type dependent ^{14}C production rates, and average $^{14}C/^{10}Be$ production rate ratios were assumed. Ignoring the shielding dependence introduces a size dependent bias into the terrestrial age database. This study enables the determination of shielding-corrected ^{14}C saturation activities and $^{14}C/^{10}Be$ production rate ratios to calculate shielding corrected terrestrial ages for meteorites reducing or eliminating a size bias in the database. In addition, this novel approach enables to give reliable uncertainty estimates of within 15% for the ^{14}C and ^{14}C-^{10}Be terrestrial ages.

4.1. Introduction

Terrestrial ages of meteorites, i.e., the time a meteorite spent on Earth before being found, provide essential information for a large variety of important scientific questions. A non-complete list includes, *first*, studying weathering effects and thereby improving our understanding of how weathering depends on the find location (hot and cold deserts, type of desert). *Second*, correcting meteorite finds for pairing, i.e., determining if two meteorites belong to the same object in space that broke up during atmospheric entry. *Third*, terrestrial ages are used to calculate ejection ages, which is the sum of the cosmic-ray exposure (CRE) age and the terrestrial age and gives the time since the meteorite has been produced in an asteroid collision event. *Fourth*, the ages are also relevant for studying the influx of meteorites to Earth. The questions are, was the influx constant over time and/or was the composition of the meteorite flux variable over time?

Terrestrial ages for stony meteorites are usually determined using the ^{14}C and/or the $^{14}C/^{10}Be$ dating techniques, which are both applicable for samples with terrestrial ages of less than 30–40 ka. The ^{14}C dating technique has also been applied, though with limited success, to iron meteorites (Schnitzer et al., 2012) and mesosiderites (Jull et al., 2009). Earlier studies assumed constant ^{14}C saturation activities for each type of meteorite and/or constant $^{14}C/^{10}Be$ saturation activity ratios. In the following the term saturation activities and production rates are used synonymously. Most terrestrial ages for H, L, and LL chondrites were obtained assuming average ^{14}C production rates of 46 dpm/kg, 51.1 dpm/kg, and 55.2 dpm/kg, respectively. Very often, these average ^{14}C production rates have assigned uncertainties in the range ~15% (e.g., Jull et al., 1989; 1993; 1998). However, experimental data on meteorite falls but also model calculations clearly indicate that the ^{14}C production rates vary significantly with meteorite size and shielding depth and that using an average value is not expected to give accurate ages (e.g., Wieler et al., 1996). The influence of the depth dependency on the ^{14}C production rates was already discussed in previous studies (e.g., Jull et al., 1994; Jull et al., 1989; Knauer et al., 1995; Wieler et al., 1996). For example, Knauer et al. (1995) discussed the shielding dependency of ^{14}C production rates and suggested combining ^{14}C production rates with $(^{22}Ne/^{21}Ne)_{cos}$ ratios to make the dating system more accurate. However, this idea was never widely implemented. One notable exception is the study by Schultz et al. (2005), which utilized the correlation between ^{14}C production rates and $(^{22}Ne/^{21}Ne)_{cos}$ to calculate shielding-corrected ages for meteorites from the Nullarbor desert in Australia. Their results revealed that, for some meteorites, the shielding-corrected ages were more than 60% lower than those calculated using

the assumed average ^{14}C saturation activity. Despite these findings, the suggestion of Jull et al. (1993) to assign an uncertainty of 15% to the ^{14}C saturation activity for meteorites with unknown shielding conditions was put into practice. Recently, we demonstrated that by using an average ^{14}C production rate, a significant size-dependent bias is introduced into the terrestrial age database. For a detailed discussion see Tauseef et al. (2024).

Other studies used the $^{14}C/^{10}Be$ production rate ratio, which internally corrects for shielding (at least partly), and therefore gives terrestrial ages that are more reliable than those calculated solely using ^{14}C (e.g., Kring et al., 2001; Jull et al., 2010). For applying this system, a $^{14}C/^{10}Be$ production rate ratio of 2.5 ± 0.1 is assumed (Jull et al., 2010; Jull et al., 1990; Kring et al., 2001; Welten et al., 2001). Again, while the ratio is assumed to be constant, experimental data and model calculations indicate otherwise. For example, some measured $^{14}C/^{10}Be$ ratios for meteorite falls differ substantially from the assumed ratio, i.e., there are ratios of 2.1 for the L/LL6 chondrite Knyahinya (Jull et al., 1994), 3.3 ± 0.1 for Carancas (H4-5) (Jull et al., 2009), and 1.54 ± 0.06 for the H5 chondrite SaU 606 (Tauseef et al., 2024). A large variation was also observed for samples from the same meteorite, St-Robert (H5), where the ratios vary from 2.3 to 3.7 (Leya et al., 2001b). In addition, based on model calculations, Jull et al. (2010) predict $^{14}C/^{10}Be$ ratios between 1.2 for small meteorites to 3.0 for large meteorites.

These findings clearly indicate that neither the ^{14}C saturation activities nor the $^{14}C/^{10}Be$ production rate ratio are constant, but both are shielding dependent. To address this problem and to establish shielding corrected, and therefore more accurate, ^{14}C and $^{14}C/^{10}Be$ dating systems, we established a new set of model calculations systematically studying the ^{14}C production rates and $^{14}C/^{10}Be$ ratios as a function of the shielding indicator $(^{22}Ne/^{21}Ne)_{cos}$. To evaluate the model predictions, we measured ^{14}C saturation activities, $^{14}C/^{10}Be$ ratios, and noble gas isotope concentrations, e.g., $(^{22}Ne/^{21}Ne)_{cos}$ ratios in a collection of freshly fallen meteorites. In a first study, the four meteorite falls Mt. Tazerzait (L5), Bensour (LL6), Boumdeid (L6), and SaU 606 (H5) were studied (Tauseef et al., 2024). While the data confirm the model predictions, it was obvious that more data are needed to fully cover the entire range of shielding conditions and meteorite types and thereby to fully evaluate all aspects of the model predictions. The goal of the present work is two-fold. *First*, we re-study the model calculations. This is because, in Tauseef et al. (2024), the modeled parameter space was artificially reduced by assuming ~80% spherical ablation losses (by mass), i.e., by considering only the innermost ~60% of the pre-atmospheric radius. In the present study we no longer assume ablation losses, and the entire database is considered. *Second*, we significantly extend

the experimental database by systematically studying the saturation activities of ^{14}C and ^{10}Be together with the light noble gas isotopes in a large collection of H, L, and LL chondrite falls.

4.2. Experimental

4.2.1. *Sample Preparation and Chemical Leaching*

We studied the recently fallen H chondrites Castalia (H5), Ehole (H5), Farmville (H4), Al-Khadhaf (H4–5) and Ochansk (H4), the L chondrites Ausson (L5), Kandahar (L6), Leedey (L6), Suizhou (L6) Renchen (L5–6), Antonin (L) and Tennasilm (L4), and the LL chondrites Kilabo (LL6), Mangwendi (LL6), Sulagiri (LL5), Moshampa (LL6), and Stubenberg (LL6). The relevant information of the studied meteorites are summarized in Table 4.1.

Selected meteorites were processed following the sample preparation techniques recently established in our laboratory by Mészáros et al. (2018) and Sliz et al. (2019, 2022). Samples were first grinded in an agate mortar and subsequently sieved, which produced a powder with a relatively large fraction of fine-grained material (<128 μm). This procedure enriched the sample material in silicates because the metal is not expected to enter the fine-grained fraction.

Table 4.1. Meteorites analysed in this study.

Meteorites	Type	Fall Year	Fall Country	TKW (kg)	References
Castalia	H5	1874	USA	7.38	Hintenberger et al. (1965)
Ehole	H5	1961	Angola	2.40	Fireman, (1962)
Farmville	H4	1934	USA	56.0	Howard et al. (2014)
Ochansk	H4	1887	Russia	500	Met. Bull. database
Al-Khadhaf	H5-6	2022	Oman	0.022	Zappatini et al. (2024)
Antonin	L5	2021	Poland	0.35	Bischoff et al. (2022)
Ausson	L5	1858	France	50.0	Met. Bull. database
Kandahar	L6	1959	Afghanistan	0.299	Krinov (1960)
Leedey	L6	1943	USA	51.5	McCoy et al. (1997)
Renchen	L5-6	2018	Germany	0.999	Bischoff et al. (2019)
Suizhou	L6	1986	China	70.0	Xie and Chen (2016)
Tennasilm	L4	1872	Estonia	28.5	Mason and Wiik (1965)
Kilabo	LL6	2002	Nigeria	19.0	Cole et al. (2007)
Mangwendi	LL6	1934	Zimbabwe	23.0	Lightfoot et al. (2018)
Moshampa	LL5	2015	Iran	2.26	Bouvier et al. (2017)
Sulagiri	LL5	2008	India	110	Mahajan et al. (2017)
Stubenberg	LL6	2018	Germany	1.47	Bischoff et al. (2017)

TKW is the total known weight, recovered from excursions.

Studying samples with non-bulk composition requires some corrections for both the radioactive and stable isotopic data, which is explained in detail below. Next, the samples were first leached in 6 M HCl for 30 min to dissolve carbonates and to remove any terrestrial contamination. After washing the leachates with MilliQ water and drying them under a UV lamp, the samples were subjected to a second leaching step for 48 h using monoethanolamine thioglycolate (EATG) 65% to remove iron oxides and hydroxides. Finally, the samples were washed in MilliQ water, dried, and the mass loss caused by leaching was measured. For some samples, the chemical composition was measured to check for changes introduced by the leaching procedure following the HF/HNO_3 digestion and analysis of the solution samples using the Quadruple ICP-MS at the Institute of Geological Sciences, University of Bern. All meteorites were measured for ^{14}C and ^{10}Be activity concentrations and noble gas isotope concentrations, except Stubenberg, Renchen, and Antonin, for which ^{10}Be measurements were not possible due to the limited sample mass available.

4.2.2. *Noble Gas Measurement*

The He, Ne, and Ar isotope concentrations were measured following the standard procedures for stony meteorites used in our laboratory at the Physics Institute, University of Bern (e.g., Leya et al., 2013). Samples of ~20 mg were wrapped in commercial aluminum foil and loaded in the sample storage system of the noble gas extraction line. The samples were pre-heated in vacuum at ~80 °C for up to 48 hours to reduce absorbed atmospheric contamination. The samples were degassed in a molybdenum crucible held at 1750 °C for ~20 minutes. Blanks were regularly measured before and after sample extractions. Typical blanks (in units 10^{-10} cm^3STP) are ~0.2, ~4, ~0.2 for ^3He, ^4He, and ^{20}Ne, respectively. For ^{36}Ar and ^{40}Ar, typical blanks (in 10^{-10} cm^3STP) are ~1 and ~300, respectively. Blanks for ^3He, ^4He, ^{21}Ne, and ^{22}Ne contribute for all samples less than 1% to the measured sample gas amounts. For ^{20}Ne, ^{36}Ar, and ^{40}Ar blanks contribute on average less than 4% and for ^{38}Ar they contribute less than 10% to the measured gas amounts. In addition, the data are corrected for interferences and instrument nonlinearities. Calibrations were performed regularly, they consisted of known amounts of standard gases having atmospheric isotope composition, except for He, which is enriched in ^3He relative to ^4He relative to the atmospheric ratio.

Released gases were purified using various SAES® getters operating at temperatures between 180 °C and 450 °C. The He-Ne fraction was separated from the Ar fraction using activated charcoal held at the temperature of liquid nitrogen (LN2). The He-Ne fraction was measured

in a small-volume static sector field mass spectrometer, constructed in-house. During measurement, the spectrometer was connected to a Ti getter for H_2 reduction and to an activated charcoal held at the temperature of LN2 to reduce the background of Ar and hydrocarbons. The Ar fraction was further purified using additional getters and was measured in a static noble gas tandem mass spectrometer, also constructed inhouse. Gas concentrations were calculated by peak-height-comparison between samples and standards. The reported uncertainties for the noble gas data include statistical uncertainties from the measurements, uncertainties related to blank corrections and to the corrections for mass fractionation. In addition, a systematic uncertainty of 4% for gas concentrations and 2% for ratios are added to the data (see Leya et al., 2013).

4.2.3. *Measurements of ^{10}Be Activity Concentrations*

Sample preparation and AMS measurements of ^{10}Be were performed at the ASTER AMS facility hosted at CEREGE, Aix-en-Provence, France. The details of the sample preparation and data handling procedure are described by Sliz et al. (2019) and Tauseef et al. (2024). Briefly, about 200 mg of each sample was treated with HF-HNO_3, spiked with a ^{9}Be carrier. Beryllium was then extracted in the form of BeO powder. Niobium (Nb) powder (Aldrich, 325 mesh, 99.8%) was added to BeO powder in a 1.5:1 ratio and pressed into the AMS cathodes. Standard reference material NIST SRM4325, with a ^{10}Be/^{9}Be ratio of $(2.79 \pm 0.03) \times 10^{-11}$ (Nishiizumi et al., 2007), along with machine blanks, were analyzed before and after the samples. The AMS results include all sources of uncertainties, i.e., statistical uncertainties, uncertainty of the standard, uncertainty of the mean of the standard measurements (instrumental), and a systematic uncertainty of ~0.5% (Arnold et al., 2010). Finally, the ^{10}Be data are converted to activity concentrations in dpm/kg via:

$$^{10}\text{Be (dpm kg}^{-1}) = \lambda_{10} \times \left(\frac{N_{10}}{M_S}\right) \times 1000 \qquad \textbf{(eq. 4.1)}$$

where N_{10} is the number of measured ^{10}Be atoms in the sample, M_s is the mass of the sample in grams, and λ_{10} is the decay constant for ^{10}Be (9.7×10^{-13} min^{-1}). Finally, the reported ^{10}Be activities are also corrected for mass loss due to leaching. To check the entire procedure for reliability and reproducibility, two aliquots of the L6 chondrite Kandahar were analyzed (<128 μm). The results are given in Table 4.2.

Table 4.2. Measured ^{10}Be atoms and activity concentrations for the studied meteorites.

Samples	Type	mass (mg)	^{10}Be/^{9}Be	^{9}Be (10^{19})	^{10}Be at (10^{9})	^{10}Be at/g (10^{10})	^{10}Be (dpm/kg)	^{10}Be Bulk (dpm/kg)
Blank	n.a.	453.2	0.001	3.03	0.002	0.001	n.a.	n.a.
Kandahar 1	L	187.5	1.16 ±0.02	3.06	3.554	1.90	18.39 ±0.24	18.46 ± 0.24
Kandahar 2	L	201.4	1.22 ±0.02	3.07	3.752	1.86	18.07 ±0.22	18.14 ± 0.22
Leedey	L	197.1	1.04 ±0.02	2.96	3.068	1.56	15.10 ±0.24	15.93 ± 2.21
Ausson 1	L	193.1	1.19 ±0.02	3.02	3.604	1.87	18.10 ±0.25	18.18 ± 0.25
Tennasilm	L	196.0	1.02 ±0.02	2.99	3.602	1.56	15.15 ±0.19	15.22 ± 0.19
Suizhou	L	195.3	1.23 ±0.02	2.98	3.671	1.88	18.23 ±0.23	18.31 ± 0.23
Ochansk	H	196.6	1.13 ±0.02	3.00	3.390	1.72	16.72 ±0.21	17.72 ± 2.08
Castalia	H	198.1	1.22 ±0.02	3.02	3.675	1.86	17.99 ±0.23	18.17 ± 0.23
Farmville	H	191.5	1.14 ±0.02	3.02	3.438	1.80	17.41 ±0.22	18.25 ± 0.77
Ehole 1	H	195.3	1.30 ±0.02	2.99	3.899	2.00	19.37 ±0.24	19.56 ± 0.24
Kilabo	LL	195.6	1.15 ±0.02	3.02	3.460	1.77	17.16 ±0.22	17.19 ± 0.22
Mangwendi	LL	200.3	1.40 ±0.02	2.99	4.192	2.09	20.30 ±0.25	20.33 ± 0.25
Sulagiri 1	LL	197.5	1.28 ±0.02	3.01	3.862	1.96	18.97 ±0.24	19.00 ± 0.24
Ehole 2	H	194.6	1.31 ±0.02	2.92	3.830	1.97	19.11 ±0.24	19.30 ± 0.24
Ausson 2	L	200.1	1.41 ±0.02	2.88	4.060	2.03	19.69 ±0.25	19.77 ± 0.25
Sulagiri 2	LL	199.5	1.24 ±0.02	3.02	3.750	1.88	18.22 ±0.23	18.25 ± 0.23

Mass loss, i.e., Fe (metal) loss % due to leaching, 4.9, 5.2 and 5.6% for H, L and LL chondrites is applied. ^{10}Be (bulk) is given after mass-balanced for iron content, i.e., by assuming total Fe of 20, 8 and 3% in H, L, and LL chondrites. In addition, ^{10}Be activity for Leedey (5%), Ochansk (5%) and Farmville (4%) are corrected for their short CRE ages. Discussed in the ^{10}Be sections below.

4.2.4. *Measurements of ^{14}C Activity Concentrations*

Carbon-14 extraction and measurement processes for meteorites follow the established protocol (e.g., Sliz et al., 2019; Tauseef et al., 2024). Briefly, ~50 mg of dried (and leached) samples were wrapped in pre-cleaned Al-foil and were loaded into the ^{14}C extraction system. Samples were pre-heated at ~500 °C for one hour before the sample gas was extracted at ~1600 °C in a platinum crucible (for details see Sliz et al., 2019). The extracted CO_2 gas was collected in glass ampoules held at the temperature of LN2. The extracted amounts of CO_2 from the samples were sufficient (>10 µg C) for reliable ^{14}C/^{12}C measurements in the AMS system. Each sample extraction was followed by a re-extraction at a slightly higher temperature to check for complete ^{14}C extraction from the samples. Since the re-extractions gave only low amounts of CO_2 and therefore low carbon, we added ^{14}C free CO_2 to produce samples with a sufficient amount of carbon for AMS measurements.

Measurements of the ^{14}C/^{12}C ratios were performed at the MICADAS at the Laboratory for the Analysis of Radiocarbon with AMS (LARA) at the Department of Chemistry, Biochemistry, and Pharmaceutical Sciences, University of Bern (Szidat et al., 2014; Szidat, 2020). Sample glass ampoules were introduced into the gas interface system (GIS) of the MICADAS, cracked

open, and the released CO_2 was mixed with helium. This mixture was then transferred to the gas ion source and was measured. In addition, the standard reference material (Oxalic acid II; NIST, Gaithersburg, USA) and blanks, were measured before and after the samples. The results from the AMS measurements, i.e., the $^{14}C/^{12}C$ ratios and the measured ^{14}C values, are given in fraction modern carbon ($F^{14}C$). The given uncertainties include the uncertainties related to the correction for isotope fractionation, blank subtraction, and standard normalization. In addition, a systematic uncertainty of 1.5‰ due to day-to-day variabilities is added to the data (Szidat et al., 2014). The ^{14}C activity concentrations (dpm/kg) were calculated based on the procedure described by Hippe et al. (2013) and Hippe and Lifton (2014).

Blank contributions were in the range of 1–3%. The ^{14}C yields in the re-extractions were typically low (<3% of total ^{14}C), except for Stubenberg, for which the re-extraction contributed ~50% to the total measured ^{14}C. This demonstrates that re-extractions are very important also for meteorite falls. Pt-crucibles was replaced every time after completing one batch of chondrite measurements. Measured ^{14}C concentrations in both procedural and system blanks, the raw ^{14}C data, and details about the calculation of ^{14}C activity concentrations, are given in Table 4.3 and 4.4 for H chondrite, L chondrites (Table 4.5 and 4.6), and for LL chondrites (Table 4.7 and 4.8), respectively. Final calculations for ^{14}C activity (dpm/kg) of samples are given in Table 4.9.

H_Chondrites

Table 4.3. ^{14}C concentration in the procedural and system blanks.

Blanks	Diluted CO_2 (10^{-2} cm^3)	C equi. (µg)	$F^{14}C$	$\delta^{13}C$ (‰)	$^{14}C/^{12}C$ (10^{-12})	N14 (10^4 at)
CB_3012	3.7 ± 0.03	18.7	0.135±0.004	-21.5	0.13±0.004	12.6±0.4
CB_0601	3.4 ± 0.03	16.8	0.145±0.006	-25.3	0.14±0.005	12.0±0.4
CB_1001	2.8 ± 0.02	14.0	0.723±0.011	-21.9	0.71±0.011	50.6±0.8
CB_0603	2.8 ± 0.02	14.0	0.113±0.005	-22.5	0.11±0.005	7.8±0.4
CB_1503	3.0 ± 0.02	14.8	0.257±0.007	-20.9	0.25±0.007	19.0±0.5
AB_0301	3.9 ± 0.03	19.69	0.237±0.005	-22.8	0.23±0.005	23.2±0.5
AB_0701	3.2 ± 0.03	16.01	0.202±0.005	-22.4	0.20±0.005	16.1±0.5
AB_0203	3.4 ± 0.03	16.95	0.434±0.007	-24.5	0.43±0.007	36.4±0.7
AB_0703	3.1 ± 0.03	15.50	0.143±0.005	-20.2	0.14±0.005	11.1±0.4
AB_0803	2.5 ± 0.02	12.67	0.089±0.005	-21.9	0.09±0.005	5.7±0.3
AB_1403	2.9 ± 0.02	14.47	0.147±0.005	-18.6	0.15±0.005	10.7±0.4

$F^{14}C$ is the fraction of modern carbon.
Average blank contributions of 1.01×10^5 ^{14}C atoms was applied to sample + re-extraction correction.

Table 4.4. ^{14}C concentration in the H chondrite samples and their re-extraction.

Meteorites	CO_2 (10^{-2} cm^3)	C (µg)	$F^{14}C$	$\delta^{13}C$ (‰)	$^{14}C/^{12}C$ (10^{-12})	N14 (10^6 at)	N14[a] (10^6 at)
Ochansk	2.9 ±0.02	14.3	12.92±0.07	-22.0	14.9±0.08	10.7±0.11	10.5±0.10
Reextraction	3.4 ±0.03	16.9	0.475±0.01	-22.3	0.54±0.01	0.46±0.01	0.26±0.01
Ehole	2.8 ±0.02	14.2	9.69±0.06	-23.1	11.2±0.07	7.9±0.08	7.80±0.01
Reextraction	3.3 ±0.03	16.6	1.228±0.01	-21.8	1.42±0.02	1.18±0.02	0.97±0.02
Farmville	36.0 ±0.3	181.6	0.891±0.01	-29.1	1.00±0.01	9.2±0.11	9.00±0.01
Reextraction	2.4 ±0.02	12	0.714±0.02	-28.6	0.81±0.02	0.49±0.01	0.28±0.01
Farmville[b]	4.5 ±0.4	22.5	7.840±0.04	-1.2	8.60±0.05	9.7±0.09	9.50±0.08
Reextraction	3.3 ±0.03	16.3	1.046±0.01	-14.6	1.11±0.01	0.91±0.01	0.83±0.02
Castalia	6.8 ±0.06	34.1	4.321±0.02	-26.7	4.90±0.03	8.4±0.08	8.30±0.01
Reextraction	3.4 ±0.03	16.8	1.397±0.01	-22.2	1.61±0.02	1.35±0.02	1.15±0.02
Al-Khadhaf	2.1 ±0.02	10.6	8.620±0.06	-23.2	9.90±0.06	5.3±0.06	5.20±0.01
Reextraction	2.0 ±0.02	10.1	1.021±0.02	-25.9	1.20±0.02	0.59±0.01	0.49±0.02
JaH 073	3.7 ±0.03	18.7	1.302±0.01	-16.7	1.40±0.01	1.30±0.01	1.10±0.02
Reextraction	3.7 ±0.03	14.0	0.279±0.01	-22.9	0.29±0.01	0.21±0.01	0.13±0.01

[a] N14 is the number of ^{14}C atoms after blank corrections.
[b] Farmville unleached sample re-extraction

L_Chondrites

Table 4.5. ^{14}C concentration in the procedural and system blanks.

Blanks	Diluted CO_2 (10^{-2} cm^3)	C equi. (µg)	$F^{14}C$	$\delta^{13}C$ (‰)	$^{14}C/^{12}C$ (10^{-12})	N14 (10^4 at)
CB_1402	3.0 ± 0.03	15.0	0.243±0.005	-22.2	0.24±0.005	18.2±0.4
CB_2002	3.0 ± 0.02	14.8	0.117±0.002	-11.3	0.12±0.002	8.8±0.2
CB_2102	2.9 ± 0.02	14.3	0.384±0.008	-11.7	0.39±0.008	28.0±0.6
CB_2802	2.8 ± 0.02	14.2	0.261±0.005	-12.2	0.26±0.005	18.8±0.4
CB_0403	2.9 ± 0.02	14.5	0.306±0.006	-10.2	0.31±0.006	22.7±0.5
CB_1303	2.5 ± 0.02	12.2	0.219±0.004	-7.4	0.22±0.005	13.8±0.3
AB_1402	2.6 ± 0.03	13.0	0.313±0.008	-22.9	0.31±0.008	20.3±0.6
AB_2702	2.9 ± 0.03	14.6	0.851±0.013	-17.1	0.86±0.013	62.5±1.0
AB_2902	3.0 ± 0.03	14.8	0.578±0.011	-15.3	0.58±0.011	43.2±0.8
AB_0503	2.4 ± 0.03	12.2	0.441±0.012	-10.2	0.45±0.012	27.4±0.8
AB_1103	2.6 ± 0.02	13.0	0.411±0.009	-11.2	0.42±0.009	27.3±0.6
AB_1303	2.0 ± 0.02	10.1	0.208±0.010	-10.6	0.21±0.009	10.7±0.5

$F^{14}C$ is the fraction of modern carbon.
Average blank contributions of 1.01×10^5 ^{14}C atoms was applied to sample + re-extraction correction.

Table 4.6. ^{14}C concentration in the L chondrite samples and re-extractions.

Meteorites	CO_2 (10^{-2} cm^3)	C equi. (µg)	$F^{14}C$	$\delta^{13}C$ (‰)	$^{14}C/^{12}C$ (10^{-12})	N14 (10^6 at)	N14[a] (10^6 at)
Ausson	7.7 ± 0.06	38.5	4.90±0.03	-34.3	5.50±0.08	10.6±0.11	10.3±0.10
Reextraction	2.9 ± 0.07	14.4	0.564±0.01	-22.9	0.65±0.01	0.47±0.01	0.26±0.01
Kandahar	4.3 ± 0.04	21.6	9.35±0.05	-28.2	10.6±0.07	11.3±0.11	11.2±0.11
Reextraction	2.6 ± 0.06	13.1	0.802±0.01	-14.4	0.94±0.01	0.62±0.02	0.41±0.02
Leedey	6.0 ± 0.05	30.1	6.10±0.03	-34.9	6.90±0.01	10.3±0.10	10.0±0.09
Reextraction	2.5 ± 0.06	12.7	0.954±0.02	-15.8	1.10±0.02	0.71±0.02	0.50±0.01
Suizhou	8.3 ± 0.07	41.4	5.08±0.03	-33.9	5.70±0.03	11.9±0.12	11.6±0.11
Reextraction	2.8 ± 0.06	13.8	0.974±0.01	-17.5	1.10±0.02	0.78±0.02	0.58±0.02
Tennasilm	4.5 ± 0.04	22.6	6.15±0.06	-33.9	6.90±0.06	7.80±0.08	7.50±0.07
Reextraction	2.6 ± 0.06	12.8	0.846±0.01	-12.8	0.99±0.02	0.64±0.02	0.43±0.02
Tennasilm[b]	4.3 ± 0.04	21.7	9.29 ± 0.05	-7.5	10.3±0.06	11.2±0.11	11.1±0.13
Reextraction	3.3 ± 0.03	16.4	0.433±0.01	-15.0	0.46±0.01	0.38±0.01	0.30±0.01
Antonin	1.5 ± 0.01	7.7	12.62±0.11	-22.5	14.5±0.02	5.60±0.07	5.30±0.06
Reextraction	2.3 ± 0.06	11.4	1.351±0.03	-9.8	1.60±0.03	0.91±0.03	0.70±0.02
Renchen	3.5 ± 0.03	17.6	6.94±0.03	-24.9	7.90±0.04	7.00±0.07	6.80±0.10
Reextraction	3.2 ± 0.03	16.1	0.547±0.01	-24.2	0.63±0.01	0.51±0.01	0.31±0.01

[a] N14 is the number of ^{14}C atoms after blank corrections. [b] Tennasilm unleached sample re-extraction.

LL_Chondrites

Table 4.7. ^{14}C concentration in the procedural and system blanks.

Blanks	Diluted CO_2 (10^{-2} cm^3)	C equi. (µg)	$F^{14}C$	$\delta^{13}C$ (‰)	$^{14}C/^{12}C$ (10^{-12})	N14 (10^4 at)
CB_1604	14.2 ±0.12	70.9	0.063±0.003	-25.0	0.06±0.003	22.3±1.0
CB_1605	2.7 ± 0.02	13.6	0.024±0.003	-27.4	0.02±0.003	1.6±0.2
CB_2205	2.9 ± 0.02	14.6	0.124±0.005	-21.9	0.12±0.005	9.0±0.3
CB_2305	3.2 ± 0.03	16.0	0.072±0.004	-23.3	0.07±0.004	5.7±0.3
CB_2905	3.3 ± 0.03	16.3	0.269±0.005	-23.8	0.26±0.005	2.2±0.5
CB_1805	3.0 ± 0.02	15.1	0.019±0.003	-25.0	0.19±0.003	1.4±0.2
AB_1604	2.7 ± 0.02	13.3	0.275±0.007	-20.8	0.27±0.007	18.2±0.5
AB_1605	3.4 ± 0.03	17.0	0.098±0.004	-21.7	0.09±0.004	8.3±1.3
AB_2105	3.2 ± 0.03	15.8	0.086±0.004	-22.9	0.08±0.004	6.7±0.3
AB_2205	1.9 ± 0.02	9.4	0.033±0.005	-25.9	0.03±0.005	1.5±0.2
AB_2405	3.0 ± 0.02	14.8	0.077±0.004	-22.9	0.08±0.004	5.7±0.3
AB_2905	2.6 ± 0.02	13.1	0.288±0.008	-23.4	0.28±0.008	18.8±0.5

$F^{14}C$ is the fraction of modern carbon.
Average blank contributions of 1.01×10^5 ^{14}C atoms was applied to sample + re-extraction correction.

Table 4.8. ^{14}C concentration in the LL chondrites samples and their re-extractions.

Meteorites	CO_2 (10^{-2} cm^3)	C equi. (µg)	$F^{14}C$	$\delta^{13}C$ (‰)	$^{14}C/^{12}C$ (10^{-12})	N14 (10^6 at)	N14[a] (10^6 at)
Kilabo	8.4 ±0.07	41.7	4.146±0.02	-29.4	4.71±0.02	9.80±0.09	9.70±0.15
Reextraction	2.4 ±0.02	12.2	0.528±0.01	-15.3	0.62±0.01	0.38±0.01	0.27±0.01
Mangwendi	7.6 ±0.06	37.7	4.803±0.02	-32.3	5.42±0.02	10.2±0.09	10.1±0.16
Reextraction	2.9 ±0.02	14.7	0.489±0.01	-24.9	0.56±0.01	0.41±0.01	0.31±0.01
Sulagiri	5.4 ±0.04	27.0	5.063±0.03	-23.6	5.82±0.03	7.90±0.02	7.80±0.13
Reextraction	3.0 ±0.02	15.0	1.864±0.02	-28.0	2.12±0.02	1.60±0.02	1.49±0.05
JaH 073	1.7 ±0.01	8.4	2.439±0.03	-24.1	2.80±0.04	1.20±0.02	1.10±0.02
Reextraction	2.7 ±0.02	13.4	0.223±0.01	-23.0	0.26±0.02	0.72±0.01	0.07±0.01
Moshampa	1.6 ±0.02	8.1	19.59±0.13	-25.2	22.4±0.15	9.20±0.09	9.10±0.15
Reextraction	3.3 ±0.03	16.3	1.155±0.01	-22.8	1.33±0.01	1.09±0.01	0.99±0.03
Stubenberg	4.1 ±0.03	20.2	3.701±0.02	-26.7	4.22±0.02	4.30±0.04	4.10±0.01
Reextraction	3.1 ±0.03	15.5	2.239±0.02	-22.6	2.58±0.02	2.01±0.02	1.80±0.03

[a] N14 is the number of ^{14}C atoms after blank corrections.

Table 4.9. Measured ^{14}C atoms and activity concentrations for the studied meteorites.

Sample ID	Mass (mg)	C (µg)	CO_2 (cm^3)	$N14^b$ $\times 10^6$	N14r $\times 10^6$	$N14_T$ $\times 10^6$	N14/g $\times 10^8$	A14 dpm/kg	A14* dpm/kg
Ochansk	48.50	14.30	0.028	10.5	0.262	10.8	2.22	51.38	48.94
Ehole	50.20	13.77	0.028	7.78	0.981	8.75	1.74	40.34	38.42
Farmville	50.20	181.6	0.363	9.00	0.284	9.29	1.85	42.79	40.76
Castalia	50.30	33.02	0.068	8.27	1.153	9.42	1.87	43.31	41.25
Al-Khadhaf	56.40	10.64	0.021	5.19	0.485	5.68	1.01	23.30	n.a.
Stubenberg	50.20	19.58	0.040	4.11	1.801	5.91	1.18	27.25	25.95
Renchen	50.40	17.01	0.035	6.83	0.301	7.13	1.42	32.74	31.19
Ausson	46.60	38.46	0.077	10.3	0.264	10.6	2.26	52.40	49.70
Kandahar	50.27	21.59	0.043	11.1	0.412	11.5	2.29	52.99	50.26
Leedey	50.24	30.06	0.060	10.1	0.503	10.6	2.11	48.73	46.23
Suizhou	50.30	41.43	0.083	11.6	0.579	12.2	2.43	56.22	53.33
Tennasilm	50.50	22.55	0.045	7.58	0.430	8.01	1.59	36.71	34.82
Antonin	50.10	7.69	0.015	5.22	0.704	5.92	1.18	27.34	25.94
Kilabo	50.39	41.72	0.084	9.75	0.276	10.0	1.99	46.01	43.44
Mangwendi	50.66	37.70	0.076	10.1	0.309	10.5	2.06	47.72	45.08
Sulagiri	50.65	26.98	0.054	7.77	1.490	9.26	1.83	42.33	39.95
Moshampa	48.26	8.13	0.016	9.05	0.987	10.0	2.08	48.12	n.a.

Note: C content (µg) is the amount of C introduced in the gas ion source of the AMS. $F^{14}C$ is the Fraction of modern ^{14}Carbon.

Ab14 is the absolute $^{14}C/^{12}C$ ratio.

N14 is the number of ^{14}C atoms (10^6) measured in the samples.

$N14^b$ is the blank corrected number of ^{14}C atoms after correcting for blanks produced in extraction line.

N14r is the number of ^{14}C atoms (10^6) measured in the re-extractions. $N14_T$ is total number of ^{14}C, i.e., sum of N14 from samples and re-extractions.

*mass-loss corrected activities, where mass correction factor for H, L and LL-chondrites are 4.9%, 5.2% and 5.6%, respectively. Al-Khadhaf and Moshampa were not leached.

4.3. Results for Noble Gases, ^{10}Be, and ^{14}C Activity concentrations

4.3.1. *Mass Losses of Leached Samples*

Although all studied meteorites are falls, we decided to leach them for two reasons. *First*, the results should be fully consistent with the samples usually studied, which are weathered and altered, and require leaching before analysis. *Second*, studies have shown that even a short terrestrial age (e.g., a few years) can lead to surface contamination or weathering effects on meteorites, necessitating leaching to remove altered material and ensure accurate analysis. The leaching procedure removes carbonates, organic compounds, and metal oxides, that were formed in the weathering process and/or due to rapid oxidation of metallic Fe. The rapid oxidation of metallic Fe has been demonstrated by Pillinger et al. (2013) using the (L/LL6) Holbrook meteorite. These authors found that the Holbrook fragments show increasing degree of weathering with increasing time they spent in the field. For example, samples that were collected immediately after its fall in 1912 are less altered than pieces found almost 100 years later that have suffered exchange of oxygen, and oxidation of metal and troilite.

The sometimes-substantial amounts of ^{14}C extracted from meteorites at low temperatures are supposed to originate from secondary CO_2 accumulation, resulting from atmospheric exchange during storage, either in our collections or in the field (Cresswell et al., 1993; Jull et al., 1984). As an example, studies on fresh meteorite falls and Antarctic meteorites (low weathering) clearly indicated that the samples contain secondary ^{14}C, termed weathering components (Cresswell et al., 1993; Jull et al., 1984). The weathering components in the L6 Bruderheim meteorite extracted at low temperatures also indicate a substantial contribution to the total ^{14}C from secondary CO_2 accumulation (Cresswell et al., 1993). The importance to remove such weathering products even in relatively fresh meteorite falls was clearly demonstrated for the Holbrook meteorite. The ^{14}C activity concentration reported by Jull et al. (1989) for a non-treated sample with no pre-heating was 67.5 ± 0.5 dpm/kg. For a second sample a pre-heating step at 500°C was performed, which reduced the measured activity concentration to 58.9 ± 0.5 dpm/kg. Both values are much higher than expected for typical L/LL chondrites. In a later study (Jull et al., 1998), the Holbrook sample was treated with phosphoric acid to remove weathering products and the resulting much lower ^{14}C activity concentration of 44 ± 1 dpm/kg is in much better agreement with the expected values for L/LL chondrites. Minami et al. (2006) also measured ^{14}C in Holbrook samples using a similar procedure as Jull et al. (1998), i.e., with phosphoric acid treatment. The results were 53.6 ± 0.7 and 54.4 ± 0.8 dpm/kg, which is 18–19% higher than the value reported by Jull et al. (1998). The discrepancy could either be due to the fact that both studies used different pieces from different shielding locations and/or, that

the leaching procedure used by Minami et al. (2006) was not efficient enough to fully remove carbonate contamination.

The effects of the leaching procedure on the composition of the studied samples have already been discussed by Mészáros et al. (2018). However, in their study weathered hot desert meteorites were studied and, even more important, the 125–250 μm grain size fraction was used. For most of our samples, however, we did not have enough material to select only this grain size fraction. Therefore, our samples also contain smaller grains, which made it necessary to re-visit the leaching procedure. In future studies, however, measuring the terrestrial ages of valuable meteorites, limited sample mass may often be an issue and the present study of leaching effects on samples of small grain size is relevant.

Leached and unleached samples of Farmville, Ehole, Kandahar, Leedey, and Sulagiri were analyzed for their chemical composition. The results (in wt%) are summarized in Table 4.4. Since leaching with 6M HCl potentially dissolves troilites, thereby further reducing the total iron content, the silicate-metal ratio is of most interest. To calculate the compositional changes (mainly the Mg-Fe ratio) caused by the leaching procedure, we follow the methodology from Mészáros et al. (2018). The results are summarized in Table 4.5. Briefly, some of the iron is incorporated into mafic silicates and some is in metal and troilites. We further assume that all the magnesium is in mafic silicates and none is in the secondary alteration products. Based on these assumptions, Mg# = Mg / (Mg + Fe) of the mafic silicates can be calculated. In fact, the Mg# of the mafic silicates should not be affected by the leaching process. In contrast, the Mg# of the bulk sample increases from being unleached to being leached because some of the total iron has been removed by dissolution of oxides and hydroxides. In addition, iron from metal and troilites might has been dissolved as well. In ordinary chondrites, about half of the total iron is contained in mafic silicates, with an average of 48% in H chondrites, 52% in L chondrites, and 57% in LL chondrites, and the rest is in metal and troilite (see Jarosewich, 1990). Following the procedure of Mészáros et al. (2018), the amount of iron in mafic silicates and the amount of iron in metal and troilite before and after leaching are calculated (see Table 4.5). If this value is positive, there is no over-leaching of the sample. For the studied samples, between 0.4% (Sulagiri) and 2.6% (Kandahar) of iron remained in the metal and troilite fraction after leaching, which is consistent with the results of Mészáros et al. (2018) and Al-Kathiri et al. (2005).

Table 4.10. Major Element concentration (wt.%) in the studied meteorites.

Samples	Type	Fe	Mg	Si	Ca	Na	Ni	Mn	Cr	Co	Al
FUL <128 µm	H4	12.3	17.6	13.6	1.6	0.82	0.61	0.26	0.38	0.007	1.05
FL <128 µm	H4	8.1	17.5	23.8	1.3	1.78	0.77	0.3	0.67	0	1.99
EUL <128 µm	H4	15	17.6	16.2	1.1	0.73	0.65	0.26	0.35	0.018	1.12
EL <128 µm	H5	7.9	13.8	14.2	2.1	0.57	1.06	0.22	0.46	0.005	0.99
ER >200 µm	H5	70.3	2.7	6.7	0.6	0.25	5.5	0.05	0.11	0.391	0.28
EL 128-200 µm	H5	12.3	17.5	19.3	3.8	0.74	0.76	0.29	0.24	0.018	1
KUL <128 µm	L6	12.5	14	18.8	1.2	0.98	0.77	0.22	0.2	0.012	0.87
KL <128 µm	L6	8.2	12	9.1	1.3	1.15	0.18	0.22	0.53	0.002	1.62
KUL 128-200µm	L6	15.7	14.7	5.1	0.5	0.55	1.08	0.25	0.22	0.019	0.81
KR >200 µm	L6	42	9.5	21.4	1.9	0.77	5.84	0.16	0.16	0.258	0.48
LUL <128 µm	L6	17.9	17.3	13.6	1.9	0.66	0.69	0.28	0.41	0.022	0.9
LL <128 µm	L6	9.1	13.9	8.9	1.4	1.05	0.34	0.24	0.48	0.003	1.46
LUL 128-200 µm	L6	20.7	14.7	23.3	0.5	1.08	1.77	0.26	0.31	0.037	0.99
LR >200 µm	L6	44.5	8.2	17.2	0.7	0.56	4.56	0.15	0.27	0.28	0.69
SZUL <128 µm	L6	14.5	14.7	6.1	1.3	0.94	0.57	0.24	0.24	0.02	1.39
SZL <128 µm	L6	0.8	1.8	12.1	1.1	0.24	0.05	0.03	0.04	0	0.16
SUL <128 µm	LL5	13.9	13.8	6.4	1.2	0.58	0.47	0.21	0.34	0.017	0.82
SL <128 µm	LL5	8.2	13.6	23	1.7	1.26	0.15	0.23	0.45	0.002	1.5

FUL= Farmville unleached, FL= Farmville Leached, EUL= Ehole unleached, EL= Ehole leached, ER= Ehole residual (grain size> 200µm, mostly metals), KUL= Kandahar unleached, KL= Kandahar leached, KR= Kandahar residual (mainly metals), LUL= Leedey unleached, LL= Leedey leached, LR= Leedey residual, SZUL= Suizhou unleached, SZL= Suizhou leached, SUL= Sulagiri unleached, SL= Sulagiri leached

Table 4.11. Results for the changes in Fe and Mg (wt.%) due to leaching.

Samples	Fe (total)	Mg (total)	Fe (silicates)	Mg# (bulk)	Mg# (silicates)	Fe (metal)
Farmville, unleached, <128 µm	12.3	17.6	5.9	58.9	74.9	6.4
Farmville, leached, <128 µm	8.1	17.5	5.9	68.4	74.9	2.2
Ehole, unleached, <128 µm	15.1	17.6	7.2	53.8	70.8	7.9
Ehole, leached, <128 µm	7.9	13.8	5.7	63.6	70.8	2.2
Kandahar, unleached, <128 µm	12.5	14.0	6.5	52.8	68.3	6.0
Kandahar, leached, <128 µm	8.2	12.0	5.6	59.4	68.3	2.6
Leedey, unleached, <128 µm	17.9	17.3	9.3	49.2	65.0	8.6
Leedey, leached, <128 µm	9.1	13.9	7.5	60.4	65.0	1.6
Sulagiri, unleached, <128 µm	13.9	13.8	7.9	49.8	63.5	6.0
Sulagiri, leached, <128 µm	8.2	13.6	7.8	62.4	63.5	0.4

Mass loss = unleached Fe (metal) – leached Fe (metal), e.g., Farmville: 5.9 – 1.7 = 4.2%. Fe (silicates) and Fe (metal + troilite) are in wt.%. Fe (silicates) in unleached samples are calculated assuming 48% of the total Fe in silicates of H chondrites, 52% in L chondrites and 57% in LL chondrites (Jarosewich, 1990). Therefore, Fe (metal + troilite) is given as Fe (total) – Fe (silicates). Mg# (silicates) and Mg# (bulk) are relative wt.% calculated following Meszaros et al. (2018). Finally, Fe loss % is given by the differences in Fe (metal + troilite) between unleached and leached samples. The adopted Fe (metal + troilite) losses are 4.9% for H, 5.2% for L, and 5.6% for LL chondrites, respectively.

Almost all of the ^{14}C and most of the ^{10}Be are incorporated into the silicate phase, which is not affected by the leaching procedure. Therefore, there is no loss of ^{14}C and/or ^{10}Be from the sample due to leaching. However, some of the iron from metal and troilite was lost during leaching and this mass loss must be considered when reporting the activity concentrations, i.e., activities per gram of sample. Doing so, we consider the loss of iron (metal + troilite), which ranges from 3.4% for Kandahar to 7.0% for Leedey. The average mass loss of metallic iron determined for Farmville and Ehole is 4.9%. This value is applied to all H chondrites in this study. The average mass loss for Kandahar and Leedey of 5.2% is used for all L chondrites, and the mass loss of 5.6% determined for Sulagiri is applied to all LL chondrites. In the following discussion, the measured ^{14}C and ^{10}Be activities and noble gas concentrations have been corrected for mass loss and therefore best represent the values expected for bulk samples.

4.3.2. *Helium and Ne Concentrations and Isotopic Ratios*

The He and Ne concentrations and isotope ratios are compiled in Table 4.6 for H chondrites, Table 4.7 for L chondrites, and Table 4.8 for LL chondrites. The data are per gram of sample material after leaching, i.e., the mass loss due to leaching (see above) is not taken into account. The data are therefore not directly comparable to data from other studies, though changes due to leaching induced mass losses are small. The last column in Tables 4.6, 4.7, and 4.8 gives the cosmogenic ^{21}Ne concentrations ($^{21}Ne_{cos}$) corrected for mass loss during leaching. Note that the isotopic ratios are not affected by such mass losses. For all samples, two aliquots were measured.

The measured (uncorrected) ^{3}He concentrations (in units 10^{-8} cm^3STP/g) range from 8.80 ± 0.46 in Leedey-2 to 97.6 ± 5.0 in Ausson-2. Cosmogenic $^{4}He_{cos}$ are calculated via $(^{4}He/^{3}He)_{cos}$ = 6 (Alexeev, 1998; Leya and Masarik, 2009) and assuming that the measured ^{3}He to be entirely cosmogenic. The latter is justified considering that all Ne isotope ratios are very close to cosmogenic (see below). The thus calculated $^{4}He_{cos}$ contributes less than ~30% to the measured ^{4}He concentrations, indicating that the measured ^{4}He is predominantly of radiogenic origin. Measured (uncorrected) ^{20}Ne concentrations (in 10^{-8} cm^3STP/g) range from 1.45 ± 0.19 in Leedey-2 to 20.6 ± 2.6 in Moshampa. The $^{20}Ne/^{22}Ne$ ratios vary from 0.775 ± 0.020 (Leedey-2) to 1.022 ± 0.06 (Moshampa), indicating that the measured Ne is dominated by cosmogenic contributions.

Cosmogenic $(^{22}Ne/^{21}Ne)_{cos}$ and $^{21}Ne_{cos}$ values are calculated using a two-component-deconvolution assuming air ($^{20}Ne/^{22}Ne$ = 9.8 and $^{21}Ne/^{22}Ne$ = 0.02878) and cosmogenic

($^{20}Ne/^{22}Ne$ = 0.81) as endmembers. For two samples (Ausson-2, Leedey-2), the measured $^{20}Ne/^{22}Ne$ ratios are lower than the assumed cosmogenic endmember of 0.81. For these samples no corrections were applied. The uncertainties given for $^{21}Ne_{cos}$ and $(^{22}Ne/^{21}Ne)_{cos}$ are either the raw uncertainties from the noble gas measurements, including counting statistics, extrapolation of the signal back to the time of gas inlet, corrections for blanks, interference, and fractionation plus assigned systematic uncertainties (see above), or half of the size of the correction applied for removing remaining air contamination, whatever is larger. The $^{21}Ne_{cos}$ concentrations (in 10^{-8} cm^3STP/g) range from 1.65 ± 0.21 (Leedey-2) to 22.1 ± 1.4 (Ausson-2). The reproducibility for $^{21}Ne_{cos}$ and $(^{22}Ne/^{21}Ne)_{cos}$ among the different aliquots is always within the 1σ standard deviations, the only exception is Ehole, for which the two aliquots differ by 30%, i.e., about 3σ. Thanks to the good reproducibility, we could calculate average $(^{22}Ne/^{21}Ne)_{cos}$ ratios and $^{21}Ne_{cos}$ concentrations, using the uncertainties as weights (Tables 4.6, 4.7, and 4.8).

Table 4.12. He and Ne isotope concentrations, cosmogenic ^{21}Ne, $(^{22}Ne/^{21}Ne)_{cos}$ and CRE ages for the studied H chondrites.

Meteorite	Mass (mg)	Concentrations are in 10^{-8} cm^3STP/g[1)]								
		^3He	^4He	^{20}Ne	$^{20}Ne/^{22}Ne$	$^{21}Ne/^{22}Ne$	$(^{22}Ne/^{21}Ne)_{cos}$	$^{21}Ne_{cos}$[1)]	$^{21}Ne_{cos}$(bulk)[2)]	T_{21} (Ma)
Castalia - 1	20.30	32.80 ± 2.8	1506 ± 110	7.37 ± 0.61	0.886 ± 0.024	0.900 ± 0.020	1.102 ± 0.024	7.49 ± 0.57	7.10 ± 0.54	21.6 ± 2.4
Castalia - 2	20.50	32.60 ± 1.7	1548 ± 68	7.05 ± 0.43	0.904 ± 0.018	0.900 ± 0.018	1.099 ± 0.022	7.01 ± 0.32	6.65 ± 0.31	19.9 ± 1.3
Mean Castalia		**32.70 ± 1.5**	**1536 ± 58**				**1.100 ± 0.016**	**7.13 ± 0.28**		**20.3 ± 1.1**
Ehole - 1	20.50	8.87 ± 0.75	322 ± 23	4.38 ± 0.37	0.882 ± 0.022	0.898 ± 0.019	1.102 ± 0.024	4.46 ± 0.45	4.24 ± 0.42	12.9 ± 1.8
Ehole - 2	20.35	28.20 ± 1.5	1380 ± 61	5.28 ± 0.30	0.809 ± 0.016	0.882 ± 0.018	1.134 ± 0.023	5.76 ± 0.24	5.46 ± 0.23	19.9 ± 1.3
Mean Ehole		**-**	**-**				**1.119 ± 0.017**	**5.07 ± 0.21**		**-**
Farmville - 1	20.60	9.32 ± 0.78	1401 ± 100	2.59 ± 0.23	0.982 ± 0.026	0.893 ± 0.019	1.099 ± 0.024	2.36 ± 0.19	2.24 ± 0.18	6.69 ± 0.8
Farmville - 2	19.60	9.04 ± 0.48	1437 ± 63	1.97 ± 0.19	0.814 ± 0.017	0.907 ± 0.018	1.102 ± 0.022	2.20 ± 0.19	2.08 ± 0.18	6.32 ± 0.8
Mean Farmville		**9.28 ± 0.41**	**1428 ± 53**				**1.101 ± 0.016**	**2.28 ±0.13**		**6.50 ± 0.6**
Ochansk - 1	20.01	9.68 ± 0.82	1448 ± 103	2.26 ± 0.23	1.013 ± 0.030	0.902 ± 0.019	1.084 ± 0.023	2.01 ± 0.19	1.91 ± 0.18	$\bar{5}.\bar{2}\bar{5} \pm \hat{0}.\bar{7}$
Ochansk - 2	20.26	9.83 ± 0.52	1603 ± 71	2.23 ± 0.18	0.819 ± 0.017	0.916 ± 0.019	1.091 ± 0.022	2.49 ± 0.18	2.36 ± 0.17	6.76 ± 0.7
Mean Ochansk		**9.78 ± 0.44**	**1553 ± 58**				**1.088 ± 0.016**	**2.26 ± 0.13**		**6.00 ± 0.5**
Al-Khadhaf[a]	48.50	11.2 ± 0.86	1414 ± 133	1.43 ± 0.09	0.843 ± 0.036	0.801 ± 0.017	1.244 ± 0.022	1.36 ± 0.10	n.a.	8.53 ± 0.9

1)The concentrations are not corrected for mass loss during leaching, 2) concentration corrected for mass loss (~5%) during leaching. [a]Measurements for Al-Khadhaf was performed in an unleached sample material. n.a. = not applicable

Table 4.13. He and Ne isotope concentrations, cosmogenic ^{21}Ne, $(^{22}Ne/^{21}Ne)_{cos}$ and CRE ages for the studied L and LL chondrites.

Meteorite	Mass (mg)	Concentrations are in 10^{-8} cm^3STP/g[1)]								
		^{3}He	^{4}He	^{20}Ne	$^{20}Ne/^{22}Ne$	$^{21}Ne/^{22}Ne$	$(^{22}Ne/^{21}Ne)_{cos}$	$^{21}Ne_{cos}$ [1)]	$^{21}Ne_{cos}$ [2)]	T_{21} (Ma)
Ausson - 1	20.70	91.4 ± 7.6	1801 ± 129	18.30 ± 1.5	0.859 ± 0.021	0.921 ± 0.020	1.080 ± 0.024	19.6 ± 1.5	18.6 ± 1.5	49.7 ± 1.1
Ausson - 2	20.31	97.6 ± 5.0	1837 ± 81	18.40 ± 1.4	0.781 ± 0.016	0.937 ± 0.019	1.068 ± 0.021	22.1 ± 1.4	21.0 ± 1.4	46.2 ± 0.9
Mean Ausson		**95.7 ± 4.2**	**1827 ± 69**				**1.073 ± 0.016**	**20.9 ± 1.0**		**48.1 ± 3.4**
Leedey - 1	20.55	10.2 ± 0.9	585 ± 42	1.88 ± 0.2	0.852 ± 0.023	0.871 ± 0.019	1.144 ± 0.025	1.9 ± 0.2	1.8 ± 0.5	6.53 ± 0.8
Leedey - 2	20.30	8.8 ± 0.5	499 ± 22	1.45 ± 0.2	0.775 ± 0.020	0.879 ± 0.018	1.137 ± 0.023	1.7 ± 0.2	1.6 ± 0.2	5.37 ± 1.0
Mean Leedey		**9.1 ± 0.4**	**518 ± 25**				**1.140 ± 0.025**	**1.8 ± 0.1**		**6.10 ± 0.6**
Tennasilm - 1	20.30	29.1 ± 2.5	1519 ± 110	5.43 ± 0.5	0.900 ± 0.023	0.875 ± 0.019	1.132 ± 0.024	5.3 ± 0.4	5.1 ± 0.4	16.7 ± 1.9
Tennasilm - 2	20.68	29.4 ± 1.5	1568 ± 69	5.57 ± 0.4	0.861 ± 0.018	0.871 ± 0.017	1.142 ± 0.023	5.6 ± 0.3	5.4 ± 0.3	18.9 ± 1.5
Mean Tennasilm		**29.3 ± 1.3**	**1554 ± 58**				**1.137 ± 0.017**	**5.5 ± 0.2**		**18.1 ± 1.2**
Kandahar - 1	21.10	36.0 ± 3.1	994 ± 71	7.48 ± 0.6	0.856 ± 0.025	0.921 ± 0.023	1.081 ± 0.027	8.1 ± 0.6	7.7 ± 0.6	19.2 ± 2.2
Kandahar - 2	23.90	33.9 ± 1.8	1025 ± 45	7.65 ± 0.4	0.839 ± 0.017	0.911 ± 0.018	1.094 ± 0.022	8.3 ± 0.3	7.9 ± 0.3	21.3 ± 1.2
Mean Kandahar		**34.4 ± 1.6**	**1016 ± 38**				**1.089 ± 0.017**	**8.2 ± 0.3**		**20.8 ± 1.1**
Suizhou - 1	20.12	44.8 ± 3.7	829 ± 59	9.71 ± 0.8	0.896 ± 0.030	0.970 ± 0.027	1.021 ± 0.029	10.5 ± 0.9	10.0 ± 0.9	19.1 ± 2.5
Suizhou - 2	20.44	44.3 ± 2.3	781 ± 34	9.71 ± 0.5	0.866 ± 0.017	0.938 ± 0.019	1.059 ± 0.021	10.5 ± 0.4	10.0 ± 0.4	22.5 ± 1.5
Mean Suizhou		**44.4 ± 2.0**	**793 ± 29**				**1.046 ± 0.017**	**10.5 ± 0.4**		**21.6 ± 1.3**
Kilabo - 1	20.76	43.5 ± 3.6	1024 ± 73	10.10 ± 0.8	0.915 ± 0.02	0.898 ± 0.019	1.102 ± 0.023	9.9 ± 0.7	9.3 ± 0.7	25.7 ± 2.7
Kilabo - 2	20.49	48.0 ± 2.5	1098 ± 48	10.50 ± 0.6	0.885 ± 0.02	0.900 ± 0.018	1.103 ± 0.022	10.6 ± 0.4	10.0 ± 0.4	27.8 ± 1.6
Mean Kilabo		**46.5 ± 2.1**	**1074 ± 40**				**1.103 ± 0.016**	**10.4 ± 0.4**		**27.3 ± 1.4**
Mangwendi -1	20.40	18.7 ± 1.6	744 ± 53	3.61 ± 0.3	0.858 ± 0.02	0.883 ± 0.019	1.126 ± 0.024	3.7 ± 0.3	3.5 ± 0.3	11.1 ± 1.2
Mangwendi -2	21.25	19.4 ± 1.0	746 ± 33	3.57 ± 0.3	0.817 ± 0.02	0.883 ± 0.018	1.132 ± 0.023	3.9 ± 0.2	3.6 ± 0.2	11.9 ± 1.1
Mean Mangwendi		**19.2 ± 0.8**	**745 ± 28**				**1.129 ± 0.017**	**3.8 ± 0.2**		**11.5 ± 0.8**
Sulagiri - 1	20.80	27.3 ± 2.3	714 ± 51	7.19 ± 0.6	0.891 ± 0.02	0.926 ± 0.020	1.070 ± 0.023	7.5 ± 0.6	7.1 ± 0.5	16.4 ± 1.8
Sulagiri - 2	20.55	27.0 ± 1.4	733 ± 33	6.84 ± 0.4	0.863 ± 0.02	0.922 ± 0.018	1.078 ± 0.022	7.3 ± 0.4	6.9 ± 0.3	16.7 ± 1.2
Mean Sulagiri		**27.1 ± 1.2**	**727 ± 28**				**1.074 ± 0.019**	**7.4 ± 0.3**		**16.6 ± 1.0**
Moshampa	20.12	79.4 ± 6.9	2540 ± 122	20.59 ± 2.6	1.022 ± 0.06	0.925 ± 0.020	1.057 ± 0.02	18.6 ± 2.7	n.a.	38.2 ± 2.7

1) The concentrations are not corrected for mass loss during leaching, 2) concentration corrected for mass loss during leaching.

4.3.3. *Cosmic Ray Exposure Ages (T_{21}) and ($^{22}Ne/^{21}Ne$) Ratios*

The cosmic ray exposure ages are calculated from measured $^{21}Ne_{cos}$ and $(^{22}Ne/^{21}Ne)_{cos}$ using the correlations for H, L, and LL chondrites given by Dalcher et al. (2013). The results are given in Table 4.9. The following discussions are based on average CRE ages for the samples, i.e., the data for the two aliquots were averaged using the uncertainties as weights.

H Chondrites: The T_{21} age for Castalia of 20.3 ± 1.1 Ma agrees with the CRE ages of 20.5 Ma and 23.8 Ma given by Schultz and Weber (1996). There are, however, slight differences in $(^{22}Ne/^{21}Ne)_{cos}$. We measured a ratio of 1.100 ± 0.016, whereas Schultz and Weber (1996) reported a slightly higher value of 1.119. The difference suggests that both samples likely came from different shielding depths from within the Castalia meteorite, which was likely an object with a pre-atmospheric radius in the range 30–40 cm.

The CRE age for the first Ehole aliquot of 12.9 ± 1.8 Ma is significantly lower than T_{21} = 19.9 ± 1.3 Ma for the second aliquot. The latter, however, is in good agreement with a previously reported value of 18.5 Ma (see Graf and Marti, 1995). The average $(^{22}Ne/^{21}Ne)_{cos}$ ratio of 1.119 ± 0.017 agrees within the uncertainties with the ratios in the range 1.129–1.134 compiled by Schultz and Franke (2004), indicating that Ehole was an object with a pre-atmospheric radius of about 20–30 cm.

For Farmville, the calculated CRE age of 6.5 ± 0.6 Ma is slightly lower but agrees within the 1σ uncertainties with the age of 7.4 ± 0.9 Ma given by Eugster et al. (1993). The $(^{22}Ne/^{21}Ne)_{cos}$ ratio of 1.101 ± 0.016 measured for Farmville is slightly lower but again agrees within the 1σ uncertainties with the value of 1.121 ± 0.010 given by Eugster et al. (1993). The data suggest that the samples derived from either a less shielded location in a 30–40 cm sized object or from a shielded location within an object with a pre-atmospheric radius in the range 20–30 cm.

Ochansk has a slightly shorter CRE history. The T_{21} age of 6.0 ± 0.5 Ma is lower than the previously reported ages of 7.5–7.8 Ma (see Graf and Marti, 1995), and 7.2 ± 0.2 and 8.6 ± 1.7 Ma given by Leya et al. (2004). The average $(^{22}Ne/^{21}Ne)_{cos}$ ratio of 1.088 ± 0.016 agrees within the uncertainties with the ratio of 1.100 ± 0.022 given by Eugster (1988) but is lower than the ratio of 1.108 (± 2%) given by Leya et al. (2001). All ratios, however, are smaller than the ratios for the other studied H chondrites, indicating that most likely Ochansk was a larger pre-atmospheric object than the other studied H chondrites. As a note, the T_{21} ages for Farmville and Ochansk suggest that both meteorites belong to the ~7 Ma CRE age peak of H chondrites, which represents ~45% of all H chondrites in our collections (e.g., Graf and Marti, 1995).

For the H5–6 chondrite Al-Khadhaf, the determined CRE age of 8.5 ± 0.9 Ma places this object also consistently into the ~7 Ma CRE age peak of H chondrites. The $(^{22}Ne/^{21}Ne)_{cos}$ ratio of 1.244 ± 0.022 determined for Al-Khadhaf indicates a small object with a pre-atmospheric radius of less than 5 cm. This finding is supported by the low ^{26}Al activity concentration of 24 dpm/kg, which also suggests a small pre-atmospheric radius of less than 5 cm (Zappatini et al., 2024).

L Chondrites: Ausson has the longest CRE age among all studied meteorites. The age of 48.1 ± 3.4 Ma is slightly shorter than the age of 57.1 ± 9.4 Ma determined by Leya et al. (2015) using the ^{81}Kr-Kr dating system; though, there is agreement within the (large) uncertainties. The $(^{22}Ne/^{21}Ne)_{cos}$ ratio of 1.073 ± 0.016 indicates that Ausson had a relatively large pre-atmospheric size, i.e., it was likely a meter-sized object in space.

The relatively high $(^{22}Ne/^{21}Ne)_{cos}$ ratio of 1.140 ± 0.025 for Leedey indicates a relatively small pre-atmospheric radius of 10–15 cm. The ratio we measured is in good agreement with the value of 1.15 given by Eugster (1988). The T_{21} age of 6.1 ± 0.6 Ma agrees with the age of 7.6 ± 1.4 Ma determined by Eugster (1988).

For Tennasilm, the CRE age of 18.1 ± 1.2 Ma is slightly lower than the T_{21} value of 22.8 ± 2.9 Ma given by Eugster (1988). The difference, however, is barely outside the 1σ uncertainties. The measured $(^{22}Ne/^{21}Ne)_{cos}$ ratio of 1.137 ± 0.017 agrees with the ratio of 1.160 measured by Eugster (1988), indicating that Tennasilm likely had a relatively small pre-atmospheric radius of 10–20 cm.

The CRE age for Kandahar is 20.8 ± 1.1 Ma, which is in perfect agreement with the ^{36}Cl-^{36}Ar age of 21.1 ± 1.4 Ma determined by Dalcher et al. (2013). There is also perfect agreement for the $(^{22}Ne/^{21}Ne)_{cos}$ ratios; the value obtained here is 1.089 ± 0.017 and Dalcher et al. (2013) give a ratio of 1.083. Both ratios also agree with the earlier value of 1.090 ± 0.04 measured by Eberhardt et al. (1966). Therefore, $(^{22}Ne/^{21}Ne)_{cos}$ consistently indicates that the samples come from shielded positions in a relatively large object, which contrasts with the recovered mass of only 299 g. Either a large part of the fallen mass is not recovered, or Kandahar experienced a complex exposure history.

The relatively small $(^{22}Ne/^{21}Ne)_{cos}$ for Suizhou of 1.046 ± 0.017 indicates a large pre-atmospheric radius and contrasts with the ratio of 1.085 ± 0.005 measured by Eugster et al. (1993). The T_{21} age determined here is 21.6 ± 1.3 Ma, which is slightly lower than the CRE age of 27.2 ± 3.0 Ma reported by Eugster et al. (1993). Taking all data at face value, the low

$(^{22}Ne/^{21}Ne)_{cos}$ ratio measured here, and the larger ratio measured by Eugster et al. (1993) likely indicates that Suizhou was a relatively large object in space, which is not really obvious considering the recovered mass of only ~70 kg.

For Renchen, Bischoff et al. (2019) estimated, based on He, Ne, and Ar isotope concentrations, a CRE age of 42 ± 3 Ma and they give $(^{22}Ne/^{21}Ne)_{cos}$ = 1.140 ± 0.004. In addition, based on ^{26}Al data, the authors estimated a pre-atmospheric radius in the range 10–20 cm. Since the piece studied here was obtained from A. Bischoff, we can safely use their noble gas data also for the present study.

LL Chondrites: The CRE age for Kilabo of 27.3 ± 1.4 Ma is slightly lower than the T_{21} age of 33.0 Ma (no uncertainty given) published by Cole et al. (2007). Significant discrepancies also exist for $(^{22}Ne/^{21}Ne)_{cos}$. Whereas the ratio measured here is 1.103 ± 0.016, suggesting moderate shielding, Cole et al. (2007) reported a significantly lower ratio of 1.040 (no uncertainty given), indicative of deeper shielding. The discrepancies imply that the samples in both studies originated from different shielding locations, which would indicate a large pre-atmospheric radius. Alexeev et al. (2008) intensively studied Kilabo using luminescence data, tracks, and radionuclides and found that it has a bimodal track distribution, indication of a complex exposure history. These authors conclude that Kilabo likely experienced significant pre-irradiation on its parent body (30–40 Ma) and that the sample studied by them was from shallow shielding in an object with a pre-atmospheric radius of 34^{+6}_{-4} cm. The second exposure stage likely lasted longer than 5 Ma.

The T_{21} age determined here for Mangwendi of 11.5 ± 0.8 Ma agrees with the CRE age of 12 Ma reported by Heymann (1965), indicating that this meteorite belongs to the LL chondrite cluster of 10–12 Myr in the CRE age histogram. The relatively large $(^{22}Ne/^{21}Ne)_{cos}$ ratio of 1.129 ± 0.017 suggests that the studied sample was irradiated in low shielding conditions in an average-sized meteorite having a pre-atmospheric radius of about 10–20 cm.

For Sulagiri, the CRE age determined here of 16.6 ± 1.0 Ma is significantly lower than the age of 27.9 ± 3.4 Ma published by Mahajan (2017). The $(^{22}Ne/^{21}Ne)_{cos}$ ratio of 1.074 ± 0.019 indicates that Sulagiri was a relatively large pre-atmospheric object in the size range of ~40 cm. This finding is supported by the substantial recovered mass of 110 kg (Mahajan, 2017).

For Moshampa, we determined a T_{21} age of 38.2 ± 2.7 Ma, which places this LL5 chondrite to the minor CRE age peak of ~40 Ma for LL chondrites. The $(^{22}Ne/^{21}Ne)_{cos}$ ratio of 1.057 ± 0.022

indicates that Moshampa was likely a meter-sized pre-atmospheric object, which is in contrast to the TKW of only 2.26 kg.

Based on cosmogenic ^{3}He and ^{21}Ne concentrations, Bischoff et al. (2017) determined for Stubenberg a CRE age of 37 ± 1 Ma. Their $(^{22}Ne/^{21}Ne)_{cos}$ ratio of 1.0826 ± 0.0026 indicates a pre-atmospheric radius ≥35 cm, in agreement with the fireball observations (600 kg). However, such a large radius is incompatible with the short-lived radionuclide data, which constrain the radius to < 20 cm. This contradiction might indicate a complex exposure history. This finding was recently confirmed by Welten and Caffee (2024), who pointed out that Stubenberg might have experienced a recent break-up event <0.1 Ma ago. Based on the results for the long-lived radioisotopes ^{10}Be, ^{26}Al, and ^{36}Cl, the authors suggested that Stubenberg had a complex exposure history with a first exposure stage in an object with R>35 cm and a second exposure stage in an object with R<20 cm. This second stage in a smaller object is evident by the absence of ^{60}Co, whose concentration is very shielding dependent.

4.3.4. *Thermal History of the Studied Chondrites using $(^{3}He/^{21}Ne)_{cos}$ vs. $(^{22}Ne/^{21}Ne)_{cos}$*

Diffusive losses of radioactive tritium (^{3}H) and/or its decay product ^{3}He are commonly used to study the thermal history of meteorites. Doing so, the data are usually discussed in the so-called Bern plot, i.e., a plot of $(^{3}He/^{21}Ne)_{cos}$ vs. $(^{22}Ne/^{21}Ne)_{cos}$ (Fig. 4.1). The solid black line represents the best fit line considering the experimental data from this study and from the study by Tauseef et al. (2024). The best linear fit gives:

$$\left(\frac{^{3}He}{^{21}Ne}\right)_{cos} = (20.1 \pm 1.7) \times \left(\frac{^{22}Ne}{^{21}Ne}\right)_{cos} - (17.5 \pm 1.9) \qquad \textbf{(eq. 4.2)}$$

The dotted line represents the best fit line through physical model calculations (Leya and Masarik 2009) for meteoroids with pre-atmospheric radii <65 cm (which covers most of the meteorites falling to Earth) and assuming 80% ablation losses (see, e.g., Leya and Masarik 2009; Dalcher et al. 2013). In addition, the dashed line shown in Fig. 4.1 represents the fitted correlation line derived from 138 chondrite data (Nishiizumi et al. 1980). This correlation line differs only slightly from the original one proposed by Eberhardt et al. (1966). Chondrites that fall below these correlation lines show a deficit in $^{3}He_{cos}$, likely due to diffusive losses of ^{3}H, which is the parent isotope of ^{3}He.

Most of the data plot close to the correlation lines, indicating there are none or only very minor $^{3}He_{cos}$ deficits; Ehole-1 being an exception (see Fig. 4.1). For the H5-6 chondrite Al-Khadhaf

and the H5 chondrite SaU 606, the new data extend the correlation line towards higher $(^3He/^{21}Ne)_{cos}$ and $(^{22}Ne/^{21}Ne)_{cos}$ ratios. The L6 chondrite Suizhou plots to the lower end of the correlation lines at low $(^3He/^{21}Ne)_{cos}$ and $(^{22}Ne/^{21}Ne)_{cos}$ ratios. The data is more in agreement with the correlation line given by Leya and Masarik (2009) than with the correlation given by Nishiizumi et al. (1980). The only clear outlier is one aliquot of Ehole (Ehole-1) with a $(^3He/^{21}Ne)_{cos}$ ratio of ~2, which plots significantly below both correlation lines. Note that the data for the other Ehole aliquot plots perfectly on the correlation line with a $(^3He/^{21}Ne)_{cos}$ ratio close to 4.9. That one aliquot shows ^3He deficits and the other aliquot shows no such deficits cannot be explained by diffusive losses of the meteorite while in space. In contrast, it could be possible that one aliquot experienced ^3He losses during sample treatment, especially during pre-heating in vacuum (see above). This hypothesis, however, is unlikely because all samples were treated similarly and ^3He losses should either occur in all or in none of them. The inconsistency for Ehole-1 is due to a too low ^3He concentration, the ^{21}Ne data for both aliquots agree, though $^{21}Ne_{cos}$ in Ehole-1 is ~30% lower than $^{21}Ne_{cos}$ in Ehole-2. Both nuclides, ^3He and ^{21}Ne were measured at the same time in the same gas fractions (see above).

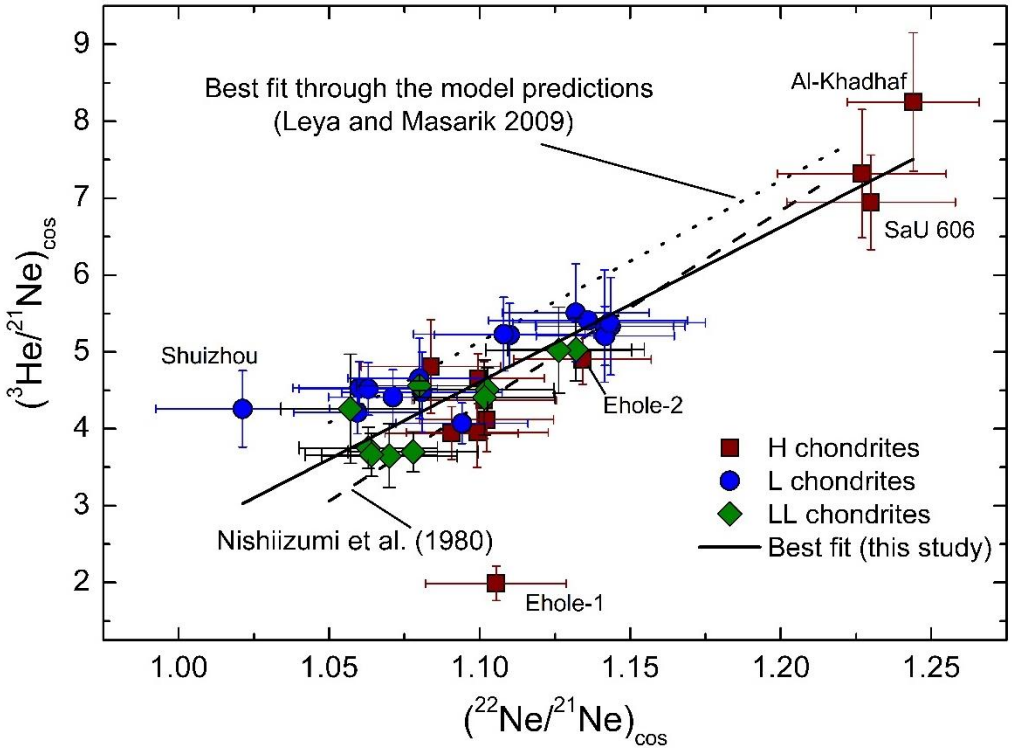

Fig. 4.1. $(^3He/^{21}Ne)_{cos}$ as a function of $(^{22}Ne/^{21}Ne)_{cos}$ for the studied H chondrites (squares), L chondrites (circles), and LL chondrites (diamonds). Also shown are the empirical correlation given by Nishiizumi et al. (1980) and the best fit line through physical model calculations given by Leya and Masarik (2009).

4.3.5. *^{10}Be Activity Concentrations*

For most of the studied samples, some solid residues remained after the HF/HNO_3 treatment. As shown by Sliz et al. (2022) using X-ray diffraction, the residual material consists almost exclusively of fluorides with no traces of original minerals. It is therefore safe to conclude, that all ^{10}Be was extracted out of the samples and therefore no further corrections are necessary. However, this assumption is questioned further below.

The results for ^{10}Be activity concentrations given in Table 4.9 are corrected for Fe (metal + troilite) loss during leaching and short CRE ages in case of Ochansk, Farmville, and Leedey. The data therefore represent ^{10}Be saturation activities in bulk samples. The values range from 15.2 ± 0.2 dpm/kg for Tennasilm (L4) to 20.3 ± 0.3 dpm/kg for Mangwendi (LL6). Some of the meteorites have been measured before for ^{10}Be. For example, the ^{10}Be activity concentration measured here for Ehole of 19.6 ± 0.3 dpm/kg agrees with 19 ± 2 dpm/kg reported by Honda and Arnold (1964). However, our value is based on the most recent half-life of $T_{1/2} = 1.36 \times 10^6$ yrs and a NIST ^{10}Be/Be standard (Nishiizumi et al., 2007), which contrasts to the value determined by Honda and Arnold (1964) obtained by assuming a half-life of 2.5×10^6 yrs. For Ausson and Kandahar, we measured a ^{10}Be activity concentration of ~18 dpm/kg, which is on average 21% lower than the 23–24 dpm/kg reported by Dalcher et al. (2013).

For Kilabo, we measured a ^{10}Be activity concentration of 17.2 ± 0.2 dpm/kg, which is more than 25% lower than the 23.5 ± 0.5 dpm/kg given by Cole et al. (2007). However, the study by Cole et al. (2007) measured the stone fraction of the meteorite. Using their data, i.e., 23.5 dpm/kg for the stone fraction and 5.2 dpm/kg for the metal fraction gives a ^{10}Be activity concentration of ~19 dpm/kg for bulk Kilabo, which is in better agreement with the data measured by us. Note that there was also a difference in the $(^{22}Ne/^{21}Ne)_{cos}$ ratios measured by Cole et al. (2007) and the one measured by us; their value is lower, indicative of higher shielding of their sample (see above). Such differences in shielding together with the complex exposure history for Kilabo can in principle explain the remaining differences in the ^{10}Be activity concentrations, because more shielded samples have, for average sized meteorite, higher ^{10}Be activity concentrations. This argument, however, fails to explain the lower ^{10}Be activity measured for Kandahar. Our $(^{22}Ne/^{21}Ne)_{cos}$ ratio for Kandahar is consistent with the value given by Dalcher et al. (2013), suggesting that both samples were irradiated at similar shielding depth and therefore should have similar ^{10}Be activity concentrations. However, our value is more than 20% lower than theirs. A possible explanation for the lower ^{10}Be in some samples could be the retention of ^{10}Be in the fluoride residues that were formed during sample

dissolutions. However, if this is the case, there is no way to correct for such trapped ^{10}Be deficits because different meteorites behave differently upon acid digestion. Considering that the assumption of ^{10}Be retention is still somewhat speculative, especially considering that for Ehole and Kilabo the new data are in accord with earlier measurements (see above), no further action is taken. It is worth emphasizing that this unresolved problem is not affecting the conclusion of the present study. Since we had not enough material for a ^{10}Be measurement of *Stubenberg* (LL6), we rely on the value of 24.0 ± 0.6 dpm/kg published by Welten and Caffee (2024).

To check our procedure for accuracy, we measured the 128–200 µm grain-size fraction of leached samples from Ehole (H5), Ausson (L5), and Sulagiri (LL5). The data indicates that there is no significant difference in the ^{10}Be activity concentrations between the grinded samples used by us (no grain-size separation) and the grain-size separates, which gives further confidence in the procedure (see Table 4.2).

4.3.6. *^{14}C Activity Concentrations*

The measured ^{14}C activity concentrations are given in Table 4.9; they range from 23.3 ± 0.4 dpm/kg for Al-Khadhaf (H5-6) to 53.3 ± 1.1 dpm/kg for *Suizhou* (L6). This large spread clearly demonstrates that ^{14}C saturation activities exhibit large variations among the different meteorites studied here, being of different types and having different pre-atmospheric radii. This further confirms that average ^{14}C saturation activities of 46, 51.1, and 55.2 dpm/kg, as often assumed for H, L, and LL chondrites, respectively (Jull et al., 1994), are not sufficient for calculating reliable ^{14}C terrestrial ages.

4.3.7. *^{14}C/^{10}Be Production Rate Ratios*

The ^{14}C/^{10}Be ratios for the studied chondrites range from 1.96 ± 0.05 for Ehole (H5) to 2.91 ± 0.07 for Suizhou (L6). Stubenberg (LL6) is a clear outlier with its extremely low ^{14}C/^{10}Be ratio of 1.07 ± 0.03. As already discussed for the noble gas data, Stubenberg likely experienced a complex exposure history with a very recent break-up (Welten and Caffee, 2024). According to them, Stubenberg might have experienced a first exposure stage in an object with R>35 cm and, after a recent break-up event less than 0.1 Ma ago, a second irradiation stage in an object with R<20 cm. In such an irradiation scenario, ^{14}C reflects exclusively the second irradiation stage as a small object. The measured ^{14}C activity concentration of 26.0 ± 0.5 dpm/kg is

possible in LL chondrites with pre-atmospheric radii of 8–10 cm. In contrast, ^{10}Be activity concentration of 24.4 ± 0.2 dpm/kg is indicative of a larger object in the size range 30–50 cm. Therefore, the ^{14}C and ^{10}Be data can be fully explained by the complex exposure history, thus the Stubenberg is not discussed any further.

The average ^{14}C/^{10}Be ratio of the remaining samples is 2.47 ± 0.02 (using uncertainties as weights). This average is within the uncertainties identical to the ratio of 2.5 ± 0.1, very often used for terrestrial age dating (Welten et al., 2001; Kring et al., 2001). However, the spread in the data indicates that an average value might not be sufficient for determining reliable ages. For example, the ratio of 2.91 ± 0.07 for Suizhou and Leedey is more than 15% higher than the average and the ratio of 2.12 ± 0.05 for Ehole is ~20% lower than the average. The data, therefore, demonstrate that a more reliable procedure for calculating terrestrial ages is necessary.

Table 4.14. ^{14}C and ^{10}Be activity concentrations, and ^{14}C/^{10}Be ratios for the studied meteorites.

Meteorites	Type	^{14}C[a] (dpm/kg)	^{10}Be[a] (dpm/kg)	^{14}C/^{10}Be
Castalia	H5	41.3 ± 0.8	18.2 ± 0.2	2.27 ± 0.05
Ehole	H5	38.4 ± 0.8	19.6 ± 0.2	1.96 ± 0.05
Farmville	H4	40.8 ± 0.8	18.3 ± 0.7[b]	2.23 ± 0.05
Ochansk	H4	48.9 ± 1.0	17.7 ± 2.0[b]	2.76 ± 0.06
Al-Khadhaf	H5-6	23.3 ± 0.4	n.d.	n.d.
Ausson	L6	49.7 ± 1.1	18.2 ± 0.2	2.73 ± 0.08
Leedey	L6	46.2 ± 0.9	15.9 ± 2.1[b]	2.91 ± 0.07
Tennasilm	L4	34.8 ± 0.7	15.2 ± 0.2	2.29 ± 0.06
Kandahar	L6	50.3 ± 1.0	18.3 ± 0.2[c]	2.75 ± 0.06
Suizhou	L6	53.3 ± 1.1	18.3 ± 0.2	2.91 ± 0.07
Renchen	L5-6	31.2 ± 0.6	n.d.	n.d.
Antonin	L6	25.9 ± 0.5	n.d.	n.d.
Kilabo	LL6	43.4 ± 0.9	17.2 ± 0.2	2.52 ± 0.06
Mangwendi	LL6	45.1 ± 0.9	20.3 ± 0.2	2.22 ± 0.06
Sulagiri	LL5	40.0 ± 0.8	19.0 ± 0.2	2.11 ± 0.05
Stubenberg	LL6	26.0 ± 0.5	24.4 ± 0.2[d]	1.07 ± 0.03
Moshampa	LL6	48.1 ± 1.0	n.d.	n.d.

[a] ^{14}C and ^{10}Be activity concentrations are given after employing mass loss corrections (see Table 4.2 and 4.3), except Al-Khadhaf and Moshampa were not leached.
[b] ^{10}Be activity concentrations are corrected for saturation for small CRE ages.
[c] ^{10}Be activity for Kandahar is the average of two measurements.
[d] CRE ages for Renchen and Stubenberg are from Bischoff et al. (2019) and Bischoff et al. (2017), respectively. ^{10}Be data for Stubenberg is taken from Welten and Caffee (2024).

4.4. Isotope Ratios and New Correlations for Determining ^{14}C and $^{14}C/^{10}Be$ Terrestrial Ages

In the following, the measured saturation activities for ^{14}C and ^{10}Be as well as the $^{14}C/^{10}Be$ and $(^{22}Ne/^{21}Ne)_{cos}$ ratios are used to evaluate the model calculations (e.g., Tauseef et al., 2024) for various meteorite types and shielding depths. Doing so, we slightly changed the model predictions. In Tauseef et al. (2024), the model calculations were limited to pre-atmospheric radii < 90 cm and 80% ablation losses were assumed. Since ablation was assumed to be spherically symmetric, only the innermost 60% of the meteorite was considered. These assumptions were based on some studies (e.g., Bhandari et al., 1980; Alexeev, 1998), which have reported ablation losses in the range 80–95%, though, such losses are unlikely to be spherical. The assumption of spherical ablation is most likely over-simplified. Studies (e.g., Halliday et al., 1989) have mentioned that mass loss due to atmospheric ablation vary significantly as a function of initial mass, size of meteoroids, orientation and entry conditions. Considering that most meteorites break up during atmospheric entry and it might well be possible that pieces from close to the pre-atmospheric surface survived and made it into the meteorite inventory. Therefore, as not to unreasonably reduce the database, atmospheric losses are ignored, and the entire database is considered. This makes the dataspace for the model calculations larger but closer to the reality.

4.4.1. *^{14}C Saturation Activity Concentration as a Function of $(^{22}Ne/^{21}Ne)_{cos}$*

Fig. 4.2 presents the model calculations for ^{14}C production rates as a function of $(^{22}Ne/^{21}Ne)_{cos}$ in H chondrites. The open symbols are the results of the model calculations for meteoroids with pre-atmospheric radii smaller than 90 cm and considering all shielding depths. The gray area shows the 1σ standard deviation of the model calculations. The solid black line is the best fit through the model calculations, as given by Tauseef et al. (2024). The results obtained here are shown by the solid dots, included is the data for SaU 606 from Tauseef et al. (2024). In addition, some literature data are plotted (see Fig. 4.2 caption for references). For Torino, Carancas and Richardton, the ^{14}C and the noble gas analysis might not have been on the same aliquot, making the data slightly less reliable. Most of the samples plot consistently close to the correlation line and within the gray area and are therefore fully consistent with the model predictions. Only two data from St. Robert plot above the correlation and above the uncertainty band at unreasonably high ^{14}C activities. The St. Robert samples have been treated with H_3PO_4 before ^{14}C analysis (Leya et al. 2001), which might have dissolved a large fraction of metal and troilite,

therefore resulting in 20–25% higher ^{14}C activities relative to bulk samples. Since the data given by Leya et al. (2001) are not corrected for mass (Fe) losses, they are not representing ^{14}C in bulk samples and are therefore not comparable to the model calculations. Al-Khadhaf has the lowest ^{14}C activity ever measured in an H-chondrite fall but is fully consistent with the model calculations. In addition, the high $(^{22}Ne/^{21}Ne)_{cos}$ ratio and the low ^{26}Al activity also suggest a small pre-atmospheric radius of less than 5 cm (Zappatini et al., 2024).

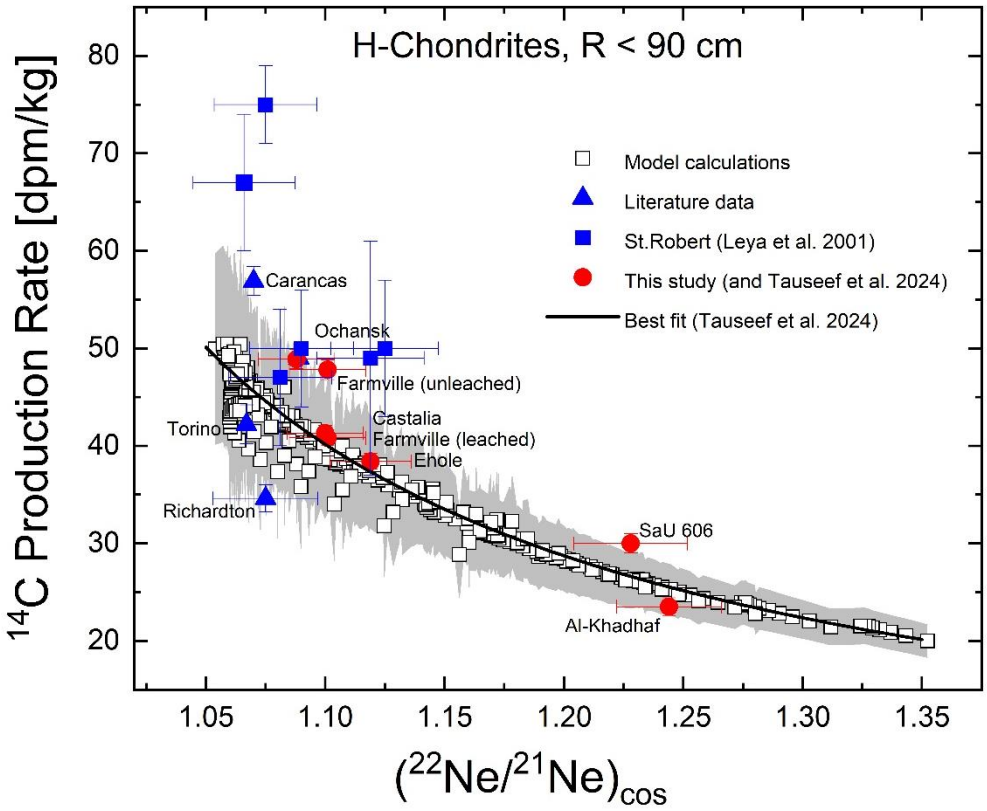

Fig. 4.2. ^{14}C production rates as a function of $(^{22}Ne/^{21}Ne)_{cos}$. The model calculations are for H chondrites with pre-atmospheric radii <90 cm. The gray area indicates the 1σ standard deviation of the model calculations. Studied H chondrites are shown by red circles, including SaU 606 data (Tauseef et al., 2024). ^{14}C data— Carancas (Jull et al., 2009), Torino (Wieler et al., 1996), Richardton (Jull et al., 1989). Noble gas data—Torino (Wieler et al., 1996), Carancas (Ott et al., 2008) Richardton Dalcher et al., 2013). The data for St. Robert is from Leya et al. (2001).

Fig. 4.3 shows the model calculations for ^{14}C production rates as a function of $(^{22}Ne/^{21}Ne)_{cos}$ in L chondrites. For a description of the model calculation see above. The experimental data obtained here and the data for Boumdeid and Mt. Tazerzait (Tauseef et al., 2024) are plotted as red dots. Literature data for Mbale, Harleton, Holbrook, Bruderheim, and Knyahinya are shown as blue triangles (see Fig. 4.3 caption for references). Again, ^{14}C and noble gas analysis might not have been performed on the same aliquot. Most data are close to the correlation line and

within the 1σ uncertainty of the model calculations. The only exception is Boumdeid, which plots significantly below the correlation line. This meteorite likely experienced a complex exposure history. The short-lived radionuclides and ^{26}Al are consistent with a pre-atmospheric radius in the range 10–20 cm (Buhl et al., 2014), the $(^{22}Ne/^{21}Ne)_{cos}$ ratio, however, clearly indicates substantial shielding in a larger object. Therefore, the data for Boumdeid can consistently be explained assuming a complex exposure history; the stable Ne isotopes are dominated by the first exposure stage as a relatively large object and all radionuclides, including ^{14}C, reflect the second exposure stage as an object in the size range 10–20 cm.

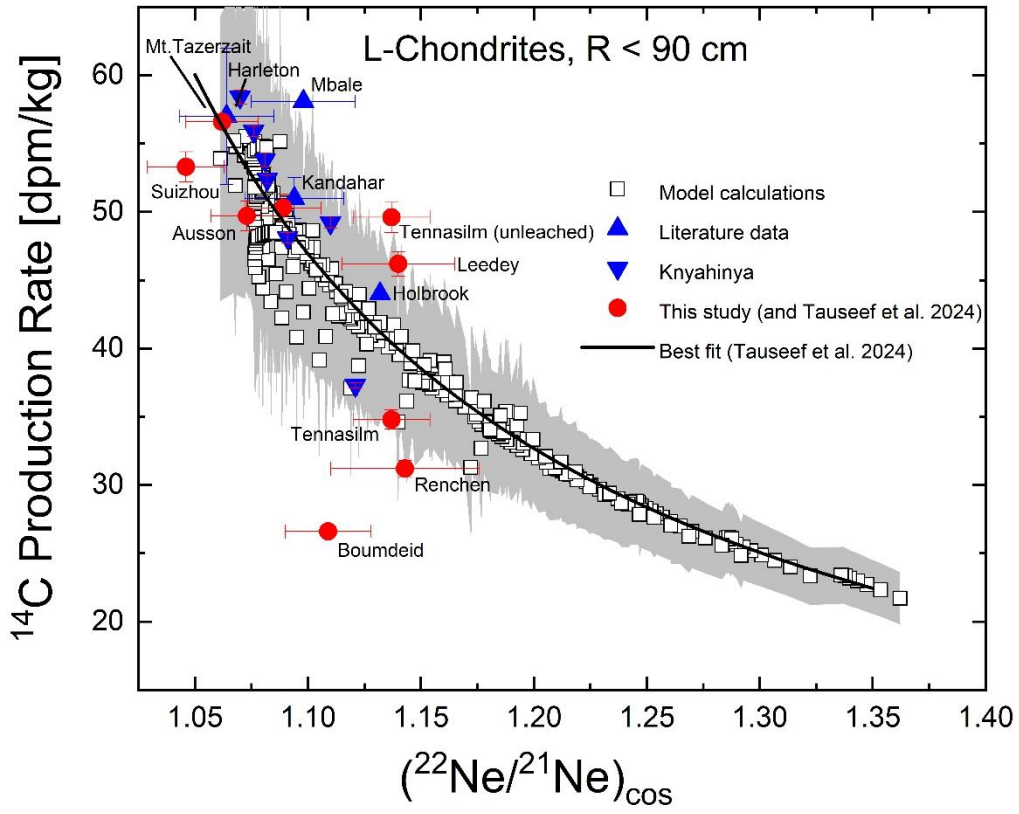

Fig. 4.3. ^{14}C production rates as a function of $(^{22}Ne/^{21}Ne)_{cos}$ for L chondrites. For details, see Fig. 4.2 caption and text. ^{14}C data—Holbrook and Mbale (Jull et al., 1998), Harleton (Goel and Kuhman, 1961), Bruderheim (Jull et al., 1993), Knyahinya (Jull et al., 1994). Noble gas data—Harleton and Mbale (Dalcher et al., 2013), Knyahinya (Graf et al., 1990), Holbrook (Gibson and Bogard, 1978), Bruderheim (Bogard and Cressy, 1973).

The relationship between ^{14}C saturation activity concentrations and $(^{22}Ne/^{21}Ne)_{cos}$ ratios for LL chondrites are shown in Fig. 4.4. In addition to the data obtained here and the data for Bensour from Tauseef et al. (2024), also the data for Dhurmsala is shown (Stelzner et al., 1999). Like for the H and L chondrites, the experimental data are fully consistent with the model predictions. Unfortunately, the experimental data are limited to meteorites with relatively low

($^{22}Ne/^{21}Ne)_{cos}$ ratios, i.e., relatively large pre-atmospheric meteorites, therefore prohibiting the evaluation of the model calculations for high ($^{22}Ne/^{21}Ne)_{cos}$ ratios, i.e., small pre-atmospheric meteorites. As mentioned before, the data for Stubenberg is not plotted due to its complex exposure history.

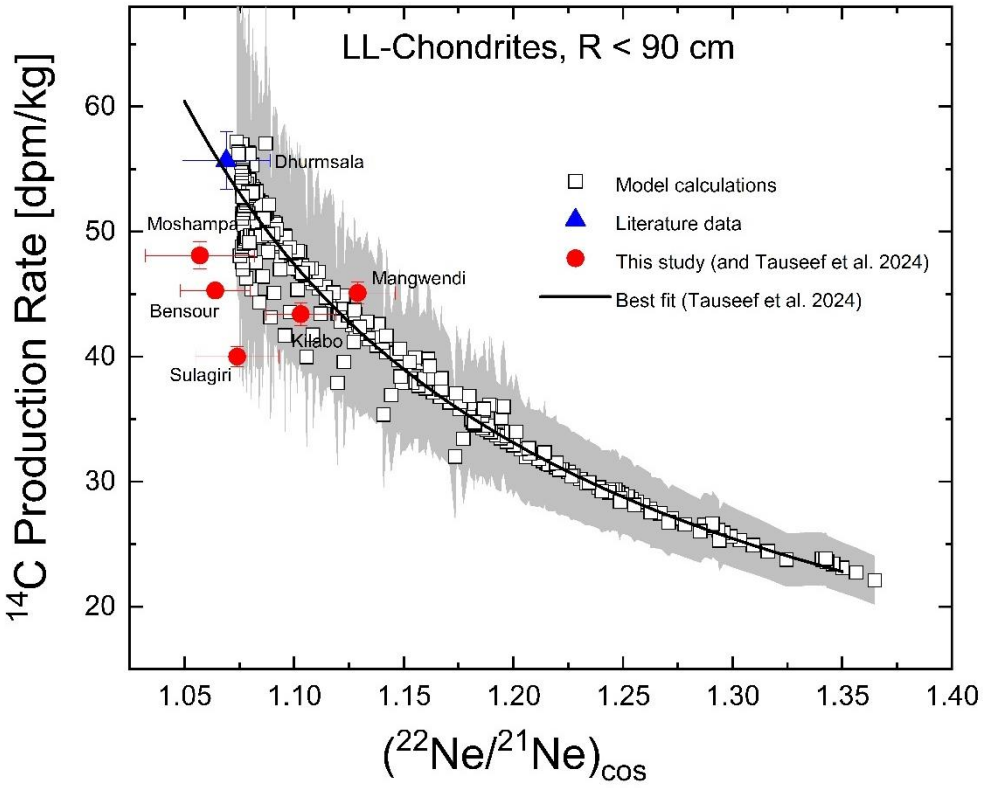

Fig. 4.4. ^{14}C production rates as a function of $(^{22}Ne/^{21}Ne)_{cos}$ for LL chondrites. Bensour Data is from Tauseef et al. (2024), Dhurmsala from Stelzner et al. (1999). For details, see Fig. 4.2 caption and text.

4.4.2. *$^{14}C/^{10}Be$ Production Rate Ratios as a Function of $(^{22}Ne(^{21}Ne)_{cos}$ Ratios*

Fig. 4.5 depicts $(^{22}Ne/^{21}Ne)_{cos}$ as a function of $^{14}C/^{10}Be$ for H chondrites with pre-atmospheric radii between 4 cm and 100 cm. The open symbols, distinguished for the different pre-atmospheric radii, are the results of the model calculations, and the gray area indicates the 1σ standard deviation of the model calculations. In contrast to our earlier study (Tauseef et al., 2024), x- and y-axis are interchanged, which makes data handling easier. The relationship can be fitted by a 2nd degree polynomial. Solving for $^{14}C/^{10}Be$ gives equations of the form:

$$\left(\frac{^{14}C}{^{10}Be}\right) = a \pm \left(b \times \sqrt{c \times \left(\frac{^{22}Ne}{^{21}Ne}\right)_{cos} - d}\right) \qquad \textbf{(eq. 4.3)}$$

Table 4.15. Parameters for the model fit to calculate $^{14}C/^{10}Be$ ratios as a function of $(^{22}Ne/^{21}Ne)_{cos}$

Meteorite	a	b	c	d
H chondrites	2.5550	3.3360	0.5996	0.6371
L chondrites	2.5755	3.3823	0.5913	0.6381
LL chondrites	2.5796	3.3697	0.5935	0.6405

The minus before the bracket refers to the left hand-side of the parabola and is for meteorites with pre-atmospheric radii ≤ 70 cm. The plus sign refers to the right hand-side of the parabola and is for meteorites with pre-atmospheric radii ≥ 70 cm. The values for the parameters *a*, *b*, *c*, and *d* for H, L, and LL chondrites are summarized in Table 4.10. The experimental data from this study and the study by Tauseef et al. (2024) are shown by the red squares and literature data are shown by the blue triangles (see Fig. 4.5 caption). All experimental data plot within the 1σ uncertainty range of the model calculations. The experimental data confirm the model calculations, and they especially confirm that $^{14}C/^{10}Be$ production rate ratios depend on meteorite size and shielding depth. The $^{14}C/^{10}Be$ ratio of the L6 chondrite Leedey shows a slight deviation from the general trend confirmed by the rest of the data. This deviation may be attributed to the lower ^{10}Be activity concentration measured for Leedey. As mentioned before, some of the chondrites studied by us have been analyzed before and some of them have ^{10}Be activity concentrations up to 20% higher than the ones measured by us. For example, while the $(^{22}Ne/^{21}Ne)_{cos}$ ratio measured by us for Kandahar (L6) agrees with the ratio given by Dalcher et al. (2013), our ^{10}Be value is more than 20% lower than theirs. Regardless of whether we use our measured values or previously reported ones, the $^{14}C/^{10}Be$ ratios remain significantly different from the average value of 2.5 ± 0.1. For example, as shown in Figure 3, the ratio for Kandahar determined in this study is 2.75 ± 0.05, whereas the ratio calculated using our ^{14}C data but the ^{10}Be data from Dalcher et al. (2013) results in a lower ratio of 2.11 ± 0.06. In contrast, the average $^{14}C/^{10}Be$ ratio considering all data is 2.47 ± 0.02, i.e., in good agreement with the ratio of 2.5 ± 0.1 assumed so far (Kring et al., 2001; Welten et al., 2001, see also above), though with a much larger uncertainty. However, the average ratio fails to describe data for small objects, like for SaU 606, for which the $^{14}C/^{10}Be$ ratio is more than 50% lower than the average. The model calculations, in contrast, describe the measured $^{14}C/^{10}Be$ ratio in this small meteorite within the uncertainties.

Although, we had not enough material to analyze ^{10}Be for Al-Khadhaf, we can nevertheless estimate its $^{14}C/^{10}Be$ ratio from the measured $(^{22}Ne/^{21}Ne)_{cos}$ ratio. The thus determined $^{14}C/^{10}Be$ ratio is 1.45 and with the measured ^{14}C activity concentration of 23.3 dpm/kg, the expected

^{10}Be activity concentration would be ~16 dpm/kg. Such a low activity concentration is possible in H chondrites with a pre-atmospheric radius in the range 4–5 cm. Such a small radius is fully consistent with the low ^{14}C and ^{26}Al activity concentrations measured in this study and Zappatini et al. (2024).

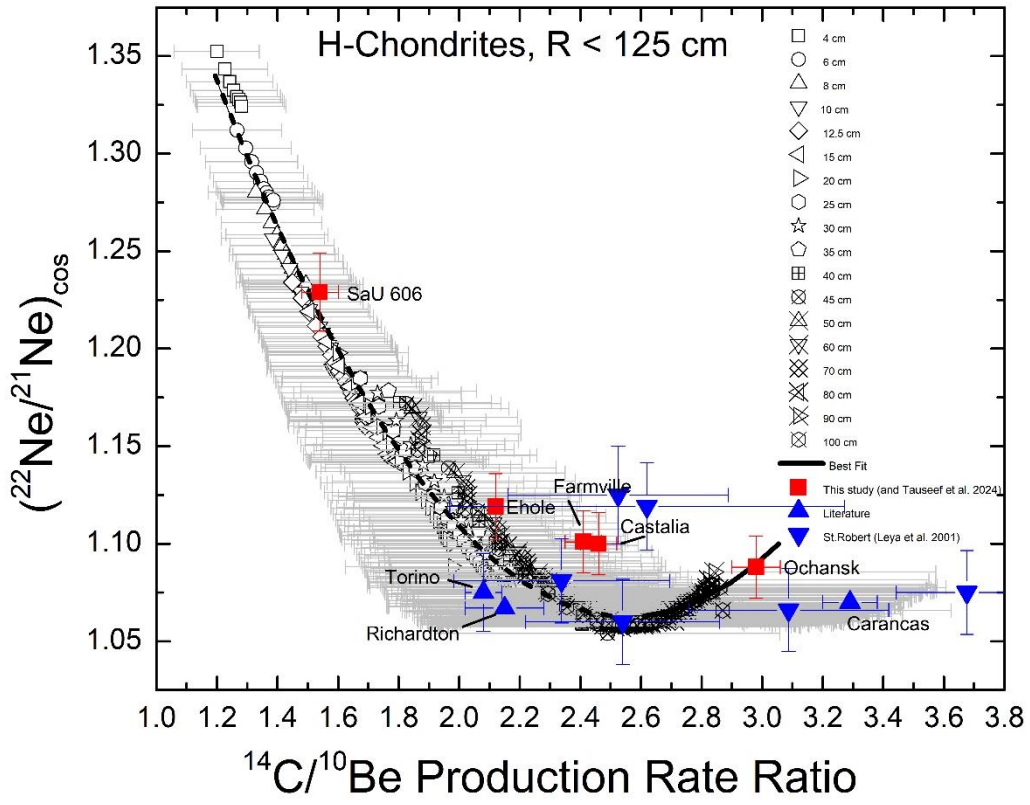

Fig. 4.5. $(^{22}Ne/^{21}Ne)_{cos}$ as a function of $^{14}C/^{10}Be$ for H chondrites. Model calculations (open symbols) are for meteorites with pre-atmospheric radii between 4 cm and 100 cm, with uncertainties shown by gray error bars. Experimental data from this study and Tauseef et al. (2024) are shown by red squares. Literature data (solid triangles) for Torino (Wieler et al., 1996), Richardton (Jull et al., 1989), Carancas (Jull et al., 2009), and St. Robert (Leya et al., 2001) are also plotted.

Fig. 4.6 depicts $(^{22}Ne/^{21}Ne)_{cos}$ as a function of $^{14}C/^{10}Be$ for L chondrites. In contrast to Fig. 4.5, the model calculations are no longer marked for the pre-atmospheric radius. Instead, the same symbol is used for all radii and all shielding depths. The experimental data from this study and from Tauseef et al. (2024) are shown by the red squares and literature data is shown by the blue triangles (for details, see Fig. 4.6 caption). The experimental data agree and therefore evaluate the model calculations. As mentioned before, Boumdeid likely experienced a complex exposure history; the stable Ne isotopes are dominated by the first exposure stage as a relatively large object and the radionuclides are dominated by the second exposure stage as a relatively

small object. Despite the complex exposure history, the data for Boumdeid nevertheless agrees with the model productions. Except for Mt. Tazerzait, Boumdeid, and Tennasilm, the $^{14}C/^{10}Be$ ratios for all studied L chondrites are higher than the often-used recommended value of 2.5 ± 0.1 (Jull et al., 2010; Welten et al., 2001; Kring et al., 2001). For the L chondrite Renchen, we can use the correlation from Fig. 4.6 to estimate the (expected) ^{10}Be saturation activity. Using $(^{22}Ne/^{21}Ne)_{cos}$ = 1.140 (Bischoff et al., 2019), we calculate a $^{14}C/^{10}Be$ production rate ratio of 1.796 for meteorites with a pre-atmospheric radius less than 70 cm and 3.315 for larger objects. Since Renchen was most likely a smaller meteorite (see Bischoff et al., 2019), we assume $^{14}C/^{10}Be$ = 1.796. With the measured ^{14}C activity concentration of 31.2 ± 0.6 dpm/kg, the (expected) ^{10}Be activity concentration is ~17 dpm/kg.

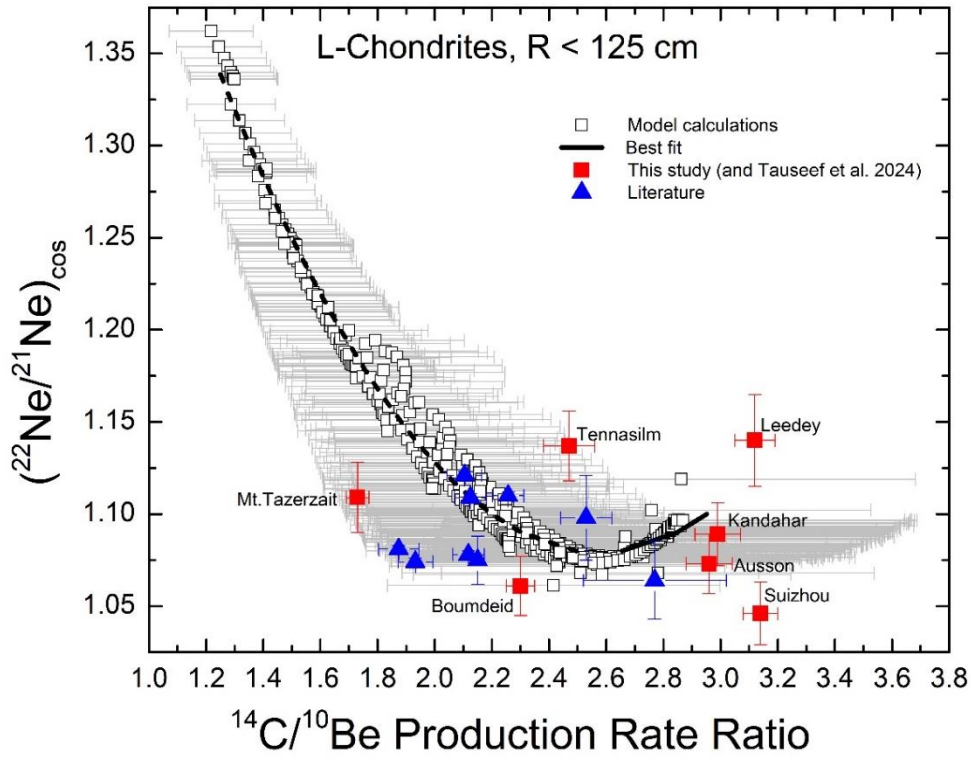

Fig. 4.6. $(^{22}Ne/^{21}Ne)_{cos}$ as a function of $^{14}C/^{10}Be$ for L chondrites. $^{14}C/^{10}Be$ data for Knyahinya are from Jull et al. (1994) and Ne isotopic data from Graf et al. (1990). For details, see Fig. 4.5 caption and text.

The $(^{22}Ne/^{21}Ne)_{cos}$ as a function of $^{14}C/^{10}Be$ ratios for LL chondrites are plotted in Fig. 4.7. The experimental data for Sulagiri, Kilabo, Mangwendi and Bensour are shown by the red squares. Their average value (using uncertainties as weights) of 2.44 ± 0.10 is relatively close to the recommended value of 2.5 ± 0.1 (Kring et al., 2001; Welten et al., 2001). However, using an average value is still not recommended. Since Stubenberg has a complex exposure history (see

above and, Bischoff et al., 2017), there are only four experimental data to evaluate the model. However, all four data perfectly agree with the model calculations.

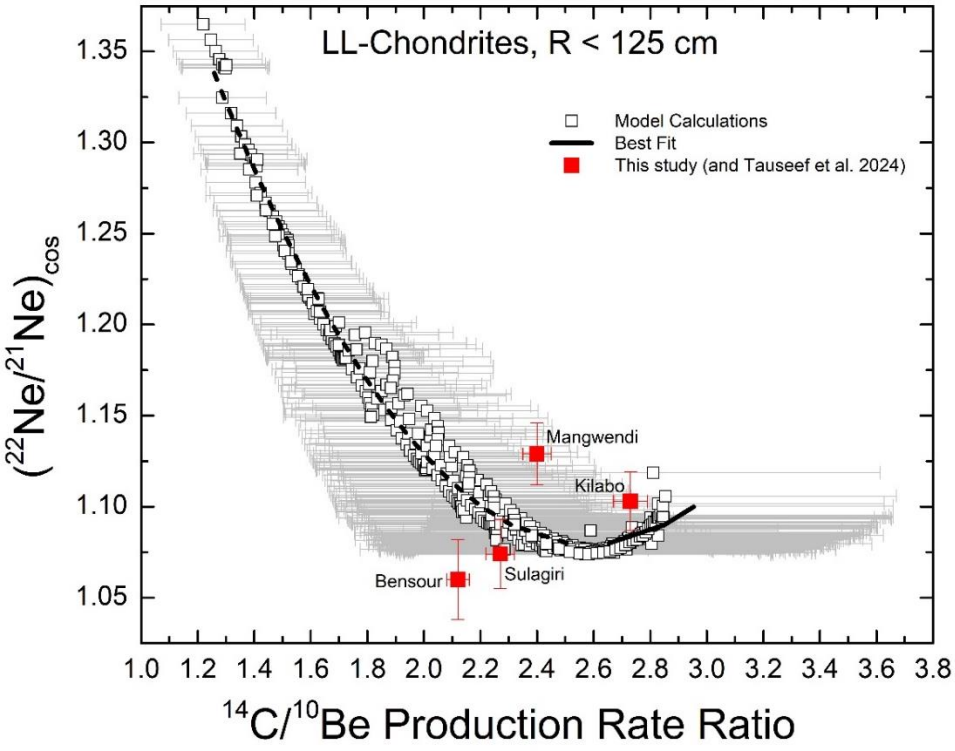

Fig. 4.7. $(^{22}Ne/^{21}Ne)_{cos}$ vs. $^{14}C/^{10}Be$ for LL chondrites. For details, see Fig. 4.5 caption and text.

4.5. Discussion and Conclusions

To evaluate the model calculations for ^{14}C production rates and $^{14}C/^{10}Be$ production rate ratios as a function of the shielding indicator $(^{22}Ne/^{21}Ne)_{cos}$, the ^{10}Be and ^{14}C saturation activity concentrations and the noble gas isotopes were measured in H, L, and LL chondrite falls. Together with the few existing literature data, the experimental data confirm the model calculations, and they especially confirm that neither the ^{14}C production rates nor the $^{14}C/^{10}Be$ production rate ratios are constant. Instead, both values show a significant dependence on shielding, indicating that using average values to calculate terrestrial ages, may not be very reliable and there may be a significant size-dependent bias in the database (Tauseef et al., 2024). Fig. 4.8 (left panel) depicts the ratios of the measured ^{14}C production rates relative to the production rates calculated using equation 3.4 as a function of $(^{22}Ne/^{21}Ne)_{cos}$. The ratios are distinguished for H, L, and LL chondrites, though, there is no trend in the data. The average ratio of production rates for H, L, and LL chondrites is 1.10 ± 0.15, 1.00 ± 0.15, and 0.91 ± 0.12, respectively. Note that the ratio for H chondrites is biased towards higher values by the

unreliable high ^{14}C data for St. Robert (Leya et al., 2001b). The average value considering all data (except St. Robert) is 1.01 ± 0.12. Therefore, the correlation between ^{14}C production rates and $(^{22}Ne/^{21}Ne)_{cos}$ ratios given by equation 3.4 (and in Tauseef et al., 2024) describes the measured production rates very accurately to within 3%. However, there is some scatter in the data, likely due to shielding effects in the meteorites considering that most of the measured data are within the 1σ uncertainty band of the model calculations. From the scatter we can conclude that the ^{14}C production rates can be estimated within an uncertainty of 12%.

Fig 4.8 (right panel) depicts the ratios of the experimental data relative to the previously assumed average (recommended) ^{14}C production rates, as a function of $(^{22}Ne/^{21}Ne)_{cos}$. Compared to left panel data, there is more scatter in the data and there are some low ratios, especially for high $(^{22}Ne/^{21}Ne)_{cos}$ ratios, i.e., smaller meteorites. The average ratio is 0.92 ± 0.18. Therefore, the ^{14}C production rates as a function of $(^{22}Ne/^{21}Ne)_{cos}$ calculated via equation 3.4 describes the experimental data more accurately than the averages used so far, i.e., within 3% relative to 8%, and more precisely, i.e., within an uncertainty of ~16% relative to ~20%. However, the greatest advantage of using equation 3.4 (Tauseef et al. 2024) relative to using averages becomes obvious for $(^{22}Ne/^{21}Ne)_{cos}$ ratios larger than ~1.15, i.e., for smaller meteorites. The average ratio for all meteorites with $(^{22}Ne/^{21}Ne)_{cos}$ larger than 1.15 for the left panel is 1.024 and for the right panel it is 0.581. Therefore, using the recommended average ratios gives erroneous ^{14}C production rates for small objects.

As a note, the relatively good average obtained by using the recommended (constant) values is due to the fact that most of the studied meteorites are of intermediate size, i.e., with $(^{22}Ne/^{21}Ne)_{cos}$ in the range ~1.10, for which the average values work reasonably well. If there were a larger number of small (or very large) meteorites in our study, the discrepancy between measured ^{14}C production rates and recommended average ^{14}C production rates would be much larger, and it would even be more obvious that the modeled correlations used by us are superior. Most of the meteorites falling on Earth are relatively small, as smaller meteoroids are more abundant and have a higher chance of being perturbed into Earth-crossing orbits. This is also evident from the total known weight (TKW) data and by the power-law size distribution of objects in interplanetary medium (see Brykina and Egorova, 2021; Dohnanyi, 1969). Thus, it is recommended to use ^{14}C production rates calculated via equation 3.4 of Tauseef et al. (2024).

Fig. 4.9 (left panel) shows the ratios of the measured $^{14}C/^{10}Be$ production rate ratios relative to the $^{14}C/^{10}Be$ production rate ratios calculated using equation 4.3 as a function of $(^{22}Ne/^{21}Ne)_{cos}$. There is no trend with meteorite type. The average ratio considering all data is 1.08 ± 0.16, i.e., the agreement is within the uncertainties.

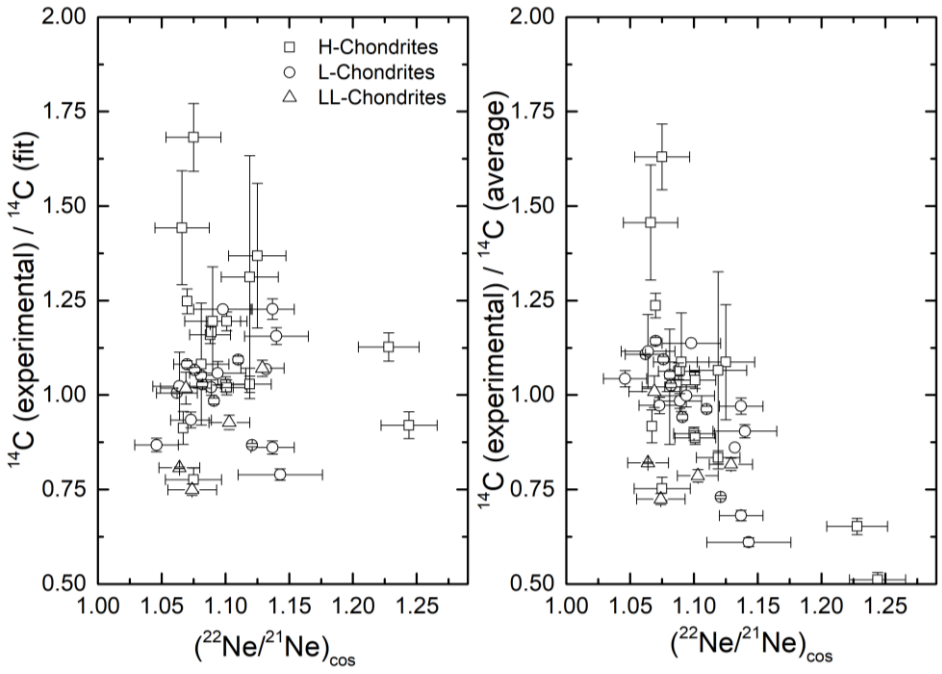

Fig. 4.8. Ratio of measured ^{14}C production rates relative to ^{14}C production rates calculated via equation 3.4 as a function of (^{22}Ne/^{21}Ne)$_{cos}$ for H, L, and LL chondrites (left panel). Ratio of measured ^{14}C production rates relative to previously assumed average values as a function of (^{22}Ne/^{21}Ne)$_{cos}$ (right panel).

Fig. 4.9 (right panel) depicts the measured ^{14}C/^{10}Be production rate ratio divided by 2.5 ± 0.1, i.e., by previously assumed average, as a function of (^{22}Ne/^{21}Ne)$_{cos}$. The average ratio considering all meteorites is 0.92 ± 0.13. As with the ^{14}C production rates, the relatively good performance of the average ^{14}C/^{10}Be production rate ratios is because most of the studied meteorites are of average size. Consider for example, the H chondrite SaU 606. While the measured/calculated ^{14}C/^{10}Be ratio (=1.02 ± 0.05), is in almost perfect agreement, the discrepancy is significant for the assumed average value, for which the measured/assumed ratio is 0.62 ± 0.03, i.e., significantly lower. This clearly demonstrates that equation 4.2 describes experimental ^{14}C/^{10}Be ratios more accurately than the assumed average ratio. Therefore, equation 4.2 should be preferred for calculating ^{14}C/^{10}Be production rate ratios.

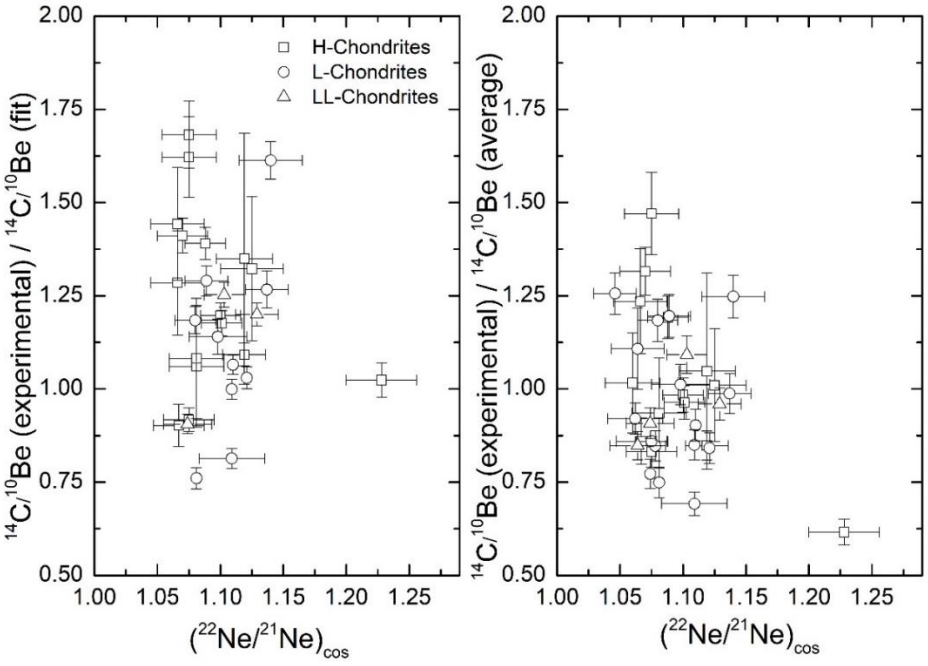

Fig. 4.9. Measured $^{14}C/^{10}Be$ production rate ratios relative to $^{14}C/^{10}Be$ production rate ratios calculated via equation 4.2 as a function of $(^{22}Ne/^{21}Ne)_{cos}$ for H, L, and LL chondrites (left panel). The right panel shows measured $^{14}C/^{10}Be$ production rate ratios relative to assumed average (2.5 ± 0.1) as a function of $(^{22}Ne/^{21}Ne)_{cos}$.

To summarize, to evaluate the model calculations for ^{14}C production rates and $^{14}C/^{10}Be$ production rate ratios as a function of the shielding indicator $(^{22}Ne/^{21}Ne)_{cos}$, we systematically studied freshly fallen H, L, and LL chondrites. The experimental database fully confirms the model predictions, clearly demonstrating that neither the ^{14}C production rates nor the $^{14}C/^{10}Be$ production rate ratios are constant but vary significantly with meteorite type, size, and shielding depth. For determining ^{14}C terrestrial ages it is therefore recommended to use the correlation of ^{14}C production rates as a function of $(^{22}Ne/^{21}Ne)_{cos}$ for H, L, and LL chondrites given by Tauseef et al. (2024). The accuracy is expected to be in the range of a few percent and the precision is in the range 16%, both independent of meteorite size and shielding depth. The only requirement is to measure the $(^{22}Ne/^{21}Ne)_{cos}$ ratios in an aliquot of the sample. Alternatively, terrestrial ages can be calculated using the $^{14}C/^{10}Be$ production rate ratios. Combining $^{14}C/^{10}Be$ production rate ratios with $(^{22}Ne/^{21}Ne)_{cos}$ ratios enable to calculate terrestrial ages with an accuracy in the range of 12% and a precision in the range of 15%, again, independent of meteorite size and shielding depth. This study therefore provides a major improvement in the terrestrial age dating systems for meteorites within the age range of 0–45 ka. The new correlations enable the calculation of shielding-corrected terrestrial ages with high accuracy and precision, thereby avoiding any bias in the terrestrial age database. In addition, thanks to the systematic nature of the study, realistic uncertainties can be assigned to the terrestrial ages.

Chapter 5

Noble gases in Omani strewnfield meteorites: new reliable terrestrial ^{14}C and $^{14}C/^{10}Be$ ages for Omani and Other Hot Desert Meteorites

Based on article published in the ***Meteoritics & Planetary Science*** Journal. h**ttps://doi.org/10.1111/maps.14355**

Numbering of the Title, tables and figures presented in this chapter are formatted to fit the layout of this thesis.

Cosmic ray exposure ages and pre-atmospheric shielding of Omani meteorites: New reliable ^{14}C and $^{14}C/^{10}Be$ terrestrial ages

Mohammad Tauseef[1*], Ingo Leya[1], Beda Hofmann[2]

Physics Institute, Space Research and Planetology, University of Bern, Sidlerstrasse 5, 3012 Bern, Switzerland
Naturhistorisches Museum Bern, Bernastrasse 15, 3005 Bern, Switzerland

Corresponding author email: mohammad.tauseef@unibe.ch

ABSTRACT

We present light noble gas isotope data from five well-defined meteorite strewnfields and two single stone from the Omani desert. Cosmogenic $(^{22}Ne/^{21}Ne)_{cos}$ ratios indicate large pre-atmospheric shielding, as expected for the strewnfields samples, and are consistent with their total known mass. A $(^{22}Ne/^{21}Ne)_{cos}$ of 1.209 suggests a small pre-atmospheric size of less than 10 cm for the single LL6 stone RaS 267, which has a recovered mass of 110 g. Using the $(^{22}Ne/^{21}Ne)_{cos}$ and previously established correlations, we calculated ^{14}C saturation activities and $^{14}C/^{10}Be$ saturation ratios, enabling refined shielding-corrected terrestrial ages. For the strewnfield meteorites, new ages slightly change, and they are also more consistent across the paired stones, compared to the ages published earlier using an assumed average saturation value. A 16% lower age is calculated for RaS 267. In addition, meteorites from other hot deserts (Acfer, Adrar, and Nullarbor regions) were re-investigated using literature data for ^{14}C and $(^{22}Ne/^{21}Ne)_{cos}$ and the correlations between ^{14}C and $(^{22}Ne/^{21}Ne)_{cos}$ established earlier. For these meteorites, the new terrestrial ages are all systematically shorter than the ages given earlier using a shielding independent approach. In some cases, the new ages are more than 50% lower. The observed differences are because the average ^{14}C production rates and $^{14}C/^{10}Be$ production rate ratios used in the earlier studies were determined using medium-sized meteorites and are therefore most precise for medium-sized objects. In contrast, most of the studied meteorites are small and for them production rates are lower and using the higher average production rates significantly overestimates the terrestrial ages. This study provides a systematic framework for precise terrestrial age determination of stony meteorites.

5.1. Introduction

Terrestrial ages of meteorites provide crucial information on the dynamics of small bodies in the solar system, the delivery of extraterrestrial material to Earth, and on weathering and erosion rates of extraterrestrial material on the Earth surface. For determining terrestrial ages up to 50 ka, the ^{14}C and $^{14}C/^{10}Be$ dating techniques are routinely used. Most of the previous studies on terrestrial ages assumed constant ^{14}C production rates (saturation activity concentration) of 46, 51.1, and 55.2 dpm/kg for H, L and LL chondrites, respectively (Sliz et al., 2022; Al-Kathiri et al., 2005; Jull et al., 1989 and references therein). For applying the $^{14}C/^{10}Be$ dating system, a production rate ratio $^{14}C/^{10}Be = 2.5$ is assumed (Welten et al., 2001; Sliz et al., 2022). Despite it is known for some time that neither the ^{14}C production rate nor the $^{14}C/^{10}Be$ production rate ratio is constant but significantly varies with pre-atmospheric radius and shielding depth of the studied sample, a rather low uncertainty in the range ~15% is typically assigned to the ^{14}C saturation activity concentration (e.g., Jull et al., 1989; 1998). However, a recent study demonstrates that ^{14}C production rates and $^{14}C/^{10}Be$ ratios significantly and systematically vary with radius and shielding depth (Tauseef et al., 2024, 2025). For example, ^{14}C activity concentrations in meteorite falls vary between 24–70 dpm/kg, i.e., by more than a factor of 2 (Tauseef et al., 2025, 2024; Minami et al., 2006, Jull et al., 1989; Leya et al., 2001). Similarly, $^{14}C/^{10}Be$ ratios vary from 1.54 to 3.30 (Tauseef et al., 2025; 2024; Jull et al., 1994), i.e., also by almost a factor of 2. The large variability experimentally determined in ^{14}C production rates and $^{14}C/^{10}Be$ ratios are fully confirmed by physical model calculations (Tauseef et al., 2024; 2025; Wieler et al., 1996; Knauer et al., 1995). If this large variability is not properly accounted for, there will be a significant size dependent bias in the terrestrial age database and the (so far) assigned uncertainties are unrealistically inaccurate.

To further validate the model predictions, i.e., to correct the ^{14}C and $^{14}C/^{10}Be$ terrestrial ages for shielding effects, but at the same time producing important scientific data, strewn-field meteorites are very useful. A strewn-field refers to a single meteorite fall that fragmented during passage through the Earth atmosphere, producing an area (usually an ellipse) with a high density of meteorite fragments. Importantly, all meteorites belonging to the same strewn-field must have an identical terrestrial age. Compared to other meteorite falls, objects producing strewn-fields are typically relatively large, which makes shielding corrections for the terrestrial age systems even more important.

Here we combine new noble gas measurements to determine shielding corrected ^{14}C saturation activities and $^{14}C/^{10}Be$ ratios (following Tauseef et al., 2024, 2025), and together with measured

^{14}C activity concentrations and $^{14}C/^{10}Be$ ratios (Sliz et al., 2022), we determine new (improved) terrestrial ages for five strewnfields and two single unpaired stones from the Omani Desert (JaH073, JaH091, SaU001, Shisr 015, Dhofar 005, SaU 163, Ras 267). The new ages replace earlier ages given by Sliz et al. (2022) calculated by assuming constant ^{14}C saturation activity concentrations and $^{14}C/^{10}Be$ ratios. In addition to the new data (re-calculated terrestrial ages using new noble gas data), this study also compiles data from the Sahara Desert and the Nullarbor region to calculate new terrestrial ages by implementing the shielding dependency on the ^{14}C saturation activities and the $^{14}C/^{10}Be$ ratios. In addition to the major topic of this study, i.e., the terrestrial ages, cosmogenic noble gases, particularly $^{21}Ne_{cos}$ and $(^{22}Ne/^{21}Ne)_{cos}$, provide valuable constraints on exposure histories. Especially important is the cosmic ray exposure age determined via $^{21}Ne_{cos}$, as this gives information if the measured ^{10}Be is in saturation and therefore if the $^{14}C/^{10}Be$ dating system can be applied without further corrections.

To summarize, by combining newly measured noble gas data with published ^{14}C activity concentrations and $^{14}C/^{10}Be$ ratios for strewn-fields, new, more reliable terrestrial ages are produced. Integrating this with literature data for other desert meteorites (corrected for shielding effects) provides a consistent database for terrestrial ages of hot desert meteorites and finally provides new insights into the meteorite flux to Earth.

5.2. Experimental Methods

5.2.1. *Studied Meteorites*

Meteorites from well-studied strewn-fields in the Sultanate of Oman were selected for noble gas studies. The strewn fields in question are: JaH073 (L6), JaH091 (L5), SaU 001 (L4-5), Shisr 015 (L4-5), and Dhofar 005 (L6). In addition, the two single unpaired stones RaS 267 (LL6) and SaU 163 (H5) are included in this study. Details of the studied samples and their internal (field) number are given by Sliz et al. (2022) and listed in Table 5.1. The measured ^{14}C and ^{10}Be activity concentrations of the samples are published by Sliz et al. (2022). This study aims at completing the dataset by measuring the cosmic ray exposure ages and shielding conditions using cosmogenic noble gases in aliquots of the samples.

Table 5.1. Meteorites in this study.

Meteorites	Internal Nr.	Type	Find Year	TKW (kg)	References
JaH073	0201–640	L6	Al Wusta, Oman	650	Al-Kathiri et al. (2005)
JaH091	0210–11	L5	Al Wusta, Oman	4600	Al-Kathiri et al. (2005)
SaU001_243	0201–243	L4-5	Al Wusta, Oman	423	Sliz et al. (2022)
SaU001_04	0201–04	L4-5	Al Wusta, Oman	423	Sliz et al. (2022)
Shisr015_1942	0212–1942	L5	Zufar, Oman	3.41	Sliz et al. (2022)
Shisr015_165	0102–165	L5	Zufar, Oman	3.41	Sliz et al. (2022)
Shisr015_78	0301–78	L5	Zufar, Oman	3.41	Sliz et al. (2022)
Dhofar 005	0102–200	L6	Dhofar, Oman	125.5	Sliz et al. (2022)
SaU 163	0101–002	H5	Al Wusta, Oman	1.88	Al-Kathiri et al. (2005)
RaS 267	0801–005	LL6	Al Wusta, Oman	0.117	Zurfluh et al. (2016)

5.2.2. *Noble Gas Measurements*

He, Ne, and Ar isotopic concentrations were measured in homogenised sample aliquots with a mass of ~50 mg, wrapped in commercial aluminium foil, and loaded into the noble gas extraction line. The measurements followed the standard procedures established at the Physics Institute, University of Bern. The details of the gas extraction, purification, and measurement can be found elsewhere (e.g., Tauseef et al., 2024; Leya et al., 2013).

Regularly measured blanks were (in units 10^{-10} cm^3STP) ~2.0, ~9, ~0.2 for ^3He, ^4He, and ^{20}Ne, respectively. Blanks for ^3He, ^4He, and all three Ne isotopes contribute for all samples less than 1% to the measured sample gas amounts. Calibrations were regularly conducted using standard gases having atmospheric isotopic composition, except for helium, which has a higher $^3He/^4He$ ratio compared to atmospheric. Gas concentrations were determined by peak height comparisons between samples and standards. Additionally, the data are corrected for interferences and instrument nonlinearities. The uncertainties given for the noble gas data include statistical uncertainties and uncertainties originating from blank corrections and calibrations. In addition, systematic uncertainties of 2% and 4% are added to isotope ratios and isotope concentrations, respectively. For some samples, ^4He was not measured in some samples due to an overloading of the digital voltmeter (DVM).

5.3. Results

5.3.1. *He and Ne Gas Concentrations and Isotopic Ratios*

The results of He and Ne isotope concentrations and ratios are given in Table 5.2. The measured ^{3}He concentrations (in units 10^{-8} cm^{3}STP/g) range from 0.61 ± 0.4 in Dhofar 005-1 to 37.8 ± 5.2 in SaU 163-1. Measured ^{20}Ne concentrations (in units 10^{-8} cm^{3}STP/g) range from 0.40 ± 0.05 in Dhofar 005-1 to 10.1 ± 0.68 in JaH073-2. The ^{20}Ne/^{22}Ne ratios vary from 0.821 ± 0.03 in Dhofar 005-1 to 1.729 ± 0.04 in SaU 001 243-2, indicating that measured Ne is dominated by cosmogenic contributions. Cosmogenic ^{22}Ne/^{21}Ne ratios, i.e., $(^{22}Ne/^{21}Ne)_{cos}$, and $^{21}Ne_{cos}$ concentrations are calculated using a two-component deconvolution, assuming cosmogenic $(^{20}Ne/^{22}Ne)_{cos}$ = 0.826, which is the lowest ratio measured for the samples, and air (^{20}Ne/^{22}Ne = 9.8 and ^{21}Ne/^{22}Ne = 0.02878) as endmembers. The results are also given in Table 5.2. The $(^{22}Ne/^{21}Ne)_{cos}$ ratios range from 1.037 ± 0.002 for Dhofar 005-1 to 1.211 ± 0.017 for RaS 267-1, indicating a large variation in the pre-atmospheric sizes and shielding depths of the studied strewn-field meteorites. For most meteorites up to three aliquots were measured. The reproducibility of the $(^{22}Ne/^{21}Ne)_{cos}$ ratios for the different aliquots is within the 1σ standard deviations, the only exception is SaU001 (stone 04), for which agreement is within the 2σ standard deviations. The good reproducibly enables one to calculate average $(^{22}Ne/^{21}Ne)_{cos}$ ratios for each studied sample. The average $(^{22}Ne/^{21}Ne)_{cos}$ ratios range from 1.037 ± 0.002 for Dhofar 005 to 1.209 ± 0.003 for RaS 267. Considering only the strewnfield meteorites, the average $(^{22}Ne/^{21}Ne)_{cos}$ ranges from 1.037 ± 0.002 for Dhofar 005 to 1.077 ± 0.038 for SaU001, i.e., indicating large pre-atmospheric objects, as expected for strewnfields. The highest $(^{22}Ne/^{21}Ne)_{cos}$ ratio has been determined for RaS 267, which is a single unpaired chondrite with a small preatmospheric size. The found mass for RaS 267 is ~100 g.

The $^{21}Ne_{cos}$ concentrations range from (in 10^{-8} cm^{3}STP/g) 0.42 ± 0.01 in SaU 001 (stone 243) to 11.1 ± 0.8 in JaH073-2. The reproducibility for $^{21}Ne_{cos}$ among aliquots of the same sample is in most cases within the 1σ standard deviations; an exception is JaH073, for which agreement is within the 2σ standard deviations. For Shişr 015, the two aliquots differ by more than a factor of 2. The same discrepancy can be seen in the ^{3}He data, aliquot 1 is about a factor of 3 lower than aliquot 2. While two aliquots for Shişr 015 gave $(^{21}Ne)_{cos}$ in agreement within the 1σ standard deviations, one aliquot is more than a factor of 2 lower. This aliquot is not considered for calculating averages (see below). For all other samples, average $(^{21}Ne)_{cos}$ are calculated and used for further discussion.

Table 5.2. He and Ne isotope concentrations, cosmogenic ^{21}Ne, and $(^{22}Ne/^{21}Ne)_{cos}$, and ^{21}Ne-CRE ages for the studied meteorites.

		Mass	Concentrations are in 10^{-8} cm^3STP/g							
Meteorite	**Type**	**(mg)**	**^3He**	**^4He**	**^{20}Ne**	**$^{20}Ne/^{22}Ne$**	**$^{21}Ne/^{22}Ne$**	**$^{22}Ne/^{21}Ne_{cos}$**	**$^{21}Ne_{cos}$**	***T_{21}* (Myr)**
JaH073_1	L6	50.67	16.8 ±2.3	n.d.	7.87 ±0.53	0.867 ±0.018	0.951 ±0.019	1.047±0.025	8.63±0.63	17.4±1.8
JaH073_2	L6	50.29	23.7 ±3.3	n.d.	10.1 ±0.68	0.868 ±0.018	0.955 ±0.019	1.042±0.025	11.13±0.8	22.0±2.3
JaH073_3	L6	50.27	17.9 ±2.6	n.d.	8.32 ±0.56	0.874 ±0.019	0.958 ±0.019	1.038±0.028	9.12±0.67	17.7±1.9
Mean JaH 073								***1.042±0.004***	***9.63±1.32***	***19.0±2.5***
JaH091_1	L5	50.45	26.2 ±3.6	n.d.	7.89 ±0.54	0.878 ±0.026	0.935 ±0.019	1.063±0.030	8.40±0.65	18.3±2.1
JaH091_2	L5	50.70	24.4 ±3.4	n.d.	7.29 ±0.49	0.872 ±0.019	0.938 ±0.019	1.061±0.028	7.83±0.58	16.9±1.8
JaH091_3	L5	50.70	23.5 ±2.8	892 ±44	7.26 ±0.36	0.862 ±0.026	0.928 ±0.020	1.073±0.026	7.81±0.48	17.9±1.6
Mean JaH 091								***1.066±0.007***	***8.01±0.33***	***17.7±0.7***
SaU 001_243_1	L4/5	50.03	1.45 ±0.4	n.d.	0.84 ±0.08	1.692 ±0.040	0.863 ±0.020	1.050±0.040	0.43±0.04	0.87±0.3
SaU 001_243_2	L4/5	50.29	1.03 ±0.1	258 ±13	0.89 ±0.05	1.729 ±0.040	0.818 ±0.017	1.104±0.030	0.42±0.03	1.13±0.2
Mean SaU 001_243								***1.077±0.038***	***0.42±0.01***	***1.00±0.2***
SaU 001_04_1	L4/5	50.29	1.82 ±0.5	n.d.	0.40 ±0.05	0.894 ±0.055	0.927 ±0.024	1.071±0.021	0.42±0.06	0.94±0.2
SaU 001_04_2	L4/5	50.41	2.08 ±0.1	736 ±37	0.56 ±0.07	1.062 ±0.093	0.903 ±0.018	1.079±0.028	0.48±0.07	1.13±0.3
Mean SaU 001_04								***1.075±0.006***	***0.45±0.04***	***1.04±0.1***
Shisr 015_1942_1	L5	50.12	5.21 ±0.9	n.d.	2.10 ±0.15	0.865 ±0.020	0.954 ±0.019	1.044±0.022	2.31±0.18	4.60±0.5
Shisr 015_1942_2	L5	50.33	15.63 ±1	667 ±63	5.90 ±0.29	0.865 ±0.027	0.941 ±0.019	1.058±0.004	6.42±0.39	13.7±1.2
Mean Shisr 015_1942								***1.051±0.010***	***4.37±2.90***	***9.13±6.4***
Shisr 015_165_1	L5	50.08	14.6 ±2.1	n.d.	5.77 ±0.40	0.846 ±0.019	0.934 ±0.019	1.068±0.012	6.37±0.48	14.3±1.5
Shisr 015_165_2	L5	50.25	18.4 ±2.2	559 ±36	6.87 ±0.49	0.865 ±0.027	0.934 ±0.019	1.066±0.021	7.42±0.60	16.4±1.9
Mean Shisr 015_165								***1.067±0.002***	***6.90±0.75***	***15.3±1.5***
Shisr 015_78_1	L5	50.35	5.46 ±0.9	n.d.	2.45 ±0.17	0.883 ±0.028	0.954 ±0.019	1.041±0.031	2.65±0.21	5.21±0.6
Shisr 015_78_2	L5	50.27	n.d.	n.d.	5.17 ±0.27	0.849 ±0.039	0.943 ±0.023	1.058±0.014	5.74±0.42	12.2±1.3
Shisr 015_78_3	L5	50.24	15.6 ±2.3	560 ±43	6.43 ±0.67	0.897 ±0.058	0.943 ±0.020	1.052±0.029	6.77±0.84	14.0±2.5
Mean Shisr 015_78								***1.050±0.008***	***5.05±2.14***	***10.5±4.6***
Dhofar 005_1	L6	50.31	0.61 ±0.5	7.0 ±2.8	0.40 ±0.05	0.821 ±0.030	0.965 ±0.021	1.037±0.002	0.47±0.06	0.90±0.2
Dhofar 005_2	L5									
Mean Dhofar 005								***1.037±0.002***	***0.47±0.06***	***0.90±0.2***
SaU 163_1	H5	50.24	37.8 ±5.2	n.d.	8.61 ±0.60	0.862 ±0.018	0.937 ±0.019	1.064±0.019	9.36±0.71	22.0±2.4
SaU 163_2	H5									
Mean SaU 163								***1.064±0.019***	***9.36±0.71***	***22.0±2.4***
RaS 267_1	LL6	50.48	n.d.	n.d.	2.42 ±0.17	0.852 ±0.024	0.823 ±0.017	1.211±0.017	2.34±0.18	11.2±1.3
RaS 267_2	LL6	50.25	n.d.	n.d.	3.42 ±0.21	0.850 ±0.041	0.824 ±0.020	1.210±0.015	3.32±0.27	15.8±1.8
RaS 267_3	LL6	50.04	1254 ±91	83.6 ±6.9	3.12 ±0.42	0.905 ±0.061	0.822 ±0.017	1.206±0.030	2.83±0.43	13.1±2.8
Mean RaS 267								***1.209±0.003***	***2.83±0.49***	***13.4±2.3***

5.3.2. *CRE Ages and Pre-atmospheric Size ($^{22}Ne/^{21}Ne_{cos}$)*

CRE ages (T_{21}) were calculated using measured $^{21}Ne_{cos}$ and $(^{22}Ne/^{21}Ne)_{cos}$ ratios following the correlations for H, L, and LL chondrites given by Dalcher et al. (2013). Ages were calculated for each aliquot separately and shown in Fig. 5.1. In the following, average CRE ages per sample are discussed and given in Table 5.2. The ages vary between 1.0 ± 0.2 Ma for SaU 001 to 22.0 ± 2.4 Ma for SaU 163. The T_{21} ages for the different aliquots of the same sample agree within the 2σ standard deviations, exceptions are one out of two aliquots for Shişr 015 (fragment 1942) and one out of three aliquots for Shişr 015 (fragment 78) (see also discussion of $^{21}Ne_{cos}$ above).

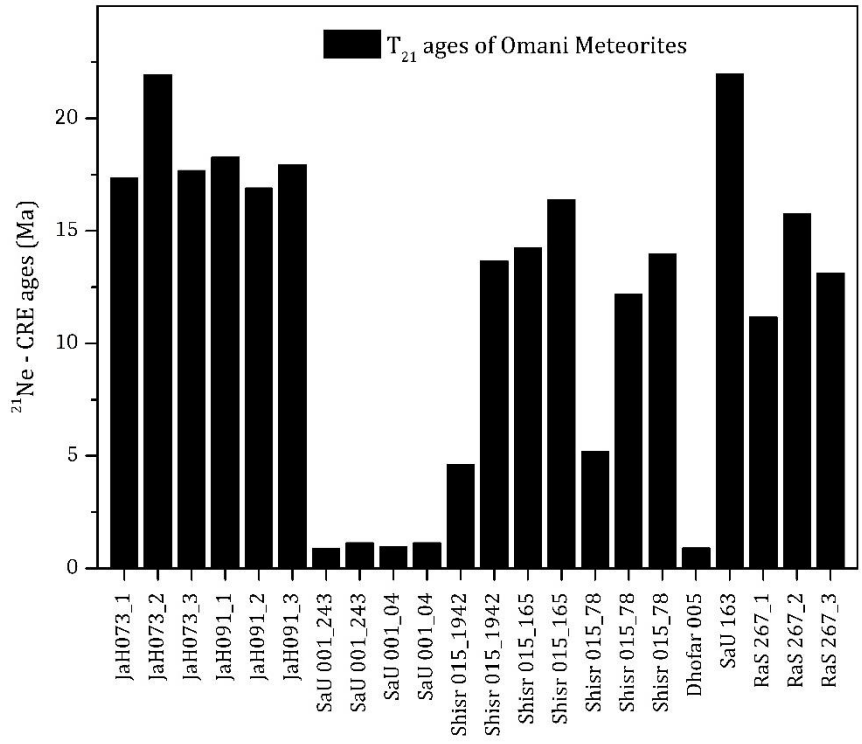

Fig. 5.1. . $^{21}Ne_{cos}$ CRE ages histogram for Omani meteorites.

The JaH 073 strewn field meteorite has been studied extensively before for its complex exposure history (Huber et al., 2008, 2007; Gnos et al., 2009). Huber et al. (2008) reported, based on radionuclide data, a first exposure stage in a large body (2π) of ~65 Ma and a second exposure age of 0.5–0.7 Ma as a large object in space. The T_{21} age of 19.0 ± 2.5 Ma for stone #640 has therefore no chronological meaning. There are differences in the $(^{22}Ne/^{21}Ne)_{cos}$ ratios. The measured ratios of 1.038–1.047 (average 1.042 ± 0.004) are lower than the previously reported ratio of 1.066 ± 0.018 for the same stone #640 (Huber et al., 2008). Low ratios (~1.04)

have been reported also for other fragments of JaH 073 (Huber et al., 2008). Such low $(^{22}Ne/^{21}Ne)_{cos}$ ratios indicate that samples were located at deep shielding depths in a large object. Ratios lower than 1.04 are typically observed in iron meteorites (Smith et al., 2019) and in some ureilites (Leya and Stephenson, 2019). In ordinary chondrites, however, modeled $(^{22}Ne/^{21}Ne)_{cos}$ ratios are higher than ~1.06. Lower ratios might actually not be the result of cosmogenic production but might instead indicate loss of Ne caused by selective weathering of Na-bearing plagioclase. Since $(^{22}Ne/^{21}Ne)_{cos}$ in Na-bearing minerals is typically higher than in other minerals, loss of Ne from such minerals would lower the remaining $(^{22}Ne/^{21}Ne)_{cos}$ for the studied sample. For further discussion see Leya and Masarik (2009), Leya et al. (2013) and Huber et al. (2008).

For the L5 chondrite JaH 091, the new T_{21} age of 17.7 ± 0.7 Ma is consistent with the reported age (average of ^{3}He, ^{21}Ne and ^{38}Ar ages) of 15.7 ± 4.6 Ma by Leya et al. (2013). However, the same authors reported a T_{21} age of 12.0 Ma for the same fragment, i.e., ~29% lower than the age determined here. There are also differences in the $(^{22}Ne/^{21}Ne)_{cos}$ ratios, the ratios of 1.061–1.073 (average 1.066 ± 0.007) are significantly lower compared to the 1.108 reported by Leya et al. (2013). The $(^{22}Ne/^{21}Ne)_{cos}$ ratio measured here for JaH 091 is similar to the values for other paired stones JaH 230 and JaH 296 reported by Leya et al. (2013). The low $(^{22}Ne/^{21}Ne)_{cos}$ indicates a relatively large pre-atmospheric size, consistent with the 100–130 cm size estimated by Weber et al. (2017) using the cosmogenic radionuclide ^{26}Al.

The strewn-field SaU 001 has not been studied before for $(^{22}Ne/^{21}Ne)_{cos}$ ratios or T_{21} ages. The CRE ages determined for the two fragments 243 and 04 are 1.0 ± 0.2 and 1.0 ± 0.1 Ma, respectively, i.e., the ages are very consistent. The same good consistency is achieved for $(^{22}Ne/^{21}Ne)_{cos}$. The average of 1.077 ± 0.038 indicates that the studied samples likely originated from a shielded location in an object having a pre-atmospheric radius in the range ~65 cm.

CRE ages for the three fragments 1942, 165, and 78 of the strewn-field Shişr 015 are 9.1 ± 6.4, 15.3 ± 1.5, and 10.5 ± 4.6 Ma, respectively. The agreement is within the 1σ standard deviation. One aliquot of stone fragment 1942 and 78 has low $^{21}Ne_{cos}$ concentration and consequently a low T_{21} ages. Other aliquots have CRE age in much better agreement with the rest of the data for Shişr 015. Ignoring the outliers, one for fragment 1942 and one for fragment 78, gives an average CRE age for Shişr 015 of 14.1 ± 0.8 Ma. Measured $(^{22}Ne/^{21}Ne)_{cos}$ ratios range from 1.052 ± 0.03 for stone 78 to 1.068 ± 0.012 in an aliquot of stone 165. The low $(^{22}Ne/^{21}Ne)_{cos}$

ratios measured here are indicative of a large pre-atmospheric size, likely a meter-sized object in space.

For Dhofar 005, the CRE age is 0.90 ± 0.2 Ma, which is shorter than any of the other CRE ages determined here and also short compared to other L chondrites. The measured $(^{22}Ne/^{21}Ne)_{cos}$ ratios of 1.037 ± 0.002 is lower than that of the other studied meteorites. Such a low ratio can be due to Ne losses caused by weathering and/or shocks. For example, plagioclase is sensitive to weathering losses, thereby lowering the $(^{22}Ne/^{21}Ne)_{cos}$ ratio of the sample. This has been observed for other large meteorites like Jilin and JaH 073 (e.g., Huber et al., 2008). Note that the low $^{21}Ne_{cos}$ concentration and lower $(^{22}Ne/^{21}Ne)_{cos}$ ratios are typical indicator of samples buried at large shielding depth. This finding indicates that Dhofar 005 (stone 200) was a part of a large object in space. The CRE age determined for the single unpaired H5 stone SaU 163 is 22.0 ± 2.4 Ma. The $(^{22}Ne/^{21}Ne)_{cos}$ ratio of 1.064 ± 0.02 indicates that the sample came from a well shielded location and that the SaU 163 meteorite was likely a meter-sized object in space. However, no other fragments or paired stones were found so far.

For the LL6 chondrite RaS 267, a CRE age of 13.4 ± 2.3 Ma is derived. This finding indicates that RaS 267 consistently belongs to the pronounced 15 Ma CRE age peak of LL chondrites (Graf and Marti, 1994). The $(^{22}Ne/^{21}Ne)_{cos}$ ratio of 1.209 ± 0.003 is reproducible across the three aliquots. This finding suggests that RaS 267 had a small pre-atmospheric size, which is in agreement with the recovered mass of 117 g (Sliz et al., 2022).

5.3.3. *Shielding-depth Dependent ^{14}C Saturation Activities and $^{14}C/^{10}Be$ Ratios*

We determined the ^{14}C saturation activities using the measured $(^{22}Ne/^{21}Ne)_{cos}$ ratios and the correlations (eq. 3.4) between the ^{14}C production rates and $(^{22}Ne/^{21}Ne)_{cos}$ given by Tauseef et al. (2024). The results are shown in Fig. 5.2 and are compiled in Table 5.3. Similarly, the $^{14}C/^{10}Be$ saturation ratios are calculated based on the average $(^{22}Ne/^{21}Ne)_{cos}$ values. The thus determined ^{14}C saturation activity concentrations and $^{14}C/^{10}Be$ ratios are corrected for shielding, a correction that sometimes is substantial, and therefore the new terrestrial ages replace earlier estimates using the same measured ^{14}C activity concentrations and $^{14}C/^{10}Be$ ratios but non-shielding corrected production rates and production rate ratios (e.g., Al-Kathiri et al., 2005; Gnos et al., 2009; Sliz et al., 2022).

The ^{14}C saturation activity range from 32.2 ± 0.5 dpm/kg for the LL6 chondrite RaS 267 to 64.7 ± 1.1 dpm/kg for L6 chondrite Dhofar 005. For the only H chondrite in this study, SaU 163, we calculated a saturation activity of 47 ± 1.1 dpm/kg (Fig. 5.2), which is similar to the assumed average activity of 46 ± 1.0 dpm/kg used so far determining terrestrial ages for H chondrites (Jull et al., 1989; Sliz et al., 2022). For the L chondrites, the calculated ^{14}C saturation activities are 2–21% higher than the previously assumed average value of 51.1 ± 1.0 dpm/kg (Jull et al., 1989). In contrast, the ^{14}C saturation activity for the LL6 chondrite RaS 267 of 32.2 ± 0.5 dpm/kg is 42% lower than the assumed constant value of 55.2 ± 1.0 dpm/kg for LL chondrites (Jull et al., 1989). The new ^{14}C saturation activities are fully consistent with the new model calculations for cosmogenic production rates in meteorites that have been extensively validated using data from freshly fallen meteorites (Tauseef et al., 2024, 2025). The calculated $^{14}C/^{10}Be$ saturation ratios range from 1.75 ± 0.01 for RaS 267 to 3.05 ± 0.18 for Dhofar 005 (Table 5.3), i.e., they vary by 30% compared to the commonly assumed constant value of 2.5 ± 0.1 (Welten et al., 2001; Kring et al., 2001; Jull et al., 2010). Overall, the calculated $^{14}C/^{10}Be$ saturation ratios align well with the determined ratios observed in recently fallen meteorites (Tauseef et al., 2025; Jull et al., 2009) and are not as constant as previously assumed.

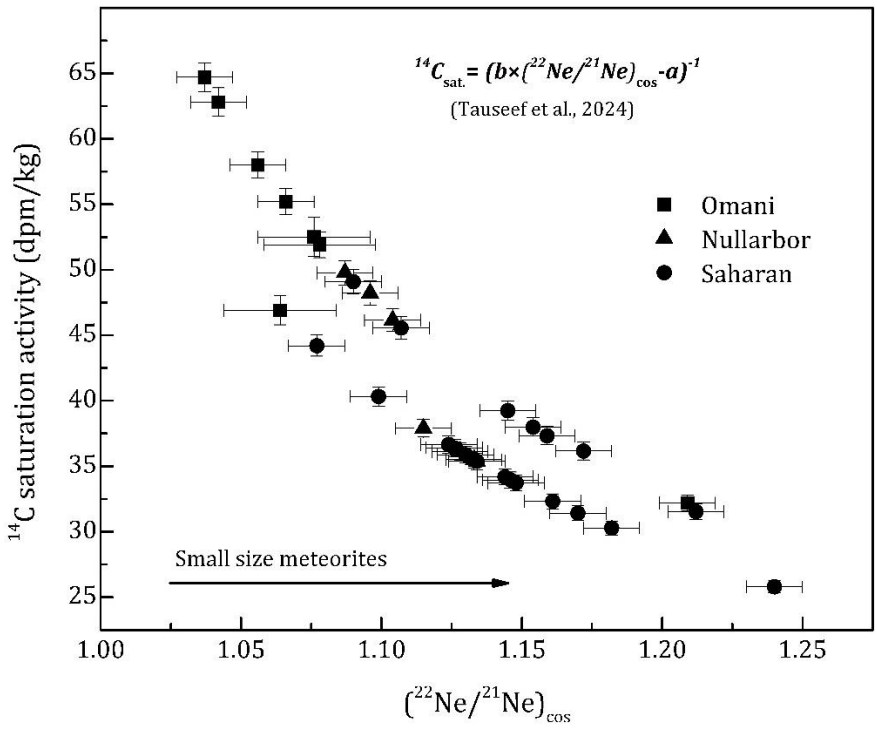

Fig. 5.2. ^{14}C saturation activity concentrations in meteorites from the desert region of Oman, Australia and Sahara, calculated using the measured $(^{22}Ne/^{21}Ne)_{cos,}$ and the correlation established between ^{14}C production rate and $(^{22}Ne/^{21}Ne)_{cos}$ (eq. 3.4; Tauseef et al., 2024). The $(^{22}Ne/^{21}Ne)_{cos}$ data for Nullarbor and Saharan meteorites are taken from the database of Schultz and Franke (2004).

5.3.4. *Revised Terrestrial Ages*

Using the ^{14}C saturation activity concentrations and the $^{14}C/^{10}Be$ production rate ratios calculated above, new terrestrial ages are calculated for the meteorites recently studied by Sliz et al. (2022). Additionally, we have also compiled data of meteorites from Sahara Desert and Nullarbor region to make a comparative study of their reported terrestrial age with new shielding-based ages derived in this study. The revised ages along with the earlier reported ages are summarised in Table 5.3 and 5.4.

5.3.5. *Revised ^{14}C and $^{14}C/^{10}Be$ Terrestrial Ages for Omani Meteorites*

For the H chondrite SaU 163, the determined ^{14}C and $^{14}C/^{10}Be$ ages are in good agreement and they agree with earlier estimates by Al-Kathiri et al. (2005) and Sliz et al. (2022). The average ^{14}C and $^{14}C/^{10}Be$ terrestrial age is 22.5 ± 1.2 ka. For the L6 chondrite JaH 073, we calculated a ^{14}C terrestrial age of 20.2 ± 0.9 ka (Fig. 5.3), which is 6% higher than the 18.6 ± 2.0 ka reported by Sliz et al. (2022) and 10% higher than the 18 ± 1.3 ka given by Gnos et al. (2009). Due to the complex exposure history, ^{14}C and ^{10}Be are not referring to the same irradiation conditions, and therefore the $^{14}C/^{10}Be$ dating system cannot be applied. The adopted terrestrial age for JaH 073 is 20.2 ± 0.9 ka. The new ^{14}C and $^{14}C/^{10}Be$ terrestrial ages for JaH 091 agree with earlier estimates by Sliz et al. (2022) but are slightly lower than the ^{14}C age given by Al-Kathiri et al. (2005) due to significantly lower ^{14}C activity concentrations (4.90 ± 0.10 dpm/kg compared to 11.8 ± 0.2 dpm/kg). The adopted new terrestrial age for JaH 091 is 12.4 ± 0.4 ka. Both fragments of SaU 001 (04 and 243) give ^{14}C terrestrial ages in good agreement. Both ages also agree with earlier data from Sliz et al. (2022). Due to the short CRE age of only 1 Ma, ^{10}Be is not in saturation and therefore, the $^{14}C/^{10}Be$ dating system cannot be applied. The adopted terrestrial age for SaU 001 is 12.9 ± 3.9 ka. Note that the ^{14}C age of fragment 290 from SaU 001, which is assumed to be part of the same strewnfield, has a ^{14}C terrestrial age of 3.0 ± 0.6 ka (Sliz et al., 2022), i.e., much lower than the other studied fragments of the strewnfield. Therefore, fragment 290 cannot be part of the SaU001 strewnfield but must be from a different fall event. All three fragments for Shişr 015 (78, 165, 1942) give consistent ^{14}C and $^{14}C/^{10}Be$ terrestrial ages. The new ages agree with earlier estimates by Sliz et al. (2022) and Al-Kathiri et al. (2005). The new terrestrial age for Shişr 015 is 32.6 ± 2.1 ka.

Dhofar 005 also had a very short CRE age of 0.9 ± 0.2 Ma, prohibiting the use of the $^{14}C/^{10}Be$ dating system because ^{10}Be is not in saturation. Despite this, the ^{14}C and $^{14}C/^{10}Be$ terrestrial ages are in reasonable agreement. This might be due to the fact, the Dhofar 005 was an

exceptionally large object is space, as indicated by the extremely low $(^{22}Ne/^{21}Ne)_{cos}$ ratio. For such large objects, the correlation between $^{21}Ne_{cos}$ production rates and $(^{22}Ne/^{21}Ne)_{cos}$ is no longer valid and $^{21}Ne_{cos}$ production rates are significantly overestimated. If this is the case for Dhofar 005, the exposure age is most likely longer than 0.9 ± 0.2 Ma, bringing ^{10}Be close to saturation and making the $^{14}C/^{10}Be$ dating system more applicable. However, for calculating the adopted terrestrial age, only the ^{14}C age is considered, which gives 39.8 ± 2.4 ka. The LL6 chondrite RaS 267 is a single unpaired stone. The new ^{14}C and $^{14}C/^{10}Be$ terrestrial ages agree with each other and they agree within the 1σ uncertainties with the ages given by Sliz et al. (2022). There is also some agreement with ^{14}C age published earlier by Al-Kathiri et al. (2005). The new adopted age (weighted average ^{14}C and $^{14}C/^{10}Be$) is 20.0 ± 1.6 ka. Fig. 5.3 depicts the new, improved terrestrial ages for the studied Omani meteorites, and compares the results to the earlier ages given by Sliz et al. (2022), Al-Kathiri et al. (2055), and Zurfluh et al. (2016). For most meteorites, the agreement is good, a notable exception is RaS 267.

Two large pieces (total mass 1.75 t) of the L5 regolith breccia Ghubara were found in the year 1954 in the Al Wusta region of Oman. This meteorite has been extensively studied due to its unique characteristics of trapped solar noble gases. Ferko et al. (2002) systematically analysed the cosmogenic radionuclides ^{14}C, ^{10}Be, ^{26}Al and noble gas isotopes in different pieces of Ghubara, including material from a drill core. The authors gave a ^{14}C terrestrial age in the range of 2–3 ka based on an average saturation activity of 51 dpm/kg. However, combining all data and using the results from Tauseef et al. (2024), we can be more accurate. Using the published $(^{22}Ne/^{21}Ne)_{cos}$ of 1.780, a ^{14}C saturation activity of 51.9 ± 1.0 dpm/kg is calculated. Using now the measured ^{14}C activity of 38 ± 1 (Ferko et al., 2002), a ^{14}C terrestrial age of 2.57 ± 0.1 ka is calculated. However, using the measured ^{10}Be data of 17.3 ± 0.3 dpm/kg (Ferko et al., 2002) gives a $^{14}C/^{10}Be$ ratio of 2.2 ± 0.07 for the same aliquot for which $(^{22}Ne/^{21}Ne)_{cos}$ was determined. This corresponds to a $^{14}C/^{10}Be$ terrestrial age of 1.15 ± 0.06 kyr, i.e., significantly lower than the ^{14}C terrestrial age. The recommended terrestrial age (average of ^{14}C and $^{14}C/^{10}Be$) is 1.86±1.0 ka. Despite the large uncertainties, the short terrestrial age for Ghubara is consistent with the finding that Ghubara belong to the least weathered meteorites (W0) that have been found from Oman so far.

5.3.6. *Recalculating Terrestrial Ages for Other Hot Desert Meteorites*

To update the terrestrial age of meteorites from Acfer and Adrar regions in Algeria, the Nullarbor region in Australia, and for one meteorite from Libya, Hammad al Hamra (HaH) 004. The references for the ^{14}C data are given in Table 5.3, the noble gas data, i.e., the $(^{22}Ne/^{21}Ne)_{cos}$ ratios, are from the compilation by Schultz and Franke (2004). Here we limit ourselves to meteorites with $(^{22}Ne/^{21}Ne)_{cos}$ below 1.250, which is the highest value measured for recently fallen chondrites, and which therefore indicates something like the upper limit of applicability for the empirical correlation between ^{14}C production rates and $(^{22}Ne/^{21}Ne)_{cos}$ (Tauseef et al., 2024). Meteorites with higher ratios, e.g., Ilafegh 013, are excluded. The newly calculated terrestrial ages, together with the originally reported ages, are compiled in Table 5.4 and are shown in Figs. 5.4 and 5.5.

The new terrestrial ages are systematically lower than the original ages. Using constant ^{14}C production rates and $^{14}C/^{10}Be$ production rate ratios gives too old terrestrial ages. The differences are larger for smaller meteorites, i.e., higher $(^{22}Ne/^{21}Ne)_{cos}$ ratios. For example, the H5 chondrite Forrest 007 from the Nullarbor region of Australia has a revised ^{14}C age of 1.14 ± 0.02 ka, which is more than 60% lower than the previously reported age 3.4 ± 1.3 ka (Jull et al., 2010). Similarly, the new ^{14}C age for the LL5 chondrite Kybo 001 of 1.04 ± 0.02 ka is more than 50% lower than the reported age of 2.2 ± 1.3 ka (Jull et al., 2010). There are similar findings for the other studied meteorites, either from Sahara or the Nullarbor region, the recalculated ages are younger than the reported ages. Notably, the revised terrestrial ages for H4 chondrite Boorabie 001 from Nullarbor region, and H5 chondrites Acfer 203 and Acfer 206 from Algeria, have a zero age, indicating that these meteorites are likely recent fall. These findings emphasize the importance of shielding-corrected ^{14}C saturation activities and $^{14}C/^{10}Be$ ratios for accurately determining meteorite terrestrial ages. The observation that the recalculated terrestrial ages are systematically shorter than the ages obtained using average ^{14}C production rates is due to the fact that the earlier studies used average ^{14}C production rates that were determined from medium sized meteorites. Therefore, the dating system was more accurate for (and strictly speaking only applicable to) medium-sized objects. In contrast, most of the meteorites are relatively small and for small objects, the ^{14}C production rates and the $^{14}C/^{10}Be$ ratios are lower than earlier used averages, resulting in shorter terrestrial ages. Therefore, using average ^{14}C production rates and $^{14}C/^{10}Be$ ratios that were determined from medium-sized objects produces a significant size dependent bias into the terrestrial age database, because most meteorites are small, and their terrestrial age is overestimated. The

database established here, which is based on shielding corrected ^{14}C production rates and $^{14}C/^{10}Be$ ratio, gives for the first time accurate terrestrial ages for meteorites independent of their size.

Table 5.3. Shielding-based **s**aturated ^{14}C activities and $^{14}C/^{10}Be$ ratios and refined terrestrial age for Omani meteorites.

Meteorites	Type	$A14_{sat}$ (dpm/kg)	Saturated $^{14}C/^{10}Be$	$A14_m$ (dpm/kg)	Measured $^{14}C/^{10}Be$	T_{14}	$T_{14/10}$	Reference
JaH 073	L6	62.8±1.1	2.98±0.06	5.36±0.21	0.37±0.02	20.2±0.9	17.2±1.0	This study
		51.1±1.0	2.50±0.20	5.36±0.21	0.37±0.02	18.6±2.0	16.1±2.0	(1)
		51.1±1.0	2.50±0.10	5.76±0.12	0.38±0.02	18.0±1.3	15.4±0.4	(2)
JaH 091	L5	55.2±1.0	2.67±0.08	11.8±0.20	0.62±0.01	12.7±0.3	12.1±0.4	This study
		51.1±1.0	2.50±0.20	11.8±0.20	0.62±0.01	12.3±1.9	10.9±1.7	(1)
		51.1±1.0	--	4.90±0.10	--	19.3±1.3	--	(3)
SaU001_243	L4/5	52.2±2.0	2.54±0.42	9.95±4.31	1.48±0.03	13.6±5.9	4.47±0.7	This study
		51.1±1.0	2.50±0.20	9.95±4.31	1.48±0.03	13.9±3.7	6.80±2.6	(1)
SaU001_04	L4/5	52.7±0.9	2.56±0.07	12.1±5.09	1.69±0.06	12.1±5.1	3.43±0.2	This study
		51.1±1.0	2.50±0.20	12.1±5.09	1.69±0.06	12.3±3.6	5.70±2.5	(1)
Shisr015_1942	L5	59.7±1.1	2.85±0.14	0.76±0.05	0.05±0.01	35.9±2.5	33.4±1.7	This study
		51.1±1.0	2.50±0.20	0.76±0.05	0.05±0.01	34.7±4.1	32.5±3.3	(1)
Shisr015_165	L5	54.8±0.9	2.65±0.02	1.27±0.06	0.07±0.01	31.0±1.6	30.0±0.5	This study
		51.1±1.0	2.50±0.20	1.27±0.06	0.07±0.01	31.1±3.8	29.7±3.1	(1)
		51.1±1.0	--	0.60±0.20	--	36.5±2.4	--	(3)
Shisr015_78	L5	59.9±1.1	2.86±0.11	1.05±0.06	0.06±0.01	33.3±2.0	31.9±1.4	This study
		51.1±1.0	2.50±0.20	1.05±0.06	0.06±0.01	32.0±3.9	30.9±3.2	(1)
Dhofar 005	L6	64.7±1.1	3.05±0.18	0.51±0.03	0.05±0.01	39.8±2.4	35.8±2.3	This study
		51.1±1.0	2.50±0.20	0.51±0.03	0.05±0.01	38.1±3.0	35.4±2.5	(1)
		51.1±1.0	--	0.37±0.13	--	40.6±3.1	--	(3)
SaU 163	H5	47.0±1.1	2.37±0.19	3.39±0.05	0.14±0.01	21.6±0.6	23.4±1.9	This study
		46.0±1.0	2.50±0.20	3.39±0.05	0.14±0.01	22.8±2.2	23.3±2.0	(1)
		46.0±1.0	--	3.56±0.15	--	21.2±1.3	--	(3)
RaS 267	LL6	32.2±0.5	1.75±0.01	2.24±0.04	0.16±0.01	21.9±0.5	19.7±0.2	This study
		55.2±1.0	2.50±0.20	2.24±0.04	0.16±0.01	26.4±2.4	23.0±2.0	(1)
		55.2±1.0	--	1.40±0.70	--	30.5±4.4	--	(4)

Note: for this study, the measured ^{14}C activity concentrations and $^{14}C/^{10}Be$ ratio are taken from Sliz et al. (2022).
References: 1= Sliz et al. (2022), 2= Gnos et al. (2009), 3= Al-Kathiri et al. (2005), 4= Zurfluh et al. (2016), respectively.
The saturated ^{14}C activity and $^{14}C/^{10}Be$ ratio are calculated using the correlations given in Tauseef et al. (2024)
[1]saturated activities are calculated using the average $(^{22}Ne/^{21}Ne)_{cos}$ of each meteorite sample (for details see Table S1)

Table 5.4. Shielding-based **s**aturated ^{14}C activities and revised terrestrial age for the Algerian and other meteorite finds.

Meteorites	Type	$(^{22}Ne/^{21}Ne)_{cos}$	$A14_{sat}$ (dpm/kg)	$A14_{m}$ (dpm/kg)	Calculated T_{14} (kyr)	Reported T_{14} (kyr)	Ref.
Ghubara	L5	1.078±0.01	51.94 ± 1.0	38.0 ± 1.0	2.57±0.08	2.0–3.0	(1)
Adrar 003	LL3	1.172±0.03	36.16 ± 0.7	19.9 ± 1.0	4.91±0.26	8.4 ± 1.3	(2)
Acfer 022	H4	1.144±0.03	34.18 ± 0.6	13.5 ± 0.6	7.64±0.37	10.1 ± 0.5	(2)
Acfer 023	H4	1.146±0.03	33.95 ± 0.6	3.5 ± 0.2	18.70±1.12	21.2 ± 1.3	(2)
Acfer 028	H4	1.134±0.02	35.38 ± 0.6	14.7 ± 0.6	7.22±0.32	9.4 ± 0.4	(2)
Acfer 129	H3	1.182±0.02	30.29 ± 0.5	4.4 ± 0.2	15.90±0.77	19.3 ± 1.0	(2)
Acfer 171	H4	1.126±0.03	36.40 ± 0.7	15.2 ± 0.8	7.18±0.40	9.1 ± 0.5	(2)
Acfer 019	L6	1.159±0.03	37.33 ± 0.7	4.7 ± 0.1	17.04±0.50	19.8 ± 1.3	(3)
Acfer 047	L4	1.107±0.02	45.56 ± 0.9	18.5 ± 0.2	7.41±0.16	8.4 ± 1.3	(3)
Acfer 199	L4	1.159±0.02	37.33 ± 0.7	24.6 ± 0.2	3.43±0.07	6.0 ± 1.3	(3)
Acfer 203	H5	1.240±0.03	25.80 ± 0.5	32.8 ± 0.2	-1.97±0.04	2.9 ± 1.3	(3)
Acfer 206	H5	1.077±0.01	44.20 ± 0.8	46.1 ± 0.6	-0.35±0.01	Rec. Fall	(3)
Acfer 210	H3	1.124±0.02	36.66 ± 0.7	2.7 ± 0.1	21.54±0.89	23.6 ± 1.3	(3)
Acfer 212	H5	1.148±0.02	33.72 ± 0.6	8.6 ± 0.1	11.24±0.24	13.9 ± 1.3	(3)
Acfer 225	H3	1.161±0.02	32.32 ± 0.7	20.2 ± 0.1	3.87±0.07	6.9 ± 1.3	(3)
Acfer 263	L6	1.145±0.02	39.24 ± 0.7	31.3 ± 0.4	1.86±0.04	4.0 ± 1.3	(3)
Acfer 280	L6	1.090±0.01	49.09 ± 0.9	10.4 ± 0.1	12.76±0.27	13.1 ± 1.3	(3)
Acfer 292	H5	1.170±0.02	31.42 ± 0.6	18.5 ± 1.3	4.36±0.32	7.6 ± 1.3	(3)
El Djouf 003	L6	1.154±0.02	37.99 ± 0.7	11.8 ± 0.2	9.62±0.20	12.1 ± 1.3	(3)
Ilafegh 011	L5	1.212±0.03	31.53 ± 0.6	6.3 ± 0.1	13.24±0.30	17.3 ± 1.3	(3)
Ilafegh 013	H3	1.537±0.10	14.67 ± 0.3	22.2 ± 1.1	-3.41±0.18	6.0 ± 0.3	(2)
Tanezrouft 006	H3	1.130±0.02	35.88 ± 0.6	13.2 ± 0.7	8.22±0.46	10.3 ± 0.6	(2)
HaH 004	H3	1.099±0.01	40.32 ± 0.7	10.5 ± 0.5	11.06±0.56	12.2 ± 0.6	(2)
Burnabbie[a]	H5	1.128±0.03	36.14 ± 0.7	2.9 ± 0.3	20.89±2.20	23.1 ± 1.4	(4)
Boorabie 001[a]	H4	1.134±0.02	35.38 ± 0.6	41.7 ± 0.3	-1.35±0.03	0.9 ± 1.3	(4)
CarlisleLake 002[a]	H4-5	1.115±0.02	37.90 ± 0.7	32.9 ± 0.2	1.16±0.02	2.8 ± 1.3	(4)
Forrest 007[a]	H4	1.133±0.03	35.50 ± 0.6	30.9 ± 0.3	1.14±0.02	3.4 ± 1.3	(4)
Forrest 009 [a]	L4	1.087±0.01	49.77 ± 0.9	25.0 ± 0.2	5.66±0.12	5.9 ± 1.3	(4)
Forrest 010 [a]	L4	1.104±0.02	46.14 ± 0.9	5.8 ± 0.1	17.00±0.43	17.9 ± 1.3	(4)
Forrest 010 [b]	L4	1.104±0.02	46.14 ± 0.9	1.4 ± 0.1	28.70±6.18	29.5 ± 2.2	(4)
Kybo 001[a]	LL5	1.096±0.01	48.23 ± 0.9	42.5 ± 0.3	1.04±0.02	2.2 ± 1.3	(4)

Noble gas data are obtained from the data collection of Schultz and Franke, 2004.
References: 1= Ferko et al. (2002), 2 = Knauer et al. (1995), 3= Wlotzka et al. (1995), 4= Jull et al. (2010).

5.4. Discussions

Cosmogenic $^{21}Ne_{cos}$ concentrations, and $(^{22}Ne/^{21}Ne)_{cos}$ ratios are determined to estimate the CRE ages and pre-atmospheric shielding of the studied samples. Fig. 5.1 shows the CRE age histogram for Omani meteorite. The reproducibility across stones of a strewnfield can be clearly seen in the histogram. By the way of example, the CRE age of ~1 Ma determined for SaU 001 are consistent across aliquots of stones 241 and 04. Good reproducibility was also

achieved for aliquots of JaH091. In addition, CRE ages are essential information to check if ^{10}Be is in saturation and therefore if the ^{14}C/^{10}Be dating system can be used. By way of example, the CRE age for strewnfield SaU 001 of ~1 Ma is too short for ^{10}Be to reach saturation and therefore the ^{14}C/^{10}Be system cannot be applied, at least not without adjusting the ^{10}Be activity concentration.

The measured $(^{22}Ne/^{21}Ne)_{cos}$ indicates large pre-atmospheric shielding for strewnfields, which is expected. However, the $(^{22}Ne/^{21}Ne)_{cos}$ ratios of 1.064 for the single stone SaU 163 suggests a large pre-atmospheric size which is not in agreement with the total known mass of 1.88 kg. On the other hand, a small pre-atmospheric shielding (< 10 cm) is derived for the single-stone LL6 chondrite RaS 267, which is consistent with its recovered mass of 110 g. Using the $(^{22}Ne/^{21}Ne)_{cos}$ ratios and the correlation established earlier (eq. 3.4), ^{14}C saturation activities are calculated for the Omani, Nullarbor and Saharan meteorites. The trend in the Fig. 5.2 shows decreasing ^{14}C saturation activities for meteorites with increasing $(^{22}Ne/^{21}Ne)_{cos}$. The variation is significantly large, i.e., from 25 dpm/kg up to 60 dpm/kg (Fig. 5.2). Such large variations have been observed in experimental data from recently fallen meteorites (Tauseef et al., 2025), and also demonstrated by model calculations (Tauseef et al., 2025, 2024; Weiler et al., 2006; Knauer et al., 1995). This means that the ^{14}C production rates decreases with decreasing pre-atmospheric size of meteorites. Therefore, terrestrial age estimates for small meteorites based on the assumption of constant saturation activity give overestimated ages rather than their true ages. Comparing the earlier data, which were all determined using average values for the ^{14}C production rates and/or ^{14}C/^{10}Be production rate ratios, with the new, shielding corrected terrestrial ages demonstrates that the new ages are systematically lower. This is due to the fact, that the average values used earlier were determined from medium-sized meteorites and therefore are strictly valid only for medium-sized objects. In contrast, the ^{14}C production rates and the ^{14}C/^{10}Be production rate ratios for small meteorites are lower and using the too high average values produces too high terrestrial ages. This is exactly what can be seen in this study. Therefore, for calculating accurate terrestrial ages, shielding corrections are necessary.

Fig. 5.3 show the terrestrial age histogram for Omani meteorites. The shielding-corrected ages for strewnfields are in general consistent with the previous reported ages, indicating that the average saturation value works fine for medium-large size meteorites. However, significant difference is observed for samples with smaller pre-atmospheric sizes, for instance, refined age for RaS 267 is 16% lower than the previous age. This suggests that earlier estimates, which assumed constant ^{14}C production rates, may have overestimated ages of other small meteorites

from Omani Desert. This size dependent bias is more pronounced in terrestrial ages of Saharan and Nullarbor meteorites, as shown in the terrestrial age histograms (Fig. 4 and 5).

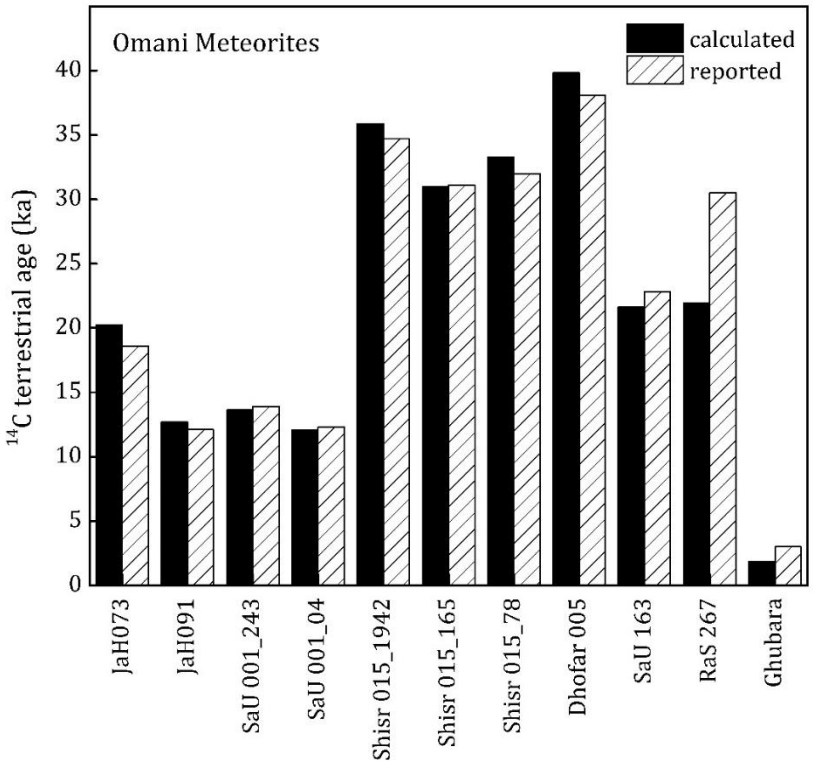

Fig. 5.3. Terrestrial age histogram for Omani meteorites. Average ages (^{14}C and ^{14}C/^{10}Be) are used to develop this histogram. For JaH073, SaU 001 and Dhofar 005, ^{14}C/^{10}Be ages are not considered due to their short CRE ages. Reported data are from Sliz et al. (2022), Zurfluh et al. (2016), Gnos et al. (2009) and Al-Kathiri et al. (2005).

Fig. 5.4 (left panel) shows terrestrial age histogram for Nullarbor meteorites. The differences in calculated and reported ages in the histogram indicate that neglecting shielding effects can lead to overestimations in cases where the meteorite size is small. The histogram reveals significant and systematic lower terrestrial ages than previously reported ages. While more than 50% lower ages are calculated for Forrest 007 and Kybo, a negative age in the histogram for the H4 chondrite Boorabie 001 suggest that it has been fallen recently and has no terrestrial age.

Fig. 5.4 (right panel) show the terrestrial age distribution for Saharan meteorites, which exhibits a prominent and systematic size-dependent bias in the histogram. It is possibly due to the fact that a large number of found and dated meteorites from Acfer and Adrar regions are smaller in size., The histogram reveal a negative age for Acfer 203, similar to that of Acfer 206, indicating

that Acfer 203 is likely a recent fall and should not have a ~3 ka terrestrial age as reported earlier by Wlotzka et al. (1995). The shielding-corrected ages show significant deviations from uncorrected values, reinforcing the importance of accounting for depth-dependent production rates.

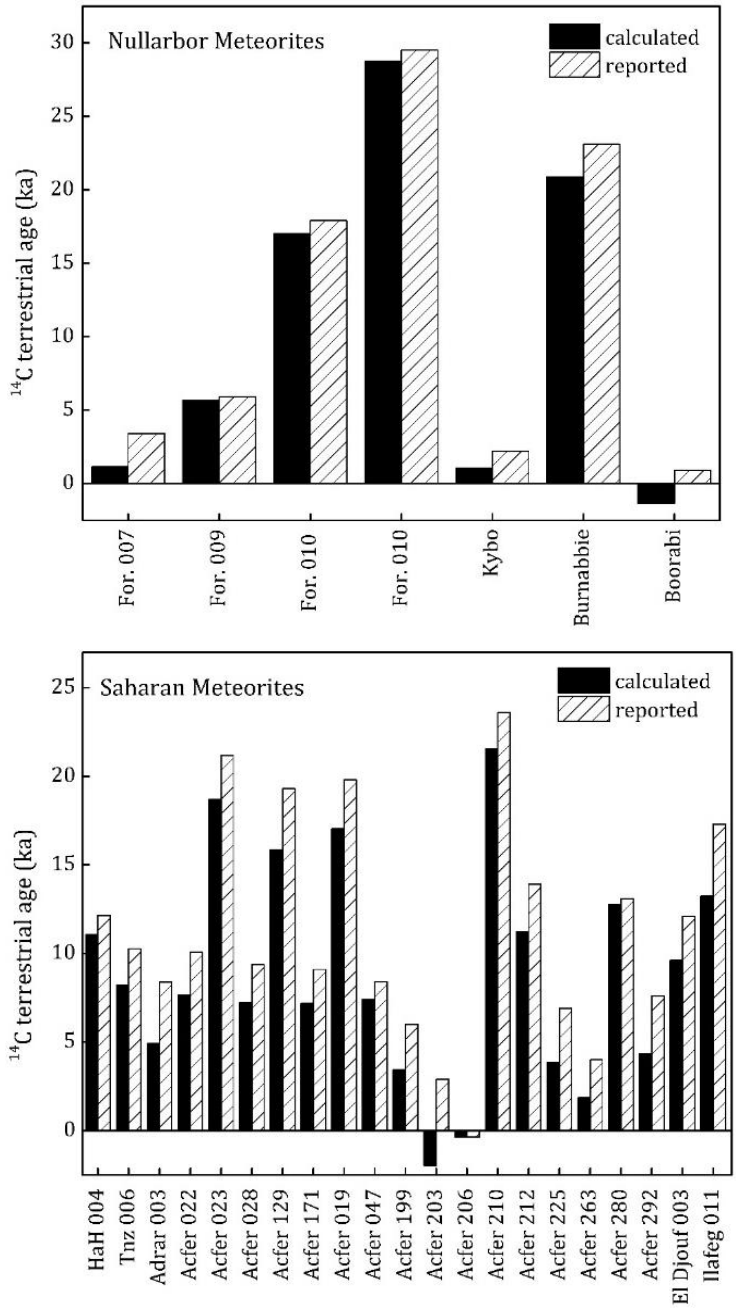

Fig. 5.4. ^{14}C terrestrial age histogram for meteorites from Nullarbor region, Australia (upper panel) and meteorites from Acfer and Adrar region of Algeria and Hammad al Hamra (HaH) 004 from Libya (lower panel). Boorabie, Acfer 203 and 206 falls below zero line are likely recently fallen meteorites. Reported ^{14}C age data are form Jull et al. (2010) for Nullarbor meteorites, and from Knauer et al., (1995), and Wlotzka et al. (1995) for Saharan meteorites.

5.5 Conclusions

In conclusion, this study presents a refined approach based on measured ^{14}C and ^{10}Be activity concentrations, noble gas isotope concentrations, and the correlations (eq. 3.4) developed by Tauseef et al. (2024) to determine shielding corrected ^{14}C and $^{14}C/^{10}Be$ terrestrial ages. our methodology allows for an accurate determination of terrestrial ages by fully considering shielding effects. It is therefore highly recommended to integrate noble gas measurements to the ^{14}C and/or ^{10}Be analyses on aliquots. The refined – and for the first time shielding corrected – terrestrial ages presented here not only resolve discrepancies reported in earlier studies but also demonstrates that the new dating framework is robust, and accurate.

There is, however, still some rooms for improvement. For example, the correlations given by Tauseef et al. (2024) for ^{14}C production rates and $^{14}C/^{10}Be$ production rate ratios as a function of $(^{22}Ne/^{21}Ne)_{cos}$ are not well validated for very small meteorites, i.e., for high $(^{22}Ne/^{21}Ne)_{cos}$ ratios. This situation is about to change thanks to the growing number of recorded meteorites falls.

These findings underscore the importance of shielding-corrected ^{14}C saturation activities (and $^{14}C/^{10}Be$ ratios as well) for accurately determining meteorite terrestrial ages. Detailed measurements of both ^{14}C and $^{14}C/^{10}Be$ ratios, provide a comprehensive view of the exposure histories and help identify influences from cosmic-ray irradiation and terrestrial weathering for each meteorite. The assumption of constant saturation values for all meteorites neglects size-shielding effects, leading to inaccuracies in the terrestrial age estimates. Some meteorites in the dataset were excluded due to their $(^{22}Ne/^{21}Ne)_{cos}$ ratios exceeding higher than the typical cosmogenic range for ordinary chondrites (> 1.5) (Leya and Masarik, 2009) and in model calculation for ^{14}C saturation activity (Tauseef et al., 2024). For those meteorite re-measuring noble gas isotopes could constrain their shielding depth and improve terrestrial age estimates. Our findings emphasize the importance of incorporating size-specific production rate models in terrestrial age calculations. By integrating noble gas ratio data as an indicator of pre-atmospheric size and shielding depth, the reliability of the terrestrial age database can be significantly improved.

Chapter 6

Terrestrial *in-situ* ^{14}C production in some of the Oldest Meteorites from the Atacama Desert, Chile

Manuscript **in preparation** to be submitted in a peer-reviewed Journal.

Numbering of the Title, tables and figures presented in this chapter are formatted to fit the layout of this thesis.

Terrestrial *in-situ* ^{14}C production in some of the oldest meteorites recovered from Atacama Desert

Mohammad Tauseef*[1], Ingo Leya[1], Jérôme Gattacceca[2], Sönke Szidat[3]

[1]Space Research and Planetology, Physics Institute, University of Bern, Sidlerstrasse 5, 3012 Bern, Switzerland

[2]CNRS, Aix Marseille Université, IRD, INRAE, CEREGE, Aix-en-Provence, France

[3]Department of Chemistry, Biochemistry and Pharmaceutical Sciences & Oeschger Centre for Climate Change Research, University of Bern, Freiestrasse 3, 3012 Bern, Switzerland

Corresponding author email: mohammad.tauseef@unibe.ch

ABSTRACT

This is a preliminary study, which investigates the possibility of detecting terrestrial production of *in-situ* ^{14}C in meteorites with terrestrial ages over 100 ka. For this, we studied meteorites from Atacama Desert, which is known for its hyper-arid conditions and long-term meteorite preservation. L chondrites recovered from the Caleta el Cobre, El Medano, and San Juan dense collection areas in Chile, with terrestrial ages ranging up to 500 ka based on ^{10}Be dating, are selected. Using accelerator mass spectrometry (AMS), we measured ^{14}C concentrations in these leached meteorites, with values ranging from 1.28×10^7 to 1.60×10^7 atoms/g. The calculated ^{14}C production rates under secular equilibrium conditions vary between 1554 and 1933 atoms/g/yr, with estimated muogenic contributions accounting for approximately 17% of the total production. These rates are more than 10 times higher than those typically observed in terrestrial quartz but still significantly lower than the cosmogenic ^{14}C production in space. Our findings suggest that ^{14}C production in meteorites is influenced by shielding effects, chemical composition, and altitude-dependent cosmic ray flux. However, the results are higher than expected and provide critical insights into the possible terrestrial production of radionuclide, contamination during $^{14}CO_2$ extraction, and understanding of the interplay between cosmogenic and muogenic production in extraterrestrial materials.

6.1. Introduction

Carbon-14 is continuously produced in pre-atmospheric meteorites (meteoroids) through interactions with cosmic rays. These interactions induce spallation reactions, where high-energy particles break apart target atomic (oxygen atom) nuclei, producing ^{14}C. A prolonged exposure of more than 30,000 years is typically sufficient for ^{14}C to reach saturation levels. This process applies to most meteorites that arrive on Earth. However, once meteorites land, they are shielded from cosmic rays, causing ^{14}C production to cease or become negligible compared to production in space. With no further production, the remaining ^{14}C (half-life of 5730 years) begins to decay, eventually becoming undetectable after several tens of thousands of years on Earth. This decay process serves as a reliable tool for determining the terrestrial ages of meteorites (T_{age}).

The preservation of meteorites also plays a critical role in determining their T_{age}, which largely depend on the environmental conditions where the meteorites reside. For example, meteorites recovered from hot deserts such as Oman, Libya, and Western Australia typically have shorter T_{age} (Sliz et al., 2022, 2019; Jull et al., 2010; Al-Kathiri et al., 2005) compared to those found in Antarctica and the Atacama Desert (Drouard et al., 2019; Hutzler et al., 2016; Gattacceca et al., 2011). The latter locations often preserve meteorites for significantly longer durations, with T_{age} extending up to 1–2 million years (Drouard et al., 2019; Hutzler et al., 2016).

Any detectable ^{14}C activity in meteorites with T_{age} exceeding 50,000 years must originate from Earth-based production mechanisms. These mechanisms include spallation by fast neutrons (cosmogenic), capture of thermal neutrons by oxygen atoms, and muogenic production. Such ^{14}C may be produced in situ from oxygen atoms in minerals like olivine and pyroxene. Alternatively, it may result from contamination by organic materials, weathering products (e.g., oxides and hydroxides), carbonates accumulated on the meteorite surface over time, or a combination of both in situ production and contamination. On Earth, the ^{14}C production rate in meteorites is significantly lower than in space due to atmospheric shielding, which attenuates cosmic rays before they reach the surface. Despite this attenuation, ^{14}C can still be produced in meteorites under continuous exposure and stable preservation conditions, particularly in arid environments where weathering and erosion are minimal.

Meteorites from the Atacama Desert are particularly suitable for studying terrestrial ^{14}C production. Recovered meteorites from this hyper-arid desert have some of the longest T_{age} recorded, up to 2 million years (Drouard et al., 2019). Studies (Dunai et al., 2005; Nishiizumi

et al., 2005) have shown that the Atacama Desert contains some of the highest concentrations of cosmogenic nuclides ever measured in terrestrial rocks. However, research by Placzek et al. (2010), based on cosmogenic nuclide data and field observations, suggests that the Central Atacama has remained geomorphically active well into the Pleistocene. Despite this activity, erosion rates and exposure ages are comparable to those in other deserts worldwide. This geomorphic activity does not diminish the Atacama Desert's status as an exceptionally hyper-arid environment. Its nitrate- and gypsum-rich soils, along with paleosols, reflect minimal rainfall over millions of years. Given these long-standing arid conditions, erosion and weathering rates of meteorites in the Atacama are assumed to be very low to negligible. Thus, there is no significant loss of terrestrially produced ^{14}C due to geomorphological processes. Furthermore, we assume continuous exposure of meteorites, with no burial under sand or soil. This allows ^{14}C in meteorites from the Atacama Desert to potentially reach saturation levels. However, the terrestrial ^{14}C saturation activity is expected to be much lower than the saturation activity observed in space for ordinary chondrites (30–60 dpm/kg; Tauseef et al., 2025; Jull et al., 1989). The higher ^{14}C production rate in space is primarily due to meteoroids being continuously bombarded by high-energy cosmic ray particles without the shielding effects of Earth's atmosphere. However, cosmic ray interactions on Earth are not negligible, and in-situ production of ^{14}C does occur in terrestrial environments, albeit at significantly lower rates. For instance, the in-situ ^{14}C production rate measured in quartz from Allan Hills, Antarctica, is 99 ± 12 atoms/g/yr—more than 200 times lower than the typical ^{14}C production observed in meteorites in space. Although we have meteorites with terrestrial ages spanning several hundred thousand years from Antarctica and hot deserts (e.g., Atacama Desert), their cosmogenic nuclide interactions and terrestrial production rates have not been studied before. Investigating these older meteorites for terrestrial ^{14}C production could provide valuable insights into long-term exposure effects, meteorite dynamics on Earth, and the influence of environmental factors on cosmogenic nuclide accumulation in meteorites from different hot or cold deserts.

The objectives of this study are twofold: (i) to determine whether it is possible to measure terrestrial *in-situ* ^{14}C in older meteorites using accelerator mass spectrometry (AMS) and chemical extraction techniques, and (ii) to estimate the terrestrial ^{14}C production rate in meteorites by using $^{36}Cl/^{10}Be$ derived terrestrial ages. Furthermore, a physical model calculation combining cosmogenic (neutron flux and reaction cross-sections) and muonic production rate, can be done to compare with the experimental data.

6.2. Meteorites and Their Find Location

Selected L chondrites in this study are from the Caleta el Cobra, El Medano and San Juan dense collection areas in the central depression (~2000 m ASL) of the Atacama Desert, Chile. These samples were recovered in systematic search campaigns in Atacama Desert conducted by CEREGE, France in collaboration with University of Chile. Located between the western central Andes and the Pacific Ocean, the Atacama Desert has designated as the oldest continuously arid and stable desert for at least 25 Ma (Clarke, 2006; Dunai et al., 2005). Classification of meteorites, petrographic studies, shock and weathering grade were carried out in CEREGE (Drouard et al., 2019; Hutzler et al., 2016; Gattacceca et al., 2011). The relevant details about the meteorites are discussed in the following sections.

6.3. Methodology

6.3.1. *Sample Preparation and $^{14}CO_2$ Extraction*

Carbon-14 extracted from leached samples as CO_2 following the standard procedure established in our lab at Physics Institute, University of Bern (Sliz et al., 2019; Tauseef et al., 2024 and 2025). About 400–800 mg sample material was grinded and leached in two steps. *First*, samples were treated with 6M HCl to remove any carbonates attached to them. *Second*, samples were treated with EGTA to remove weathering products, mainly FeO and FeOH. These leaching steps helps get rid of terrestrial contaminations and to achieve the original composition of meteorites at the time of fall. About 50 mg of sample materials wrapped in Al-foil were extracted in Platinum crucible in the presence of O_2 partial pressure of ~30 mbar. Before gas extraction, samples were heated at 500 °C for an hour to remove any adsorbed atmospheric gas. ^{14}C extracted at 1600 °C subjected to further cleaning with water trap and cold trap to remove moisture and other unwanted gas. Extracted CO_2 was collected in glass ampoules using LN. Sample extraction yield more than enough carbon (>10 µg) for a reliable AMS measurement. Sample re-extraction yields low carbon (< 10 µg) to which ^{14}C-free cylinder CO_2 was added. In addition, we systematically perform extraction and measurement of Al-foil and ^{14}C-free cylinder CO_2 blanks to control the blank contribution to extracted samples. We also perform routine measurements of L6 chondrite JaH 073, which act as an internal standard for our extraction line.

6.3.2. *^{14}C AMS Measurement and Data Reduction*

$^{14}C/^{12}C$ ratios were measured using the MICADAS system at the Laboratory for the Analysis of Radiocarbon with AMS (LARA) in the Department of Chemistry of University of Bern (Szidat, 2020; Szidat et al., 2014). Sample glass ampoules were introduced to the gas interface system of the MICADAS, cracked open, mixed with carrier gas He, and transferred to the gas ion source of AMS. Standard reference material (Oxalic acid II; NIST, Gaithersburg, USA) and blanks were measured before and after the samples for calibration and quality check. The AMS results are given in fraction of modern carbon ($F^{14}C$) and $^{14}C/^{12}C$ ratios with uncertainties related to the correction for isotope fractionation, blank subtraction, and standard normalization. The uncertainty also includes systematic uncertainty of 1.5‰ due to day-to-day variabilities (Szidat et al., 2014). ^{14}C activity concentrations were calculated in disintegration per minute per kg of sample (dpm/kg) based on the procedure given by Hippe et al. (2013) and Hippe and Lifton (2014).

6.4. Results and discussions

6.4.1. *^{14}C Concentrations in Procedural and System Blanks*

The ^{14}C extraction line has been successful in producing low blanks. The very first blanks after replacing the platinum crucible are typically higher than the rest. First cylinder blank (CB_1410) yielded 13.6 (±0.03) $\times 10^4$ ^{14}C atoms. In rest of the cylinder CO_2 blanks, the ^{14}C activity concentrations ranges from 0.40 (±0.01) $\times 10^4$ to 3.5 (±0.02) $\times 10^4$ ^{14}C atoms, contributing an average of ~3% to the measured sample concentrations. ^{14}C activity concentrations measured in six Al-Blank ranges from 3.4 (±0.02) $\times 10^4$ to 8.4 (±0.02) $\times 10^4$ ^{14}C atoms. The average contribution of Al-blank to the ^{14}C concentration measured in samples is about ~7%. Combined, both the blanks account for ~10% of the total ^{14}C concentration observed in the sample. Note, blank measurements were performed at the same extraction conditions as samples. Therefore, the Al-blanks and cylinder CO_2 blanks were also held at extraction temperature of 1600 °C in UHP O_2 for 10 min before trapping CO_2 in helix trap and collection in glass capillaries. Thus, the measured blanks (12%) account for the maximum background ^{14}C contribution from the extraction system. The detailed of blank calculations and corrections are provided in Table 6.1.

Table 6.1. ^{14}C concentration in the procedural (Al-foil) and system (cylinder) blanks.

Blanks	Diluted CO_2 (10^{-2} cm^3)	C equi. (µg)	$F^{14}C$	$\delta^{13}C$ (‰)	$^{14}C/^{12}C$ (10^{-12})	N14 (10^4 at)
CB_1410	3.6 ± 0.03	17.89	0.154 ± 0.004	-24.5	0.15 ± 0.003	13.6 ± 0.3
CB_2210	3.1 ± 0.03	15.61	0.045 ± 0.003	-25.6	0.04 ± 0.001	3.5 ± 0.02
CB_2410	2.6 ± 0.02	13.01	0.006 ± 0.002	-29.1	0.01 ± 0.001	0.4 ± 0.01
CB_2810	2.9 ± 0.02	14.71	0.045 ± 0.003	-26.2	0.04 ± 0.003	3.3 ± 0.02
CB_3010	3.0 ± 0.03	15.20	0.036 ± 0.003	-26.5	0.04 ± 0.002	2.7 ± 0.02
AB_1510	3.9 ± 0.03	19.69	0.086 ± 0.003	-25.6	0.08 ± 0.003	8.4 ± 0.03
AB_1810	3.2 ± 0.03	16.01	0.069 ± 0.003	-26.3	0.07 ± 0.003	5.5 ± 0.03
AB_2210	3.4 ± 0.03	16.95	0.059 ± 0.003	-26.2	0.06 ± 0.003	5.0 ± 0.02
AB_2410	3.1 ± 0.03	15.49	0.085 ± 0.004	-25.6	0.08 ± 0.003	6.5 ± 0.03
AB_2810	2.5 ± 0.02	12.67	0.054 ± 0.003	-26.2	0.05 ± 0.002	3.3 ± 0.02
AB_3010	2.9 ± 0.02	14.47	0.048 ± 0.003	-26.4	0.05 ± 0.003	3.4 ± 0.02

$F^{14}C$ is the fraction of modern carbon. Avg. blank contributions of 1.01×10^5 ^{14}C at applied to sample correction.

6.4.2. *^{14}C Activity Concentrations in Meteorite Samples and Re-extractions*

The number of ^{14}C atoms (in units 10^4) in the samples (blank-corrected) range from 64.8 ± 1.1 in P39 to 77.4 ± 1.3 in J35. The re-extraction contributes 2–7% to the total ^{14}C measured in the samples. The re-extraction of P39 yield ^{14}C atoms even lower than the blanks. Detailed ^{14}C concentrations for the samples and the re-extraction are provided in Table 6.2. The determined ^{14}C atoms/g concentrations in the four L chondrites show a small variation, ranging from 1.28 (±0.02) $\times 10^7$ ^{14}C atoms/g in P39 to 1.60 (±0.02) $\times 10^7$ ^{14}C atoms/g in J35. These values represent the sum of ^{14}C atoms measured in the sample and the corresponding re-extraction, both corrected for blank contributions. We also extracted $^{14}CO_2$ from Caleta el Cobre 06 (J14) (T_{age} ~2 Ma), but unfortunately the glass capillary broke and we lost the gas during AMS measurement. The re-extraction of this meteorite does not yield any detectable ^{14}C.

Table 6.2. Detailed ^{14}C concentrations measured in the meteorite samples.

Samples	Diluted CO_2 (10^{-2} cm^3)	C equi. (µg)	$F^{14}C$	$\delta^{13}C$ (‰)	$^{14}C/^{12}C$ (10^{-12})	N14[a] (10^4 at)	N14[b] (10^4 at)
P18	9.7 ± 0.03	48.4	0.266 ±0.004	-20.9	0.31 ±0.005	74.7 ±1.1	69.3 ±1.3
Reextract	2.5 ± 0.02	12.4	0.113 ±0.001	-24.9	0.13 ±0.005	8.1 ±0.3	3.4 ±0.2
P39	5.6 ± 0.05	27.9	0.439 ±0.005	-26.0	0.50 ±0.005	70.2 ±0.9	64.8 ±1.1
Reextract	3.1 ± 0.03	15.7	0.052 ±0.001	-27.6	0.06 ±0.004	4.6 ±0.3	-0.06
J35	5.4 ± 0.04	26.9	0.532 ±0.005	-21.3	0.61 ±0.006	82.8 ±1.0	77.4 ±1.3
Reextract	2.4 ± 0.02	12.3	0.109 ±0.001	-27.1	0.12 ±0.005	7.7 ±0.3	3.0 ±0.2
M34	17.6 ± 0.10	88.3	0.142 ±0.003	-28.5	0.16 ±0.003	71.4 ±1.5	66.0 ±1.6
Reextract	2.2 ± 0.02	11.2	0.094 ±0.001	-29.8	0.11 ±0.006	6.0 ±0.3	1.3 ±0.1
JaH073	2.7 ± 0.02	13.7	1.116 ±0.015	-26.8	1.27 ±0.017	87.5 ±1.4	82.2 ±1.6
Reextract	2.6 ± 0.02	13.2	0.153 ±0.001	-27.6	0.17 ±0.007	11.0 ±0.4	6.8 ±0.4

[a] N14 is the number of ^{14}C atoms measured in samples. [b] N14 is the number of ^{14}C atoms after blank correction.

The calculated activity concentrations (dpm/kg) before mass correction are 2.97 ± 0.01, 3.10 ± 0.01, 3.35 ± 0.01 and 3.70 ± 0.01 dpm/kg for P39, M34, P18, and J35, respectively. M34 (San Juan 034) has not been dated for terrestrial age, but was measured before (Gattacceca et al., 2011) for ^{14}C, resulted in a negative ^{14}C activity of –0.715 dpm/kg (pers. Comm.) and thus was not published. Applying a mass loss correction of 5.15% for L chondrites (Tauseef et al., 2025) due to leaching-removal of some metals, slightly decreases the activity concentration to 2.82 ± 0.01, 2.94 ± 0.01, 3.18 ± 0.01 and 3.50 ± 0.01 dpm/kg for P39, M34, P18 and J35, respectively (Table 6.3).

Table 6.3. ^{14}C concentration after blank corrections and ^{14}C production rate in the studied meteorites.

Meteorites	Field Id	T_{age} (ka)	Mass (mg)	[a]N14 (10^5 at)	N14 (10^7 at/g)	^{14}C dpm/kg	^{14}C dpm/kg	P14 (at/g/y)
Caleta el Cobre 06	J14	2590	n.d.	n.d.	n.d.	n.d.	n.d.	n.d.
Caleta el Cobre 15	P18	520	50.20	7.27±0.5	1.45±0.02	3.35±0.01	3.18±0.01	1752±2
El Medano 026	P39	300	50.39	6.46±0.5	1.28±0.02	2.97±0.01	2.82±0.01	1554±2
El Medano 029	J35	160	50.36	8.04±0.5	1.60±0.02	3.70±0.01	3.50±0.01	1933±2
San Juan 34	M34	n.d.	50.28	6.73±0.6	1.34±0.02	3.10±0.01	2.94±0.01	1620±2

T_{age}= terrestrial age determined via ^{10}Be (Drouard et al., 2019; Hutzler et al., 2016).
[a] N14 is the total ^{14}C atoms measured in samples and re-extractions, for details see Table 6.2.
Caleta el Cobre 06 sample was lost during AMS measurement.

6.4.3. *Estimating Terrestrial ^{14}C Production in Meteorites*

For meteorites, focusing on bulk composition and accurately accounting for shielding effects, muogenic contributions, and depth-dependent production is more critical than isolating specific minerals like quartz, which is a terrestrial rock-specific method. If there is evidence of secondary carbonates or weathering products (e.g., calcite, gypsum) formed after terrestrial exposure, these phases must be chemically removed to avoid contamination. This step is already standard practice in meteorite studies (Jull et al., 1984), as we have performed chemical leaching of the studied samples following the work of Tauseef et al. (2024). Further, Lifton (1997) has shown that a two-step heating procedure can effectively separate atmospherically adsorbed gases from in situ ^{14}C. Therefore, pre-heating of samples in vacuum at 500 °C can essentially diffuse any adsorbed gases, which can be pumped out and in situ ^{14}C can be extracted at higher temperatures. The author demonstrated this experiment for quartz where in situ ^{14}C starts to diffuse at temperature >1200°C. In case of meteorites similar observations were recorded by Jull et al. (1984) and Creswell et al. (1993). The production rate of ^{14}C is generally expressed as: $P_{14C}(h) = P_0 \cdot e^{-h/\Lambda}$ where $P_{14C}(h)$ is the production rate (atoms/g/yr) at given altitude h (m) above sea level, P_0 is the production rate at sea level and high latitude

(164.64 atoms/g/y) and Λ is the attenuation length (150–160 g cm^{-2}). For a continuously produced radionuclide with a finite half-life, the activity approaches saturation after some time, given as: $A_{(t)} = P \cdot (1 - e^{-\lambda t})/ \lambda$

When $t = \infty$, the exponential term ($e^{-\lambda t}$) approaches zero and the activity reaches saturation level, i.e., $A_{sat} = P/\lambda$. In case of ^{14}C, where the decay constant (λ) is 1.21×10^{-4}, the saturation activity at sea level would be 1.36×10^{6} atoms/g. For a radionuclide, it takes about 5 half-lives to reach saturation level. For ^{14}C (5×5730 years) radionuclides, the required time to reach saturation level is ~28,650 years.

For the studied meteorites, based on the ^{10}Be ages, the ^{14}C activities are in secular equilibrium with its production rate, which means that the production rate of ^{14}C equals its decay rate, implying that the system has reached a steady state where no net accumulation or loss occurs over time. Except for San Juan 34, where terrestrial age is unknown. The production rate in secular equilibrium condition given as: $\mathbf{P = N \cdot \lambda}$, where N is the number of ^{14}C atoms per gram at present and λ is the decay constant. Further, we assume a continuous exposure, and that all the measured ^{14}C atoms are from in situ production without any contamination, diffusion or losses due to weathering and chemical leaching. Thereby, the calculated ^{14}C production rate for Caleta el Cobre 15, El Medano 26, El Medano 29 and San Juan 34 are 1752, 1554, 1933 and 1620 atoms/g/yr (Fig. 6.1). These production rate can be a combination of cosmogenic and muons contribution. Heisinger et al. (2002a,b) conducted experiment where SiO_2 target was bombarded by muon fluxes, which produces 3.34 ± 0.27 atoms/g/yr by negative muon capture and 0.44 ± 0.25 atoms/g/yr by fast muon reactions. The author suggested a total of 17% production by muons to the total ^{14}C produced. If we assume this number then muons alone produced 298, 264, 329 and 275 ^{14}C atoms/g/yr in the studied samples. These numbers are a factor of ~100 higher than what is generally used as a fixed rates for muon-induced productions at sea level at high latitudes, and cosmogenic produced ^{14}C in quartz samples in terrestrial materials. These production rates which should be the saturation activity are not constant. There seem to have no relation with T_{age}, for example, El Medano 026 is older with a T_{age} of 300 kyr gave a production rate ~20% lower compared to El Medano 029 with T_{age} of 160 kyr (see Fig. 6.1). This indicate that the non-constant saturation activity may depend on meteorite chemical composition, its size and to some extent at the altitude.

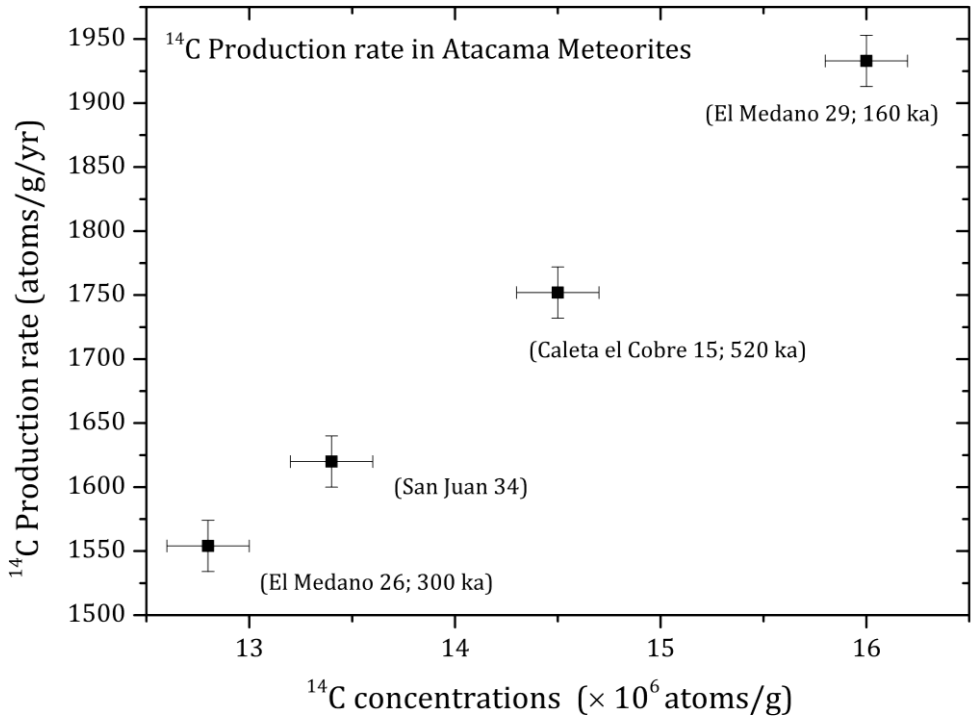

Fig. 6.1. Measured ^{14}C concentrations (atoms/g) as a function of calculated terrestrial *in-situ* ^{14}C production rate in the selected L chondrites from Atacama Desert. Terrestrial ages of the meteorites are given in the brackets.

In comparison, ^{14}C production rates in ordinary chondrites in space are typically in the range (1–3) × 10^{8} atoms/g (Fig. 6.2), as observed in recent falls (Tauseef et al., 2025; 2024 and references therein). These values represent cosmogenic production under different shielding conditions, where high-energy galactic cosmic rays (GCRs) dominate the interaction with meteoroidal matter. The production rate measured in our study (1–2) ×10^{7} atoms/g, are only a factor of 10 lower than these space-based values. Notably, this relatively small reduction contrasts sharply with production rates observed in terrestrial materials, which are typically 100–1000 times lower than those in meteorites exposed to space. Lal et al. (1990) reported a ^{14}C production rate of 99 ± 12 atoms/g/yr in quartz from Allan Hills, Antarctica (Fig. 6.2), which is up to 20 times lower than that measured in the meteorite samples and more than 200 times lower than the production observed in meteorites in space.

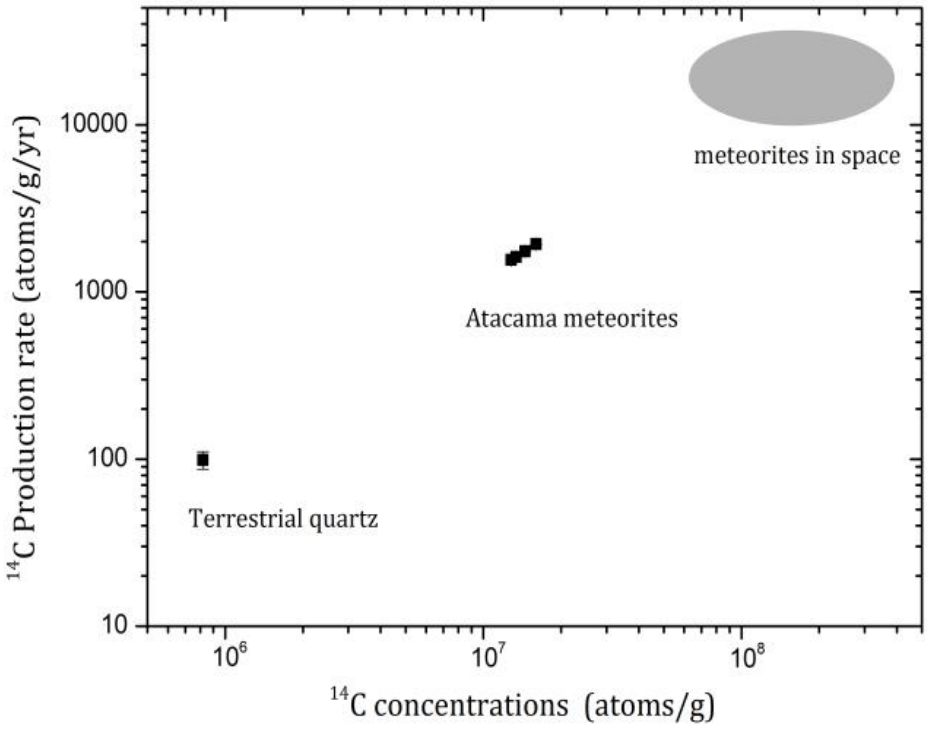

Fig. 6.2. ^{14}C production rate in Atacama meteorites scaled to production in space and terrestrial quartz from Allan Hills, Antarctica, (Lal et al. 1990).

6.5. Conclusions and Outlook

This study presents a detailed investigation of in-situ ^{14}C production in meteorites with terrestrial ages of 100–500 ka, recovered from the Atacama Desert. The Atacama Desert is one of the oldest and most stable hyper-arid regions on Earth. By analyzing L chondrites from the Caleta el Cobre, El Medano, and San Juan dense collection areas, we provide new insights into the terrestrial production rates of ^{14}C in meteoritic materials. Terrestrial ages of the studied meteorites, dated using ^{10}Be technique, suggest that these meteorites have reached a secular equilibrium for ^{14}C production and decay. To ensure that no carbonates or weathering products are attached to the samples, we leached them with 6M HCl and EGTA in order to remove any terrestrial contamination. The measured ^{14}C concentrations range from 1.28×10^7 to 1.60×10^7 atoms/g. These concentrations are a factor of 10 lower than freshly fallen L chondrites, which typically ranges from 1–3 $\times$ 10^8 atoms/g. The calculated ^{14}C production of (1554–1933) atoms/g/yr, indicates a higher-than-expected rate, and a complex interplay between cosmogenic and muogenic contributions, with muons accounting for ~17% of total production. The meteorites studied here show production rates more than a factor of 10 higher than the production rate in terrestrial materials. In-situ ^{14}C measured in terrestrial quartz samples exhibit

significantly lower ^{14}C production rate. For instance, a maximum of ~99 atoms/g/yr ^{14}C atoms estimated for quartz from Allan Hills, Antarctic (Lal et al., 1990). This relatively small reduction in production rate from space to terrestrial conditions underscores the strong contribution of secondary cosmic rays, particularly neutron- and muon-induced reactions, even at moderate shielding depths in meteoritic material.

Our findings also reveal that the terrestrial production rates of *in-situ* ^{14}C in meteorites are not constant and do not scale directly with terrestrial age. For example, El Medano 026 (T_{age} ~300 kyr) exhibits a ~20% lower production rate than El Medano 029 (T_{age} ~160 kyr). This suggests that factors such as chemical composition, weathering and environment, shielding depth, and altitude-dependent cosmic ray flux play a significant role in determining the in-situ ^{14}C production in these extraterrestrial materials. These observations emphasize the need for a more refined approach in using in-situ ^{14}C as a tool for terrestrial age dating, accounting for shielding effects, chemical weathering, and production rate variations across different meteorite types and environmental conditions.

Future studies should focus on expanding the dataset, by systematically analyzing meteorites with terrestrial ages over 50 ka, and to include a broader range of meteorite types, and developing models to quantify cosmogenic and muogenic ^{14}C production in extraterrestrial materials. Additionally, I encourage to perform chemical treatment in clean-lab environment and using high-grade ultra-pure solvents to ensure zero contamination. Such efforts will significantly improve the quality of data and will enhance the precision of ^{14}C production rate estimates, and contribute to a more comprehensive framework for interpreting cosmic ray and muons interactions with meteorites.

Chapter 7

Outlook and Future Work: Developments for Potential Projects

7.1. Outlook: Terrestrial Age Dating of Meteorites

The goal of this project was to investigate shielding-dependency of ^{14}C production rate and $^{14}C/^{10}Be$ production rate ratios in recently fallen ordinary chondrites to improve terrestrial age dating system. To achieve our goal, we combined model calculations and experimental data from a variety of recently fallen H, L and LL chondrites. Meteorite samples were measured for ^{14}C activity concentrations and $^{14}C/^{10}Be$ activity ratios. To evaluate shielding depth of samples, noble gas isotopes, He and Ne, were measured, and cosmogenic $(^{22}Ne/^{21}Ne)_{cos}$ ratios were determined. Our results clearly demonstrated that neither the ^{14}C saturation activity nor the $^{14}C/^{10}Be$ saturation ratios are constant, as assumed in earlier studies. Instead, they vary significantly with shielding-depth. Based on our findings, we argued that the small meteorites were systematically dated older than their true ages, and this creates a size-dependent bias in the terrestrial age histogram. We employed our framework to recalculate terrestrial ages of meteorites from Omani, Nullarbor, and Saharan Desert. The new ages slightly change for the Omani strewnfield meteorites due to their large sizes, but the ages for small single-stone meteorites (e.g., RaS 267) came out 16–20% lower than previous estimates. In case of Nullarbor and Saharan meteorites, the differences in age-histograms were quite prominent that for some of the meteorites the new ages were more than 50% lower. This is because most of the meteorites from the Saharan Desert (Acfer and Adrar regions) are small stones. There are also meteorites from these regions dated 2–3 ka old but the new ages suggest zero age, i.e., they are recently fallen, consistent with their weathering grades. Our framework of ^{14}C and ^{14}C-^{10}Be terrestrial age dating system considering shielding-depth dependency has significantly improved terrestrial age dating of meteorites. Though some room for improvement is still there, for instance, extending the database by including more data from small size meteorites. Moving forward, we encourage to adapt similar framework for other nuclide based terrestrial age dating.

7.2. Studying Shielding Dependence of Nuclide Production in other Meteorite Types

One should emphasize to evaluate ^{14}C and noble gases in meteorites which are not observed fall but their physical and chemical characteristic suggest they have recently fallen. This approach will avoid any discrepancies and help in their classification as falls. The study of shielding-dependent cosmogenic nuclide (^{14}C, ^{10}Be) production in H, L and LL chondrites has provided valuable contribution in improvising the terrestrial age dating system. However, to

develop a more comprehensive model for meteorite flux studies and so the terrestrial ages, future research should focus on extending ^{14}C and ^{14}C-^{10}Be terrestrial age dating system to other meteorite types, such as carbonaceous chondrites, and stony-iron. This would be challenging because CCs or Iron meteorites will need different setups for extraction, which means developing parallel or do modifications in the existing line. Additionally, similar framework, that is, studying the shielding dependency on nuclide production should be developed for other nuclide systems, e.g., ^{26}Al, ^{36}Cl, ^{41}Ca dating systems.

7.3. Systematic Study of Meteorites from Atacama Desert and Antarctica

We started investigating terrestrial ^{14}C production in meteorites and measured few samples to test whether it is possible to detect any ^{14}C in such old meteorites. We have been successful in terms of analysis of ^{14}C, but the results were too high than expected. The calculated production rates are a factor of 10 higher than the maximum production measured in terrestrial quartz samples, and a factor of 10 lower than the typical ^{14}C production in meteorites in space. To evaluate terrestrial ^{14}C production in meteorites, a systematic study of samples from Atacama is needed to be done. We already have samples in our collection from Jérôme. This project can be started. Additionally, there are older meteorites from Antarctica that should be included in this project. This will help evaluate difference between nuclide production in hot and cold desert meteorites, and also cosmic ray flux studies.

7.4. Development of New ^{14}C Extraction line

The extraction line has been successfully developed, producing low-blank, high-quality ^{14}C data. However, there is still room for improvement. One potential enhancement is making the system semi-automated to increase efficiency (although I prefer it manual and having more control in my hand). Technical improvement would be automating the continuous 30 mbar of O_2 supply to the crucible during extraction. Additionally, there are plans to develop a new extraction line incorporating cryogenic techniques, including a cryopump for improved gas separation and collection.

References

Agostinelli, S., et al. 2003. GEANT4 – A Simulation Toolkit. *Nuclear Instruments and Methods in Physics Research* A 506: 250–313.

Alexeev, V. A. 1998. Parent bodies of L and H chondrites: Times of catastrophic events. *Meteoritics & Planetary Science* 33: 145–52.

Alexeev, V.A., Gorin, V.D., Ivliev, A.I., Kashkarov, L.L., Ustinova, G.K. 2008. Recently fallen Bukhara (CV3) and Kilabo (LL6) chondrites: A parallel study of luminescence, tracks, and cosmogenic radionuclides. *Geochemistry International* 46, 849–66 (2008).

Al-Kathiri, Hofmann, B.A., Jull., A.J.T., Gnos, E. 2005. Weathering of meteorites from Oman: Correlation of chemical and mineralogical weathering proxies with ^{14}C terrestrial ages and the influence of soil chemistry. *Meteoritics & Planetary Science* 40(8): 1215–39.

Alvarez, L. W., Alvarez, W., Asaro, F., Michel, H. V., 1980, Extraterrestrial cause for the Cretaceous Tertiary Extinction, *Science* 208: 1095–1108.

Arnold, M., Aumaitre, G., Bourlès, D. L., Keddadouche, K., Braucher, R., Finkel, R. C., Nottoli, E., Benedetti, L., Merchel, S. 2013. The French Accelerator Mass Spectrometry Facility ASTER after 4 Years: Status and Recent Developments on ^{36}Cl and ^{129}I. *Nuclear Instruments and Methods in Physics Research Section B: Beam Interactions with Material and Atoms* 294: 24–9.

Arnold, M., Merchel, S., Bourlès, D. L., Braucher, R., Benedetti, L., Finkel, R. C., Aumaitre, G., Gottdang, A., Klein, M. 2010. The French Accelerator Mass Spectrometry ASTER: Improved Performance and Developments. *Nuclear Instruments and Methods in Physics Research Section B: Beam Interactions with Material and Atoms* 268: 1954–59.

Bhandari N., Lal D., Arnold J. R., Marti K., Rajan R. S., and Moore C. B. 1980. Atmospheric ablation in meteorites based on cosmic-ray tracks and neon isotopes. *Nuclear Track Detection* 4: 213–262.

Bischoff, A., et al. 2019. The Renchen L5-6 chondrite breccia – The first confirmed meteorite fall from Baden-Württenberg (Germany). *Geochemistry* 79: 125525

Bischoff, A., et al. 2017. The Stubenberg meteorite – An LL6 chondrite fragmental breccia recovered soon after precise prediction of the strewn field. *Meteoritics & Planetary Science* 52: 1683–1703

Bischoff, A., Patzek, M., T. M. Peters, S., Barrat, J-. A., Di Rocco, T., Pack, A., Ebert, S., Jansen, C. A., Kmieciak, K. 2022. The chondrite breccia of Antonin (L4-5) - A new meteorite fall from Poland with a heterogeneous distribution of metal. *Meteoritics & Planetary Science* 57: 2127–42.

Bland P. A., Spurny P., Bevan A. W. R., Howard K. T., Towner M. C., Benedix G. K., Greenwood R. C., Shrbeny L., Franchi I. A., Deacon G., Borovicka J., Ceplecha Z., Vaughan D., Hough R. M. 2012. The Australian Desert Fireball Network: A new era for planetary science. *Australian Journal of Earth Sciences* 59, 177–187. doi: 10.1080/08120099.2011.595428

Bogard, D.D., Cressy, P.J., 1973. Spallation production of ^{3}He, ^{21}Ne and ^{38}Ar from target elements in the Bruderheim chondrite. *Geochimica Cosmochimica Acta* 37, 527–46

Bouvier, A., Gattacceca, J., Grossman, J., Metzler, K. 2017. The Meteoritical Bulletin, No. 105. *Meteoritics & Planetary Science* 52(11): 2411.

Brykina, I.G., and Egorova, L.A. 2021. On the Mass Distribution of Fragments of an Asteroid Disrupted in the Earth's Atmosphere. *Advances in Astronomy*. Article 9914717, doi. 10.1155/2021/9914717

Buhl, S., Toueirjenne, C., Hofmann, B., Laubenstein, M., Wimmer, K. 2014. The meteorite fall near Boumdeid, Mauritania, from September 14, 2011. *Meteorites* 3(1–2): 5–18.

Cassidy, W. A. 2003. Meteorites, Ice, and Antarctica. New York: *Cambridge University Press*.

Colas F., Zanda B., Bouley S., Jeanne S., Malgoyre A., Birlan M., Blanpain C., Gattacceca J., et al. 2020. FRIPON: a worldwide network to track incoming meteoroids. *Astronomy & Astrophysics*, 644 (6), pp. A53. doi: https://doi.org/10.1051/0004-6361/202038649.

Cole, K. J., Schultz, L., Sipiera, P. P., Welten, K. C. 2007. Kilabo and Bensour, two LL6 chondrite falls from Africa with very similar mineralogical compositions but different cosmic-ray exposure histories. *38th Lunar and Planetary Science Conference*, abstract #1338, pp. 1477.

Clarke, J. 2006. Antiquity of aridity in the Chilean Atacama Desert. *Geomorphology* 73, 101–114. https://doi.org/10.1016/j.geomorph.2005.06.008

Cresswell, R. G., Miura, Y., Beukens, R. P., Rucklidge, J. C. 1993. ^{14}C terrestrial ages of nine Antarctic meteorites using CO and CO_2 temperature extractions. *Antarctic Meteorite Research* 6, 381–90. https://ui.adsabs.harvard.edu/abs/1993AMR6381C

Dalcher, N., Caffee, M.W., Nishiizumi, K., Welten, K.C., Vogel, N., Wieler, R., Leya, I. 2013. Calibration of cosmogenic noble gas production in ordinary chondrites based on ^{36}Cl-^{36}Ar ages. Part 1: refined produced rates for cosmogenic ^{21}Ne and ^{38}Ar. *Meteoritics & Planetary Science* 48: 1841–62.

Dohnanyi, J. S. 1969. Collisional models of asteroids and their debris. *Journal of Geophysical Research,* 74(10), 2531–2554.

Drouard, A., Gattacceca, J., Hutzler, A., Rochette, P., Braucher, R., et al. 2019. The meteorite flux of the last 2 Myr recorded in the Atacama desert. *Geology*, 47(7), 673–676.

Dunai, T., Lopez, G., Jeuz-Larre, J. 2005. Oligocene–Miocene age of aridity in the Atacama Desert revealed by exposure dating of erosion-sensitive landforms. *Geology* 33(4), 321–324. doi: 10.1130/G21184.1

Eberhardt P., Eugster O., Geiss J. and Marti K. 1966. Rare Gas Measurements in 30 Stone Meteorites. *Z. Naturforsch*. 21a: 414–26

Eugster, O. 1988. Cosmic-ray production rates for ^{3}He, ^{2l}Ne, ^{38}Ar, ^{83}Kr, and ^{126}Xe in chondrites based on 81Kr-Kr exposure ages. *Geochimica et Cosmochimica Acta* 52: 1649–62

Eugster, O., Micheal, T., Niedermann, S., Wang, D., Yi, W. 1993. The record of cosmogenic, radiogenic, fissiogenic, and trapped noble gases in recently recovered Chinese and other chondrites. *Geochimica et Cosmochimica Acta* 57 (5): 1115–42.

Farley, K. A., Vokrouhlický, D., Bottke, W. F., Nesvorný, D. 2006. A late Miocene dust shower from the break-up of an asteroid in the main belt. *Nature* 439: 295–297.

Ferko, T.E., Wang, M-S., Hillegonds, D.J., Lipschutz, M.E., Hutchison, R., Franke, L., Scherer, P., Schultz, L., Beniot, P.H., sears, W.G., Singhvi, A.K., Bhandari, N. 2002. The irradiation history of the Ghubara (L5) regolith breccia. *Meteoritics & Planetary Science* 37:311–327

Fireman, E.L. 1962. The Ehole Meteorite, Its Acquisition and Its Radioactivity. *Journal of Geophysical Research* 67(6): 2592–94

Gattacceca, J., Valenzuela, M., Uehara, M. et al. 2011. The densest meteorite collection area in hot deserts: the San Juan meteorite field (Atacama Desert Chile): *Meteoritics and Planetary Science* 46(9), 1276–1287. doi: 10.1111/j.1945-5100.2011.01229.x.

Gibson, E., Bogard, D., 1978. Chemical alteration of the Holbrook chondrite resulting from terrestrial weathering. Meteoritics 13, 277–289. https://doi.org/10.1111/ j.1945-5100.1978.tb00467.x

Gnos, E., Eggimann, M., Al-Kathiri, A., and Hofmann, B. A. 2006. The JaH 091 strewn field. *Meteoritics & Planetary Science* 41:A64–230.

Gnos, E., Lorenzetti, S., Eugster, O., Jull, A. J. T., Hofmann, B. A., Al-Kathiri, A., and Eggimann, M. 2009. The Jiddat al Harasis 073 Strewn Field, Sultanate of Oman. *Meteoritics & Planetary Science* 44:375–87.

Graf, T., Marti, K. 1995. Collisional history of H chondrites. *Journal of Geophysical Research* 100 (l0): 21,247–63

Graf, T., and Marti, K. 1994. Collisional records in LL chondrites. *Meteoritics* 29 (5): 643–648.

Graf, Th., Signer, P., Wieler, R., Herpers, U., Sarafin, R., Vogt, S., Fieni, Ch., Pellas, P., Bonani, G., Suter, M., Wölfli, W. 1990. Cosmogenic nuclides and nuclear tracks in the chondrite Knyahinya. *Geochimica et Cosmochimica Acta* 54: 2511–2530.

Halliday, I., Blackwell, A.T., Griffin, A.A. 1989. The flux of meteorites on the Earth's surface. *Meteorites* 24: 173–178.

Heck, P. R., Schmitz, B., Bottke, W, Rout, S. S., Kita, N. T., Cronholm, A., Defouilloy, C., Dronov, A., Terfel, F. 2017. Rare meteorites common in the Ordovician period. *Nature Astronomy* 1, id 0035.

Herzog, G. F., Vogt, S., Aylmer, D., Signer, P., Graf, Th., Wieler, R., Tuniz, C., Klein, J., Fink, D., Middleton, R., and Jull, A. J. T. 1991. Multi-stage exposure history of the Torino, H6, meteorite. *22nd Lunar and Planetary Science Conference*: 563–564.

Heymann, D. 1965. Cosmogenic and Radiogenic Helium, Neon and Argon in Amphoteric Chondrites. *Journal of Geophysical Research* 70: 3735–43.

Heisinger, B., Lal, D., Jull, A.J.T., Kubik, P., Ivy-Ochs, S., Neumaier, S., Knie, K., Lazarev, V., Nolte, E., 2002a. Production of selected cosmogenic radionuclides by muons: 1. Fast muons. *Earth and Planetary Science Letters* 200, 345–355.

Heisinger, B., Lal, D., Jull, A.J.T., Kubik, P., Ivy-Ochs, S., Knie, K., Nolte, E., 2002b. Production of selected cosmogenic radionuclides by muons: 2. Capture of negative muons. *Earth and Planetary Science Letters* 200, 357–369.

Hildebrand, A. R., Penfield, G. T., Kring, D. A., Pilkington, M., Camargo, Z. A., Jacobsen, S. B., Boynton, W. V. 1991. Chicxulub Crater: A possible Cretaceous/Tertiary boundary impact crater on the Yucatan Penninsula, Mexico. *Geology* 19: 867–871.

Hintenberger, H., König, H., Schultz, L., and Wanke, H. 1965. Radiogene, spallogene und primordiale Edelgase in Steinmateoriten III, *Z. Naturforsch.* 20a, 983–989.

Hippe, K., Kober, F., Wacker, L., Fahrni, S. M., Ivy-Ochs, S., Akar, N., Schluechter, C., and Wieler, R. 2013. An Update on In Situ Cosmogenic ^{14}C Analysis at ETH Zurich. *Nuclear Instruments and Methods in Physics Research B* 294: 81–86.

Hippe, K., and Lifton, L. 2014. Calculating Isotope Ratios and Nuclide Concentrations for in Situ Cosmogenic ^{14}C Analyses. *Radiocarbon* 56: 1167–74.

Honda, M., and Arnold J.R. 1964. Effects of Cosmic Rays on Meteorites. *Science* 143, 203–212. DOI:10.1126/science.143.3603.203

Howard, C., Ferm, M., Cesaratto, J., Daigle, S., Iliadis, C. 2014. Radioisotope studies of the Farmville meteorite using γγ-coincidence spectrometry. *Applied Radiation and Isotopes* 94: 23–29. https://doi.org/10.1016/j.apradiso.2014.07.001

Huber, L., Gnos, E., Hofmann, B., Welten, K. C., Nishiizumi, K., Caffee, M. W., Hillegonds, D. J., and Leya, I. 2008. The Complex Exposure History of the Jiddat al Harasis 073 L-Chondrite Shower. *Meteoritics & Planetary Science* 43:1691–708.

Hutzler, A., Gattacceca, J., Rochette, P. et al. 2016. Description of a very dense meteorite collection area in western Atacama: Insight into the long-term composition of the meteorite flux to Earth: *Meteoritics & Planetary Science* 51(3), 468–482. doi : 10.1111/maps.12607 9.tb00959.x

Jarosewich E. 1990. Chemical analyses of meteorites: a compilation of stony and iron meteorite analyses. *Meteoritics and Planetary Science* 25:323–37.

Jull, A. J. T., Cloudt, S., and Cielaszyk, E. 1998. ^{14}C terrestrial ages of meteorites from Victoria Land, Antarctica, and the infall rates of meteorites. In *Meteorites: Flux with time and impact effects*, edited by Grady M. M. London: Geological Society. pp. 75–91.

Jull, A. J. T., Donahue, D. J., Cielaszyk, E., and Wlotzka, F. 1993. Carbon-14 Terrestrial Ages and Weathering of 27 Meteorites from the Southern High Plains and Adjacent Areas (USA). *Meteoritics & Planetary Science* 28: 188–95.

Jull, A. J. T., Donahue, D. J., Reedy, R. C., and Masarik, J. 1994. A Carbon-14 Depth Profile in the L5 Chondrite Knyahinya. *Meteoritics* 29: 649–738.

Jull, A. J. T., Donahue, D. J., and Linick, T. W. 1989. Carbon-14 Activities in Recently Fallen Meteorites and Antarctic Meteorites. *Geochimica et Cosmochimica Acta* 53: 2095–2100.

Jull, A. J. T., Donahue, D. J., and Zabel, T. H., Fireman, E.L. 1984. Carbon-14 ages of Antarctic meteorites with accelerator and small-volume counting techniques. *Journal of Geophysical Research: Solid Earth* 89, C329–C335.

Jull, A. J. T., Giscard, M. D., McHargue, L. R., Kim, K. J., and Reedy, R. C. 2009. Production Rates of ^{14}C and ^{10}Be in Vaca Muerta (Mesosiderite), Carancas, and some Recent Falls (Abstract). *Meteoritics & Planetary Science* 72: 5276.

Jull, A. J. T., McHargue, L. R., Bland, P. A., Greenwood, R. C., Bevan, A. W., Kim, K. J., LaMotta, S. E., and Johnson, J. A. 2010. Terrestrial Ages of Meteorites from the Nullarbor Region, Australia, Based on ^{14}C and ^{14}C-^{10}Be Measurements. *Meteoritics & Planetary Science* 45: 1271–83

Jull, A. J. T., Donahue, D. J., Zabel, T. H., Fireman, E.L. 1984. Carbon-14 ages of Antarctic meteorites with accelerator and small-volume counting techniques. *Journal of Geophysical Research: Solid Earth* 89, C329–C335

Jull, A. J. T., McHargue, L. R., Bland, P. A., Greenwood, R. C., Bevan, A. W. R., et al. 2010. Terrestrial Ages of Meteorites from the Nullarbor Region, Australia, Based on ^{14}C and ^{14}C–^{10}Be Measurements. *Meteoritics & Planetary Science* 45: 1271–83.

Jull, A. J. T., Wlotzka, F., Palme, H., Donahue, D. J. 1990. Distribution of terrestrial ages and petrologic type of meteorites from western Libya. *Geochimica et Cosmochimica Acta* 54: 2895–2899.

Jull, A. J. T., Bland, P., Klandrud, S. E., McHargue, L. R., Bevan, A. W. R, Kring, D., Wlotzka, F. 2000. Using ^{14}C and ^{14}C-^{10}Be for terrestrial ages of desert meteorites. In *Workshop on Extraterrestrial Material from Cold and Hot Deserts* (eds. L. Schultz, I. Franchi, A. Reid and M. Zolensky), pp. 41–43. LPI Contribution No. 997, Lunar and Planetary Institute, Houston, Texas, USA.

Jull, A. J. T., Bland, P.A., Bevan, A. W. R., Klandrud, S. E., McHargue, L. R. 2001. ^{14}C and ^{14}C-^{10}Be terrestrial ages of meteorites from Western Australia (abstract) *Meteoritics & Planetary Science* 36:A91.

Jull, A. J. T., Kim, K. J., Reedy, R. C., McHargue, L. R., Johnson, J., A. 2004. Modelling of ^{14}C and ^{10}Be production rates in meteorites and lunar samples. *25th Lunar and Planetary Science Conference*, abstract #1191.

Jull, A. J. T. 2006. Terrestrial Ages of Meteorites. In *Meteorites and the Early Solar System II*, edited by D. Lauretta, and H. Y. McSween, Jr., 889–905. Tucson, Arizona: The University of Arizona Press.

Jull, A. J. T., Giscard, M. D., Hutzler, A., Schnitzer, C. J., Zahn, D., Burr, G. S., McHargue, L. R., Hill, D. 2013. Radionuclide Studies of Stony Meteorites from Hot Deserts. *Radiocarbon* 55(03): 1779–1789.

Knauer, M. Neupert, U., Michel. R., Bonani, G., Dittrich, B., Hajdas, I., Ivy Ochs, S., Kubik, P.W., Suter, M. 1995. Measurement of the long-lived radionuclides Beryllium-10, Carbon-14 and Aluminum-26 in meteorites from hot and cold deserts by Accelerator mass spectrometry (AMS), *Proceedings*, *Workshop on Meteorites from Cold and Hot Deserts*. 38–42.

Koeberl, C., Montanari, A. 2009. The late Eocene Earth: Hothouse, icehouse, and impacts. In: *Geological Society of America*, Special Paper No. 452.

Korschinek, G. Bergmaier, A. Faestermann, T. Gerstmann, U.C. Knie, K. Rugel G., Wallner, A. Dillmann, I. Dollinger, G. Lierse von Gostomski, Ch. Kossert, K. Maiti, M. Poutivtsev, M. Remmert, A. 2010. A new value for the half-life of ^{10}Be by Heavy-Ion Elastic Recoil Detection and liquid scintillation counting, *Nuclear Instruments and Methods in Physics Research Section B: Beam Interactions with Materials and Atoms* 268 (2): 187–91.

Kring, D. A., Jull, A. J. T., McHargue, L. R., Bland, P. A., Hill, D. H., and Berry, F. J. 2001. Gold Basin Meteorite Strewn Field, Mojave Desert, Northwestern Arizona: Relic of a Small Late Pleistocene Impact Event. *Meteoritics & Planetary Science* 36: 1057–66.

Krinov, E.L. 1960. *The Meteoritical Bulletin*, No. 19. Moscow.

Lal, D., Jull, A.J.T., Donahue, D.J., Burtner, D., Nishiizumi, K., 1990. Polar ice ablation rates measured using in situ cosmogenic ^{14}C. *Nature* 346, 350–352.

Lifton, N.A., 1997. A new extraction technique and production rate estimate for in situ cosmogenic ^{14}C in quartz. Ph.D. Thesis, University of Arizona.

Leya, I., Dalcher, N., Vogel, N., Wieler, R., Caffee, M.W., Welten, K.C., Nishiizumi, K. 2015. Calibration of cosmogenic noble gas production based on ^{36}Cl-^{36}Ar ages. Part 2. The ^{81}Kr-Kr dating technique. *Meteoritics & Planetary Science* 50: 1863–79.

Leya, I., Hirtz, J., David, J.-C. 2021. Galactic Cosmic Rays, Cosmic-Ray Variations, and Cosmogenic Nuclides in Meteorites. *The Astrophysical Journal* 910:136(17pp).

Leya, I., Ammon, K., Cosarinsky, M., Dalcher, N., Gnos, E., Hofmann, B., Huber, L. 2013. Light noble gases in 12 meteorites from the Omani desert, Australia, Mauritania, Canada, and Sweden. *Meteoritics & Planetary Science* 48 (8): 1401–14.

Leya, I., Graf, T., Nishiizumi, K., Wieler, R. 2001a. Cosmic-ray production rates of helium, neon and argon isotopes in H chondrites based on chlorine-36/argon-36 ages. *Meteoritics & Planetary Science* 39: 963–73.

Leya, I., Masarik, J. 2009. Cosmogenic nuclides in stony meteorites revisited. *Meteoritics & Planetary Science* 44(7): 1061–86.

Leya, I., Wieler, R., Aggrey, K., Herzog, G. F., Schnabel, C., Metzler, K., Hildebrand, A. R., Bouchard, M., T. Jull, A. J., Andrews, H. R., Wang, S., Ferko, T. E., Lipschutz, M. E., Wacker, J. F., Neumann, S., & Michel, R. 2001b. Exposure history of the St-Robert (H5) fall. *Meteoritics & Planetary Science* 36(11): 1479–94. https://doi.org/10.1111/j.1945-5100.2001.tb01840.x

Leya, I. and Stephenson, P. 2019. Cosmic ray exposure ages for ureilites—New data and a literature study. *Meteoritics & Planetary Science* 54 (7):1512–1532.

Lightfoot, B., Macgregor, A.M., Golding, E. 2018. The meteoric stone seen to fall in the Mangwendi native reserve, Southern Rhodesia, on March 7, 1934. *Mineralogical magazine and journal of Min. Society* 24(148):1–12. doi.org/10.1180/minmag.1935.024.148.04

Mahajan, R. 2017. Noble gases, nitrogen and cosmic ray exposure age of the Sulagiri Chondrite. *Geoscience Frontiers* 8: 205–10.

Mancusi, D., Boudard, A., Cugnon, J., David, J.-C., Pekka, K., Leray, S. 2014. Extension of the Liège intranuclear-cascade model to reactions induced by light nuclei. *Physical Review C* 90: p054602.

Marboeuf, U., Thiabaud, A., Alibert, Y., Cabral, N., Benz, W. 2014. From planetesimals to planets – volatile elements. *Astronomy & Astrophysics* 570, id. A36.

Marty, B. 2012. The origins and concentrations of water, carbon, nitrogen and noble gases on Earth. *Earth and Planetary Science Letters* 313: 56–66.

Mason, B., Wiik, H.B. 1965. The composition of the Forest city, Tennasilm, Weston and Geidam Meteorites. *American Museum of Natural History*, New York, No. 2220.

McCoy, T. J., Ehlmann, A.J., Moore, C.B. 1997. The Leedey, Oklahoma chondrite: Fall, petrology, chemistry and an unusual Fe, Ni-FeS inclusion. *Meteoritics & Planetary Science* 32: 19–24.

Mészáros, M., Leya, I., Hofmann, B., and Szidat, S. 2018. Current Performance and Preliminary Results of a New ^{14}C Extraction Line for Meteorites at the University of Bern. *Radiocarbon* 60: 601–615.

Minami, M., Terui, A., Takaoka, N., and Nakamura, T. M. 2006. An Improved Extraction System to Measure Carbon-14 Terrestrial Ages of Meteorites and Paring of the Antarctic Yamato-75097 Group Chondrites. *Meteoritics & Planetary Science* 49(4): 529–540.

Muller, R. A., MacDonald, G. J. 1997. Glacial cycles and astronomical forcing. *Science* 277:215–218.

Nishiizumi, K., Caffee, M.W., Finkel, R.C., Brimhall, G., Mote, T. 2005. Remnants of a fossil alluvial fan landscape of Miocene age in the Atacama Desert of northern Chile using cosmogenic nuclide exposure age dating. *Earth and Planetary Science Letters* 237, 499–507.

Nishiizumi, K., Elmore, D., Ma, X.Z., Arnold, J.R. 1984. ^{10}Be and ^{36}Cl depth profiles in an Apollo 15 drill core. *Earth and Planetary Science Letters* 70: 157–163.

Nishiizumi, K., Imamura, M., Caffee, M. W., Southon, J. R., Finkel, R. C., and McAninch, J. 2007. Absolute Calibration of ^{10}Be AMS Standards. *Nuclear Instruments and Methods in Physics Research Section B: Beam Interactions with Materials and Atoms* 258: 403–13.

Nishiizumi K., Regnier S., and Marti K. 1980. Cosmic ray exposure ages of chondrites, pre-irradiation and constancy of cosmic ray flux in the past. *Earth and Planetary Science Letters* 50:156–70.

Norton, O. R. (2002) The Cambridge Encyclopedia of Meteorites. *Cambridge University Press.*

Ott, U., Franke, L., Grau, Th. 2008. Noble gases in the Carancas (Puno, Peru) meteorite. *71st Annual Meteoritical Society Meeting*, Abstract #5088

Pillinger, C.T., Greenwood, R.C., Gibson, J.M., Gibson, E.K. 2013. Weathering effects in Holbrook meteorite and their possible removal. *76th Annual Meteoritical Society Meeting*, Abstract #5325.

Placzek, C.J., Matmon, A., Granger, D.E., Quade, J., Niedermann, S. 2010. Evidence for active landscape evolution in the hyperarid Atacama from multiple terrestrial cosmogenic nuclides. *Earth and Planetary Science Letters* 295, 12–20.

Rosén, A. V., Hofmann, B. A., von Sievers, M., Schumann, M. 2020. Radionuclide activities in recent chondrite falls determined by gamma-ray spectrometry: Implications for terrestrial age estimates. *Meteoritics & Planetary Science* 55: 149–163.

Scherer, P., Schultz, L. 2001. Noble gases in Baszkówka and Mt. Tazerzait. *Geological Quarterly* 45: 313–314.

Schlichting, H. E., Sari, R., Yalinewich, A. 2015. Atmospheric mass loss during planet formation: the importance of planetesimal impacts. *Icarus* 247: 81–94.

Schmieder, M., Jourdan, F., Tohver, E., Cloutis, E. A. 2014. ^{40}Ar/^{39}Ar age of the Lake Saint Martin impact structure (Canada) - Unchaining the Late Triassic impact craters. *Earth and Planetary Science Letters* 406: 37–48.

Schmitz, B., Heck, P. R., Alvarez, W., Kita, N. T., Rout, S. S., Cronholm, A., Defouilloy, C., Martin, E., Smit, J., Terfelt, F. 2017. Meteorite flux to Earth in the Early Cretaceous as reconstructed from sediment-dispersed extraterrestrial spinels. *Geology* 45: 807–810.

Schmitz, B., Fesit, R., Meier, M. M. M., Martin, E., Heck, P. R., Lenaz, D., Topa, D., Busemann, H., Maden, C., Plant, A. A., Terfelt, F. 2019a. The micrometeorite flux to Earth during the Frasnian-Famennian transition reconstructed in the Coumiac GSSP section, France. *Earth and Planetary Science Letters* 522: 234–243.

Schmitz, B., et al. 2019b. An extraterrestrial trigger for the mid-Ordovician ice age: Dust from the breakup of the L-chondrite parent body. *Science Advances* 5: eaax4184.

Schnitzer, C. J., Jull, A. J. T., Biddulph, D., Zahn, D., Cheng, L., Burr, G. S., McHargue, L. 2012. New studies of ^{14}C and ^{10}Be in iron meteorites (abstract). *Meteoritics & Planetary Science* 75:5085.

Schulte P., et al. 2010 The Chicxulub asteroid impact and mass extinction at the Cretaceous-Paleogene Boundary. *Science* 327: 1214–1218.

Schultz, L., Weber, H. W. 1996. Noble gases and H chondrite meteoroid streams: No confirmation. *Journal of geophysical research*, vol. 101(9), pages 21,177–81.

Schultz, L., Franke, L. 2004. Helium, neon, and argon in meteorites: a data collection. *Meteoritics and Planetary Sciences* 39: 1889–90.

Sliz, M., Espic, C., Hofmann, B. A., Leya, I., and Szidat, S. 2019. An Update on the Performance of the In Situ ^{14}C Extraction Line at the University of Bern. *Radiocarbon* 62:1371–88.

Sliz, M., Hofmann, B.A., Leya, I., Szidat, S., Espic, C., Gattacceca, J., Braucher, R., Borschneck, D., Gnos, E., ASTER Team. 2022. Terrestrial ages of seven meteorite strewn fields and two single unpaired meteorites from the Sultanate of Oman determined using ^{14}C and ^{10}Be. *Meteoritics & Planetary Sciences* 57: 2170–91.

Smith, T., Cook, D.L., Merchel, S., Pavetich, S., Rugel, G., Scharf, A., Leya, I. 2019. The constancy of galactic cosmic rays as recorded by cosmogenic nuclides in iron meteorites. *Meteoritics & Planetary Science* 54 (12): 2951–2976.

Szidat, S. 2020. ^{14}C Research at the Laboratory of the Analysis of Radiocarbon with AMS (LARA), University of Bern. *CHIMIA* 74: 1010–14.

Szidat, S., Salazar, G. A., Vogel, E., Battaglia, M., Wacker, L., Synal, H. A., and Türler, A. 2014. ^{14}C Analysis and Sample Preparation at the New Bern Laboratory for the Analysis of Radiocarbon with AMS (LARA). *Radiocarbon* 56: 561–66.

Stelzner, T., Heide, K., Bischoff, A., Weber, D., Scherer, P., Schultz, L., et al. (1999). An interdisciplinary study of weathering effects in ordinary chondrites from the Acfer region, Algeria. *Meteoritics and Planetary Science* 34: 787–94.

Tauseef, M., Leya, I., Gattacceca, J., Hofmann, B., Szidat, S., Braucher, R., ASTER Team. 2024. ^{14}C and ^{14}C-^{10}Be terrestrial age dating system for meteorites—New data for four recently fallen meteorites. *Meteoritics and Planetary Science* 59(6): 1219–35.

Tauseef, M., Leya, I., Gattacceca, J., Szidat, S., Kruttasch, P., Braucher, R., Zappatini, A., ASTER Team. (2025). Evaluating ^{14}C and $^{14}C/^{10}Be$ terrestrial age dating systems for meteorites using experimental data and model calculations *Meteoritics & Planetary Sciences* (**In press**).

Van Schmus W. R., Wood J. A. 1967. A chemical-petrologic classification for the chondritic meteorites. *Geochimica et Cosmochimica Acta* 31, 747-765.

Vogt, S. K., Aylmer, D., Herzog, G. F., Wieler, R., Signer, P., Pellas P., Fiéni, C., Tuniz, C., Jull, A. J. T., Fink, D., Klein, J., Middleton, R. 1993. On the Bur Gheluai H5 chondrite and other meteorites with complex exposure histories. *Meteoritics* 28: 71–85.

Weber, P., Hofmann, B. A., Tolba, T., and Vuilleumier, J. L. 2017. A Gamma-Ray Spectroscopy Survey of Omani Meteorites. *Meteoritics & Planetary Science* 52: 1017–29

Welten K. C., Caffee M. W. 2024. Cosmogenic Radionuclides in the Stubenberg LL6 Chondrite Fall — Evidence for a Recent Breakup Event of a Meter-Sized Object in Space. *86th Annual Meteoritical Society Meeting*, abstract #6460.

Welten, K. C., Nishiizumi, K., Masarik, J., Caffee, M. W., Jull, A. J. T., Klandrud, S. E., and Wieler, R. 2001. Cosmic-Ray Exposure History of Two Frontier Mountain H-Chondrite Showers from Spallation and Neutron- Capture Products. *Meteoritics & Planetary Science* 36:301–317.

Weiler, R. 2002. Cosmic ray produced noble gases in meteorites. *Reviews in Mineralogy and Geochemistry* 47: 125–170. https://doi.org/10.2138/rmg.2002.47.5

Weisburg, M. K., McCoy, T. J. and Krot, A. N. (2006) Systematics and Evaluation of Meteorite Classification in *Meteorites and the Early Solar System II*. University of Arizona Press, Tuscon, pp. 19-52.

Wieler, R., Graf, Th., Signer, P., Vogt, S., Herzog, G. F., Tuniz, C., Fink, D., Fifield, L. K., Klein, D., Middleton, R., Jull, A. J. T., Pellas, P., Masarik., J., Dreibus, G. 1996. Exposure history of the Torino meteorite. *Meteoritics & Planetary Science* 31: 265–272.

Wlotzka, F. (1993) A Weathering Scale for the Ordinary Chondrites. *Meteoritics & Planetary Science* 28, pp. 460.

Wlotzka, F., Jull, A.J.T., Donahue, D.J. 1995. Carbon-14 terrestrial ages of meteorites from Acfer, Algeria. *Proceedings*, *Workshop on Meteorites from Cold and Hot Deserts*. 72–73.

Xie, X., Chen, M. (2016). General Introduction of the Suizhou Meteorite. In: Suizhou Meteorite: Mineralogy and Shock Metamorphism. *Springer Geochemistry/Mineralogy*. Springer, Berlin, Heidelberg. https://doi.org/10.1007/978-3-662-48479-1_1

Zappatini, A. Hofmann, B.A., Gnos, E., Eggenberger, U., Gfeller, F., Kruttasch, P.M., et al. (2024). Al-Khadhaf: A camera observed H5-6 fall from Oman. *86th Annual Meteoritical Society Meeting*, Abstract #6140.

Zurfluh, F.J., Hofmann, B.A., Gnos, E., Eggenberger, U., Jull, A.J.T. 2016. Weathering of ordinary chondrites from Oman: Correlation of weathering parameters with ^{14}C terrestrial ages and a refined weathering scale. *Meteoritics & Planetary Science* 51(9):1685–1700.

Declaration of consent

on the basis of Article 18 of the PromR Phil.-nat. 19

Name/First Name:

Registration Number:

Study program:

Bachelor ☐ Master ☐ Dissertation ☐

Title of the thesis:

Supervisor:

I declare herewith that this thesis is my own work and that I have not used any sources other than those stated. I have indicated the adoption of quotations as well as thoughts taken from other authors as such in the thesis. I am aware that the Senate pursuant to Article 36 paragraph 1 litera r of the University Act of September 5th, 1996 and Article 69 of the University Statute of June 7th, 2011 is authorized to revoke the doctoral degree awarded on the basis of this thesis.
For the purposes of evaluation and verification of compliance with the declaration of originality and the regulations governing plagiarism, I hereby grant the University of Bern the right to process my personal data and to perform the acts of use this requires, in particular, to reproduce the written thesis and to store it permanently in a database, and to use said database, or to make said database available, to enable comparison with theses submitted by others.

Place/Date

Signature